Modelling the biological membrane

Lemon, A. P.

Award date:
1995

Awarding institution:
University of Bath

Modelling the Biological Membrane

Submitted by A.P. Lemon

For the degree of Ph.D.
of the University of Bath
1995

ProQuest LLC
789 East Eisenhower Parkway
P.O. Box 1346
Ann Arbor, MI 48106-1346

Abstract

Modelling the Biological Membrane
Submitted by A.P. Lemon for the degree of Ph.D.
of the University of Bath
1994

The aim of this thesis is to provide a realistic model for the biological membrane. The experimental and theoretical literature is reviewed, examining the available data and theoretical approaches to reproducing such data. The methodologies used in this study for both production and analysis of the molecular dynamics trajectories are reviewed. The details of the analysis tools developed specifically for analysis of membrane simulations are discussed in detail.

The starting conformation and configuration of bilayer models has been found to be fundamental to the progress of their molecular dynamics trajectory. A number of different approaches to this problem have been undertaken and are discussed.

A molecular dynamics trajectory of 18 DMPC molecules (in the crystal structure A conformation), arranged in a 3x3 square lattice bilayer configuration has been sampled and analysed. The DMPC molecule exhibits restricted flexibility and there is no evidence of the formation of the L_α phase. An interdigitated model has also been simulated and the results are discussed.

An alternative approach is to use the crystal structure unitcell of DLPC. This is a bilayer consisting of two monolayers of 8 DLPC molecules. The molecular dynamics trajectory has been sampled and analysed. The DLPC molecule is also found to exhibit low flexibility. In order to probe the effect of density and area per head group of these systems an expanded crystal structure system has been sampled and analysed. It has been found that this system exhibits increased flexibility and evidence of the formation of an L_α phase.

The effect of cholesterol on the dynamics of the DLPC bilayer systems has been investigated using a 1:1 cholesterol:DLPC bilayer. The molecular dynamics trajectory has been sampled and analysed. It has been found that cholesterol decreases order in the unexpanded bilayer model and increases order in expanded system. This agrees with the experimentally observed trend.

The effect of water on the bilayer systems has been investigated using hydrated models of the unexpanded DLPC model, the expanded DLPC model and the expanded cholesterol doped system. The molecular dynamics trajectories have been sampled and analysed. The hydrogen bonding behaviour of waters has been examined and their penetration into the hydrophobic core followed. Waters are observed to penetrate down to the glycerol backbone on the phospholipid molecules.

The effect of density on the populations of gauche torsional states in the acyl chain torsions of these molecules has been examined using a series of decane simulations. A narrow density range is found in which increased flexibility is observed. A number of problems with these simulation results are highlighted and possible solutions are discussed.

Acknowledgements

I would like to thank the following people for their help and assistance in both compiling this thesis and in my development while in Bath:

David Osguthorpe for his supervision and general discussions on all aspects of science, politics and life. Pnina Osguthorpe for her help with proof reading of my thesis, and general help and scientific collaboration. Prem Paul and Jan Pedersen for their enthusiasm and interrest.

Indeed all members past and present of the molecular graphics unit in Bath including:
Dave Evans(evo) and Gareth Adams(gazza), scientific and rugby banter,
and all things that keep a computational scientist from going insane.
Richard Sessions, Paul Hodgson, Steve Joyce(captain), Oz Parchment, Colette Maunder, Phil Tollington, Dave Webster, Andy Henry, Steve Searle and Paul Calleja for making my time in Bath more colourful.
For their specific help with thesis preparation, Paul Fortun, George Forsythe, and my father Peter Lemon.

The SERC for financial support and the Molecular Graphics Society for providing funds for international conferences, a welcome injection of ideas and collaboration.

I dedicate this thesis to my wife Angie Lemon who has trodden down every step of this long and winding road with me.

1. Introduction.

1.1. The Biological Membrane

The biological membrane is one of the most fundamental structures on which the biochemistry of the body and in particular the cell is based. It defines the barrier between the outside and inside of the biological cell. This allows for chemically different environments to coexist within the same organism, and is the basis for the organism's ability to store and transport energy, to maintain its viability . An understanding of the structure, function and chemistry of the biological membrane is a prerequisite for knowledge of any higher organism.

Membranes are composed of approximately 40% lipid and 60% proteins.[1,2] Their diversity in structure and function[3] depends upon their specific lipid and protein content. However they do share a number of common characteristics.

1. Membranes are sheet like structures, forming in a closed boundary.
2. Membrane lipids are relatively small molecules characterised by their amphiphilic nature.
3. Specific proteins mediate the various functions of membranes. These may act as pumps, gates and enzymes to regulate the flow of material in and out of the cell.
5. Lipid and protein molecules are held together by noncovalent co-operative interactions.
6. Membranes are asymmetric: the extra- and intra-cellular membrane portions are both chemically and structurally asymmetric.[4]
7. Membranes are fluid structures in which lipids and proteins diffuse rapidly in the plane of the membrane. However lipids do not transverse the membrane.

Lipids are a common component of biological membranes and can be regarded as forming a matrix or substrate into which are incorporated more biochemically active constituents such as membrane proteins.[5,6] The nature of protein-lipid interaction has a profound effect on the structure of such proteins.

1.2. Lipids

Lipids are molecules of intermediate molecular weight consisting of a substantial portion of aliphatic/aromatic hydrocarbon, containing both hydrophobic and

hydrophilic moieties in an asymmetric distribution.

Phospholipids

The phosphoglycerides are quantitatively the most important class of lipid.[7] All phosphoglycerides have a glycerol-3-phosphate backbone, but vary with respect to the groups esterified to the hydroxyls. This provides the backbone structure of the molecule and exacts important effects on the physical properties of the molecule, forcing the acyl chains to adopt a parallel conformation.[8] There is a fine balance between the properties of each connected moiety. The fluidity of the membrane is therefore controlled by both the lipid content and the interplay of the constituent lipid moieties. This has corresponding implications on the structural and dynamic properties of material within and in association with the membrane.

The hydroxyls on C1 and C2 of glycerol (Figure 1.1) are esterified with fatty acids. In most naturally occurring phosphoglycerides the Sn1 chain is saturated and the Sn2 chain is unsaturated. The phosphate is esterified to one of several alcohols, which further modify the properties of the lipid. The common moieties are serine, ethanolamine, choline, glycerol and inositol. The phosphoglyerides are optically active, the chiral centre being on the C1 of the glycerol and most naturally occurring molecules exist in the L enantiomer. In biological membranes only the L enantiomer is found.

In nature the fatty acids chains are nearly always of even carbon number and commonly C12,C14 and C16 (Lauryl, Myristyl, and Palmityl from their fatty acids). This study concentrates on the properties of diacylphosphatidylcholine (PC) and diacylphosphatidylethanolamine (PE). Some of the most widely studied glycerolphospholipids are phosphatidic acid, phosphatidylcholine (lecithin), phosphatidylethanolamine, phosphatidylserine, phosphatidylglycerol, and phosphatidylinositol. All have two acyl chains, but differ in the head group region, some being charged and some zwitterionic (pH7). When one acyl chain is removed a lysophospholipid is formed, these tend to be detergents.

Sphingolipids

These are based on a backbone structure of sphingosine. This may be esterified to one or two fatty acids and phosphate head groups, in the same manner as the phospholipids. They are found predominantly in the nerve tissues, providing a membrane protection for the nerve fibres. The fatty acid chains tend to be of considerably longer length, than for phospholipids.

Figure 1.1 Lipids

(a) DLPC

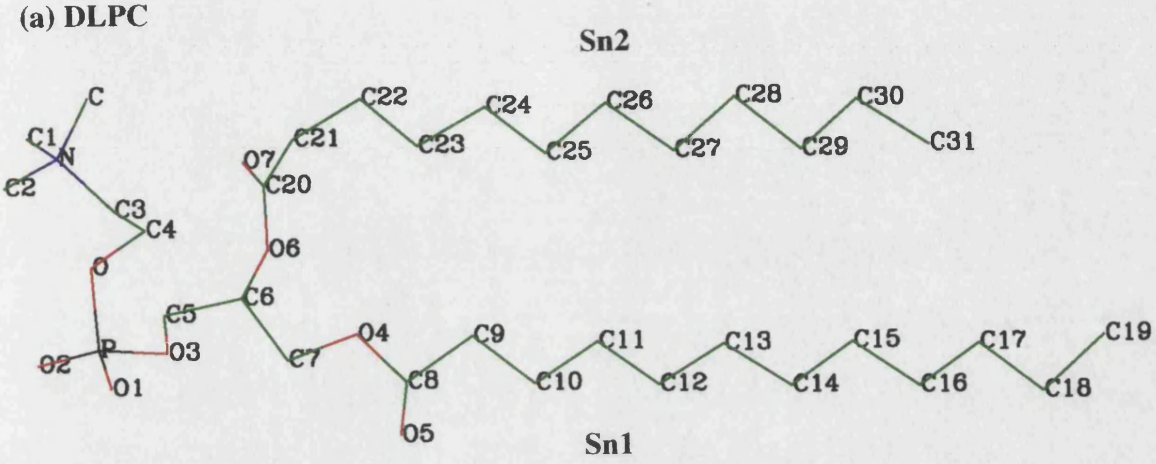

(b) DMPC

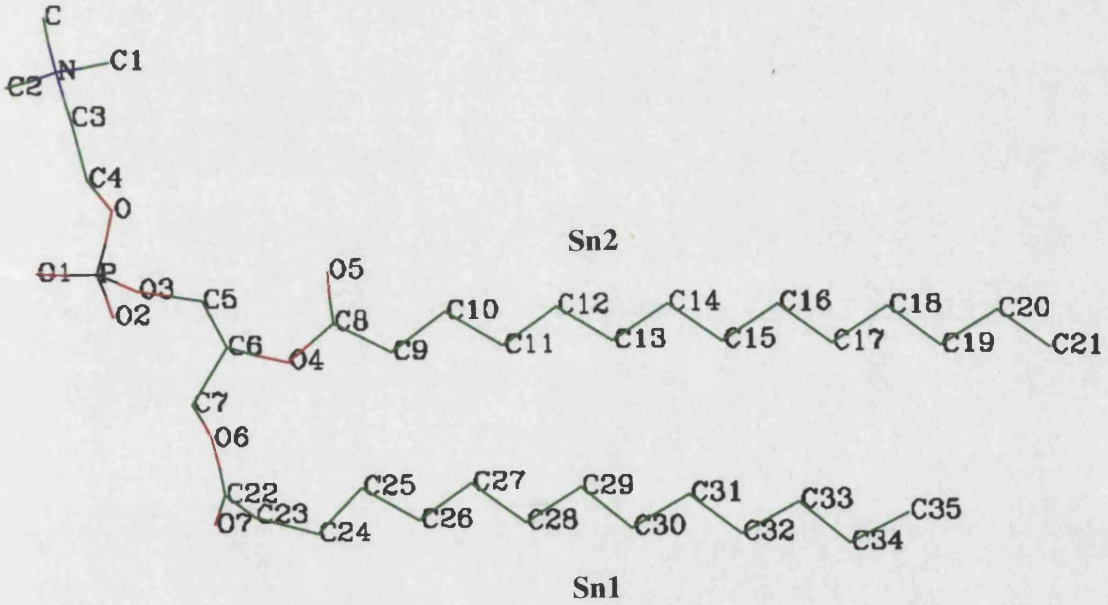

(c) Cholesterol

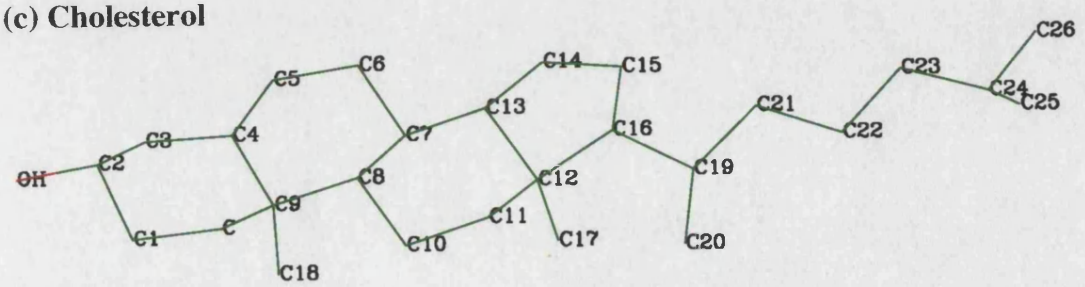

Sterols

Another important class of lipids are the sterols. Based on the sterol ring system of three fused six membered rings and a five membered ring. Many stereo isomers are possible. The most common sterol is cholesterol, which is the only sterol lipid considered in this study.

Phospholipids exhibit a variety of thermodynamically stable structures.

1.3. Bilayers

1995 marks the seventieth anniversary of the proposal that the biological membrane consists of a double layer of lipid molecules.[9,10]

Phospholipids under physiological conditions are formed into bimolecular sheets, called "bilayers", which are curved to form the walls of cells. The bilayer structure is a stable thermodynamic arrangement of lipids in aqueous or polar media. The stability of the bilayer structure is a direct consequence of the structure of phosholipids, specifically due to their amphipathic nature. Hydrophobic interaction is the major driving force for the formation of bilayers, although there is a contribution from van der Waals interactions. In biological membranes the bilayer structure contains predominantly the same head group structure, but the nature of the fatty acid chains varies considerably.

The bilayer structure minimises the contact between the hydrophobic acyl chains of the phospholipids and surrounding water molecules.[5] The thermodynamic stability of the membrane structure is due to a number of interactions.

1. Hydrophobic interactions among fatty acid acyl chains.
2. Electrostatic interactions between the zwitterionic head groups and water molecules.
3. Electrostatic interactions between negatively charged head groups and water molecules.
4. Electrostatic interactions of charged head groups with each other and any ions present.

1.4. Membrane proteins

Membrane proteins are responsible for most dynamic processes carried out by membranes. Membrane lipids form the appropriate environment for the action of such proteins.[3]

There are two basic types of membrane proteins peripheral and integral (Figure 1.4c). Peripheral membrane proteins are associated with the membrane surface and other membrane proteins. They are non-covalently linked to the surface by electrostatic interactions with the lipid head groups. They may be easily dissociated from the membrane surface by agents which disrupt ionic or hydrogen bonding. In contrast, integral proteins are not easily removed from the membrane, usually requiring the disruption of the membrane core. They are embedded in the membrane interacting with the hydrophobic lipid acyl chains. Some span the membrane, providing a channel for polar material to pass across the hydrophobic (nonpolar) interior of the lipid bilayer. Their removal in vitro is achieved with detergents which disrupt the lipid chain packing, replacing hydrophobic interactions. This causes irreversible damage to the structure of both the membrane and protein. This has made structural study of membrane proteins difficult or even impossible.

Integral proteins range from small polypeptides which are completely embedded in the hydrophobic core to larger proteins which have considerable structure within the hydrophilic region either side of the membrane. It is thought that these proteins provide receptor domains, which sense the presence of external stimuli and cause response by the protein.

Pure phospholipid bilayers have been shown to have very low permeability to ionic and polar material.[3] However membranes are highly selective permeability barriers rather than impervious walls, due to the presence of specific molecular pumps and gates. These proteins regulate the transport of ionic and molecular material across the membrane. In this way membranes control the flow of information between cells and their environment. They contain specific receptors and may in turn generate either chemical or electrical signals, in response to external stimuli. An imbalance of ionic material between the intra and extra-cellular sides of the membrane leads to a membrane potential. Ion channels are included in the membrane which sense this potential and open or close in response, allowing ions to move across the membrane and reduce the potential. It is this response or switch which shows potential as a new bioelectronic device.[11-20] Current research in synthetic chemistry is being undertaken to synthesise analogues to these ion-channels[21,22] with the aim of including them in a synthetic bilayer architecture.

1.5. Physical properties of lipid bilayers

1.5.1. Phase Behaviour of Lipids

Amphiphilic lipids dispersed in water display thermotropic and lyotropic mesomorphism (their phase depends on temperature and solvent). [23] Raising the temperature leads to an "endothermic" transition at T_c. The hydrocarbon chains of the phospholipid "melt" gaining liquid like mobility. The polar moieties, including the head group of the phospholipid remain in a semi-rigid, quasi-crystalline state. At constant pressure the Gibbs free energy for this transition is zero.

$$\Delta G_p = \Delta H - T\Delta S = 0$$

This leads to a discontinuous change in enthalpy at the phase transition. The phase transition can therefore be detected from the thermodynamic, geometric and kinetic components of the lipids fatty acid chains at the transition.

Two chain phospholipids tend to be insoluble, swelling in aqueous dispersions. Polar head groups can be zwitterionic such as phosphatidylcholine, or charged, such as phosphatidic acid. Charged phospholipids exhibit phase behaviour dependent upon their state of ionisation. Their transition temperature is therefore pH dependent. Even zwitterionic phospholipids interact with ions. An example is the interaction of PC with Ca^{+2}. The degree of swelling is particularly affected by the presence of ions.

Many general principles of hydrocarbon chain interactions apply to phospholipids. The specific changes of state depend on the nature of the polar head group, the conformation of the linkage moiety, the nature of the hydrocarbon chains and interactions of the head group with the solvent.

Lipid water phase diagrams (Figure 1.2) can be determined using a combination of calorimetric or spectroscopic techniques to determine the phase boundaries, and X-ray diffraction, electronmicroscopy and ^{31}P NMR to determine the specific structure of the phases.[24,25]

In the single lipid water dispersions examined in this study, there are three important phase regions (Figure 1.3):

1. L_α is the liquid crystalline phase in which the head groups are in a crystalline lattice, whilst the acyl chains are liquid in nature.

Figure 1.2

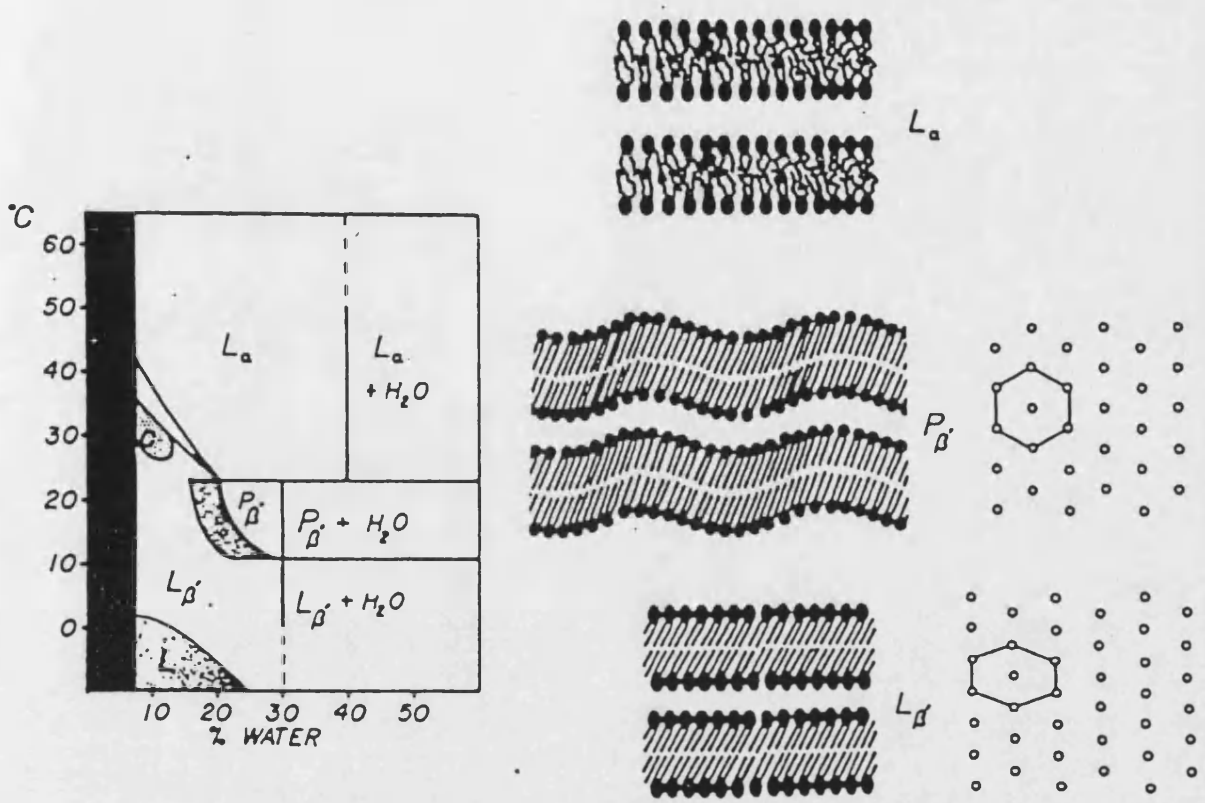

Phase diagram of hydrated dimyristoyl phosphatidylcholine bilayers, together with representations of the $L_{\beta'}$, $P_{\beta'}$, and L_α phases. The hydrocarbon chain packing is a hexagonal array for the $P_{\beta'}$ phase and a "distorted" hexagonal lattice of the $L_{\beta'}$ phase.

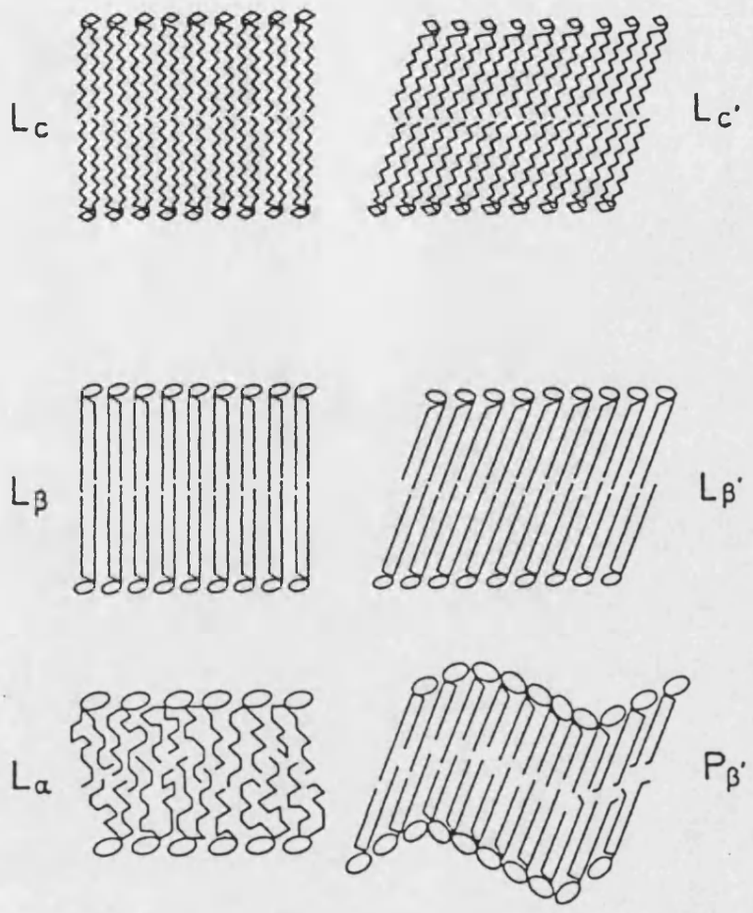

Schematic representation of various lamellar and quasilamellar (periodic) bilayer states. L_c is a crystalline phase, L_β is a gel phase, P_β is an intermediate periodic or ripple phase, and L_α is the fluid phase. Primes indicate that the chains are tilted with respect to the bilayer normal.

Table 1.1

A letter characterises the type of long range order and a subscript the short range order.

Symbols for phase states	
	Long Range Order
L	one-dimensional, lamellar
P	two-dimensional oblique or centred (ripple)
C	three-dimensional crystalline
	Short Range Order
α	disordered fluid
β	untilted, partially ordered gel
β'	tilted, partially ordered gel

2. $P_{\beta'}$ is the ripple phase, in which the head groups are in a crystalline lattice and the acyl chains are tilted with respect to the bilayer normal, in the all trans gel state. There is a long wavelength displacement of the lipids along the bilayer normal forming a "ripple". This phase cannot be observed in the simulations in this study as the unit cell is smaller than twice the wavelength of this ripple.

3. $L_{\beta'}$ is the tilted gel phase in which the head groups are in a crystalline matrix and the acyl chains in the all trans gel state.

These phase states are summerised in table 1.1.

DPPC in aqueous dispersions exhibits four phases including the three important phase regions:

1. Subgel, < 286K in which rigid packing of the Sn1 and Sn2 hydrocarbon chains is observed.
2. Gel ($L_{\beta'}$), 286-307K exhibits a different packing of hydrocarbon chains.
3. Ripple (P_{β}), 307-315 exhibits dynamic surface rippling whilst in the $L_{\beta'}$ structure.
4. Liquid Crystal (L_{α}), > 315K in which hydrocarbon chains exhibit liquid-like mobility.

The thickness of the hydrocarbon region in the two gel phases corresponds to the length of two fully extended, but tilted hydrocarbon chains.[26] The terminal methyl groups are localised near the geometric centre of the bilayer. Hydrocarbons from one monolayer do not appreciably interdigitate with those of the opposite monolayer. In the melted L_α phase the bilayer thickness is decreased due to isomerisations in the hydrocarbon chains, but on average are still only slightly interdigitated. The hydrocarbon chains of natural membrane lipids are believed to be in the fluid L_α phase under physiological conditions, although the presence of sterols may have a restrictive effect, leading to mixed phase regions.

The phase transition temperature is strongly dependent upon the percentage water present. The transition temperature is decreased with increasing water content to a limiting value at 25-30%wt H_2O. It has been shown from differential scanning calorimetry(DSC) and X-ray diffraction that 30%wt water is enough to fully hydrate the DPPC. Waters bound to the lipid are prevented from participating in co-operative interactions with bulk waters. This binding results in a reduction of the T_c by 4K per H_2O per PC. The gel phase has a maximum hydration of 30%wt H_2O. Additional water results in detection of the freezing transition for bulk waters and separation of the bilayers, which can be detected by X-ray diffraction. The phase transition temperature increases as the water content decreases and the ripple phase disappears.

From ^2H NMR[27] and DSC studies of hydrated DPPC multilayers, three species of water have been identified.

1. Free water, (>35%wt of water).
2. Water trapped between adjacent bilayers, but free to exchange, (20-35%wt water).
3. Waters bound to DPPC molecules.

Trapped waters have a critical role in the phase behaviour of these multilayers. It has been suggested that more sensitive studies of the bound waters will distinguish different types of hydrating water.

Effect of Pressure on the chain melting transition

This is expressed in the Clausius-Clapeyron Equation

$$\frac{\delta P}{\delta T} = \frac{\Delta H}{T_m \Delta V}$$

Where P is the pressure, T temperature, ΔH enthalpy change, ΔV volume change and T_m the temperature of melting.

From the behaviour of alkanes it is known that the phase transition temperature is increased with pressure.[28] The relationship dp/dt depends on the nature of the phase transition, but in general $dP/dT \approx 43.5 atm K^{-1}$

Dilatometric Properties

A discontinuous change in the specific partial volume is observed at T_c. The net volume change is small ($\Delta V_t/V_t \approx +4\%$). This suggests that lipid chain disordering is highly co-operative and does not disrupt chain packing. This is energetically unfavourable due to large stabilizing effects from hydrophobic and van der Waals interactions.

The increase in volume is consistent with the increase in volume expected from chain rotational isomerism. However the absolute change is much less than the free volume of the equivalent hydrocarbons. The free volume created by an isolated kink ($^{+}gtg^{-}$) is $0.25 Å^3$.[29] However the measured ΔV_t values for DPPC are $0.46 Å^3$, suggesting that there are two kinks per molecule, if ΔV_t is caused by kink formation only. This kink only model does not explain the observed order parameter profiles from NMR, hence it has been postulated that there is a contribution from the formation of gauche states in proximity to the terminal carbon of the acyl chains.[30]

1.5.2. Molecular Motions of bilayer lipids

Many functions of the biological membrane require mobility of both the lipid and protein components. This has lead to the *fluid mosaic*[31] model of the membrane (Figure 1.4a). In a membrane or bilayer molecules are subject to various types of movement.

1. Rotational movement about an axis normal to the membrane surface.
2. Limited oscillation in and out of the plane of the membrane along the bilayer normal.
3. Lateral diffusion within the membrane layer.

Some molecular motions are highly unfavoured thermodynamically. The transverse movement of phospholipids from one monolayer to the other monolayer, called a "flip flop", is such a motion and is observed very infrequently. Various forms of lipid mobility are described below.

A: Lateral and vertical motions of lipids

Lateral motions are very rapid with diffusion coefficients in the region of 10^{-8} $cm^2 s^{-1}$. Spin labelling techniques are used to probe the diffusion of lipids within membranes. It has been shown that lipids randomise rapidly in E Coli fatty acid auxotrophs(mutants).[32] The rate

of diffusion of pyrene in pure lecithin has been measured as $1.4 \times 10^{-7} cm^2 s^{-1}$ at 323K. At 293K the self diffusion coefficient for phosphatidylcholines was measured as $0.9 \times 10^{-8} cm^2 s^{-1}$ comparable with similar results from ESR studies.

B: Lateral Diffusion

Molecular diffusion is by a series of jumps from one lattice vacancy to another, with a frequency of $10^7 - 10^8 s^{-1}$. This can be broken down to a two dimensional diffusion problem dependent upon the free area per molecule, the temperature and the energy of activation for breaking the transient bonds to neighbouring molecules (London forces).

Typical values for the diffusion rate (D_L) are:

DMPC (L_α) 303K $7 \times 10^{-8} cm^2 s^{-1}$, and ($L_{\beta'}$) 288K $3 \times 10^{-11} cm^2 s^{-1}$.

The distance travelled by a lipid molecule in a lipid vesicle is in the order of $\mu m s^{-1}$, very slow compared to molecular dynamics time scales (ps).

C: Transbilayer Movement

The so called "flip flop" motion of lipids is very slow, in the order of seconds. This is due to the energy barrier for the polar head group passing through the hydrophobic interior of the membrane. This slow rate is observed even for cholesterol with its polar hydroxyl group, due to hydrogen bonding interactions with neighbouring groups. The half-life time for the flip flop motion is approximately $10^4 - 10^6 s$ in most lipid membranes, although this may be reduced in the proximity of proteins.

This has been elegantly measured using the paramagnetic destroying properties of ascorbate on N-O substituted fatty acid lipids in liposomes. The introduction of ascorbate into the outer solution causes destruction of the paramagnetism of the outer monolayer. The destruction of the paramagnetism of the inner lipids can then be measured, as it is a function of the transfer of lipids from intra to extra liposome layer.

There is also an undulatory movement of the bilayer ("ripple") membrane with an amplitude which may exceed the thickness of the bilayer itself. This is thought to be involved in protein transport and membrane fusion. There are two types of vibrational mode associated with this movement.

(a) Symmetric stretching or squeezing of the two monolayers with respect to each other, which results in thickness variations and even rupture of the membrane.

(b) Antisymmetric stretching or buckling of the membrane due to mechanical stress or

osmotic pressure. This gives rise to variation of local curvature, but maintains thickness. The translational diffusion can also be measured using a variety of techniques.

Lateral Diffusion

Spin Labeling $D_{diff} = 2.5 \times 10^{-8} cm^2 s^{-1}$

ESR $D_{diff} = 1.0 \times 10^{-8} cm^2 s^{-1}$

NMR $D_{diff} = 1.8 \times 10^{-8} cm^2 s^{-1}$.

D: Lipid Chain Rotational Isomerism

The dynamics of acyl chains have their origin in rotational isomerism of the C-C bonds of the lipid acyl chains. These have been studied by ^2H NMR[33] of specifically deuterated lipids. The nuclear quadrupole splittings are used to measure the order parameter or time averaged angular amplitude of motion of chain segments. These are dependent upon the orientation of chains with respect to the static field of the NMR spectrometer. The angular amplitude of motion increases on proceeding from the glycerol back bone to terminal methyl. The C2 carbon segment is significantly out of alignment in this trend due to the turn at the C2 to allow the acyl chains to pack parallel to each other.

There are three stable rotamers of the C-C bond, +gauche (60°), trans (180°) and -gauche (-60°). Formation of gauche isomers is enthalpically unfavoured: there is a 0.5kcal-mol^{-1} energy barrier to rotation for each CH_2. However this is more than compensated for by the entropic gain from the creation of rotational disorder. The conformational restriction imposed by the glycerol group acts to reduce the rotational disorder in its proximity. It also has an intermolecular effect reducing populations of gauche rotamers in the upper part of the chain.

These effects on the gauche population can be observed from the segmental order parameters for chain segments from C1-C16 in the acyl chains of DPPC bilayers at 323K.[34-39] The order parameter of the carbon segments C3-C8 decreases only slowly with chain position. This region is known as the "order-parameter-plateau", and has its origin in the intermolecular interactions of the chains. Since gauche isomer formation causes large angular deviations in the chain axis, it is concluded that only co-operative tilting and those combinations of gauche conformations that minimise lateral displacement and preserve the lateral packing are allowable disorder in the upper region of the chain. In the terminal region of the chain lateral displacement due to gauche rotamer formation is reduced, and hence their

formation favoured. This torsional freedom also creates more free volume in the chains by shortening the chain length from the all trans conformation, which in turn favours gauche rotamer formation. On average a population of 4 gauche conformations per chain is observed in the L_α phase of lipid chains. Spin-lattice relaxation measurements allow for the measurement of rotational correlation times, which are approximately 100ps for the plateau region, decreasing to approximately 10ps for the terminal carbon segments.[33]

The properties of the fluid phase represent the weighted average over all other interconverting rotational states of the lipid chains. The functional representation of the potential energy due to rotation of the C-C bond is three fold in nature (see Chapter 2). The true relationship between the potential energy of the molecule and rotation about that bond is also reflected by the non-bonded interaction of connected atoms. The Energy of individual states and transitions from one state to another can be calculated from this potential, $E_g^{\pm} = 0.5 - 0.6 \text{kcalmol}^{-1}$, $E_{t \rightarrow g^{\pm}} = 3.6 \text{kcalmol}^{-1}$, $E_{g^{+} \rightarrow g^{-}} \approx 10 \text{kcalmol}^{-1}$. It should be noted that both gauche minima are displaced towards the trans conformation by 5-10° due to strong interaction in the cis conformation. There is a coupling of adjacent C-C bond rotations due to strong steric interactions of non-bonded atoms. Hence the formation of $g^{+}g^{-}$ and $g^{-}g^{+}$ conformations is highly sterically hindered. However formation of $g^{\pm}g^{\pm}$ conformations is not significantly hindered with respect to isolated $g^{\pm}$ conformations. Only correlations over two C-C bonds away are required in lipid chains as these account for all possible steric restrictions. Packing restrictions must also be taken into account in the intermolecular interactions, for example the formation of $g^{\pm}tg^{\pm}$ kinks may be favoured as it maintains packing of the acyl chains.

Below T_c, the acyl chains are packed in a highly ordered hexagonal array, and the motion of chains is anisotropic. Above T_c the lipid acyl chains become more disordered and the hydrocarbon chains undergo rapid rotation. The degree of order is reduced in the centre of the bilayer.[40] ^{13}C NMR and ^{2}H NMR studies[41,42] have produced evidence for the rotational motion about C-C bonds. Rotational diffusion coefficients (D_{rot}) have also been determined[43,44] for phospholipid acyl chains (DMPC) and n-alkanes.

D_{rot} for the terminal carbons is approximately equal to that of n-alkanes ($1.0 \times 10^{-11} \text{cms}^{-1}$). However D_{rot} for carbons in the middle of the acyl chains are about 10% of the n-alkane values.

E: Rotation of lipid molecules

Lipids rotate about their long axis with correlation times of about 10ns. This is known as "rotational diffusion", [45] and depends on the viscosity, and geometric constraints of the molecule (ie. its shape). The rate of axial rotation about the long axis of the molecule has been determined for DMPC $7 \times 10^{-9} s^{-1}$ ($0.05 radps^{-1}$).

F: Mobility within Lipid Membranes

Rotational motion of intramolecular bonds and rotation about C-C bonds has a rotational correlation time (τ_c) of 0.1 ns. The resulting kinks have an average life time of approximately 1ns. There are also various bending and rotational movements of the head group and chains which are extremely rapid.[46] The mobility of CH_2 segments, the longitudinal spin relaxation time τ_1, has been measured by NMR.[47] DPPC/H_2O τ_1(glycerol) = 0.1ns, τ_1 (C10) = 0.6ns and τ_1 (terminal c) = 3.3s. Hence there is a longer relaxation time for carbon segments closer to the terminal carbon of the acyl chains, and further from the glycerol moiety.

Statistical Mechanics of Chain Rotational isomerism

Using statistical mechanical theory, the percentage gauche bonds in a C20 chain is $\approx$ 20%.[48] This corresponds to approximately 4 gauche bonds per C20 chain. The probability of a g^+tg^- kink conformation is 3-4%, 0.7 per C20 chain. However these calculated values take no account of the preference for kink formation on packing grounds.

The configurational entropy is a quantity directly related to chain rotational isomerism. It is possible to measure the change in entropy ΔS_t, between the all trans gel phase to the liquid crystalline L_α phase. The increase in chain conformational freedom is the largest contribution to the configurational entropy, others being negligible. The relationship between the change in entropy with carbon segment ΔS_{CH_2} and the energy of the gauche state E_g has been measured by DSC as $\partial \Delta S_t / \partial n CH_2 \approx 1.3 calmol^{-1}K^{-1}CH_2^{-1}$. However calculated values from statistical mechanical theory are consistently higher $\partial \Delta S_t / \partial n CH_2 \approx 1.6 calmol^{-1}K^{-1}CH_2^{-1}$. This difference is assigned to ordering effects caused by acyl chain packing restrictions in the extended structure.

Membrane Microviscosity

This is not true viscosity as it is not isotropic in all directions. Therefore microviscosity averages out all anisotropic effects. This is the measure of the ease with which individual molecules move with respect to each other. The correlation time of a spherical particle is

inversely proportional to the rate of rotation.

$$\tau_c = \frac{4}{3}\pi r^3 \frac{\eta}{K_B T}$$

Where τ_c rotational correlation time, r radius of molecule, η viscosity, k_b Boltzmann constant, and T temperature.

Hence τ_c depends on the size and shape of the molecule. In ESR studies of fatty acids in membranes τ_c is 1ns for the first carbon after the glycerol and 12ps for the last carbon.

The fluidity of a molecule is related to the free volume present in the system. The relationship between fluidity and molecular volume for most organic compounds is linear. It is known that when the area per chain in the bilayer plane reaches $20Å^2$ the system becomes solid. This corresponds to the area in the hexagonally packed chain. Another factor is applied pressure. Changes in membrane volume depend on compressibility under isothermal conditions. Hence pressure may bring about a phase transition as does temperature. The pressure temperature dependency is 0.2 K/Pa for most biological membranes. The effects of pressure on the microviscosity (mediated by changes in volume) differ, depending on whether pressure is applied isotropically (hydrostatic pressure) or anisotropically (osmotic pressure), acting normal to the bilayer. Lateral and transverse compressibilities are very different for membranes.

A membrane potential also gives rise to a volume decrease and a resulting change in viscosity. Therefore the phase behaviour of the membrane may also be effected by an imposed membrane potential.[49]

$$p = C\Delta\phi_m/2\gamma$$

p pressure (7KPa), C membrane capacitance ($10mFm^{-2}$), $\Delta\phi_m$ membrane potential (0.1V), and γ membrane thickness (70Å).

This expression underestimates the actual value. It is therefore assumed that there must be barrier to liquid flow within the membrane. This is taken into account by adding a Boltzmann factor, for flow activation.

Distribution of lipids in bilayers and membranes

There is increasing evidence that bilayers are asymmetric with respect to their constituent lipids. It has been shown that in mixed PE/PC liposomes the outer monolayer contains preferentially more PC than the inner layer. This is a function of the increased head group

surface area of PC with respect to PE. Therefore in the closer packed inner layer the more compact PE is sterically selected. This has also been demonstrated from NMR studies of cholesterol doped bilayers. When at >30%wt cholesterol, it is preferentially partitioned into the inner layer. However below this concentration its distribution is homogeneous.[50]

Phospholipid Interactions with Cholesterol

Cholesterol is amphipathic by virtue of the β hydroxy group and is found in up to 1:1 ratio in some membranes. The sterol ring system is in contact with 10 or more carbons of the surrounding acyl chains. Monolayer studies have indicated that cholesterol causes condensation of lipids due to increased packing efficiency. However this effect is not mimicked in bilayers, which by nature of their structure are already packed efficiently. Spin labelled Fluorescence, NMR and DSC techniques have been used to elucidate the role of cholesterol in packing and molecular motion of phospholipids in membranes.

Cholesterol is found to decrease motion only above the transition temperature. Below this temperature (more crystalline phase) cholesterol increases disordering by disrupting this crystalline packing. Cholesterol is observed from DSC studies to disrupt the phase transition.[51,52] In bilayers containing less than 1:1 cholesterol, phase separation is observed into regions of pure lipid and in those containing 1:1 cholesterol (Figure 1.4a and Figure 1.4b), co-operative motions are impossible for lipids at the boundary of these microphases. DPPC bilayers have completely homogeneous and saturated chains. Below the transition temperature these are closely packed due to strong hydrocarbon and head group interactions. Introducing cholesterol forces apart the lipid molecules, the sterol inserting between them replacing the side chain interactions. The asymmetric shape of the cholesterol decreases lipid - lipid interactions leading to an increases amplitude of fatty acid motion.[53,54]

In contrast egg lecithins tend to be rigidified by cholesterol. Fluidisation is accompanied by a decrease in lateral separation and rigidisation by an increase in lateral separation. Hence a phase separation and the formation of "islands" of 1:1 cholesterol and free lipid phases is observed. Proton NMR has indicated that there are 10 CH_2's in contact with each cholesterol. Bilayers are therefore functionally economic, laterally packing to a density dependent upon the pressure and temperature. While lateral (surface) pressure does not vary more than an order of magnitude (1-20 mNm^{-1}), temperature may vary drastically.

Above T_c there is greater translational freedom of the lipid acyl chains, reflected in a cross sectional area of 0.3-0.4nm^2 per chain, twice that of most common diacyl lipids. Below

T_c they are in a liquid condensed state with cross sectional area of 0.20-0.23 nm^2 per acyl chain. If the lateral pressure is increased the condensed solid state is achieved with the acyl chains in the all trans conformation resulting in a cross-sectional area of 0.2nm^2 per chain. This is called the $L_{\beta'}$ phase and is of thickness 40-50Å.

Static organisation of membrane lipids in bilayers is dependent upon temperature. T_c for a single component bilayer is sharp, +/- 1 °C, due to co-operative nature of melting. In actual membranes this may extend over several K due to heterogeneity.

The sterol ring system prevents acyl chains from moving freely to assume gauche conformations. Hence cholesterol has a rigidifying effect at temperatures above T_c. Below T_c cholesterol remains *in situ* preventing formation of the $L_{\beta'}$ phase. In mixed PC/cholesterol systems there is an enthalpic change at the transition temperature T_c, which disappears at greater than 22% cholesterol. This agrees with computed structural arrangement of cholesterol within membranes, in which it is calculated that each cholesterol is surrounded by 7 acyl chains (3.5 per PC). At above 27% cholesterol this changes to 9 acyl chains (4.5 per PC). The enthalpic change on adding cholesterol is due to the hydrogen bond formed between the $\beta-OH$ of the cholesterol and the PC carbonyl oxygen. This stabilizes the $L_{\beta'}$ phase. These are finite in number, after which the enthalpic change disappears.

Asymmetry of membrane lipids

All biological lipids are inserted into membranes from the cytoplasmic face. They are directly synthesised at the face. An enzyme is therefore required to transport lipids to the non-cytoplasmic (external to cell) side of the membrane. Specificity of these enzymes accounts for the asymmetry of membranes. Membranes are thermodynamically unstrained due to their curvature and lack of alignment of the hydrophilic ends. Lipids pack according to size and shape dependencies. Lipid asymmetry depends on the degree of nonideality of lateral mixing of membrane components.

The Role of Lipids in Membrane Function

Lipids provide a hydrophobic environment for intrinsic membrane proteins. For solutions with low to moderate viscosity the membrane will behave as a two-dimensional fluid. There is a finite number of lipid-protein contacts exchanging in a liquid-like manner. The solvent action of the lipid chains provides a non-polar medium of high viscosity.

Physical state of lipids in membranes

The presence of cis double bonds increases the cross-sectional area of the acyl chains in the L_α phase, leading to increased lateral freedom and rotational motion. Trans-gauche isomerisation takes place among the acyl chains of the lipids giving rise to a more liquid state. Trans-gauche isomerisation in a torsion is often followed by a gauche-trans transformation one or two carbons down the chain, which is known as a kink. Below T_c the number of such kinks per CH_2 (N_k) < 0.01, at $T_c \approx 0.07$ and above $T_c > 0.4$.

General Properties of Lipids conferred by the Aliphatic chain

The aliphatic hydrocarbon chain is an important constituent of many lipid molecules, from substituted alkanes to complex glycosphingo lipids. An understanding of the properties of the hydrocarbon chain in the solid, liquid crystalline, and liquid states is fundamental to understanding the behaviour of a given type of lipid. There are many similarities between chain packing in n-alkanes and aliphatic lipids.

The hydrocarbon chain in its most stable state forms the all trans conformation. The packing of the hydrocarbon chains relative to each other is dependent upon the conditions of crystalisation.

There are two classes of packing.

(I) Tight packing with specific chain-chain interactions.

(II) Looser packing where the specific interactions are lost due to partial rotation of the chain of CH_2 segments relative to each other.

The problem therefore is one of two-dimensional packing in which there are four types of lattice packing arrangement.

1. Square (no carbon chains pack in a square lattice).
2. Rectangular
3. Oblique
4. Hexagonal

a: Specific chain-chain interactions

In complex lipids, particularly those with two acyl chains tethered to a central moiety (glycerol) packing is restricted. In some cases this leads to a super lattice structure consisting of several chains packed in a hybrid lattice, reflecting the restrictions of their tethering. Typical arrangements for chain packing are triclinic and orthorhombic arrangements. In general the volume per CH_2 is $\approx 24\text{Å}^3$ with a cross-sectional area of $\approx 18.8\text{Å}^2$ per chain. These values

obviously vary with conformational freedom.

b: Non-specific chain-chain interactions

This is a less restrictive mode of packing in which a few degrees of freedom are allowed within the lattice, leading to the loss of specific interactions. The packing is essentially based on a hexagonal lattice with consequently larger volumes per CH_2 ($\approx 25.5 Å^3$) and cross-sectional areas ($\approx 20.0 Å^2$ per CH_2). The hydrocarbon chains therefore have greater mobility, relative to the tighter packing mode although they are restricted in comparison to the liquid state.

1.5.3. Lipid Hydration

Lipid and bilayer hydration are determined by the interaction of solvent molecules with the lipid head group, and therefore depend on the nature of that head group. Hydration of the chains is much smaller, and restricted to interaction at the polar-apolar interface (glycerol and carbonyl region). The fluid state of the chains does however have a secondary effect on hydration, due to the increased surface area of the lipid head group, after the transition temperature. This allows for increased exposure of the head group to hydration.

In pure water, long chain phosphatidylcholines are hexagonal, amphiphilic lipids, swelling in an aqueous solvent. Above T_c they swell to contain a limited number of waters (DLPC contains 23 H_2O, and DPPC 34 H_2O). The most stable thermodynamic state of DPPC in an aqueous dispersion above T_c is a series of stacked planar sheets of bilayers (lamellar) in equilibrium with low concentration of dissolved lipid. Sonication of these lamellar give rise to unilamellar vesicles.

Interfacial waters differ from bulk waters by perturbation of the highly ordered hydrogen bonded network ("clathrate water structure"). There is a fine balance between waters forming the bulk structure and local ordering around the head group. Coupling between adjacent water molecules propagates this perturbation away from the interface. Hence all the interlamellar water interact with the surface.

This change in the properties of this interlamellar water can be detected by NMR, X-ray diffraction, dielectric relaxation, IR, DSC and solubility measurements. It is found that steric fluctuations contribute little to bilayer hydration.

1.6. Phospholipid Assemblies as a Model for the Biological Membrane

Phospholipid bilayers in aqueous media have been studied extensively as a model system for biological membranes. These bilayers undergo phase transitions as a function of temperature, pressure and water content. The study of phase transitions in non-aqueous media also provides valuable information relating to the fundamental role of solvent in the stability of model and biological membranes.[55]

Other phospholipid assemblies include multilayers of bilayers, known as lamella, and highly curved vesicles.[56,57] These have been used to study the nature of the characteristic lipid motions and interactions.

The phase behaviour and physical properties of a bilayer are a function of the nature of the phospholipid from which it is constructed. Therefore an analysis of the conformation and flexibility of the phospholipid is a prerequisite for any study of such assemblies. The manner in which these molecules then pack and interact to form these extended bilayer structures and the forces which stabilize their structure can be elucidated by evaluating intermolecular interactions, as well as intramolecular conformation. The bilayer structure is a feature of an aqueous (or at least a polar solvent) environment. It is therefore important that hydration of the molecule and it's effect on the various intramolecular and intermolecular interactions be assessed.

It is the purpose of this study to simulate the environment of the biological membrane at its most simple level and to examine the impact of that environment on the chemistry of material in its proximity. The ultimate aim of such studies is the ability to model the effect of the biological membrane environment on both trans-membrane proteins and molecules which are transported across that membrane. This will allow the theoretical study of many biological systems, not previously accessible to conventional methods of study.

1.7. Sources of Structural and Dynamic Data

1.7.1. Systems for Experimental Study

Phospholipids can be assembled into a number of thermodynamically stable structures. They must be both stable with respect to the experimental data collection time and representative of the membrane environment. These represent attempts to build simplified systems approximating the biological membrane, allowing the elucidation of the co-operative interactions within such systems.

1. Lipid monolayers(Langmuir Films)

Langmuir films are made by spreading lipids on the surface of a liquid and are constricted using a moving barrier. They used to measure surface pressure - surface area isotherms for lipid monolayers at the interface between either air/water, or hydrocarbon/water. This is achieved by measuring the surface tension as a function of the area of the lipid surface. In the presence of excess hydrocarbon the effects of chain-chain cohesion are minimised and the hydrophobic interactions remain constant independent of the area per molecule. The surface pressure therefore is proportional to the repulsive interactions between lipids, arising from electrostatic, hydration and steric interactions.

2. BLM (Black lipid membranes)

BLM are contructed by smearing amphipathic molecules which are at a temperature above their gel to liquid phase transition across a hole between two aqueous compartments. This has the disadvantage of requiring a neutral hydrocarbon to be present, usually n-hexane. It is therefore seen as unphysiological. The electrical capacitance of the resulting membrane can then be measured ($0.38 \mu Fcm^{-2}$) as can its electrical resistance ($10^6 - 10^9 \Omega cm^{-2}$). A biological membrane has resistance $10^2 - 10^5 \Omega cm^2$. This large resistance is related to the large electrostatic potential for an ion travelling from the aqueous to head group region of the membrane. This resistance is consistent with a 50Å layer of pure hydrocarbon.[58] BLM's are also used to look at optical reflectance and atomic detail using electronmicroscopy. By spreading two types of lipid over a hole between the two aqueous phases and allowing them to interact it is possible to make bilayers having different compositions on the two sides of the bilayer. This property is known as "anisotropy": biological membranes are generally thought to be anisotropic or asymmetric. [4]

3. Orientated Lipid Multilayers

Orientated lipid multilayers are formed by building up successive bilayers on plates leading to the formation of a "lipid lamella". This is a stack of bilayers with or without solvent between the layers. They have the advantage of being relatively stable and because of the repeat nature of their structure, give strong X-ray Bragg reflections.

4. Bilayer Vesicles / Liposomes

When amphipathic lipids are allowed to swell in water above their transition temperature, "onion" like lamellae are formed, with water filling the spaces between the layers. Each layer forms a continuous permeability barrier. This allows the study of permeability of isotropic tracers from the outer/inner layers of the vesicle to the outside/inside environment, measuring rates of eflux.[59, 60]

Ultrasonication of these lamellae gives rise to spontaneous formation of vesicles of about 200-300Å diameter containing $1.0 - 2.7 \times 10^3$ lipids per vesicle. These are large single bilayer spherical structures, similar in structure to a simplified cell, with inner and outer solvent. It is also possible to measure the diffusion rates for ions through the membrane skin of the vesicle. They are also used to study the effect of curvature on the structure of membrane lipids. Vesicles swell in hypotonic (lower concentration) and shrink in hypertonic (excess concentration) solutions.

1.7.2. Experimental Methods

A number of experimental methods are available to probe both the time averaged properties and dynamics of the above experimental systems.

1. Differential Scanning Calorimetry (DSC) - enthalpic and entropic changes.

The temperature of the sample and reference is kept equal, using electrical heating, and the power required to maintain this equality is measured as a function of the increasing temperature. The power is related to the heat absorption of the sample. Endothermic transitions are sharp for homogeneous lipids. The gel to liquid crystalline acyl chain transition (T_c), is decreased by hydration reaching a limiting value at greater than 40% H_2O. Bound water does not show a phase change earning it the name of "iceberg" water. The transition temperature depends on the relationship between the apolar and polar moieties of the lipid. Their fatty acids interact by van der Waals interactions and dispersion forces. In unsaturated fatty acid

chains cis double bonds decrease chain cohesion. Increasing chain length gives enhanced interaction energy amongst chains and the transition will occur at higher temperatures. [30] The T_c for PE is greater than that for PC due to decreased chain cohesion in PC as a consequence of its larger head group volume (DMPE T_c 318K, and DMPC T_c 293K).

Ions can have an effect on the transition temperature. For example Ca^{2+} increases T_c of zwitterionic lipids. The pH affects T_c due to increased charge build up on the head groups of lipids. Charged phospholipids exhibit phase behaviour dependent upon their state of ionisation. This affects the electrostatic interaction between the head groups. Mixing different types of phospholipid gives rise to transient phases within the phase diagram for the mixture of the two components, dependent upon the difference in the number of hydrocarbon segments on the fatty acid chain. A difference of 4 or more hydrocarbons leads to multiple T_c. The integral of the DSC curve yields the enthalpy change for the transition. Calculating thermodynamic limits in thermotropic transitions is important in defining the effect of agents such as cholesterol, peptides and proteins on the membrane structure.

2. X-Ray Diffraction - bilayer repeat distance, hydration and volume changes.

This method cannot distinguish between the ensemble average of statistically frozen and dynamic structures whose time averaged properties are identical. It is useful for looking at the phases below and above the transition rather than during or at the transition. In DPPC lamellae strong crystalline packing Bragg reflections are observed, specifically a sharp reflection at 4.15Å and a broader peak at 4.5Å above the transition. This is explained as a thinning of the hydrocarbon region in the post transition phase leading to a change in inter acyl chain separation.[61]

3. Electronmicroscopy - low resolution structure.

Freeze fracture pictures of the lipid surface can yield some information about the phase behaviour of the lipids. This is tempered by the extreme physical conditions involved in the preparation of samples, and the coarse nature of the results, which are often open to different interpretations.

4. Spin Labelling - molecular dynamics.

This technique uses spin labelled probes to elucidate some structural information about both the bilayer structure and the nature of the membrane environment. It uses the N-O group, which contains a paramagnetic electron, which absorbs electromagnetic radiation in

the presence to an external magnetic field. The interaction of the unpaired electron with its environments nuclear spin leads to hyperfine splitting of the absorption spectrum, giving three lines at increase field. The shape and intensity of these peaks reflect the motion of the spin label and the polarity of its environment. Specific probes can be chosen to examine the environment of the hydrophobic region and hydrophilic head group region. The shape of the paramagnetic spectrum is sensitive to the rotational motion of the probe (rotational correlation time). An order parameter (S) can also be measured, reflecting the rotational polarisation of the probe as a function of chain segment position.[62, 63]

One problem with this technique, which always tempers any results, is that it has been found that some probes are phase sensitive, being preferentially partitioned into the more liquid regions, giving misleading results and over estimating fluidity. It has been found however, from N-O substituted fatty acid probes, that the fluidity of the bilayer increases from the polar head group surface to the centre of the hydrophobic core. Methylenes in close proximity to the glycerol moiety are motionally restricted.

5. Fluorescence Probes - molecular dynamics and environmental information.

These probes are photoexcitable molecules which can be inserted into the membrane, and by measurement of their fluorescence yield, information can be obtained about the environment around the probe. The quantum yield depends on the amount of collisional quenching in thermal cascades available from the environment of the phospholipid. Polarisation of the fluorescence is a function of viscosity of the solvent rotationally restricting the probe. Examples of such probes include ANS (anilinonaphthalene -8 sulphonate) which absorbs at 475nm, and is quenched by water to 520nm. It is found to locate in the glycerol region of the lipid, and is partitioned between the aqueous and bilayer core environment and measures the degree of penetration of water into the bilayer. The membrane binding of ANS is a function of the difference in hydrophobicity between the aqueous and membrane phases. The quantum yield of ANS is also sensitive to the microenvironment, detecting phase changes through increased thermal quenching in more fluid phases of the membrane core. This is observed by a large decrease in fluorescence at T_c. Again, as with spin labelling, the probe is selective for fluid regions and partitions into them preferentially.

It should be noted that there are various problems associated with using molecular probes.

(I) They cause extra perturbation of the system.

(II) They may not equipartition in all phases present.

(III) The probe may not have the same molecular shape and size as the sample and therefore behave differently to a variation in free volume.

Therefore caution should always be taken in interpretting the results.

6. Nuclear Magnetic Resonance Spectroscopy - molecular dynamics and structure.

This method is used extensively to probe the physical state of the lipids in bilayers and biological membranes. A number of different isotopes can be utilised to give structural data (^{1}H, ^{2}H, ^{13}C, ^{14}N, ^{15}N and ^{31}P). These can be used to probe the molecular environment of most atoms in a phospholipid bilayer.[64] Anisotropic interactions are not motionally averaged, leading to a broadened NMR spectra. Such spectra contain orientational and conformational information, and through relaxation and line shape studies also give dynamic information. Anisotropic features which have been most frequently exploited are quadrapolar splittings for labelled ^{2}H groups, chemical shift anisotropy from ^{13}P of the phosphate head group, and ^{13}C labelled backbone carbonyls. Dipolar interactions are resolved only for magnetically dilute nuclei, therefore ^{1}H are difficult to resolve.

Phospholipid vesicles produced by sonication of lipid lamella give high resolution spectra because of dipole-dipole interactions and chemical shift anisotropies are averaged. They do have the disadvantage that vesicles are generally small and highly curved, therefore lipids in the inner layer are strained compared with those in an extended bilayer.

In general it is possible to distinguish between the chemical shifts of atoms from the head group, backbone and certain chain segments. ^{31}P NMR can be used to characterise the composition of vesicles and detergent membranes. ^{13}C NMR can be used to provide conformational analysis of lipid chains. ^{13}C NMR T_1 relaxation times provide information on the dynamics of chain segments. The life time of the spin states (the spin state relaxation time, T) is proportional to the rotational correlation time and therefore its viscosity. The line width is proportional to the low frequency dipole interactions between neighbouring nuclei. The molecular motion gives rise to time averaged dependency and narrow line width, increased chain motion results in line narrowing. An example of this is the proton NMR of phosphatidylcholines in water, which exhibits a broad spectrum, with the exception of choline group protons. Sonication gives rise to a high resolution spectrum with clear $(CH_2)_n$ signals from the fatty acid chains. This is due to motional averaging of the choline interactions giving a zero component to their nuclear spin. However sonication may disrupt the molecular packing of the

acyl chains.

Solid state NMR of unsonicated lipid dispersions has been achieved, making use of magic angle spinning techniques to remove residual dipolar coupling and obtain high resolution ^{1}H spectra. These have demonstrated the relative conformational distortion of lipid molecules in sonicated dispersions compared with more extended bilayers. The segmental rotational mobility of specifically ^{2}H labelled chains can be studied in detail. The quadrapolar splitting in the ^{2}H NMR spectrum depends on the angular orientation of the labelled group and the extent to which this is averaged by molecular motion.[33,40] Hence by specific ^{2}H labelling of phospholipid chains in membranes, it is possible to study conformation, molecular ordering and segmental dynamics.

Broad line spectra can also elucidate dynamic information. The ^{13}P chemical shift anisotropy is partially averaged by the molecular motion within the phospholipid head group. Additional motional averaging is observed from translational diffusion of lipid molecules.

7. IR Spectroscopy - molecular dynamics and structure.

Fourier transform IR can be used to measure the characteristic antisymmetric ($2918cm^{-1}$) and symmetric ($2850cm^{-1}$) CH_2 stretching bands in lipid aqueous dispersions, and their temperature dependence.[65] These stretching values are combined to define an order parameter for the acyl chains of these lipids, which shows a dramatic reduction on the gel to liquid crystalline phase transition. The molecular dynamics of the choline head group can also be measured using the symmetric PO_2^- stretching ($1090cm^{-1}$) and the asymmetric $N^+(CH_3)_3$ stretching ($970cm^{-1}$) modes. These bands increase at the pretransition temperature (T_p). The water dynamics in these lipid lamellar can also be examined: the symmetric OH stretching ($3380cm^{-1}$) and OH_2 bending ($1640cm^{-1}$) bands show the same temperature relationship as the polar head groups. This can be interpreted as reorientation of the polar head group in the pretransition phase, and its effect on the water dynamics.

Raman IR spectroscopy can be used to describe lipid aggregate structures. Conformational changes in both the glycerol backbone and head group can be measured through changes in the spectral frequencies and intensities. It is most commonly applied to the study of the dynamics and conformation of the lipid acyl chains, concentrating on spectral features which allow for examination of their lattice packing and trans-gauche isomerisation. The gel and liquid crystalline phase regions can be unambiguously identified using the characteristic

spectral transitions in the CH stretching (2800-3100cm^{-1}), CH_2 deformation (1400-1500cm^{-1}) and C-C stretching (1000-1200cm^{-1}) mode regions. [66]

The study of the rotational isomerisation of liquid alkanes has previously been examined using Raman IR spectroscopy, allowing a comparison of the lipid acyl chain behaviour with alkanes.[67]

8. Enzymatic Probes - phase and structure.

The secondary effect of phase changes on the activity of "enzyme probes" can be measured and used as a tool to infer structural changes.

9. Neutron Diffraction Studies - structure and molecular dynamics.

Neutron diffraction experiments[68] on selectively deuterated phospholipids can elucidate to a segmental resolution, the conformation of the lipid with respect to the bilayer normal. This has the advantage of not only being able to ignore the high disorder of the system, but provides a time averaged picture of the extent of positional fluctuations of individual segments with respect to the bilayer normal.

Quasielastic neutron scattering measurements[45, 69] can give an accurate description of the diffusional properties of phospholipids within the bilayer environment. This has the advantage of being able to follow fast motions over molecular distances, whilst other techniques such as spin labelling are used for macro-diffusion. Unlike spin labelling it is a non-perturbing technique.

Specular neutron reflection[70] can be used to study the hydration of the lipid head group by virtue of its sensitivity to the distribution of protons. The application of contrast matching techniques allows the isolation of the lipid, and solvent phases specifically with respect to the neutrons.

1.8. Experimental Structural Data

1.8.1. NMR studies

Two principle structural features have been elucidated from ^2H NMR studies of labelled phospholipid chains in membranes, the inequivalence of the sn1 and sn2 chains and the chain flexibility gradient profile. The chain configuration about the glycerol backbone is found to be consistent with that observed in the crystal structure of PE and PC phospholipids.[71,72]

^2H NMR studies have indicated that signal from C2 protons of the Sn2 chain is split, interpreted as a gauche bend at C2 bringing the chains parallel. This is further confirmed by the relatively higher order parameter at C2 of the Sn1 chain, caused by its different orientation with respect to the bilayer normal.

Membrane Order

Order is defined as submicroscopic deviations from the crystal like arrangement of a liquid. This is quantified using the segmental order parameter.

$$S_n = 0.5(3 < \cos^2 \beta_i > -1)$$

Where β_i is the instantaneous angular orientation of the chain segment i relative to the bilayer normal,($< \cdots >$ averaged over the whole motion).[64]

An order parameter tensor can be defined such that

$$S_z = 0.5(3 < \cos^2 \beta_z > -1)$$

$$S_{ij} = 0.5 < 3\cos\beta_i \cos\beta_j - \delta_{ij} >$$

Where S_{ij} are elements of the order tensor, β_i is the instantaneous angular orientation and δ_{ij} is the Kronecker delta function.

The order parameter values supply information about lipid chain packing. Increased temperature reduces the order parameters and reduces the plateau region.

Membrane order can be measured from ESR, or NMR studies. However it does not necessarily yield true information about fluidity. This is a point observed by many researching in the area.[73] The order parameter S_n is related to the area per lipid and the chain length.

One can define a molecular order parameter S, in order to quantify the torsional variation.

$$S \propto \frac{1}{A}$$

where A is the cross sectional area of each chain and

$$Z = l / l_t$$

where l is the observed length, and l_t is the all trans length.

Then

$$Z^3 < S < Z^2$$

DPPC in 5% H_2O at < 303K Z =0.91 S = 0.81 (L'_β);

at > 321K Z = 0.61 S = 0.29 (L_α).

Phospholipid model membranes have been studied mostly by ^2H NMR of DMPC and DPPC membranes. The X-ray structure of only a few phospholipids has been determined, for example DMPC.$2H_2O$. DMPC in excess water at 296K spontaneously forms a lamellar of bilayers in the liquid crystalline state. The equivalence of the Sn1 and Sn2 chains persists in excess water, which is characteristic of the structure of phospholipid membranes. ^2H_2O / DPPC systems have been used to study the effect of the proximity of the phospholipid head group on the environment of the ^2H_2O and probe the phase behaviour [74] of the bilayer.

With orientated samples that are in the liquid crystalline state, the normal to the bilayer acts as an axis of symmetry for motions on the ^2H NMR time scale. ^2H labelled DPPC has a flexibility gradient along the chain[75,76] found from the variation of quadrapolar splittings with position at 323K. The order parameter (S_n) measures an inequivalence of the Sn1 and Sn2 chains. S_n depends on the average orientation and degree of motional averaging of the labelled atoms. Phospholipids are observed to conserve the configuration of the head group from the crystal structure of the dihydrate crystals in the liquid crystalline and gel states. Hydrogen bonding is observed only in the phosphate head group with waters.[77] Because of its strategic location at the membrane surface and the possibility of interactions of its permanent dipole moment with other lipid head groups, ions and water, the DPPC glycerophisphoryl-choline (GPC) head group moiety has been extensively studied by a variety of techniques.[78,79] From X-ray studies of analogous racemic DLPE[72] and DMPC dihydrate[71] it has been found that the glycerol backbone lies approximately perpendicular to the bilayer plane and parallel to the Sn1 chain. ^2H NMR of the glycerol C2 protons suggests that this configuration is conserved in the fully hydrated liquid crystal phase. ^2H NMR studies of the C3

protons suggests that the two labelled hydrogens are inequivalent, suggesting no rapid reorientation about the C2-C3 bond. The obtained spectra are axially symmetric about the bilayer normal indicating an axial rotation of the molecule about the bilayer normal axis. In addition a "Wobbling" motion of the glycerol about the bilayer normal is observed,[80] resulting in a decrease in the C3 deuterium splittings.

^{31}P NMR studies of DPPC.H_2O crystals demonstrate that the plane containing the non-esterified oxygens and the phosphorus is orientated at 50° to the bilayer normal and the O-O vector in that plane is approximately parallel to the bilayer plane.[81,82] Neutron diffraction studies[83-85] of the head group of ^{2}H labelled DPPC indicate that the deuterium nuclei at C1, C3 and C4 of the choline are all located the same distance from the centre of the bilayer, implying that the P-N vector is approximately parallel to the bilayer plane. ^{2}H labels on C3 of the glycerol and C1, C3 and C4 of PC have been used to construct a model of head group conformation.[86] This consists of two conformational states with rapid interconversion between the two enantiomeric structures found for free GPC. However in another study [87] a range of related conformations were found to fit the experimental data. High resolution ^{1}H NMR of phospholipids in vesicles and other dispersions have indicated that the head group conformations are consistent with those in bilayers. On the basis of the temperature dependence of quadrapolar splittings, there are no significant changes in torsion angles, and from neutron diffraction experiments, GPC has the same orientation in the liquid crystal phase.

The dynamics of the head group atoms has been measured from ^{2}H spin relaxation time measurements for head group and glycerol atoms. The longest relaxation time is for choline (C,C1,C2) hydrogens. Most of the quadrapolar interactions are modulated by the rapid methyl rotation and reorientation about the C3-N bond. Relaxation of C1, C3 protons should be sensitive to conformational changes in the two state model. Activation energies for N-(C,C1,C2) rotations can be measured as follows:

C,C1,C2 7.5 kcal/mol

C3 6.5 kcal/mol

C4 and C_{chain} 3.7 kcal/mol

A relaxation time $\tau_c \approx 2 \times 10^{-9}$s for P-N vector was measured.[88,89]

These values are measured from a ^{2}H NMR study of DMPC and DPPC in the $L_{\beta'}$ phase. A large fraction of the chains are found to be in a rigid state on the ^{2}H NMR time range. These show no characteristic axial symmetry. From ^{31}P NMR studies[81] PC is observed to undergo

axially symmetric reorientations. In the gel phase DPPC acyl chains are found to be 93-98% trans in conformation.[90]

Cholesterol in Model Membranes

The presence of high concentrations of cholesterol in many natural membranes and the strong influence of cholesterol on membrane properties makes investigation of its interactions a fruitful avenue of enquiry. The position of cholesterol in the phospholipid bilayer has been determined by neutron diffraction of specifically deuterated cholesterol in egg DPPC/H_2O dispersions.[91] The hydroxyl group at the head of the molecule has been found to be located at the PC/H_2O interface at the level of the phospholipid glycerol - fatty acid ester bonds. The body of the cholesterol is orientated approximately parallel to the bilayer normal and is in direct contact with the hydrocarbon chains of surrounding phospholipids. The order parameters from ^2H NMR for carbons in the acyl chains of the phospholipids is found to increase dramatically with cholesterol concentration.[92] Comparison of the quadrapolar splittings for 7:3 DMPC/cholesterol and 100% DMPC[93] confirm this result, the cholesterol doped membrane having much increased order. This effect is specific to PC head groups, PE phospholipids do not show this effect and in some cases may have reduced order on addition of cholesterol. This is probably due to the increased free volume of PC chains brought about by increased head group surface area.

The rigidity of the cholesterol sterol ring system inhibits the motion of phospholipid acyl chains, especially near the PC/H_2O interface and increased space between the lipid head groups decreases inter lipid head group interactions allowing readjustment of chain torsion angles and increased flexibility.

The motions of Cholesterol are summerised below:

1. Axial rotation.
2. "Wobble" about an axis parallel to the bilayer normal.
3. Diffusion in the bilayer plane.

The ^2H NMR order parameters for cholesterol have been determined[94,95] as S_{mol} 0.87 at 298K in egg DPPC/H_2O.

^{31}P NMR has been used to study the dynamics of phosphate head groups in biomembranes.[46] A DMPC model membrane was used and measurements taken over the temperature range 203-343K. A number of characteristic motions have been observed.

Intramolecular motions: Two hindered motions and a free rotation around bonds linking

Figure 1.4

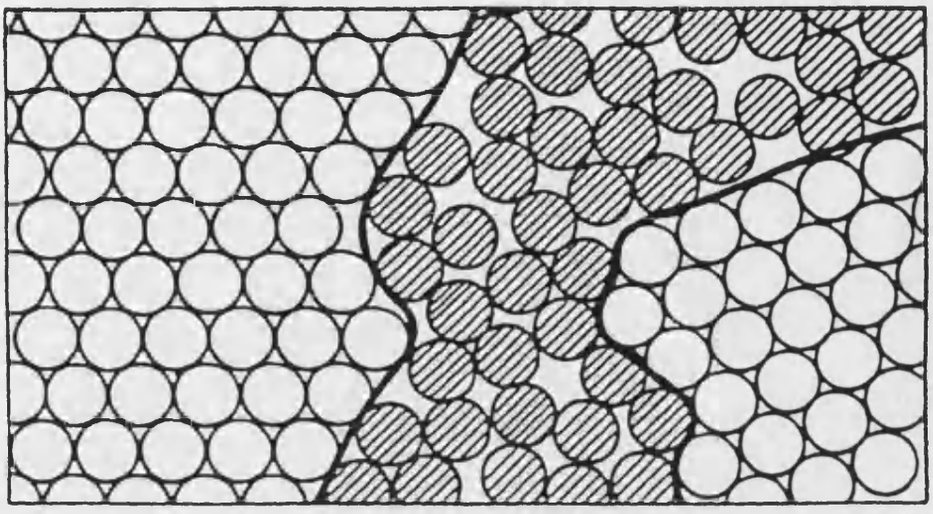

(a)

The "Fluid Mosaic"

in a mixed lipid system.

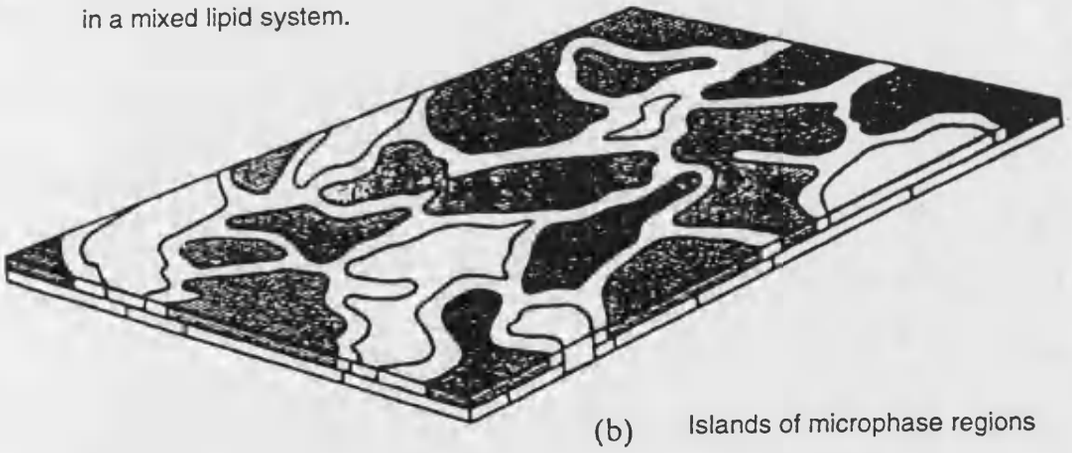

(b) Islands of microphase regions

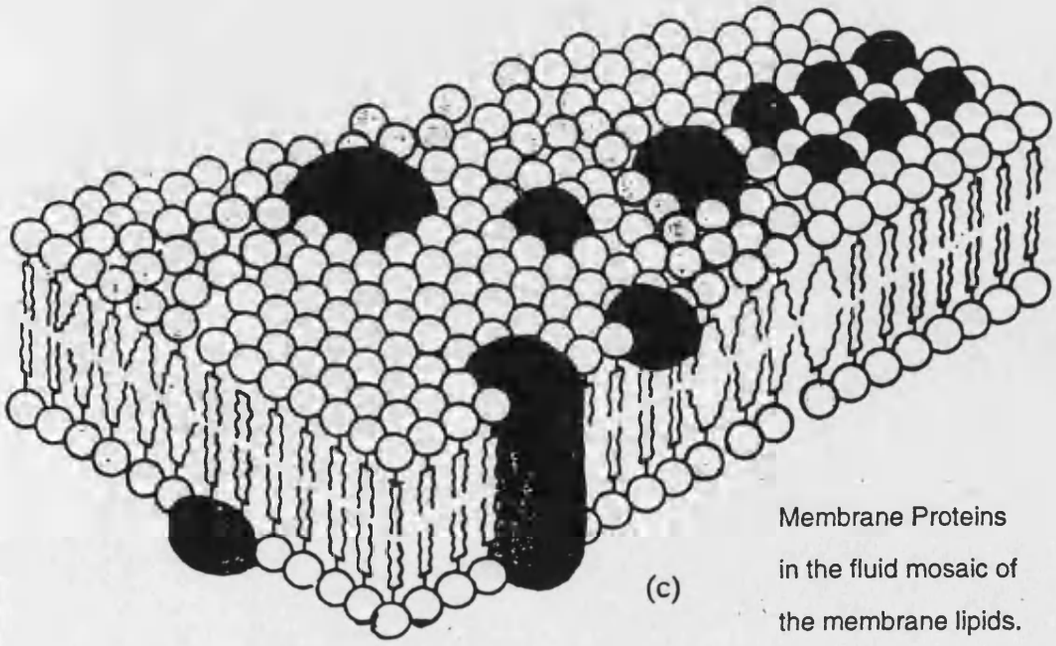

(c)

Membrane Proteins

in the fluid mosaic of

the membrane lipids.

phosphate to glycerol have been measured. $10^{-12} < \tau_c < 10^{-6}$s between 203-343K.

Intermolecular motions: A long axial rotation about the bilayer normal has been measured, in addition to small fluctuations about the other two axes, the "wobble" motion: $10^{-11} < \tau_c < 10^{-3}$s 203-343K.

Collective motions: Larger wavelength motions due to collective interactions of the DMPC molecules were observed. These involve deformations of the bilayer structure including "buckling".

Additional hydration has apparently no effect on head group conformation.[96,97] The preferred all trans conformation of the backbone glycerol moiety is conserved (subject to rotational isomerism about the C2-C3 bond). Hence geometric parameters of the head group remain constant throughout the the different phases. The angle of tilt θ_n characterises the orientation of the glycerol with respect to the bilayer normal. In the $L_{\beta'}$ phase θ_n is 30° transforming to 0° in the L_α phase.

Molecular Order

The orientational order of the whole lipid molecule is described by the order parameter $S_{zz} = \frac{1}{2} < (3\text{Cos}\theta_D{}^2 - 1) >$, where θ_D is the orientation of the molecule with respect to the bilayer normal. This can be plotted against temperature and clearly shows the phase transitions.

In the $L_{\beta'}$ phase there is high order (S_{zz} 0.97 – 0.89). On the transition from $L_{\beta'}$ to L_α the order parameter drops dramatically (S_{zz} 0.72 – 0.65). There is a much weaker coupling of order parameter and temperature in the L_α phase.

Small angle vibrations are observed in the O1-C1-C2 angle, which is reflected in the Euler angles ($\Delta\theta_3 \pm 15°$, $\Delta\theta_4 \pm 15°$). This leads to the conclusion that the glycerol backbone is the principal axis of order in glycerophospholipids. Free rotation about the P-O1 bond is observed ($4 \times 10^{-10} < \tau_c < 7 \times 10^{-10}$s). Collective lipid motion correlation times extend over 6 orders of magnitude ($10^{-9} < \tau_c < 10^{-3}$s). In biological membranes the coupling of collective lipid motions to membrane bound transporters may enhance the conformational changes required for their function.

1.8.2. DSC studies

Phase Transition Temperatures

The phase transition temperature depends on:

1. Acyl chain length. $T_c \alpha n$
2. Degree of saturation. $T_c \alpha 1/sat$
3. Location of the long chain relative to the phosphate
4. Acyl chain branching.
5. Nature of the head group T_c for PE > PS > PC >> PG
6. pH (charge build up)

The enthalpy of the liquid crystal transition can be determined using DSC.

DMPC $\Delta H_t = 5.4 kcalmol^{-1}$

DPPC $\Delta H_t = 8.7 kcalmol^{-1}$

DSPC $\Delta H_t = 10.5 kcalmol^{-1}$

DMPE $\Delta H_t = 5.8 kcalmol^{-1}$

The phase transition for mixed lipid systems and single chain lipids is broadened, the effect being entropic in nature. The gel $L_{\beta'}$ phase contains lattice defects, the number of which is proportional to temperature; areas with more defects melt first. Hence transient domains or microphases are formed. Heating the crystal leads to fluid areas within a matrix of crystal, and cooling the liquid results in crystalline "islands" in a sea of liquid. Interphasal lipids do not contribute in either co-operative motion.

These areas have relatively high free energy and it is the enthalpic and entropic terms which control the extent of these "zones". The interfacial regions represent areas through which small molecules may translate more freely. As a result artificial membranes have a high passive permeability to both charged and neutral molecules at T_c.

Heat and Enthalpy changes

Using differential scanning calorimetry it is possible to measure the relative enthalpic changes for the various phase transitions. These transitions give information about the relative proportion of molecules involved in any of the phase transitions or co-operative motions of chains. Measurements on DMPC indicate that the acyl chains start in a tightly packed crystalline arrangement (orthorhombic packing), but on heating they undergo a transition to the

Transition temperatures are systematically higher for phosphatidylethanollamines compared to phosphaditylcholines of the same acyl chain length. The transition temperature increases with increased chain length linearly. This is due to the dominance of contributions to the enthalpy and entropy of transition from chain length dependent contributions. Hence at longer chain lengths other effects are dominant.

1.8.3. Electrical Measurements

Electrostatic properties of membranes

All biomembranes carry on their surface substantial charge which varies from $1-100 mCm^{-2}$ of negative charge, spread over 10^7-10^8 anionic and 10^6-10^7 cationic groups in the average mammalian cell. This charge affects a number of membrane properties including, ion partitioning and transport.

The membrane/aqueous solution interface resembles other interfaces between electrically charged phases by the presence of an electric double layer. It is therefore possible to measure the capacitance of that membrane, a measure of its thickness. The membrane capacity consists of three components from the two phases (s1,s2), in contact with the membrane and the internal capacitance of the membrane.

$$\frac{1}{C_m} = \frac{1}{C_{s1}} + \frac{1}{C_{s2}} + \frac{1}{C_i}$$

It has been shown that the membrane surface potentials depend on the ionic composition of the two solutions either side of the membrane. The determination of the membrane interfacial tension is achieved by contact angle measurement at the boundary of the bilayer and the aqueous solution. The unit area resistivity of the simple unmodified bilayer membrane is high: $10^{15}\Omega cm^{-2}$. The capacitance of a bilayer membrane mainly arises from the low permittivity of the hydrocarbon region ($\varepsilon_r \approx 2.1$) and have typical values $< 1\ \mu Fcm^{-2}$.

Above T_c $0.83 \pm 0.02 \mu Fcm^{-2}$

Below T_c $0.74 \pm 0.04 \mu Fcm^{-2}$

The decrease in capacitance between $L_\alpha - L_{\beta'}$ is due to an increase in the thickness of the hydrocarbon region. Applying an external potential difference causes membrane thinning.

There is a large surface potential relative to surface dipoles and charge distribution in the head group region. This in turn relates to the microviscosity and specific volume of the

membrane.

1.8.4. X-Ray

Volume changes

Using X-ray data[101] combined with careful measurement of the density of hydrocarbons it is possible to calculate the mean volume per CH_2. At the transition there is a sharp increase in the volume of the CH_2. The transition from the tightly packed orthorhombic packing to looser hexagonal packing is associated with an increase of CH_2 volume of $4.4Å^3$ per CH_2 and an increase in cross-sectional area of $1.9Å^2$ per CH_2. The hexagonal lattice then melts to an isotropic liquid, and the volume per CH_2 changes to $26-29.5Å^3$, an increase of 26.6%. This corresponds to an increase in cross-sectional area from 20.4 - 23.4 $Å^2$ per chain. The measurement of volume changes in the more complex phospholipids is more difficult.[100] These have been measured as 25.7 - 26.0 $Å^3$per CH_2 below T_c, and at the liquid crystalline transition as 26.8 - 27.7 $Å^3$per CH_2.[101]

Changes in aliphatic chain behaviour conferred by polar substitution

Interaction of polar groups at the end of the acyl chain with other polar groups and solvent molecules imposes marked changes on the physical properties of the lipid. While the aliphatic chain retains many of its properties, they are modulated by the effect of the polar substituent. Such properties affected include absolute crystalline lattice arrangement, specific T_c values, associated enthalpies, liquid crystal formation, solvent interaction and solubility. Many of the factors which decrease T_c relative to the pure acyl chain, do so by disrupting chain packing; conversely those which increase T_c do so by stabilizing the packing of chains.

X-ray diffraction can measure inter head group distances accurately for crystal structures. The liquid crystalline state has the characteristics of both liquid and crystal: some degree of order and some degree of fluidity. When a given molecule is heated, instead of melting directly into an isotropic liquid it may pass through intermediate states, so called "mesophases". These are characterised by residual order in specific directions. This phenomenon is known as "thermotropic mesomorphism". Molecules with long acyl chains undergo this transition when the acyl chains melt.[23]

Lyotropic liquid crystals form in the presence of solvent. It should be noted that molecules which form liquid crystals in aqueous dispersions have a polar moiety which interacts strongly with water.

$L_{\beta'} \rightarrow P_{\beta'}$ low energy first order transition

$P_{\beta'} \rightarrow L_{\alpha}$ high energy first order transition

T_c is effected by the amount of water present and the number of carbons in the acyl chains.

X-Ray Crystallography Studies of Aliphatic lipids

A number of phospholipid crystal structures have been determined.[71,72,102-105]

From the above crystal structures there are two observed conformations of the polar head groups. Both have the P-N vector parallel to the bilayer surface. From X-ray, NMR and neutron diffraction data, it is observed that this general structural feature is conserved in both the gel and liquid crystalline phases.[82,83] Deuteration at specific locations within the lipid structure and study using neutron diffraction may elucidate characteristic internal geometries. Studies of the L_{α} and $L_{\beta'}$ phases with deuterated choline protons indicate that the head group - head group distance in $L_{\beta'}$ is 24-25 Å and 21Å in L_{α}.

Phosphatidylethanolamine

The crystal structure of DLPE[72] is taken from crystals grown from the acetic acid solution and the lipids are arranged in a bilayer formation with acetate counter ions between the bilayers. There are some features of the crystal structure which should be noted as general features of phospholipid conformation.

These include:

(a) A bend at C2 of the Sn2 chain.

(b) Acyl chains are in the antiplanar (all trans) conformation.

(c) The hydrocarbon chains are close packed.

(d) The PE head group is orientated approximately parallel to the bilayer surface, the P-N vector is at 15° to the bilayer plane.

(e) The torsion angle α_1 about the glycerol-phosphate bond is always in the antiperiplanar (trans) conformation. Other torsion angles in the head group have correlated values, but are generally syn-clinal (gauche).

(f) Torsion angles α_2 and α_3, within the phosphate group are correlated with torsion θ_1, about the C1 - C2 glycerol bond.

Crystalline State

A number of characteristic measurements can be made.

(a) Mean cross-sectional area(A_{xhc}) of the chain perpendicular to the axis of the α-chain.

(a) The angle of the chain with respect to the plane of the bilayer, θ.

(b) Thickness of the polar region, d_p.

(c) Surface area at the bilayer plane, S.

(d) Molecular volume, V_m.

(e) Volume per CH_2, V_{CH_2}.

DMPC.2H_2O monoclinic P_{2_1}			
Property	Value	Property	Value
a / Å	8.72	A_{chain} / Å^2	19.5
b / Å	8.92	V_{polar} / Å^3	404.6
c / Å	55.4	$V_{polar} - V_{Solv}$ / Å^3	344.8
β	97.4	A_{xhc} / Å^2	19.0
N_{cell}	4	V_{CH_2} / Å^3	23.9
d_p / Å	54.9	ϕ	12
d_{polar} / Å	10.4	S / Å^2	38.9

(g) The intermolecular packing in DLPE crystal is close packed in terms of the hydrocarbon chains, with average intermolecular spacing of 4.6Å. The hydrocarbon chains are arranged in a centred orthorhombic subcell, a common feature of hydrocarbon packing.[106]

(h) There is a network of hydrogen bonding between the NH_3^+ and PO_4 groups with hydrogen bond distances of 2.86 and 2.74Å in the plane of the bilayer.[107]

DMPC dihydrate

This crystal structure exhibits many of the general features of phospholipid packing from DLPE including:

(a) The crystal structure is essentially a bilayer with two molecular conformations (A and B).

(b) The two different conformations are displaced with respect to the bilayer normal, allowing the bulky head groups to pack while maintaining the close packing of the acyl chains. This may be responsible for the $P_{\beta'}$ ripple phase.

(c) The conformations A and B differ in the value of the torsion angle θ_1 about the C1 - C2 bond. This suggests that there is no preferred conformation about this bond.

(d) The two water molecules per DMPC provide a hydrogen bonding network between adjacent molecules. These provide head group stability within the bilayer plane and cohesion between adjacent bilayers.

Bilayer Dimensions

X-ray diffraction is the most accurate method of determining bilayer structure. A number of such studies have been undertaken.[108] Multibilayer dispersions of phospholipids give strong X-ray reflections in

(1) Low angle region: Inter bilayer repeat distances.

(2) High angle region: Chain packing characteristic distances.

This data can be interpreted to give chain tilt angles, interchain packing statistics, and chain cross-sectional area. The largest repeat distance gives the thickness of the bilayer and water layer. DPPG d_1 = 54.5Å in all trans conformation. The area per molecule can also be calculated from the bilayer thickness.

$$A_o = 2M\overline{v_i}/(N_A d_1)$$

where

d_1 = Thickness of bilayer

A_o = Area per molecule in the bilayer plane $\approx 4.8Å^2$

M = Molecular Mass

$\overline{v_i}$ = Specific volume of the bilayer

N_A = Avogadros Number

The chain tilt angle θ can be calculated from the chains cross sectional area A_c measured

from the high angle portion of the diffraction pattern.

$$\cos\theta = 1A_c/A_o$$

DPPG $\theta = 32°(L_{\beta'})$

Hence the change in d-spacing and A_o can be used to follow the phase transition.[108]

Bilayer thinning is observed at the transition of about 15%. This is assigned as the creation of rotational isomers in the lipid acyl chains. A kink ($^{+}gtg^{-}$) reduces the chain length by 1.25Å in DAPE, equivalent to one CH_2 group. The length reduction in DAPE is equivalent to 3-4 kinks per molecule although some length reduction is thought to be due to the formation of isolated gauche states near to the terminal segment of the chain. This decrease in length is accompanied by a lateral expansion in bilayer area ($\Delta A_o/A_o \approx 20\%$). An overall expansion in bilayer volume is observed, which has a profound effect on properties of rotational isomerism and hydration of the bilayer.

More general structural information can be found by reference to the relationship between bilayer repeat distance and chain length. This is effectively linear in the crystalline phase (1.24Å per CH_2 per molecule length increase). In the gel phase this value is slightly reduced, due to limited rotational isomerism. These incremental changes in molecules with chains up to C16 correspond to approximately the CH_2 length and therefore they are assumed to be parallel to the bilayer normal.

In the $L_{\beta'}$ gel phase considerably smaller length increments are observed, interpreted as chain tilting. The L_α phase also shows a linear relationship with smaller increments, due to rotational isomerism and other shortening effects such as gauche bond formation and hydration.

1.9. Theoretical studies of bilayers

Bilayer Models

Any model of lipid chains in the bilayer environment must take into account the intermolecular restrictions of chain packing. This includes principally hard-core repulsive (excluded volume) interactions, Lennard-Jones and attractive van der Waals interactions. Treatment of the head group and backbone regions must include, either implicitly or explicitly, terms for the contribution by hydrophobicity, electrostatics and hydration interactions. The goal of such models is the accurate representation of the dynamics of chains in the fluid state. Comparison of theoretical models for bilayers with available experimental data has been previously made.[109,110]

1.9.1. Molecular Dynamics Simulations

A wealth of data has been collected using molecular dynamic calculations on both n-alkanes and lipid acyl chains.[111-153] These studies have varied from simulations of clusters of simple hydrocarbon chains in a membrane like structure, to full atomistic simulations of phospholipid bilayers, including their water environment. Systems treated range in size from less than 10 molecules to 50-100 molecules, requiring the use of high performance computing techniques. Most studies have used either constraints or simplifications in the treatment of the potential energy of the bilayer system. These include constraining head group atoms into the plane of the bilayer, the use of constraining algorithms to keep bond lengths to their equilibrium values and reduced atom representations of the phospholipid allowing the trajectory of a larger system to be explored.

The analysis of these systems has generally concentrated on the available experimental data, calculating the segmental order parameters for the acyl chains, the density distribution within the bilayer and other conformational and configurational properties. Other studies have attempted to examine the dynamics of these molecules, calculating the frequencies of motion within the bilayer, and examining the correlation between certain characteristic motions, within the bilayer environment.

An example of such studies is a molecular dynamics simulation of 16 C10 chains performed using periodic boundary conditions to represent the extented solution.[146] One end of the chains is tethered in the Z direction using a restoring potential, which applies an energy penalty for deviation from the starting position of the terminal carbon segment in the Z

direction. The segmental order parameters for all carbon segments were calculated, and show the characteristic plateau region. The principal contribution to the S_n values comes from the collective chain tilting which fluctuates with a period of 10-20ps. These are non collective occurring by formation of disordered configurations. Rapid migration of kinks up and down the chain are found to make negligible contribution to the order parameter plateau, since their relative frequency of occurrence was not enhanced due to favourable packing, gauche conformations not migrating as intact kinks.

1.9.2. Monte-Carlo Simulations

A wealth of data has been collected using Monte-Carlo calculations on both n-alkanes and lipid chains.[115, 154-165] A simulation of 10 C10 molecules using Monte-Carlo has been performed sampling the S_n profile of the chains from the 60,000 steps of configurations. At sufficiently high packing density an order parameter plateau was observed, demonstrating that it is possible to explain its formation using hard core repulsive interactions alone.[166] This demonstrates the importance of the packing density to phase transition, kink formation being relatively unimportant to fluidity.

Other important bilayer models include more simplified techniques, such as lattice type models where possible sites for the carbon segments are represented by a lattice.[167] A chain flux is defined as a vector with direction normal to the bilayer plane and magnitude of the number of chains intersecting per unit area. For a given chain length the model is totally characterised by the surface packing density of lipid chains, taken from X-ray diffraction.

Another technique employed to model lipid chains is Mean Field Theory[168, 169] in which the dynamics of a single chain is modelled under the influence of a molecular field. This has allowed for the calculation of S_n values across the membrane with depth. Because not all carbon segments occur at the same depth, the order parameter profile of the bilayer is smoothed with respect to that of the carbon segments alone.

Order parameter values give information on the effect of chain conformation on the angular properties of lipid chains. Information can also be obtained from the spatial characteristics of chains and bilayer dimensions. From X-ray and dilatometric measurements it has been observed that the length of the chains is decreased by 6-10Å for DPPC on T_c, allowing for the chain tilting effect of the $L_{\beta'}$.[170] From this length change the change in cross sectional area of the chains can be calculated: $A = 5.9\text{Å}^2$ per molecule in L_α (L_α exp = $5.8 - 6.8\text{Å}^2$ per

molecule. More detailed information on the average location of chain segments can be obtained from neutron diffraction studies on specifically deuterated lipids. The neutron scattering results can be analysed to give the mean positions of the methylene segments projected onto the bilayer normal.[83] Theoretical models can then be used to elucidate the spatial distribution (extent of motion) of CH_2 segments projected onto the bilayer normal. Comparison of distribution functions for DPPC projected onto the bilayer normal at less than the maximum hydration are within experimental limits.[110] These also allow for comparison with the percentage conformations, to interpret the neutron diffraction results for relative conformational populations. It has been found that 38% of palmitic chains extend beyond the midpoint and that 0.6% are in the all trans conformation. One can plot the positional fluctuations for the carbon segments along the chain. These increase linearly with segment number, with no plateau effect. They are effected by connected segments, but unlike orientational ordering the effect is accumulative. For the first 8 segments the positional disorder (probability of an occurrence of an all-trans segment) decays exponentially. Beyond the plateau region it then decays more rapidly, mirroring the increase in orientational disorder. One can define probability contours from theoretical models, showing the variation in position of chain segments. These isoprobability maps are symmetric about the plane defined by the C-C bonds in the all trans configuration. This is due to the equivalence of the $g^{\pm}$ states. Calculations throughout the chain fragments indicate that the positional fluctuations increase more rapidly that lateral fluctuations. Summation over all chain elements gives the density distribution throughout the whole width of the hydrophobic region of the bilayer, indicating homogeneous volume occupancy by all chains.

It is also possible to calculate electron density profiles throughout the bilayer and compare them with experimental profiles for DPPC obtained from x-ray diffraction. In order to make this comparison it has been assumed that water penetrates to within 1.1Å of the carbonyl group, an assumption backed by experimental data. These models compare well with experiment providing a description of the degree of delocalisation of the terminal methyls. The thickness of the hydrocarbon region was predicted as 27.3Å, for DPPC at 314K, the molecular area being $63Å^2$.[169] The probability of finding a specific conformation at specified segments of the carbon chain has also been calculated, using molecular field theory.[168] There is interest in not only the conformational state at the segment, but also its relationship to the chain segment vector, relative to the bilayer normal. Whilst the chain segment may be trans or gauche the

orientation of the chain segment vector may be 0°, 60°, 90°, 120°, or 180°. The probabilities of finding all of these conformations have been calculated. The main disordered configurations are (t, 60°) and (g, 60°), the latter being half as probable as the former. Certain configurations are found to reflect the S_n values more than others. Configurations with the chain vector at angles greater than 90° although low in probability are not negligible. These give rise to hair-pin loops in chains and are found to increase in probability towards the end of the chains. The kink configuration (g^+, 60°), (t, 60°), and (g^-, 60°), although sterically favoured, is not preferentially enhanced with respect to the gauche and trans states. This is in agreement with other models.[146] There is a predicted 0.5 kinks, 4 gauche, and 10 trans conformations per chain. This agrees with Raman spectroscopic results.[171] The two main disordered configurations (t, 60°) and (g, 60°) are strongly correlated in terms of their relationship to segment number. Due to steric packing considerations it is expected that a (t, 60°) can only be followed by another (t, 60°) or (g, 60°). The greater population of (t, 60°) may then explain the fact that (g, 60°) are often found to be followed by several (t, 60°). It has been suggested that that is responsible for chain packing rather than kink formation. On increasing the temperature the relative number of (g, 60°) and (t, 60°) increases. These are the important configurations of disorder and hence disorder increases with temperature. The number of kinks remains fairly constant, (t, 60°) and (g, 60°) remain the dominant configurations in the fluid phase.

The greater disorder beyond the order parameter plateau is caused principally from an increase in 90° and 120° conformations. These are allowed because of an increase in free volume. The order parameter profile does not accurately describe the bilayer packing, since single angular fluctuations may correspond to a number of spatial fluctuations. One possible indicator is the probability of the all trans configuration. This decreases exponentially in the plateau region and more rapidly beyond.

References

1. Capaldi RA, in *Membrane Proteins and their interaction with lipids*, Membrane Proteins, vol. 5, 1977.
2. Arnost, Kotyk, Karel, Janacek, Jiri, and Koryta, in *Biophysical chemistry of membrane functions*, Chichester Wiley, 1988.
3. Stryer L, *Biochemistry 3rd Ed*, vol. New York, W.H.Freeman & Co.
4. *Biochem Biophysica Acta*, vol. 298, p. 750, 1973.
5. Quinn PJ, Koynova RD, Lis LJ, Tenchov BG, and Kohlwein SD, *J Chem Edu*, vol. 69, no. 1, pp. 3-9, 1992.
6. Vogel H, Nilsson L, Rigler R, Vogues K, and Jung G, *Proc Natl Acad Sci USA*, vol. 85, pp. 5067-5071, 1988.
7. Zubay G, in *Biochemistry*, MacMillan Pubisher, 1983.
8. Small DM, in *The Physical Chemistry of Lipids*, vol. 4, Plenum Press, 1986.
9. Kint JA and Leroy JG, *Nature*, vol. 319, p. 17, 1986.
10. Gorter E and Grendel F, *J Exp Med*, vol. 41, pp. 439-444, 1925.
11. Ahluwalia A, Rossi DED, Monici M, and Schirone A, *Biosens Bioelec*, vol. 6, pp. 133-141, 1992.
12. Jendrasiak GL, Madison GE, and Smith R, *Biosens Bioelec*, vol. 7, pp. 291-300, 1992.
13. Stenger DA, Cribbs DH, and Flare TL, *Biosens Bioelec*, vol. 6, pp. 425-430, 1991.
14. Zviman M and Tien HT, *Biosens Bioelec*, vol. 6, pp. 37-42, 1991.
15. Stenger DA, Cribbs DH, Flare TL, and Rusin KM, *Biosens Bioelec*, vol. 7, pp. 11-20, 1992.
16. Bryce M and Findlay J, *Chem Britain*, p. 707, 1991 Aug.
17. Tien TB, *Adv Material*, vol. 2, no. 6/7, p. 316, 1990.
18. Miller JS, *Adv Mater 2*, no. 8, p. 378, 1990.
19. Miller JS, *Adv Mater 2*, no. 10, p. 495, 1990.
20. Miller JS, *Adv Mater 2*, no. 10, p. 499, 1990.
21. Miller JS, *Adv Mater 2*, no. 11, p. 601, 1990.

22. Lear JD, Wassermann ZR, and Degrado WF, *Science*, vol. 240, p. 1177, 1988.

23. Lenaz G, Curatola G, and Masotti L, *J Bioenergetics*, vol. 7, p. 233, 1975.

24. Janiak MJ, Small DM, and Shipley G, *J Biol Chem*, vol. 247, pp. 6068-6078, 1979.

25. Marsh D, in *Handbook of Lipid Bilayers Crc Press*, 1991.

26. Tardieu A, Luzzati V, and Reman FC, *J Mol Biol*, vol. 75, pp. 711-733, 1973.

27. Hauser H et al, *J Col Sur Sci*, vol. 117, pp. 497-504, 1987.

28. Kalkura, Sachidhar, and Venkatesh, *Mol Cryst Liq Cryst*, vol. 84, p. 275, 1982.

29. Trauble H and Haynes DH, *Chem Phys Lipids*, vol. 7, pp. 324-335, 1971.

30. Cevc G and Marsh D, in *Phospholipid Bilayers*, Wiley-interscience, 1987.

31. Singer J and Nicholson G, *Science*, vol. 175, pp. 710-731, 1972.

32. Esfahani EM et al, *Proc Natl Acad Sci USA*, vol. 64, p. 1057, 1969.

33. Seelig J and Seelig A, *Quart Rev Biophys*, vol. 13, pp. 19-61, 1980.

34. Seelig A and Seelig J, *Biochemistry*, vol. 13, pp. 159-175, 1974.

35. Davis JH, *Biophysical J*, vol. 27, pp. 339-358, 1979.

36. Fenske DB and Cullis PR, *Biophysical J*, vol. 64, no. 5, pp. 1482-1491, 1993.

37. Morrow MR, Singh D, Lu D, and Grant CWM, *Biophysical J*, vol. 64, no. 3, pp. 654-664, 1993.

38. Morrow MR, Whitehead JP, and Lu D, *Biophysical J*, vol. 63, no. 1, pp. 18-27, 1992.

39. Boden N, Jones SA, and Sixl F, *Biochemistry*, vol. 30, no. 8, pp. 2146-2155, 1991.

40. Seelig J, *Quart Rev Biophys*, vol. 10, pp. 353-418, 1977.

41. Lee AG, *Prog Biophys Mol Biol*, vol. 29, p. 3, 1975.

42. Horwitz AF, *Proc Natl Acad Sci USA*, vol. 69, p. 590, 1972.

43. Levine YK et al, *J Chem Phys*, vol. 60, p. 2890, 1974.

44. Levine YK, Partington P, Roberts GCK, Birdsall NJM, Lee AG, and Metcalf JC, *Febs Lett*, vol. 23, p. 203, 1972.

45. Pfeiffer W, Henkel T, Sackmann E, Knoll W, and Richter D, *Europhys Lett*, vol. 8, pp. 201-206, 1989.

46. Dufourc EJ, Mayer C, Stohrer J, Althoff G, and Kothe G, *Biophysical J*, vol. 61, no. 1, pp. 42-57, 1992.

47. Baenziger JE, Jarrell HC, Hill RJ, and Smith ICP, *Biochemistry*, vol. 30, pp. 894-903, 1991.

48. Marsh D, *J Membrane Biol*, vol. 18, pp. 145-162, 1974.

49. Yakovleva NB and Pasechnik VI, *Biophysical J*, vol. 28, no. 6, pp. 1092-1097, 1983.

50. Haung CH, *Proc Natl Acad Sci USA*, 1974.

51. *Biochimica et Biophysica Acta*, vol. 330, p. 269, 1973.

52. *Biochimica et Biophysica Acta*, vol. 150, p. 333, 1968.

53. Marsh D, *Chem Phys Lipids*, vol. 10, p. 11, 1973.

54. Rothman JE, *Nature New Biology*, vol. 237, p. 42, 1972.

55. McIntosh TJ, McDaniel RV, and Simon SA, *Biochimica et Biophysica Acta*, vol. 731, pp. 97-108, 1983.

56. Cornell BA, Middlehurst J, and Separovic F, *Biochimica et Biophysica Acta*, vol. 598, pp. 405-410, 1980.

57. Lawrence B, Lawrence ML, and Barlow DJ, *Biochem Soc Trans*, vol. 18, pp. 942-943, 1990.

58. Frinkelstein A and Cass A, *J Gen Physiol*, vol. 52, p. 145, 1968.

59. Bittman R, Fugler F, Clejan S, Lister MD, and Hancock AJ, *Biochimica et Biophysica Acta*, vol. 1106, pp. 40-44, 1992.

60. De La Maza A, Parra JL, Garcia MT, Ribosa I, and Sanchez Leal J, *J Colloid and Interface Science*, vol. 148, no. 2, p. 310, 1992.

61. Nagle JF, Wiener MC, and Suter RM, *Biophysical J*, vol. 55, pp. 315-325, 1989.

62. Schinder H and Seelig J, *Chem Phys*, vol. 61, p. 2946, 1974.

63. Israelachivili J et al, *Biochimica et Biophysica Acta*, vol. 382, p. 125, 1975.

64. Knowles PF and Marsh D, *Biochem J*, vol. 274, pp. 625-641, 1991.

65. Okamura E, Umemura J, and Takenaka T, *Biochimica et Biophysica Acta*, vol. 1025, pp. 94-98, 1990.

66. O'leary TJ and Levin IW, *Biochimica et Biophysica Acta*, vol. 776, pp. 185-189, 1984.

67. Szasz GJ, Sheppard N, and Rank DH, *J Chem Phys*, vol. 16, no. 7, pp. 704-711, 1948.

68. Gally HU, Buldt G, and Seelig J, *J Mol Biol*, vol. 134, pp. 673-691, 1979.

69. Tabony J and Perly B, *Biochimica et Biophysica Acta*, vol. 1063, pp. 67-72, 1990.

70. Bayerl TM, Thomas RK, Penfold J, Rennie A, and Sackmann E, *Biophysical J*, vol. 57, no. 5, pp. 1095-1098, 1990.

71. Pearson RH and Pascher I, *Nature*, vol. 281, pp. 499-501, 1974.

72. Hitchcock P, Mason R, Thomas DB, and Shipley GG, *Proc Natl Acad Sci USA*, vol. 71, pp. 3036-3040, 1974.

73. *NATO International Conference: Supramolecular Chemistry*, Strasbourg, France, 1993.

74. Ulmius J, Wennerstrom H, Lindblom G, and Arvidson G, *Biochemistry*, vol. 16, pp. 5742-5745, 1977.

75. Seelig A and Seelig J, *Biochemistry*, vol. 13, no. 23, pp. 4839-4845, 1974.

76. Seelig A and Seelig J, *Biochimica et Biophysica Acta*, vol. 406, pp. 1-5, 1975.

77. Kimmich R and Voigt G, *Z Naturforsch*, vol. 33a, pp. 1294-1306, 1978.

78. Buldt G and Wohlgemuth R, *J Membrane Biol*, vol. 58, pp. 81-100, 1981.

79. Sudaralingham M, *Ann NY Acad Sci*, vol. 195, pp. 324-355, 1972.

80. Gally HV, Niederberger W, and Seelig J, *Biochemistry*, vol. 16, pp. 3647-3652, 1975.

81. Griffin RG, Powers L, and Pershan PS, *Biochemistry*, vol. 17, pp. 2718-2722, 1978.

82. Seelig J, *Biochimica et Biophysica Acta*, vol. 505, pp. 105-140, 1978.

83. Buldt G, Gally HU, Seelig A, Seelig J, and Zaccai G, *Nature*, vol. 271, pp. 182-184, 1978.

84. Buldt G, Gally HU, Seelig A, Seelig J, and Zaccai G, *J Mol Biol*, vol. 139, pp. 673-692, 1979.

85. Zaccai G, Buldt G, Seelig A, and Seelig J, *J Mol Biol*, vol. 134, pp. 693-706, 1979.

86. Seelig J, Gally HU, and Wohlgemuth R, *Biochimica et Biophysica Acta*, vol. 467, pp. 109-119, 1977.

87. Skarjune R and Oldfield E, *Biochemistry*, vol. 18, pp. 5903-5909, 1979.

88. Shepherd JCW and Buldt G, *Biochimica et Biophysica Acta*, vol. 514, pp. 83-94, 1978.

89. Shepherd JCW and Buldt G, *Biochimica et Biophysica Acta*, vol. 558, pp. 41-47, 1979.

90. Rice DM, Blume A, Herzfield U, Wittebort RJ, Haung TM, Das Gupta SK, and Griffin RG, in *Biomolecular Stereodynamics*, vol. 2, pp. 255-270, Adenine Press NY, 1981.

91. Worcester DL and Franks NP, *J Mol Biol*, vol. 100, pp. 359-378, 1976.

92. Stockton GW and Smith ICP, *Chemistry and Physics of Lipids*, vol. 17, pp. 251-263, 1976.

93. Oldfield E, Meadows M, Rice D, and Jacobs R, *Biochemistry*, vol. 17, pp. 2727-2739, 1978.

94. Taylor MG, Akiyama T, and Smith ICP, *Chemistry and Physics of Lipids*, vol. 29, no. 4, pp. 327-339, 1981.

95. Taylor MG, Akiyama T, Saito H, and Smith ICP, *Chemistry and Physics of Lipids*, vol. 31, no. 4, pp. 359-379, 1982.

96. Hauser H, Pascher I, Pearson RH, and Sundell S, *Biochemistry*, vol. 27, pp. 9166-9174, 1981.

97. Hauser H, Pascher I, Pearson RH, and Sundell S, *Biochimica et Biophysica Acta*, vol. 650, pp. 21-51, 1981.

98. Ladbrooke and Chapman D, *Chem Phys Lipids*, vol. 3, p. 304, 1969.

99. Hinz and Sturtevant, *J Biol Chem*, vol. 247, p. 6071, 1972.

100. Nagle JF and Wilkinson DA, *Biophysical J*, vol. 23, p. 159, 1978.

101. Schaerer AA, Busso, Smith AE, and Skinner LB, *J Am Chem Soc*, vol. 77, p. 2017, 1955.

102. Hitchcock P, Mason R, Thomas DB, and Shipley GG, *J Chem Soc Chem Comm*, 1974.

103. Hauser H, Pascher I, Pearson RH, and Sundell S, *J Mol Biol*, vol. 153, p. 807, 1981.

104. Hauser H, Pascher I, Pearson RH, and Sundell S, *J Mol Biol*, vol. 153, p. 791, 1981.

105. Hauser H et al, *J Mol Biol*, vol. 137, p. 249, 1980.

106. Segerman E, *Acta Crysta*, vol. 19, p. 789, 1965.

107. Elder M, Hitchcock P, Mason R, and Shipley GG, *Proc Roy Soc London A*, vol. 354, pp. 157-170, 1977.

108. Seddon JM, Cevc G, Kaye RD, and Marsh D, *Biochemistry*, vol. 23, no. 12, pp. 2634-2644, 1984.

109. Meraldi JP and Schlitter J, *Biochimica et Biophysica Acta*, vol. 645, pp. 183-192, 1981.

110. Meraldi JP and Schlitter J, *Biochimica et Biophysica Acta*, vol. 645, pp. 193-210, 1981.

111. Fukada T, Okazaki S, and Okada I, *Biophysical J*, vol. 64, no. 4, pp. 1344-1353, 1993.

112. Ohishi H, Fujii L, Tomoo K, Ishida T, Ikeda K, Tanabe K, and Kitamura K, *J of Biochemistry*, vol. 114, no. 2, pp. 210-214, 1993.

113. Lesage L, Genot C, Record E, Pouliquen C, and Richardmolard D, *J of General Microbiology*, vol. 139, no. 7, pp. 1653-1661, 1993.

114. Clarke JHR, *Chemistry in Britain*, p. 349, 1990.

115. Hardy BJ and Pastor RW, *J Comp Chem*, vol. 15, no. 2, pp. 208-226, 1994.

116. Alam TM, *Biophysical J*, vol. 64, no. 6, pp. 1681-1690, 1993.

117. Pastor RW, Venable RM, and Karplus M, *Proc Natl Acad Sci USA*, vol. 88, no. 3, pp. 892-896, 1991.

118. Rykaert J and Bellemans A, *Chem Phys Lett*, vol. 30, pp. 123-125, 1975.

119. Rykaert J and Bellemans A, *Chem Phys Lett*, vol. 30, pp. 94-106, 1978.

120. Chiu SW, Novotny JA, and Jakobsson E, *Biophysical J*, vol. 64, no. 1, pp. 98-109, 1989.

121. Ram P, Kim E, Thomson DS, Howard KP, and Prestegard JH, *Biophysical J*, vol. 63, no. 6, pp. 1530-1535, 1992.

122. Xiang TX and Anderson BD, *Biophysical J*, vol. 66, no. 3, pp. 561-572, 1994.

123. Xiang, TX, *Biophysical J*, vol. 65, no. 3, pp. 1108-1120, 1993.

124. Edholm O and Johansson J, *European Biophysics J*, vol. 14, no. 4, pp. 203-209, 1987.

125. Edholm O and Nyberg AM, *Biophysical J*, vol. 63, no. 4, pp. 1081-1089, 1992.

126. Edholm O and Jahnig F, *Biophysical J*, vol. 30, pp. 279-292, 1988.

127. Karaborni S, *Langmuir*, vol. 9, no. 5, pp. 1334-1343, 1993.

128. Damodaran KV, Merz KM Jr, and Gaber BP, *Biochemistry (usa)*, vol. 31, no. 33, pp. 7656-7664, 1992.

129. Damodaran KV and Merz KM, *Biophysical J*, vol. 66, no. 4, pp. 1076-1087, 1994.

130. Damodaran KV and Merz KM, *Langmuir*, vol. 9, no. 5, pp. 1179-1183, 1993.

131. Stouch TR, *Molecular Simulation*, vol. 10, no. 2-6, pp. 335-362, 1993.

132. Miklavic SJ and Granfeldt MK, *J Phys Chem*, vol. 95, pp. 6351-6360, 1991.

133. Bassolinoklimas D, Alper HE, and Stouch TR, *Biochemistry*, vol. 32, no. 47, pp. 12624-12637, 1993.

134. Israelachvili JN and Wennerstrom H, *J Phys Chem*, vol. 96, pp. 520-531, 1992.

135. Benjamin I, *J Phys Chem*, vol. 95, no. 17, pp. 6675-6683, 1991.

136. Raghavan K, Reddy M, and Berkowitz M, *Langmuir*, vol. 8, pp. 233-240, 1992.

137. Smit B, Hilbers PAJ, K Esselink, Rupert LAM, van Os NM, and Schlijper AG, *Nature*, vol. 348, pp. 624-625, 1990.

138. Marrink SJ, Berkowitz M, and Berendsen HJC, *Langmuir*, vol. 9, no. 11, pp. 3122-3131, 1993.

139. Watanabe K and Klein ML, *J Phys Chem*, vol. 93, pp. 6897-6901, 1989.

140. Watanabe ML and Klein ML, *J Phys Chem*, vol. 95, pp. 4158-4166, 1991.

141. Bocker J, Schlenkrich M, Nicklas N, Brickmann J, and Bopp P, *J Chim Phys*, vol. 88, pp. 2535-2541, 1991.

142. Khalatur PG, Pavlov AS, and Balabaev NK, *Makromolekulare Chemie-macromolecular Chemistry and Physics*, vol. 188, no. 12, pp. 3029-3040, 1987.

143. Berendsen HJC and Marrink SJ, *Pure and Applied Chemistry*, vol. 65, no. 12, pp. 2513-2520, 1993.

144. Egberts E, Marrink SJ, and Berendsen HJC, *European Biophysics J*, vol. 22, no. 6, pp. 423-436, 1994.

145. Egberts E and Berendsen HJC, *J Chem Phys*, vol. 89, no. 6, pp. 3718-3732, 1988.

146. van der Ploeg P and Berendsen HJC, *J Chem Phys*, vol. 76, no. 6, pp. 3271-3276, 1982.

147. Rich MR, *Biochimica et Biophysica Acta*, vol. 1178, no. 1, pp. 87-96, 1993.

148. Zhou F and Schulten K, *Biophysical J*, vol. 66, no. 2, p. 399, 1994.

149. Heller H, Schaefer M, and Schulten K, *J Physical Chemistry*, vol. 97, no. 31, pp. 8343-8360, 1993.

150. Essex JW, Hann MM, and Richards WG, *Philosophical Transactions of The Royal Society of London Series B-biological Sciences*, vol. 344, no. 1309, pp. 239-260, 1994.

151. Robinson AJ, Richards WG, Thomas PJ, and Hann MM, *Biophysical J*, vol. 67, pp. 2345-2354, 1994.

152. Robinson AJ, Richards WG, Thomas PJ, and Hann MM, *Biophysical J*, vol. 68, pp. 164-170, 1995.

153. Schulten K and Zhou F, *J Phys Chem*, vol. 99, pp. 2194-2207, 1995.

154. Scott HL, *Biochimica et Biophysica Acta*, vol. 469, pp. 264-271, 1977.

155. Scott HL, *Biochimica et Biophysica Acta*, vol. 14, pp. 2283-2287, 1977.

156. Scott HL and Cheng WL, *J Colloid and Interface Science*, vol. 62, pp. 125-130, 1977.

157. Scott HL and Cherng S, *Biochimica et Biophysica Acta*, vol. 510, pp. 209-215, 1978.

158. Scott HL and Cheng WL, *Biophysical J*, vol. 28, pp. 117-132, 1979.

159. Scott HL, *Biochemistry*, vol. 25, no. 20, pp. 6122-6126, 1986.

160. Scott HL and Kalaskar S, *Biochemistry*, vol. 28, pp. 3687-3691, 1989.

161. Scott HL, *Biophysical J*, vol. 59, no. 2, pp. 445-455, 1991.

162. Sperotto MM and Mouritsen OG, *Biophysical J*, vol. 59, pp. 261-270, 1991.

163. Milik M, Skolnick J, and Kolinski A, *J Phys Chem*, vol. 96, pp. 4015-4022, 1992.

164. Siepmann JI and McDonald, *Langmuir*, vol. 9, pp. 2351-2355, 1993.

165. Zhao S and Reichert WM, *Biophysical J*, vol. 66, pp. 305-309, 1994.

166. Mouritsen OG, Boothroyd A, Harris R, Jan N, Lookman T, McDonald L, Pink DA, and Zuckermann MJ, *J Chem Phys*, vol. 79, no. 4, pp. 2027-2041, 1983.

167. Dill KA and Flory PJ, *Proc Natl Acad Sci USA*, vol. 77, pp. 3115-3119, 1980.

168. Marcelja S, *Biochimica et Biophysica Acta*, vol. 367, pp. 165-176, 1974.

169. Gruen DWR, *Biochimica et Biophysica Acta*, vol. 595, pp. 161-183, 1980.

170. Janiak MJ, Small DM, and Shipley G, *Biochemistry*, vol. 15, pp. 4575-4580, 1976.

171. Yellin N and Levin IR, *Biochemistry*, vol. 16, pp. 233-250, 1977.

2. Methods

2.1. Potential Energy Force Field

The potential energy of the molecular system, V, is represented by an analytical function of the internal coordinates. Simulations were performed using the Valence Force Field,[1] an empirical potential energy function. The Valence Force Field includes terms for bond stretching, angle bending and torsional variation.

$$V = E_{bond} + E_{angle} + E_{torsion} + E_{oop} + E_{cross} + E_{vdW} + E_{electrostatic} \quad (2.1)$$

The bond strain energy is represented by an exponential 'Morse' function.

$$E_{bond} = \sum_b \left(K_b[1 - \exp(-\alpha(b - b_0))]^2 - K_b \right)$$

b and b_0 are the observed and equilibrium bond lengths respectively. The parameters K_b and α represent the 'stiffness' of the bond, hence K_b is referred to as the bond stretching force constant.

$$E_{bond} = \tfrac{1}{2} \sum_b K_b'(b - b_0)^2$$

This is the harmonic representation of the bond strain. This was used for distorted structures which are minimized back to their equilibrium positions, using a harmonic potential for the equilibrium bond position.

The angle strain is represented by a harmonic function.

$$E_{angle} = \tfrac{1}{2} \sum_\theta K_\theta(\theta - \theta_0)^2$$

K_θ is the force constant for angle bending. θ and θ_0 are the observed and equilibrium angles.

The torsional energy is represented by parameters producing the required number of minima for the three states of hybridisation.

$$E_{torsion} = \tfrac{1}{2} \sum_\phi K_\phi[1 + T\cos(n\phi)]$$

K_ϕ is the force constant for torsional deformations and T takes values 1,0,-1 depending on the hybridisation of the atoms. ϕ is the observed torsion angle.

Sp^2 hybridised atoms require an out-of-plane term.

$$E_{oop} = \tfrac{1}{2}\sum_{\chi} K_{\chi}\chi^2$$

K_{oop} is the force constant for out of plane deformations by the angle χ.

Other terms describe the coupling between these terms (the energy required to deform one internal coordinate depends on the current value of another internal coordinate).

$$E_{cross} = E_{bb'} + E_{\theta\theta'} + E_{b\theta} + E_{\phi\theta\theta'} + E_{\chi\chi'} \quad \cdots \text{ Cross Terms} \tag{2.2}$$

$$E_{bb'} = \sum_{b}\sum_{b'} F_{bb'}(b - b_0)(b' - b_0')$$

$$E_{\theta\theta'} = \sum_{\theta}\sum_{\theta'} F_{\theta\theta'}(\theta - \theta_0)(\theta' - \theta_0')$$

$$E_{b\theta} = \sum_{b}\sum_{\theta} F_{b\theta}(b - b_0)(\theta - \theta_0)$$

$$E_{\phi\theta\theta'} = \sum_{\phi} F_{\phi\theta\theta'}\cos\phi(\theta - \theta_0)(\theta' - \theta_0')$$

$$E_{\chi\chi'} = \sum_{\chi}\sum_{\chi'} F_{\chi\chi'}\chi\chi'$$

The non-bonded interactions are described by a Lennard-Jones 6-12 term.

$$E_{vdW} = \sum_{nb} \varepsilon[(r^*/r_{ij})^{12} - 2(r^*/r_{ij})^6]$$

r^* is the equilibrium bond distance for atoms i and j, ε the minimum energy value at r^*.

The electrostatic interactions are represented using a Coulombic term based on point charges.

$$E_{electrostatic} = \sum_{nb}(q_i q_j)/\varepsilon r_{ij}$$

q_i and q_j are the partial charges of the two nonbonded atoms in the nonbonded pair. ε the dielectric takes the value 1.0, r_{ij} is the distance between the two nonbonded atoms. Values for q_n the atomic partial charges have been derived from *ab initio* quantum mechanics calculations.[2-5]

The importance of the quality of the form and parameterisation of the force field has been shown in several studies.[6-11] The potential energy function and parameters for lecithin molecules have been derived from molecular dynamics and molecular mechanics simulations of dilaurylglycerol and glycerolphosphatidylcholine,[4] developed using the same implementation of the force field[12] and compatible with parameters from our standard library. Atomic

partial charges were also taken from this study, derived from a linear least squares fit to the value of the electrostatic potentials of the molecules in the unit cell and those molecules surrounding it. This used a single point *ab-initio* calculation[2] with STO-3G basis set. Charges were scaled according to the observed and calculated dipole moments. A final set of charges was obtained using a calculation on the entire zwitterionic molecule with STO-3G basis set.

The first and second derivatives of the potential energy function with respect to the Cartesian coordinates can be obtained analytically.[13]

The first derivatives are given by:

$$\frac{\partial V}{\partial x_i} = \sum_a \frac{\partial V}{\partial l_a} \frac{\partial l_a}{\partial x_i} \tag{2.3}$$

The second derivatives are given by:

$$\frac{\partial^2 V}{\partial x_i x_j} = \sum_a \sum_b \frac{\partial^2 V}{\partial l_a \partial l_b} \frac{\partial l_b}{\partial x_j} \frac{\partial l_a}{\partial x_i} + \sum_a \frac{\partial V}{\partial l_a} \frac{\partial^2 l_a}{\partial x_i \partial x_j} \tag{2.4}$$

l_a and l_b are the internal coordinates (bonds, angles etc.)

The derivatives of the energy with respect to the internals can be derived directly from equation 2.1. The derivatives of the internals with respect to the Cartesian can be derived from the equations defining the internals in terms of the Cartesian coordinates, obtained from geometric considerations.

2.2. Energy Minimisation

The energy of the system is minimized by solving the equation:

$$\delta V/\delta x_i = 0 \qquad i = 1, 2, 3, \cdots, 3n \tag{2.5}$$

x_i are the Cartesian coordinates of the system and n is the number of atoms.

Energy minimisations were carried out using the *steepest descents* minimisation algorithm. This makes use of the slope of the energy surface, as given by the first derivatives to determine the search direction.

$$x_n = x_{n-1} + \lambda_n s_n \qquad s_n = -g_n/|g_n| \tag{2.6}$$

x_n is the coordinate vector at iteration n, λ_n is the step size,

s_n is the direction of the step as determined by the energy gradient vector, g_n.

If the energy is increased the step size is reduced and the previous step repeated; if the

energy decreases the step size is increased, with the updated search direction. This is repeated until such a time as the structure is relaxed (Eq. 2.5) or the number of required iterations has been performed. Its convergence near to the minimum is very slow, but for relaxation of strained structures it is very efficient as it requires less evaluations of the energy derivative than other minimisation algorithms. For the purposes of this study in which minimisation is used as a method of removing strain and close contacts from initial coordinate systems, steepest descents provides the most efficient algorithm.

For some systems the absolute lowest derivative was required, and once the system had been relaxed to a low derivative using steepest decents, the *Conjugate Gradients* algorithm was used to further reduce the derivative. Whereas steepest decents chooses the step direction from the current gradient only, the conjugate gradient makes use of information from gradients at previous minimisation steps to determine the an optimum step size and direction.

$$s_n = -g_n + b_n s_{n-1} \qquad b_n = |g_{n-1}|^2 \tag{2.7}$$

g_n and s_n are the gradient and step size at iteration n, and b_n is a weighting factor determined by the ratio of the magnitudes of the current and previous gradients. The first step is taken in the direction of the first gradient. To avoid accumulated errors in s_n, b_n is occasionally reset to zero.

2.3. Molecular Dynamics

The motion of a molecular system is described in classical mechanics by the Lagrange equations of motion:[13]

$$\frac{d}{dt}\frac{\partial K}{\partial \dot{q}_i} + \frac{\partial V}{\partial q_i} = 0 \qquad i = 1, 2, 3, \cdots, 3n \tag{2.8}$$

where K and V are the kinetic and potential energy of the system, and $\dot{q}_i$ and q_i are the velocities and coordinates.

In a system of Cartesian coordinates, x_i, (and corresponding velocities and accelerations, $\dot{x}_i$ and $\ddot{x}_i$, respectively) the kinetic energy is given by :

$$K = \tfrac{1}{2} \sum_{i=1}^{3n} m_i \dot{x}_i^2 \tag{2.9}$$

and the forces are defined by:

$$F_i = -\frac{\partial V}{\partial x_i} \tag{2.10}$$

Using (Eq. 2.10) and (Eq. 2.9) in the Lagrange equation, (Eq. 2.8), we obtain the familiar form of Newton's equations of motion:

$$F_i = m_i\ddot{x}_i \qquad i = 1, 2, 3, \ldots, 3n \tag{2.11}$$

Molecular dynamics can be used to solve this equation of motion. The force on atom *i* can be computed directly from the derivative of the potential energy, V, with respect to the coordinates, x_i.

$$-\frac{\delta V}{\delta x_i} = m_i \frac{\delta^2 x_i}{\delta t^2} \tag{2.12}$$

Hence the accelerations can be obtained from these forces (Eq. 2.11).

The motion of an atom can be expressed in terms of a standard Taylor series. From the coordinates at time t, x(t), the coordinates at a short time later $x(t + \Delta t)$, can be calculated.

$$x(t+\Delta t) = x(t) + \frac{\delta x}{\delta t}\Delta t + \frac{\delta^2 x}{\delta t^2} \tfrac{1}{2}\Delta t^2 + \cdots \tag{2.13}$$

This can be repeated to produce an atomic trajectory for the system.

This requires x(t), $\delta x/\delta t$, and $\delta^2 x/\delta t^2$. Initial velocities are assigned on the basis of a Maxwell-Boltzmann distribution (Eq. 2.27) corresponding to the required temperature. Accelerations are calculated from (Eq. 2.11). Higher terms must also be approximated.

In practice a number of algorithms have been used.

The *Verlet* algorithm.[14]

From x(t), a(t), and $x(t + \delta t)$.

$$x(t+\Delta t) = x(t) + v(t).\Delta t + \tfrac{1}{2}a(t).\Delta t^2 \tag{2.14}$$

$$x(t-\Delta t) = x(t) - v(t).\Delta t + \tfrac{1}{2}a(t).\Delta t^2 \tag{2.15}$$

$$x(t+\Delta t) = 2x(t) - x(t-\Delta t) + a(t).\Delta t^2 \tag{2.16}$$

$$v(t) = \frac{x(t+\Delta t) - x(t-\Delta t)}{2\Delta t} \tag{2.17}$$

The *Leap frog* algorithm.[15]

$$x(t+\Delta t) = x(t) + v(t+\tfrac{1}{2}\Delta t).\Delta t \tag{2.18}$$

$$v(t+\tfrac{1}{2}\Delta t) = v(t-\tfrac{1}{2}\Delta t) + a(t).\Delta t \tag{2.19}$$

x(t), a(t), and $v(t - \frac{1}{2}\Delta t)$ are stored

$$v(t) = \frac{1}{2}.[v(t + \frac{1}{2}\Delta t) + v(t - \frac{1}{2}\Delta t)] \quad (2.20)$$

This is time reversible due to the symmetric roles of $x(t + \frac{1}{2}\Delta t)$ and $x(t - \frac{1}{2}\Delta t)$.

The *Velocity Verlet* algorithm.[14]

$$x(t + \Delta t) = x(t) + v(t).\Delta t + a(t).\Delta t^2/2 \quad (2.21)$$

$$v(t + \frac{1}{2}\Delta t) = v(t) + \frac{1}{2}a(t).\Delta t \quad (2.22)$$

$$a(t + \Delta t) = -\delta V/\delta x.\, 1/m \quad (2.23)$$

$$v(t + \Delta t) = v(t + \frac{1}{2}\Delta t) + \frac{1}{2}a(t + \Delta t).\Delta t \quad (2.24)$$

Hence the velocities, acelerations and coordinates at each time step are known.

The highest frequency motion is the water O-H stretch 3700cm-1 or $11.09 \times 10^{15} s^{-1}$, a time step of 1fs is therefore used in order to sample this mode.

2.4. Statistical Ensembles

The molecular dynamics described thus far samples the constant NVE ensemble, where the number of particles, N, the volume V and the energy of the system is constant. It is also required that the molecular dynamics of the system be examined under isobaric and isothermal conditions.

2.4.1. NVT Ensemble

The temperature of the system is proportional to its kinetic energy, and hence atomic velocities. This is expressed in kinetic theory of gases:

$$U = 3/2.\, kT \quad (2.25)$$

where U is kinetic energy and k is the Boltzmann constant.

The kinetic energy of atom i is $U_i = 3/2\ m_i v_i^2$, m_i mass of the atom, v_i velocity. The factor of 3/2 is the sum of the kinetic energy in each of its degrees of freedom. Hence we can derive an expression for the temperature in terms of velocity:

$$T_i = \frac{m_i v_i^2}{k} \quad (2.26)$$

$$\rho(v_i) = \left(\frac{m_i}{2\pi k_b T}\right)^{\frac{1}{2}} e^{-m_i v_i^2/2k_b T} \quad (2.27)$$

$\rho(v_i)$ is the probability density for the velocity v.

Initial velocities are assigned using a Maxwell-Boltzmann distribution (Eq. 2.27) at the simulation temperature. The process of equilibration of the system leads to a transfer of energy between kinetic energy and potential energy to achieve equipartition. Therefore during the simulation, after each step (or after a specified number of steps) if the temperature deviates more than a specified amount, the velocities are rescaled to match the target temperature T_0. This is achieved by multiplying the velocities by a scaling factor λ.

$$\lambda = 1 + \frac{\Delta t}{2\tau}\left(\frac{T_0}{T} - 1\right) \tag{2.28}$$

Δt is the time step size, τ is the relaxation time, T_0 is the target temperature, and T is the instantaneous temperature.

For the Velocity Verlet integration algorithm the "ad hoc" rescaling algorithm[16] is used.

$$r(t + \Delta t) = r(t) + \beta \Delta t v(t) + (2 - \beta)\frac{\Delta t^2}{2} a(t) \tag{2.29}$$

where

$$\beta = \sqrt{(1 + \frac{\Delta t}{\tau_t})(\frac{T_0}{T} - 1)} \tag{2.30}$$

where τ_t is the coupling time constant, T_0 is the target termperature and T is the actual temperature.

2.4.2. NPE Ensemble

Experimental results are generally obtained at atmospheric pressure. In order to compare these results with those of the simulation, a constant pressure constraint must be imposed on the system.

Pressure can be thought of as the energy per unit volume of a system. There are two contributions to the pressure of the system, from the ideal behaviour of the system and the non-ideal. The ideal contribution is so called as it is the only contribution to the pressure in an ideal gas (in which the potential energy is zero).

$$(PV)_{ideal} = Nk_bT = 1/3 < \sum_{i=1}^{N} |p_i|^2/m_i > \tag{2.31}$$

N is the number of atoms, k_b is the boltzmann constant, p_i is the momentum and m_i is

the mass of atom i.

The non-ideal component, the virial ω, comes from the potential energy of the system.

$$\omega = -1/3 \sum_{i=1}^{N} r_i \nabla_{r_i} V = 1/3 \sum_{i=1}^{N} r_i f_i \qquad (2.32)$$

r_i is the coordinate of atom i, $\nabla_{r_i} V$ is the derivative of the potential energy V.

Hence for intermolecular interactions:

$$PV = Nk_bT + < \omega > \qquad (2.33)$$

The instantaneous pressure P_i is

$$P_i = Nk_bT_i + \omega / V \qquad (2.34)$$

T_i is the instantaneous temperature as calculated from the velocities. V is the volume of the unit cell.

The following expression is used to scale the pressure.[17]

$$\delta P/\delta t = (P - P_i)/t_p \qquad (2.35)$$

P is the target pressure and t_p is the pressure scaling time constant. At each step the volume of the box is scaled by χ the pressure scaling matrix, which for orthorhombic systems is diagonal, and the coordinates of the molecular centres of mass by χ in each direction.

$$x_i' = \chi_i x_i \qquad (2.36)$$

where

$$\chi_i = 1 + 1/3\beta_T \frac{\delta t}{t_p} P_i - P \qquad (2.37)$$

β_T is the isothermal compressibility of the system, δt the time step of the simulation. t_p takes the value 0.5ps.

The volume of the box is changed by scaling the unit cell lengths by the pressure scaling matrix diagonals (for orthorhomic systems).[15]

2.4.3. NPT Ensemble

One may also sample the molecular dynamics of the system using both of the above constraints. Hence the system is both isothermal and isobaric.

2.5. Periodic Boundary Conditions

For the purposes of this study it is required that an extended bilayer structure be modelled. This requires that no surface or edge effects are observed. This is achieved using *Periodic Boundary Conditions.*[15] The coordinates of the system are defined within a cubic box known as, the "unit cell". This box is then replicated in 3-dimensions throughout space in an infinite lattice. Thus if a molecule leaves the unit cell, a replica of this molecule enters the unit cell from the opposite face. This is implemented by assigning molecules from the unit cell as "basic" and those within adjacent cells "ghosts". When a basic molecule crosses a periodic boundary, its coordinates are translated such that it re-enters on the opposite side of the cube. This process is known as "swapping". Basic molecules interact with both basic and ghost molecules, however ghost molecules only interact with basics. Thus molecules in the basic unit cell sense interactions as if in an infinite lattice. The coordinates of the system are maintained in their non-swapped or periodic boundary independent form in the molecular dynamics trajectory output.

References

1. Lykos P and Shavitt I, 173, p. 161, Acs Symposium.
2. Besler BH, Merz KM, and Kollman PA, *J Comp Chem*, vol. 11, no. 4, pp. 431-439, 1990.
3. Stouch TR and Williams DE, *J Comp Chem*, vol. 14, pp. 1066-1076, 1993.
4. Stouch TR, Ward KB, Altieri A, and Hagler AT, *J Comp Chem*, vol. 12, no. 8, pp. 1033-1046, 1991.
5. Charifson PS, Hiskey RG, and Pedersen LG, *J Comp Chem*, vol. 11, no. 10, pp. 1181-1186, 1990.
6. Hagler AT, *J Hermans Ed*, p. 133, 1985.
7. Billeter M, Howard AE, Kuntz ID, and Kollman PA, *J American Chemical Society*, vol. 110, p. 8385, 1988.
8. Hagler AT, Lifson S, and Dauber P, *J American Chemical Society*, vol. 101, p. 5122, 1979.
9. Mapel JR, Dinur U, and Hagler AT, *Proc Natl Acad Sci USA*, vol. 85, p. 5350, 1988.
10. Hagler AT, Lifson S, and Ariel S, *J American Chemical Society*, vol. 101, p. 813, 1979.
11. Dauber-Osguthorpe P, Roberts VA, Osguthorpe DJ, Wolff J, Genest M, and Hagler AT, *Proteins: Structure, Function, and Genetics*, vol. 4, p. 31 47, 1988.
12. Snyder RG and Schachtschneider JH, *Spectrochim Acta*, vol. 19, p. 116, 1963.
13. Dauber-Osguthorpe P, in *PhD Thesis, Bath*, 1990.
14. Verlet L, *Phys Rev*, vol. 159, p. 98, 1967.
15. Allen MP and Tildesley DJ, in *Computer Simulation of Liquids*, Oxford Clarendon Press, 1987.
16. Brown D and Clarke JHR, *Molecular Physics*, vol. 51, no. 5, pp. 1243-1252, 1984.
17. Berendsen HJC, Postma JPM, van Gunsteren WF, Dinola A, and Haak JR, *J Chem Phys*, vol. 81, pp. 3684-3690, 1984.

3. Software

3.1. VFF: Minimisation and Molecular Dynamics

The program VFF [1] is a combined molecular mechanics and molecular dynamics program for calculating the structural, energetic and dynamic properties of molecular systems. It requires the following information:

Cartesian coordinates in the coordinate space of the system.

A residue library, which describes both the connectivity and bond hybridization of the moleculer system.

The force field parameters used in the energy calculations (Eq. 2.1).

A control file containing the control information for the simulation including the number of iterations and physical conditions of the calculation.

This information is used to calculate first the internals and intermolecular distances, followed by the energy and first and second derivates of the energy with respect to Cartesian coordinates.

This allows for the energy and structure of the closest local energy minimum to be calculated using a minimization technique. A trajectory of the atomic coordinates, velocites and energy components of the systems can then be calculated, using molecular dynamics.

3.2. SLICER: Generation of unit cell coordinates from the crystal coordinates

SLICER[2] takes fractional crystal coordinates[3] and transforms them to Cartesian coordinates, performing the required crystal transformations to build the crystal unit cell. It requires a potential parameter file, residue library file, and control file.

3.3. PACKER: Generation of van der Waals packed lipid models

PACKER[4] is a "Monte-Carlo" lipid packing program for building close packed lipid bilayer assemblies. It minimizes the solvent accessible surface in the bilayer plane, whilst maintaining the bilayer structure, and the random packing of the molecules. The Cartesian coordinates of a single lipid must be orientated such that the long axis of the acyl chains are parallel to the z axis. This is achieved by removing the head group from the lipid and calculating the principle moment of inertia of the glycerol and acyl chains using the program **ORTHO**.[5] Rigid body rotation are then applied to the complete lipid orientating the molecule parallel to this axis. Other

information required includes the number of lipids and the number of valid conformations to generate in the calculation. These are generated by randomly placing copies of the lipid molecule in a box containing an initial lipid at its centre and checking for van der Waals overlap until a valid arrangement is generated. The sum of the squares of the inter-geometric distances (centre to centre) is used to maximise the packing. Restart calculations may be performed as the random number seed is saved for generation of a new set of random numbers at each iteration. This is found to converge after about 2000 iterations.

3.4. BUILDER: A lattice bilayer model builder

BUILDER[6] packs lipid molecules regularly in a lattice structure. The dimensions of the lattice can be adjusted in order to increase or decrease the amount of free volume in the unit cell. This again is based on the coordinates of the lipid molecule orientated parallel to the z axis as above using ORTHO. The molecule is first translated to the origin of the coordinate space. Copies of that molecule are then translated in the x and y directions, filling the intersection points of the lattice. This lattice can be hexagonal or square and the two monolayers can be positioned with equivalent lipids opposite each other or offset. This allows for both a regular lattice and no close contacts, providing suitable lattice dimensions are used. Once one monolayer has been built a second copy of this monolayer is rotated 180° and placed below the previous copy. The separation of the two monolayers is another control variable, in addition to both the size of the matrix and the resulting unit cell size of the coordinate system. All these models are orthorhombic, as they have unit cell angles of 90 °.

3.5. INSIGHT: A Molecular Graphics Program

INSIGHT[7] is a molecular graphics program, which combines the use of a graphics station and software to allow for the construction, manipulation and anlysis of molecular systems. It is possible to construct molecular systems, obtain cartesian coordinates, and display structures. The molecular dynamics trajectories of these systems may then be calculated and visualised. A limitted number of internal properties of the simulation may also be calculated and displayed. In addition molecular systems may be visualised within a periodic system. Molecules can be surrounded by solvent, using a Monte Carlo box of waters to sample the bulk structure of water and surround the molecule with solvent, avoiding van der Waals clashes between solvent and solute within the periodic system.

3.6. RasMol: A molecular visualisation program

RasMol[8] is a menu and command driven interactive utility for the visualisation of molecular structures. It accepts coordinates in the standard Brookhaven Protein Data Bank (PDB) format. Structures may be visualised in a variety of formats including spacefilling respresentation.

3.7. ELIM_H2O: A Program to remove solvent molecules from hydrophobic volumes

ELIM_H2O[9] allows for the elimination of water from hydrophobic volumes of the unit cell. This is achieved by removing all solvent from the acyl region of the bilayer model. This is required because the "Soak" feature of Insight places solvent molecules in any available volume that is large enough to contain a solvent molecule. Hence in lattice built systems solvent is placed within the hydrophobic core of the bilayer.

3.8. GENTOR: Generates lists of torsion angles

GENTOR[10] constructs lists of atoms to make up torsion angles within a molecular system. These include both unimolecular and polymolecular systems. Extracting the atom numbers referring to a specified torsion is a tedious process and may introduce errors which are not identified until significant CPU time has been wasted calculating the required torsion values. GENTOR automates this process. The molecule must be uniquely numbered. A list of the required torsion angle atom labels is then created with their atom numbers, replicated for all molecules within the appropiate torsion.

3.9. FOCUS: A Molecular Dynamics Analysis Program

FOCUS[11] allows for the analysis of molecular dynamics trajectories, by making available at each time step, the coordinates of the system, atomic velocities and energetics of the system. These may then be used to calculate both the time average and instantaneous value of a property.

3.10. Analysis of Trajectories

3.10.1. Time Averages and Standard Deviations:

The statistical average and standard deviation of a property, P, are given by:

$$< p > = 1/N \sum p(t_k) \quad (3.1)$$

$$\sigma = (< p^2 > - < p >^2)^{1/2} \quad (3.2)$$

where $p(t_k)$ is the value of the property at time t_k; <p> and $<p^2>$ are the time averages of the property and the square of the property respectively, and σ is the standard deviation.

3.10.2. Structural Properties

A number of properties of the system can be calculated from its coordinates at each time step. This allows for the time dependence of selected structural properties to be examined and ensemble averages to be calculated.

3.10.2.1. Average Coordinates

The average coordinates of the system can be calculated for part or all of the trajectory.

3.10.2.2. Distances

The distance between any two coordinates can be calculated. This may be a bonded pair of atoms or a non-bonded distance.

3.10.2.3. Angles

The angle between any three coordinates can be calculated. This may be an internal valence angle or three non-bonded atoms.

3.10.2.4. Torsion Angles

The torsion angle between any four coordinates may be calculated. The ensemble average, and distribution can then be calculated, measuring the distrubtion of trans and gauche conformations for example.

3.10.2.5. Diffusion

The diffusive motion of the centre of mass of a molecule or arbitary cluster of atoms may be calculated, relative to either the initial time step or some defined reference point in the trajectory. This is calculated as the linear distance travelled from the reference point at each time step, and may be calculated for any part of the system.

3.10.2.6. Vectors

The three coordinate space vectors of any bonded or non-bonded distance may be calculated. These may be used to follow the dynamics of particular functional groups in a molecule.

3.10.2.7. Radial Distribution Function

The pair-wise radial distribution function[12] of any atom or group of atoms may be calculated with reference to either all atoms, or some reference atom type (for example the water oygen). All pairwise distances (or distances from a target atom or group of atoms) are calculated and their number and distribution recorded in distance bins, the size of which depends on the resolution. δr.

$$n(i) = \sum_{N} n_{r<d<(r+\delta r)}/N \tag{3.3}$$

where n(i) number of particles in bin i, r is the radial distance for bin i ($i\delta r$), d is the pairwise distance between two particles and N is the total number of particles evaluated.

The ensemble average is then taken of each distance bin. For periodic boundary simulations, the coordinates of the system are "swapped" into the central unit cell before the distance search is performed. The radial distribution is then normalised by the expected density of atoms.

$$g(r+\delta r) = n(i)/n^{nrm}(i) \tag{3.4}$$

$$n^{nrm}(i) = \frac{4\pi\rho}{3}[(r+\delta r)^3 - r^3] \tag{3.5}$$

where $n^{nrm}(i)$ is the number of particles found in the radial segment $r-(r+\delta r)$ and ρ is the bulk density of particles.

This provides a direct comparison with experimentally obtained radial distribution

functions from neutron diffraction experiments. The heavy atom radial distribution function may also be compared with X-ray diffraction Bragg reflections.

3.10.2.8. Density Profiles

This allows one to examine the distribution of the density of ranges of atoms or molecules with respect to a specific coordinate axis. The unit cell is subdivided along the selected coordinate axis, by the required resolution. For each subdivision of the until cell axis the masses of the selected range of atoms are summed, resulting in a density. A density profile for the unit cell is thus obtained. The coordinate axis is defined relative to the centre of the unit cell in order to compensate for possible unit cell volume changes which may occur when sampling from the NPT or NPE ensemble. A unit cell vector expansion factor is used to take account of this expansion, scaling the selected unit cell axis, to ensure values are in range for the selected time period.

3.10.2.9. Fourier Transforms

Fourier transformation[13] of coordinates into the frequency domain allows for the examination the frequencies of motion of the system, from bond vibration to low frequency conformational motions.[14-17] It is also possible to fourier transform any time dependent property of the system from the time to frequency domain, in order to examine any characteristic variation.

3.10.2.10. Filtering

This method is based on digital signal processing techniques, to remove "noise" from an electrical signal. A filtering function is applied to the fourier transformed property, removing frequencies outside the selected range. The inverse fourier transform is then applied transforming the property back to the time domain with only the selected frequencies remaining. This may be applied not only to the coordinates of a system to examine low frequency motions, but also to other time dependent properties, such as the potential energy of a system, to filter out high frequency "noise".

3.10.2.11. Hydrogen Bonds

The number and position of hydrogen bonds within the system can be examined. This performs a distance check between the selected atoms, marking the interaction as a hydrogen bond if it is less than a specified distance. The hydrogen bond acceptor and donor atoms are differentiated using a list containing the search atom potential type and a list containing the other hydrogen bond pair atom label.

3.10.2.12. Euler Angles

The Euler angles of a phospholipid molecule can be calculated for each set of coordinates of the trajectory, and hence the ensemble averages. These provide a direct comparison between the obtained molecular dynamics trajectory and the NMR experimental results.[18] The Euler angle is defined using C2 and C1 of the glycerol, the esterified oxygen and phosphorus of the phoshate and the reference unit cell axis (bilayer normal). It is only valid for orthogonal systems.

3.10.2.13. Electrostatic Potential

The surface potential is defined as the drop in electrostatic potential experienced by a charge of +1 passing across the membrane / solvent interface.[19-21] The surface potential, $\Delta\Phi$, across the bilayer-water interface can be calculated by integrating the electric field, $E_z(z)$, in the z direction (assuming the bilayer normal lies along the z axis).

$$\Delta\Phi = \int_{z1}^{z2} E_z(z)\, dz \qquad (3.6)$$

where z1 and z2 are located in the middle of the water and bilayer lamella. The electric field $E_z(z)$ can be expressed as

$$E_z(z) = \frac{2\pi < q_-(z) - q_+(z) >}{S} \qquad (3.7)$$

where $q_-(z)$ and $q_+(z)$ are the total charges above and below the plane located at z, S is the xy cross-sectional area of the simulation box and <..> represents the ensemble average.

3.10.2.14. Pseudorotational Angle

Non-aromatic ring systems, which are flexible and may interconvert between conformational states (chair and boat), do so by a process known as pseudorotation. This involves the systematic rotation of each torsion angle around the ring, thus "puckering" the ring. The torsional strain in one torsion is relieved by rotation of an equivalent torsion around the ring. The pseudo rotation angle, ξ can be calculated at each step of the trajectory and the pseudorotation of a ring system under conformational interconversion may be followed.

In the case of cyclopentane:

$$\xi = \frac{((\theta_3 + \theta_5) - (\theta_2 + \theta_4))}{(\sin 36 + \sin 72).\, 2\theta_1} \tag{3.8}$$

θ_{1-5} are the five torsion angles around the ring.

3.10.2.15. Segmental Order Parameters

The segmental order parameters for C-H bonds (in experiment C-D bonds) in the acyl chains of lipid molecules can be calculated with respect to the bilayer normal. This assumes that the bilayer normal is parallel to one of the coordinate axes. This is done by calculating the component of the C-H vector in the bilayer normal.

$$S_{zz} = \tfrac{1}{2} < 3\cos^2\theta - 1 > \tag{3.9}$$

where θ is the angle that the C-H vector makes with the bilayer normal. The order parameter for each segment is both the ensemble average and the average of all equivalent segments.[22-25]

3.10.2.16. Moment of Inertia

The moment of inertia of a molecule or group of atoms can be calculated from their coordinates and velocities.[26] The centre of mass velocity must first be calculated and removed. The three components of the angular momentum can then be calculated.

$$H = \sum_N m_i(r_i x v_i) \tag{3.10}$$

where H is the angular momentum, m_i is the mass of atom i, r_i its coordinate, and v_i its velocity.

The moment of inertia tensor is then calculated and inverted. The angular velocity (ω) is the product of the inverted moment of inertia tensor and the angular momentum (H). The unit vector along ω is then

$$\omega^{uv}_{(i)} = \frac{\omega_{(i)}}{(\omega_{(1)}{}^2 + \omega_{(2)}{}^2 + \omega_{(3)}{}^2)^{1/2}} \tag{3.11}$$

The moment of inertia about the unit vector is then

$$I = \sum_i m_i(r_i{}^2 - (r_i \,.\, \omega^{uv})^2) \tag{3.12}$$

where I is the moment of interia about an axis (unit vector) running through the centre of gravity. m_i is the mass of atom i, r_i is the coordinate (principle component coordinate system) of atom i. ω^{uv} is the unit vector in the direction of the angular momentum ω.

The eigen values (components of the moment of inertia ellipsoid) and the eigen vectors (principle axes) are calculated from the moment of inertia tensor. This can then be used to characterise complex motion in part or all of the molecule.

3.10.2.17. Radius of Gyration

The radius of gyration of a molecule or group of atoms can be calculated.

$$R_g = \sqrt{I/M} \tag{3.13}$$

where R_g is the radius of gyration of the molecule. M is the molecular mass, and I is the moment of inertia.

3.10.3. Thermodynamic Properties

A number of thermodynamic properties can also be calculated or examined from the molecular dynamics trajectories. These are based on both the atomic coordinates, velocities and unit cell dimensions.

3.10.3.1. Thermodynamic Information

Information about the conditions of the simulation at each step are stored on the molecular dynamics trajectory. These include unitcell lengths and angles, unitcell volume, pressure, temperature, total energy, kinetic energy, potential energy, E_b, E_θ, E_ϕ, E_χ, E_{vdw},

E_{e^-}, $E_{bb'}$, $E_{b\theta}$, $E_{\theta\theta'}$, $E_{\theta\phi}$, $E_{\chi\chi'}$, and the Pressure Tensors (components of pressure).

3.10.3.2. Atomic/Molecular Temperature

The temperature of any range of N atoms can be calculated from their atomic velocities.

$$KE = \frac{3}{2} RT = \tfrac{1}{2}mv^2 \tag{3.14}$$

$$T = \sum_{i=1}^{N} \frac{m_i v_i^2}{3R} \tag{3.15}$$

where m_i and v_i are the mass and velocity of atom i. This allows for the examination of the partitioning of temperature and its effect on the dynamics of the system.

References

1. Osguthorpe DJO, 1986. VFF, Molecular Graphics Unit, Bath UK
2. Sessions RB. SLICER, Molecular Recognition Centre, Bristol UK
3. CSSR, Cambridge Crystalographic Database, Daresbury UK.
4. Lemon AP, 1992. PACKER, Molecular Graphics Unit, Bath UK
5. Reich K. ORTHO, Unknown
6. Lemon AP, 1992. BUILDER, Molecular Graphics Unit, Bath UK
7. INSIGHT, BIOSYM Technologies, San Deigo, USA.
8. Sayle R. RasMol V2.2, Biocomputing Research Unit, Edingburgh UK
9. Lemon AP, 1992. ELIM_H2O, Molecular Graphics Unit, Bath UK
10. Lemon AP, 1992. GENTOR, Molecular Graphics Unit, Bath UK
11. Sessions RB, Lemon AP, Dauber-Osguthorpe P, and Osguthorpe DJO, 1993. FOCUS, Molecular Graphics Unit, Bath, UK
12. Allen MP and Tildesley DJ, in *Computer Simulation of Liquids*, Oxford Clarendon Press, 1987.
13. Dauber-Osguthorpe P, in *PhD Thesis, Bath*, 1990.
14. Dauber-Osguthorpe P and Osguthorpe DJ, *J Comp Chem*, vol. 14, no. 11, pp. 1259-1271, 1993.
15. Osguthorpe DJ and Dauber-Osguthorpe P, *J of Molecular Graphics*, vol. 10, pp. 178-184, 1992.
16. Dauber-Osguthorpe P and Osguthorpe DJ, *Biochemistry*, vol. 29, pp. 8223-8228, 1990.
17. Dauber-Osguthorpe P and Osguthorpe DJ, *J American Chemical Society*, vol. 112, pp. 7921-7935, 1990.
18. Dufourc EJ, Mayer C, Stohrer J, Althoff G, and Kothe G, *Biophysical J*, vol. 61, no. 1, pp. 42-57, 1992.
19. Wilson MA and Pohorille A, *J of the American Chemical Society*, vol. 116, no. 4, pp. 1490-1501, 1994.
20. Wilson MA, Pohorille A, and Pratt LR, *J Chem Phys*, vol. 88, no. 5, pp. 3281-3285, 1988.

21. Wilson MA, Pohorille A, and Pratt LR, *J Phys Chem*, vol. 91, no. 19, pp. 4873-4878, 1987.

22. Marsh D, in *Handbook of Lipid Bilayers Crc Press*, 1991.

23. Seelig A and Seelig J, *Biochemistry*, vol. 13, no. 23, pp. 4839-4845, 1974.

24. Knowles PF and Marsh D, *Biochem J*, vol. 274, pp. 625-641, 1991.

25. Davies JH, *Biochimica et Biophysica Acta*, vol. 737, pp. 117-171, 1983.

26. Goldstein H, in *Classical Mechanics*, Addison-Wesley, 1977.

4. System Configuration

4.1. Molecular Conformations

Before molecular dynamics trajectories can be sampled the initial coordinates of the system must be constructed. The starting configuration of the system and the starting conformation of the molecules are chosen to reproduce the configuration and conformation of the "real" bilayer system. However it is important that certain features of the system are not imposed on the initial configuration of the simulation, but are allowed to develop under the interactions of the potential energy force field.

4.1.1. Phospholipids

The molecular conformations of the lipid molecules have been determined from the crystal structures of both the lipid and related molecules.[1-7] The crystal structure of DLPC was unavailable, it was therefore constructed from the crystal structure of DLPE,[8] the choline group methyls being added using INSIGHT. This conserves the important conformational features (head group and glycerol conformation) of the related PC crystal structures, and the chain separation of DLPE. The bilayer crystal structure unit cell of DLPC was then constructed.[9]

The molecular conformation A was chosen from the crystal structure of DMPC.[10] This extended head group conformation was chosen to examine the head group dynamics. This was then used to construct the regular lattice bilayer model. The crystal structure simulation of DMPC was not undertaken due to the complication of two molecular conformations in the unit cell.

4.1.2. Cholesterol

The coordinates of cholesterol [11] were used to construct the unit cell of the cholesterol crystal structure. This contains 8 cholesterol molecules in the P1 space group. A crystal minimization was then used to remove strain from the unit cell. A molecular dynamics trajectory of 25ps was then sampled,[12] the first 3ps from the NVE ensemble and the remaining 22ps from the NPT ensemble using 298K and 1bar temperature and pressure constraints. The RMS fit between the initial coordinates and the average of the last 5ps was 0.15Å. The main deviation

is in the acyl portion of the cholesterol molecule. The sterol ring system remained in a relatively rigid state. The parameterization of cholesterol was therefore stable with respect to the initial structure and the NPT ensemble. This result was confirmed in the 300ps mixed cholesterol DLPC trajectories analysed later in this study.

4.2. Bilayer Models

Data relating to the spatial arrangement of the lipids in a bilayer system have been used to construct the initial configuration. These include the measured area per head group,[13] inter-lipid spacing, [14] density, and bilayer repeat distance.[15,16] Caution must be used in the construction of the configuration with respect to the conditions of the simulation and the starting conformation of the lipids. The crystal structure of DLPC (DLPE) for example is a bilayer system, the molecules are in the all trans conformation. This gives rise to an inter-monolayer head group distance of 42Å, which is not reproduced in the "real" bilayer system, due to conformational freedom in the acyl chains compressing the hydrophobic region, leading to membrane thinning. This can be seen from X-ray diffraction experiments, in which the membrane thickness is seen to decrease by up to 40% on the gel to liquid crystaline transition. [17] Constant pressure calculations in which the unit cell vectors are scaled by the components of the pressure tensor, should however compensate for this effect, as membrane thinning should reduce the pressure tensor in the bilayer normal direction.

Another challenge associated with the construction of the starting configuration is how to avoid imposing a large electrostatic energy in the system from the starting configuration. The head group of the phospholipids contains a large concentration of electrostatic charge, both from the zwitterionic charge of the PC group and the relatively large partial charges on the oxygen, phosphorus and nitrogen atoms (See Appendix I). If the system is built in a crystaline configuration, a large electric field is imposed on the system from the start of the simulation. To avoid this various approaches were taken to introduce a randomness to the system.

4.2.1. Builder(I)

Random rotations about the three coordinates axes (±180° about z and ±5° about x,y) were applied to each molecule before being placed into its lattice position. This proved a problem, especially for the extended head group conformation of DMPC, as avoiding serious van der Waals over lap of head group atoms was difficult. The free volume required by each

molecule to avoid contact leads to a bilayer with a large area per head group, and low hydrocarbon density.

4.2.2. Packer

A lipid molecule is placed at the centre on the unit cell. Copies of that molecule are then placed randomly within the box in the plane of the bilayer surface. Random rotations are applied about the long axis of the molecule. Translations of 0-3Å are then applied along the bilayer normal direction in order to reproduce the pitch offset observed in the PC crystal structures.[2] A van der Waals overlap check is then applied to each molecular position and a new configuration generated if clashes occur. Once a full unit cell (monolayer) has been generated, the sum of the distance between the centre of mass of the central molecule and all those in the unit cell is calculated. This is then used as a convergence criteria for the configuration generated. It was found to converge after 2000 iterations. The alternative method of calculating the solvent accessible surface using a Connolly surface was is too computationally expensive. The resulting monolayer was then rotated in order to form the other envelope of the bilayer.

A 50ps NVE ensemble, molecular dynamics trajectory of the minimized coordinates (200 steps of steepest decents) was sampled from the NVE ensemble. The integrity of the bilayer system was not maintained with respect to the periodic boundary system. Lipid molecules were observed to move out of the bilayer plane, creating vacuum in the hydrophobic region and exposing the remaining acyl chains. This was attributed to a problem of excess free volume in lipids at the edges of the unit cell, due to the random nature of the packing algorithm. A concerted cooperativity of interactions between acyl chains in the hydrophobic region of the bilayer is required to maintain the bilayer stability. This is not achieved in this randomly spaced bilayer system.

4.2.3. Builder(II)

A lattice model in which lipid molecules are placed in a regular lattice was therefore used. This was seen as the only reliable method of building a stable bilayer model, despite the high initial electrostatic energy of the crystaline lattice.

4.2.4. Cholesterol Systems

These systems were built using the DLPC crystal structure template. Most properties of cholesterol doped bilayer systems are observed in 1:1 lipid:cholesterol mixtures.[18] Alternate DLPC molecules were therefore replaced with cholesterol molecules, the cholesterol hydroxyl group located level with the central glycerol atom. This position has been indicated in experimental results.[19-21] The lattice positions of the cholesterols were alternated between the two layers. Hence cholesterol molecules are not located adjacent to other cholesterol molecules, with respect to the bilayer normal. There is sufficient free volume in the DLPC crystal unit cell to accomodate the cholesterol molecule without van der Waals overlap.

4.2.5. Hydrated Systems

The "soak" module from INSIGHT was used to hydrate the minimized coordinate system. This requires generation of the unit cell using the "cell" command. The unit cell parameters were directly transferred from the minimised unit cell, and the P1 space group was used. The unit cell vector along the bilayer normal was increased by at least twice the non-bond cut off value, in order to allocate sufficient free volume for waters. This provides water which does not directly interact with the lipid, and removes any interaction between head groups across the water phase. Because of the free volume available to each lipid in the initial model, waters were placed within the hydrophobic region of the bilayer. Any waters within the volume of the glycerol and acyl chain region were removed.[22] Experimental results indicate that water penetrates down to the carbonyl groups of such bilayer systems. [23] It is important that such features are allowed to develop rather than being imposed on the starting coordinates.

4.2.6. Coordinate partitioning

The coordinate system was partitioned into its subcomponents (lipid, cholesterol and water see Table 4.1). This improves the efficiency of analysis with respect to the density profile as well as other component specific properties. It also improves the efficiency of the non-bond calculation, in terms of the localization of data (important on vector machines).

Table 4.1

Composition

Model bilayer systems					
System	DMPC	DLPC	CHOL	Water	Molwt/gmol^{-1}
dmpc	18	-	-	-	12203.1
dmpc_i	18	-	-	-	12203.1
dlpc	-	16	-	-	9949.4
dlpc_y1	-	16	-	-	9949.4
dlpc_wat	-	16	-	201	13282.3
wat_dlpc_y2	-	16	-	715	22830.4
dlpcchol	-	8	8	-	8068.0
dlpcchol_s	-	8	8	-	8068.0
wat_dlpcchol	-	8	8	319	13814.9

4.3. Strain removal

Coordinate models built using the above methodologies were then minimized using steepest decents minimization. 100 steps of minimization without periodic boundary conditions was performed. A series of 100 step steepest decents minimizations were then performed until the RMS derivative of the coordinate system reduced to approximately 1 ± 1Å, using the periodic system. The unit cell dimensions were chosen by examination of the maximum and minimum coordinates of the system. The exact values being derived from several single point calculations of the non-bond energy of the system (5.0Å cut off) under periodic boundary conditions. An orthorhombic unit cell was used ($\alpha = \beta = \gamma = 90°$). A cut off for the non-bonded interactions was then chosen, this being approximately half the smallest unit cell vector (see Table 4.3). In order to make analysis of the coordinate trajectories more elegant most coordinates were first translated to the positive quadrant of the coordinate system.

Table 4.2

Spacial Configuration

Model bilayer systems										
System	x/Å	y/Å	z/Å	D_{c-c}/Å	D_i/Å	D_{p-p}/Å	L^t	α	β	A_{PC}/Å
dmpc	9.0	-	9.0	2.0	-	46.4	S	-	-	99.89
dmpc_i	9.5	-	9.5	-	-12.6	31.0	S	-	-	109.1
dlpc	-	7.7	9.95	2.0	1.5	41.8	H	108.8	75.8	38.66
dlpc_y1	-	7.7	11.9	2.0	1.5	42.0	H	104.7	75.3	57.71
dlpc_wat	-	7.8	9.3	2.0	-1.0	40.6	H	125.9	67.83	40.08
wat_dlpc_y2	-	7.7	11.7	6.9	-1.0	42.7	H	110.5	75.3	80.48
dlpcchol	-	6.1	10.0	4.7	-2.0	39.8	H	145.6	75.3	40.08
dlpcchol_s	-	9.4	14.9	4.6	-0.5	41.1	H	142.7	37.3	59.75
wat_dlpcchol	-	9.4	14.9	4.6	-0.5	41.1	H	142.7	37.3	59.75

where x,y and z are the interlipid spacing in the monolayer plane, D_{c-c} is the distance along the bilayer normal of equivalent C segments, D_i is the distance along the bilayer normal that the two monolayers are interdigitated, D_{p-p} is the distance between the plane containing the phosphate P in the two monolayers, L^t is the lattice type (S, square, H, hexagonal) angles α and β defining the hexagonal lattice shape and A_{PC} is the area per head group.

4.4. Ensemble Sampling

The molecular dynamics trajectory of these minimized coordinates was then sampled using a time step of 1fs, velocities and coordinates stored every 10fs. All systems were orthorhombic ($\alpha = \beta = \gamma$ = 90 °),and unit cell vectors were directly transferred from the minimization cells. The temperature of the initial Boltzman distribution of velocities was chosen on the basis of the transfer of potential to kinetic energy in the initial 1000 steps of dynamics. In

Table 4.3

Minimization

Bilayer Model Systems					
System	NB_c/Å	A/Å	B/Å	C/Å	RMSd/Å
dmpc	10.0	31.0	55.0	29.0	0.738
dmpc_i	11.0	32.5	38.7	30.2	1.842
dlpc	9.9	47.7	15.54	19.9	1.335
dlpc_y1	10.0	50.08	23.2	27.75	1.313
dlpc_wat	8.0	67.7	16.0	20.4	1.663
wat_dlpc_y2	10.0	81.17	23.2	27.75	1.489
dlpcchol	8.0	47.7	16.0	20.4	1.141
dlpcchol_s	9.0	50.085	19.2	24.48	1.019
wat_dlpcchol	9.0	66.085	19.2	24.48	1.622

where NB_c is the non-bond interaction cut off, A, B, and C are the unit cell vectors and RMSd is the root mean square of the first derivative of the minimized coordinates with respect to the potential energy.

most simulations the first 1-10ps was sampled from the NVE ensemble after which constraints were imposed and the remaining trajectory sampled from either the NVT, or NPT ensembles. The precise conditions of the ensemble will be discussed in further chapters. A number of models have been constructed, and the following table summarises the key features of the starting conditions.

Table 4.4

Molecular Dynamics

Bilayer Model Systems							
			Pressure		Temperature		
System	NB_c/Å	MD Alg	P/bar	t_p/ps	T/K	t_0/K	t_T/ps
dmpc	10.0	LF	1.0	80	310	310	100
dmpc_i	11.0	LF	1.0	80	310	310	100
dlpc	9.9	LF	-	-	310	310	100
dlpc_y1	10.0	VV_{ah}	1.0	500	320	600	150
dlpc_wat	8.0	LF	1.0	500	310	310	600
wat_dlpc_y2	10.0	VV_{ah}	1.0	500	320	600	600
dlpcchol	8.0	LF	-	-	310	310	100
dlpcchol_s	9.0	VV_{ah}	1.0	500	320	600	100
wat_dlpcchol	9.0	VV_{ah}	1.0	500	320	600	150

where NB_c is the non-bond cut off used, MD alg is the Molecular dynamics integration algorith used (LF is the leap frog, VV_{ah} is the Velocity Verlet with "ad hoc" rescaling), t_p and t_t are the two time constants for the pressure and temperature constraints (MT refers to a Multiple Temperature Bath).

References

1. Hauser H, Pascher I, Pearson RH, and Sundell S, *Biochimica et Biophysica Acta*, vol. 650, pp. 21-51, 1981.

2. Pascher I, Lundmark M, Nyholm PG, and Sundell S, *Biochimica et Biophysica Acta*, vol. 1113, no. 3-4, pp. 339-373, 1992.

3. Kjaer K, Als-Nielsen J, Helm CA, Laxhuber LA, and Mohwald H, *Pre-Print*, 1988.

4. Craven BM, *Acta Crysta*, vol. B39, pp. 1123-1128, 1979.

5. Vanderkooi G, *J Phys Chem*, vol. 94, pp. 4366-4372, 1990.

6. Small DM, *J Lipid Research*, vol. 8, pp. 551-557, 1967.

7. Ruocco MJ and Shipley G, *Biochimica et Biophysica Acta*, vol. 684, pp. 59-66, 1982.

8. Elder M, Hitchcock P, Mason R, and Shipley GG, *Proc Roy Soc London A*, vol. 354, pp. 157-170, 1977.

9. Sessions RB. SLICER, Molecular Recognition Centre, Bristol UK

10. Pearson RH and Pascher I, *Nature*, vol. 281, pp. 499-501, 1974.

11. Shieh HS, Hoard LG, and Nordman CE, *Acta Crystallography Sect B*, no. 37, p. 1538, 1981.

12. Evans DE, *Personal Communication.*

13. McIntosh TJ and Simon SN, *Biochemistry*, vol. 25, pp. 4948-4952, 1986.

14. Small DM, *J Lipid Research*, vol. 25, pp. 1490-1500, 1984.

15. Hitchcock P, Mason R, Thomas DB, and Shipley GG, *Proc Natl Acad Sci USA*, vol. 71, pp. 3036-3040, 1974.

16. Nagle JF, *Biophysical J*, vol. 64, no. 5, pp. 1476-1481, 1993.

17. Miller IR, *Biophysical J*, vol. 45, pp. 643-644, 1984.

18. Lunt GG and Harrison R, in *Biological Membranes*, Blackie & Son Glasgow, 1980.

19. Bittman R, Fugler F, Clejan S, Lister MD, and Hancock AJ, *Biochimica et Biophysica Acta*, vol. 1106, pp. 40-44, 1992.

20. Scott HL and McCullough WS, *Biophysical J*, vol. 64, no. 5, pp. 1398-1404, 1993.

21. Worcester DL and Franks NP, *J Mol Biol*, vol. 100, pp. 359-378, 1976.

22. Lemon AP, 1992. ELIM_H2O, Molecular Graphics Unit, Bath UK

23. Scherer JR, *Biophysical J*, vol. 55, pp. 957-964, 1989.

5. Analysis Setup

5.1. Crystal structures and atomic labels

Figure 5.1.1 shows the crystal structure coordinates of the dilaurylphoshatidylcholine, dimystoylphosphatidylcholine and cholesterol molecules used in this study. The atomic labels as used in the minimisations and molecular dynamics simulations are shown. They are required in order to select the correct coordinates for calculating physical properties. If atoms are to be selected by name it is essential that atom labels within a molecule are unique. However in this study most atoms are selected by atom numbers. Hydrogens are labelled using their bonded atom label (C12 → H121 and H122).

Figure 5.1.1 Atom labels

(a) DLPC

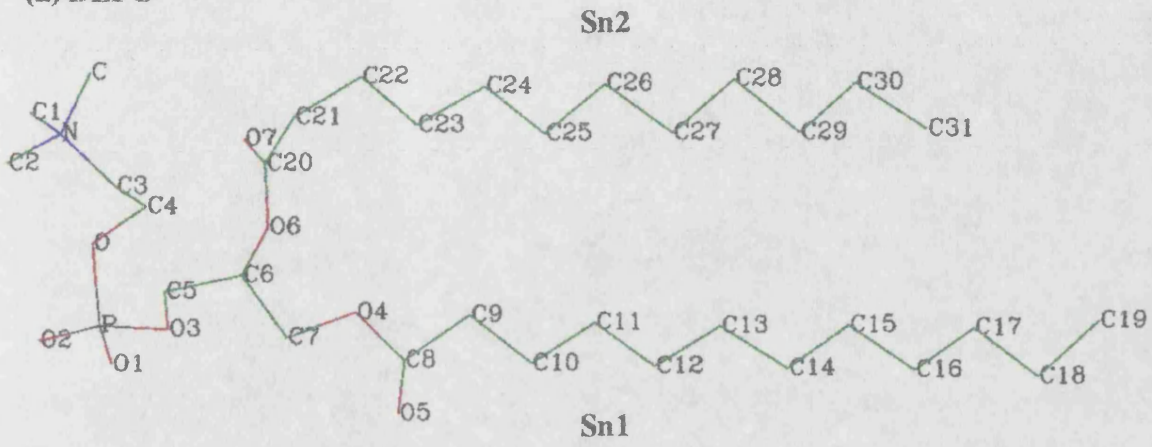

(b) DMPC

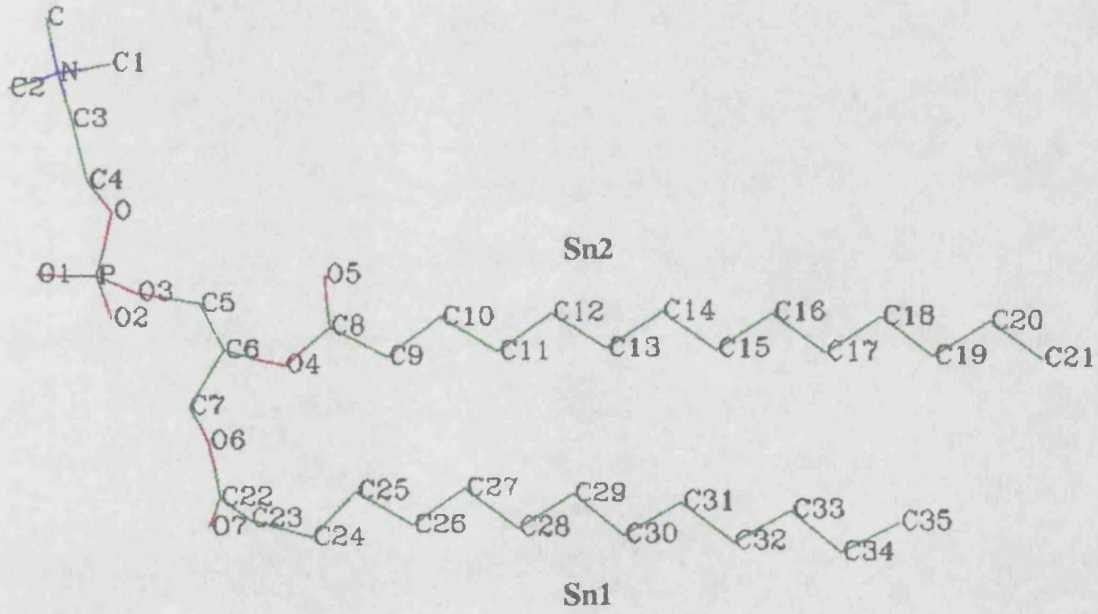

(c) Cholesterol

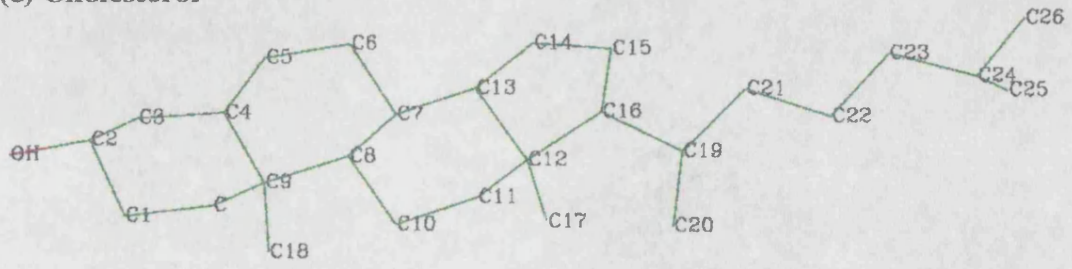

5.2. Internal Geometry

Various internals are defined to characterise the conformational transitions of the molecule and allow comparison with experimentally measured values.

5.2.1. DLPC Torsion Angles

Torsion Angles				
ϕ_n	T_1	T_2	T_3	T_4
1	C	N	C3	C4
2	N	C3	C4	O
3	C3	C4	O	P
4	C4	O	P	O3
5	O	P	O3	C5
6	P	O3	C5	C6
7	O3	C5	C6	C7
8	C5	C6	C7	O4
9	C6	C7	O4	C8
10	C7	O4	C8	C9
11	O4	C8	C9	C10
12	C8	C9	C10	C11
13	C9	C10	C11	C12
14	C10	C11	C12	C13
15	C11	C12	C13	C14
16	C12	C13	C14	C15
17	C13	C14	C15	C16
18	C14	C15	C16	C17
19	C15	C16	C17	C18
20	C16	C17	C18	C19
21	C7	C6	O6	C20
22	C6	O6	C20	C21
23	O6	C20	C21	C22
24	C20	C21	C22	C23

Torsion Angles				
ϕ_n	T_1	T_2	T_3	T_4
25	C21	C22	C23	C24
26	C22	C23	C24	C25
27	C23	C24	C25	C26
28	C24	C25	C26	C27
29	C25	C26	C27	C28
30	C26	C27	C28	C29
31	C27	C28	C29	C30
32	C28	C29	C30	C31

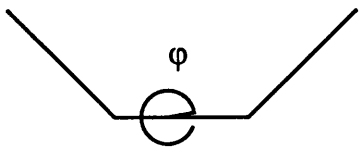

5.2.2. DMPC Torsion Angles

Torsion Angles				
ϕ_n	T_1	T_2	T_3	T_4
1	C	N	C3	C4
2	N	C3	C4	O
3	C3	C4	O	P
4	C4	O	P	O3
5	O	P	O3	C5
6	P	O3	C5	C6
7	O3	C5	C6	C7
8	C5	C6	C7	O6
9	C6	C7	O6	C22
10	C7	O6	C22	C23
11	O6	C22	C23	C24
12	C22	C23	C24	C25
13	C23	C24	C25	C26
14	C24	C25	C26	C27
15	C25	C26	C27	C28
16	C26	C27	C28	C29
17	C27	C28	C29	C30
18	C28	C29	C30	C31
19	C29	C30	C31	C32
20	C30	C31	C32	C33
21	C31	C32	C33	C34
22	C32	C33	C34	C35
23	C7	C6	O4	C8
24	C6	O4	C8	C9
25	O6	C8	C9	C10
26	C8	C9	C10	C11
27	C9	C10	C11	C12
28	C10	C11	C12	C13

Torsion Angles				
ϕ_n	T_1	T_2	T_3	T_4
29	C11	C12	C13	C14
30	C12	C13	C14	C15
31	C13	C14	C15	C16
32	C14	C15	C16	C17
33	C15	C16	C17	C18
34	C16	C17	C18	C19
35	C17	C18	C19	C20
36	C18	C19	C20	C21

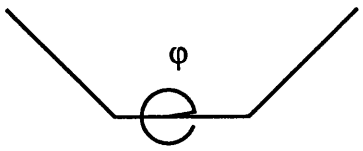

5.2.3. Cholesterol Torsion Angles

Torsion Angles				
ϕ_n	T_1	T_2	T_3	T_4
1	C15	C16	C19	C21
2	C16	C19	C21	C22
3	C19	C21	C22	C23
4	C21	C22	C23	C24
5	C22	C23	C24	C25

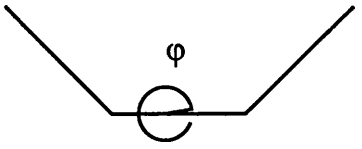

5.2.4. DLPC Non-Bonded Internal Angles

Angles			
θ_n	A_1	A_2	A_3
1	N	P	C6
2	C19	C6	C31
3	N	C6	C31
4	N	C6	C19

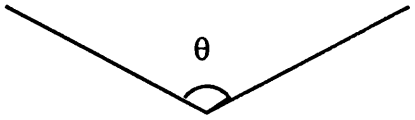

5.2.5. DMPC Non-Bonded Internal Angles

Angles			
θ_n	A_1	A_2	A_3
1	N	P	C6
2	C21	C6	C35
3	N	C6	C35
4	N	C6	C21

5.2.6. Cholesterol Non-Bonded Internal Angles

Angles			
θ_n	A_1	A_2	A_3
1	C2	C16	C24

5.2.7. DLPC Non-Bonded Internal Distances

Defined internal NB distances.

Non-Bonded Internals		
NB_n	A_1	A_2
NB_1	N	P
NB_2	N	C6
NB_3	C6	C19
NB_4	C6	C31
NB_5	C8	C19
NB_6	C20	C31
NB_7	C19	C31

5.2.8. DMPC Non-Bonded Internal Distances

Defined internal NB distances.

Non-Bonded Internals		
NB_n	A_1	A_2
NB_1	N	P
NB_2	N	C6
NB_3	C6	C21
NB_4	C6	C35
NB_5	C8	C21
NB_6	C22	C35
NB_7	C21	C35

5.2.9. Euler Angles

The Euler angles for DLPC and DMPC.

Euler Angle Atoms				
E_n	A_1	A_2	A_3	A_4
E_1	BN	C6	C5	

Euler Angle Atoms				
E_2	C6	C5	O3	
E_3	C5	O3	P	

These atoms define the Euler angles, comparable with NMR measurements. BN refers to the angle measured with respect to the bilayer normal cell axis.

5.2.10. DLPC Segmental Order Parameter

C - D pair lists.

Segmental Order Parameter Pairs		
S_n	A_1	A_2
Sn1		
S_1	C9	H91,H92
S_2	C10	H101,H102
S_3	C11	H111,H112
S_4	C12	H121,H122
S_5	C13	H131,H132
S_6	C14	H141,H142
S_7	C15	H151,H152
S_8	C16	H161,H162
S_9	C17	H171,H172
S_{10}	C18	H181,H182
S_{11}	C19	H191,H192,H193
Sn2		

Segmental Order Parameter Pairs		
S_1	C21	H211,H212
S_2	C22	H221,H222
S_3	C23	H231,H232
S_4	C24	H241,H242
S_n	A_1	A_2
S_5	C25	H251,H252
S_6	C26	H261,H262
S_7	C27	H271,H272
S_8	C28	H281,H282
S_9	C29	H291,H292
S_{10}	C30	H301,H302
S_{11}	C31	H311,H312,H313

5.2.11. DMPC Segmental Order Parameter

C - D pair lists.

Segmental Order Parameter Pairs		
S_n	A_1	A_2
Sn1		
S_1	C9	H91,H92
S_2	C10	H101,H102
S_3	C11	H111,H112
S_4	C12	H121,H122
S_5	C13	H131,H132
S_6	C14	H141,H142
S_7	C15	H151,H152
S_8	C16	H161,H162
S_9	C17	H171,H172
S_{10}	C18	H181,H182
S_{11}	C19	H191,H192
S_{12}	C20	H201,H202
S_{13}	C21	H211,H212,H213
Sn2		
S_1	C23	H231,H232
S_2	C24	H241,H242

Segmental Order Parameter Pairs		
S_n	A_1	A_2
S_3	C25	H251,H252
S_4	C26	H261,H262
S_5	C27	H271,H272
S_6	C28	H281,H282
S_7	C29	H291,H292
S_8	C30	H301,H302
S_9	C31	H311,H312
S_{10}	C32	H321,H322
S_{11}	C33	H331,H332
S_{12}	C34	H341,H342
S_{13}	C35	H351,H352,H353

5.2.12. Cholesterol Segmental Order Parameters

C - D pair lists.

Segmental Order Parameter Pairs		
S_n	A_1	A_2
S_1	C19	H19
S_2	C21	H211,H212
S_3	C22	H221,H222
S_4	C23	H231,H232
S_5	C24	H241
S_6	C26	H261,H262,H263

5.3. Intermolecular Properties

5.3.1. Radial Distribution Functions

In order to study the effect of the bilayer on the solvent structure and dynamics, the radial distribution function of water oxygens has been calculated relative to the following atoms. The resulting radial distribution function is the ensemble average and average over all such atoms in the bilayer.

Radial Distribution Functions	
A_1	Type
	DLPC and DMPC
O,O3	phophate ether oxygen
O1,O2	phosphate charged oxygen
O4,O6	glycerol ether oxygens
O5,O8	carbonyl oxygens
	Cholesterol
OH	cholesterol hydroxyl oxygen
	Water
O1	water oxygen

The pairwise radial distribution function for all water oxygens is measured and the pairwise heavy atom radial distribution function in the mixed DLPC and cholesterol bilayer models.

5.3.2. DLPC and DMPC Hydrogen Bonds

These atoms are hydrogen bond acceptor atoms within the DLPC and DMPC molecules. The water hydrogens are searched on a distance only criteria (2.5 Å).

Hydrogen bond acceptor atoms	
A_1	O
A_2	O1
A_3	O2
A_4	O3

Hydrogen bond acceptor atoms	
A_5	O4
A_6	O5
A_7	O6
A_8	O7

Hydrogen bonds acceptors are the water hydrogen ("h*") and cholesterol hydroxyl hydrogen ("ho").

5.3.3. Cholesterol Hydrogen Bonds

There are hydrogen bond donor and acceptor atoms within the cholesterol molecule. The water hydrogen are searched on a distance only criteria (2.5 Å).

Hydrogen bond donor and acceptor atoms	
A_1	OH
D_1	HO

Hence both the water hydrogen bond donating atom ("h*") and the acceptor atom ("o*") must be selected and differentiated.

5.3.4. Water Hydrogen Bonds

Hydrogen bond donor and acceptor atoms	
A_1	O1
D_1	H11,H12

Where more than one hydrogen bond acceptor or donor atom exists the property is given as a linear list atoms, each type sequentially. This is then refered to as the atom index.

5.4. Thermal Properties

5.4.1. Component Temperature

In these multi-component systems, which are non-isotropic and contain areas of relatively high and low charge, it is important to check the partitioning of kinetic energy within the system. The temperature of the water, cholesterol and lipid are calculated (Eqn 3.1.15) at regular intervals across the trajectory. The ensemble average can also be calculated. Phospholipid molecules contain moieties of high (PC) and low (acyl chains) charge density. The temperature of each moiety (PC, glycerol, Sn1 and Sn2 chains) was calculated from their atomic velocities.

5.4.2. Methylene Temperature

The ensemble average of the acyl chain methylene units is calculated from the velocities of each unit, in a similar manner to the segmental order parameters. The Sn1 and Sn2 chains are differentiated, as is the cholesterol acyl chain. These values are used to examine the kinetic energy distribution within the acyl chain and rationalize the segmental order parameters.

5.5. Distribution

A number of properties of the system vary with the bilayer normal. These reflect both the integrity of the bilayer structure and the transport properties of the bilayer.

5.5.1. Density profiles

The distribution of atomic density along the bilayer normal is calculated for each of the two monolayers, and subcomponents of the bilayer system. The distribution of the water can therefore be examined as well as the diffusion of water from its starting position. The penetration of water into the hydrophilic region of the bilayer can also be followed. The density distribution of the acyl chains, glycerol and phosphatidylcholine groups of the phospholipid may be determined with respect to the bilayer normal. This can be used to examine the stability of the bilayer as the trajectory is sampled, elucidating any changes in acyl chain density.

The coordinate system is partitioned into its subcomponents (lipid, cholesterol and water). This improves the efficiency of analysis with respect to the density profile as well as other component specific properties.

5.5.2. Electrostatic Potential

The surface potential experienced by a +1 charged particle passing from one side of the membrane to the other along the bilayer normal can be calculated. The contribution from the partial charges of subcomponents of the system can be determined. In this study all partial charges are used in the calculation.

6. DMPC Bilayer Models

6.1. System I dmpc (18xDMPC)

The bilayer model dmpc consisting of 18 DMPC molecules in the A crystal structure conformation was constructed.[1] A regular 3x3 lattice in the xz plane was used, the bilayer normal lying along the y axis. Lattice points are separated by 9.0Å in x and z. A copy of this monolayer was then rotated 180° and translated such that a separation of 2.0Å is created between adjacent lipid chains, forming the other envelope of the bilayer. The mean distance between the two planes containing the phosphate P is 46.4Å (See Table 4.2). The resulting coordinates were then minimised and used as the starting configuration for sampling the molecular dynamics trajectory (See Table 4.4).

The molecular dynamics trajectory was sampled from the NPT ensemble (See Table 4.4) for 260ps. The bilayer normal unit cell vector B was expanded to 61.1Å, to remove interactions between head groups and their periodic images.

6.1.1. Thermodynamics and Energetics

Figure 6.1.1 contains the extracted thermodynamics information. There is a large reduction in the volume of the unit cell of 60% (from 50971Å^3 to 20313Å^3) in 8ps. This is a consequence of the time constant used for the pressure scaling (80ps). This volume reduction was non-isotropic, the bilayer normal (B vector) reducing by 35.4%, and the other two vectors (A and C) by 32.7% and 20.2% respectively. This reflects the dominance of the pressure scaling algorithm by the starting configuration and the difficulty of building a model with isotropic density distribution. The large reduction of the bilayer normal unit cell vector was expected, a vacuum existing above and below the lipid coordinates in the unit cell reduces the pressure in that direction causing the unit cell vector to reduced to compensate. After 50ps the system appears to have reached equilibrium in terms of the pressure scaling algorithm, the unit cell vectors reaching average values of A=20.82±0.18Å, B=39.50±0.48Å. C=23.79±0.27Å, giving an average volume of 20689±153Å^3.

The temperature of the system and hence kinetic energy was constrained and result in an average value of 309.6±3.8K. There is a significant contribution to the potential energy of the system from the internal energies: the bond and theta energies increase while the system

reaches equilibrium, and the torsion energy decreases. This indicates that energy is being transferred from the torsion modes into the angle bending and bond stretching modes. The relative energies are not however large. E_b increases from 73.6kcal/mol to ≈ 800kcal/mol in 40ps, reaching an average value of 757.5±19.3kcal/mol, and E_θ increases from 1035.8kcal/mol to ≈1040kcal/mol in 40ps, reaching an average value of 1048.6±20.4kcal/mol. E_ϕ increases from 200.0kcal/mol to 504kcal/mol in the first pecosecond of the trajectory and then decreases to an average of 440.5±12.8kcal/mol.

The standard deviations of the relative energy components (Table 6.1.1) indicate that the electrostatic energy of the system is dominating the potential energy.

Table 6.1.1

Energy Components (kcal/mol) dmpc			
Energy	Average	SD	%SD
E_b	757	19	2.5
E_θ	1049	21	2.0
E_ϕ	440	13	3.0
E_{rep}	3852	35	1.0
E_{dsp}	-5373	42	0.7
E_{est}	-1005	135	13.4

All averages and SD over sampled range (50-260ps).

The form of the potential energy of the system matches that of the electrostatic energy. This may be a consequence of the pressure scaling, because the scaling of the unit cell vectors and repositioning of the coordinates of each molecule preferentially increases the electrostatic energy relative to other non-bond energies, which is a direct consequence of the inverse relationship between the electrostatic energy and separation r. However an examination of the energetics of the bilayer model dlpc (See Chapter 7.1) indicates that even when sampling the NVT ensemble, the potential energy is dominated by the electrostatic contribution.

Figure 6.1.1a

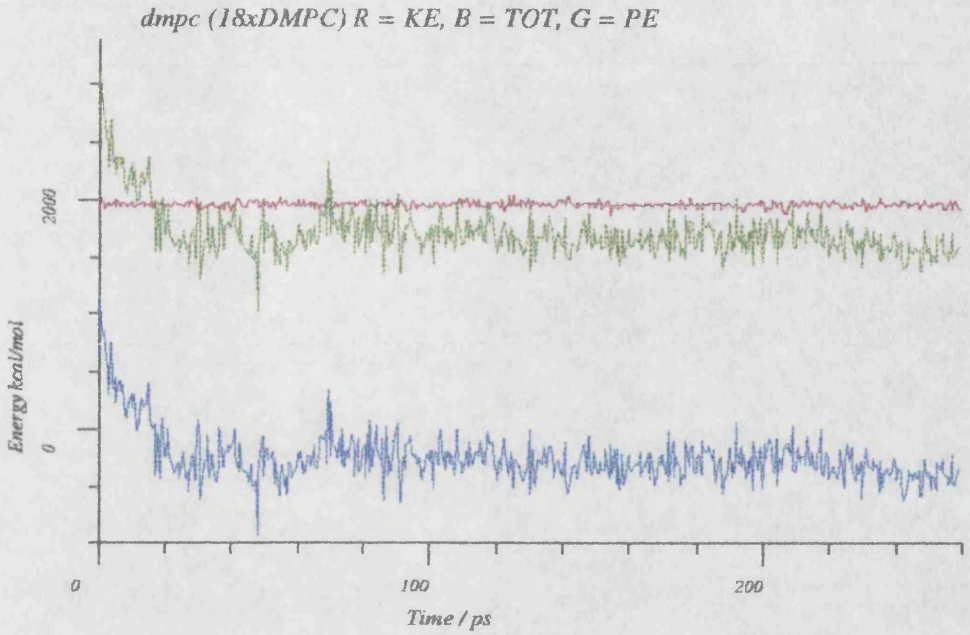
dmpc (18xDMPC) R = KE, B = TOT, G = PE
2000
0
Energy kcal/mol
0
100
200
Time / ps

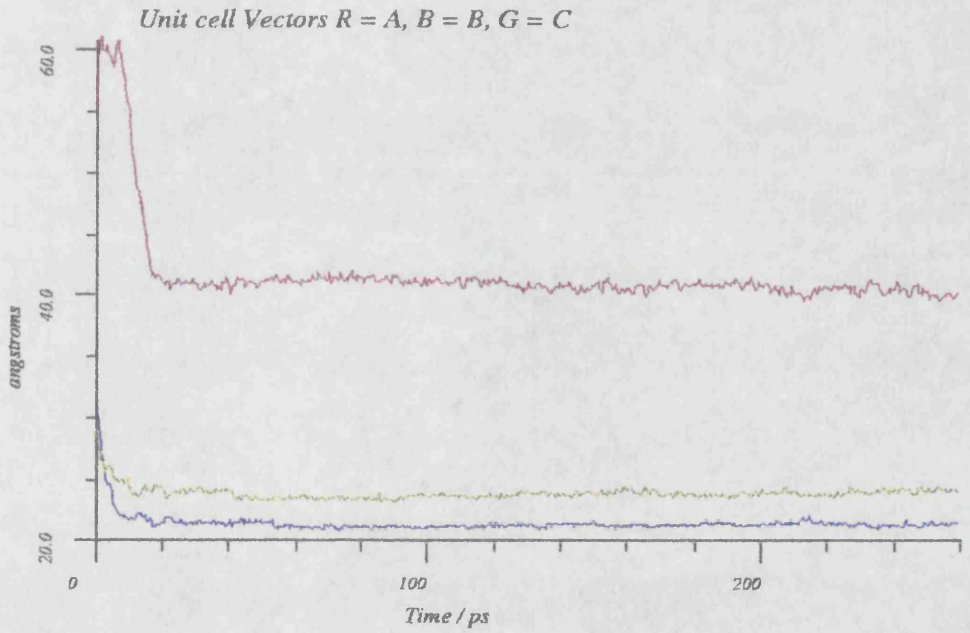
Unit cell Vectors R = A, B = B, G = C
60.0
40.0
20.0
angstroms
0
100
200
Time / ps

Figure 6.1.1b

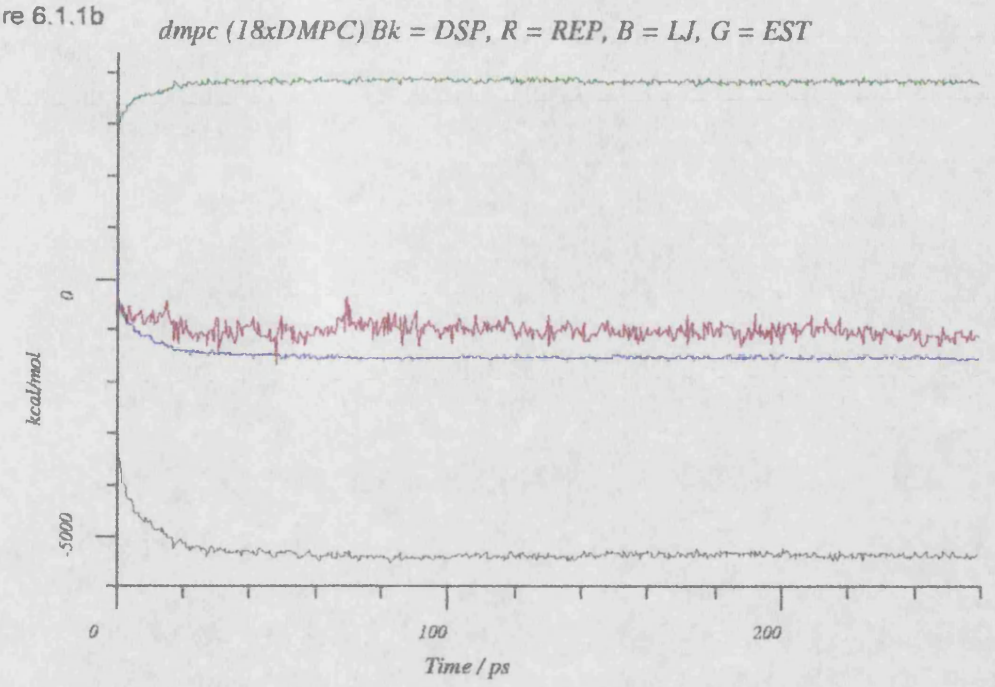
dmpc (18xDMPC) Bk = DSP, R = REP, B = LJ, G = EST
kcal/mol
0
-5000
0
100
200
Time / ps

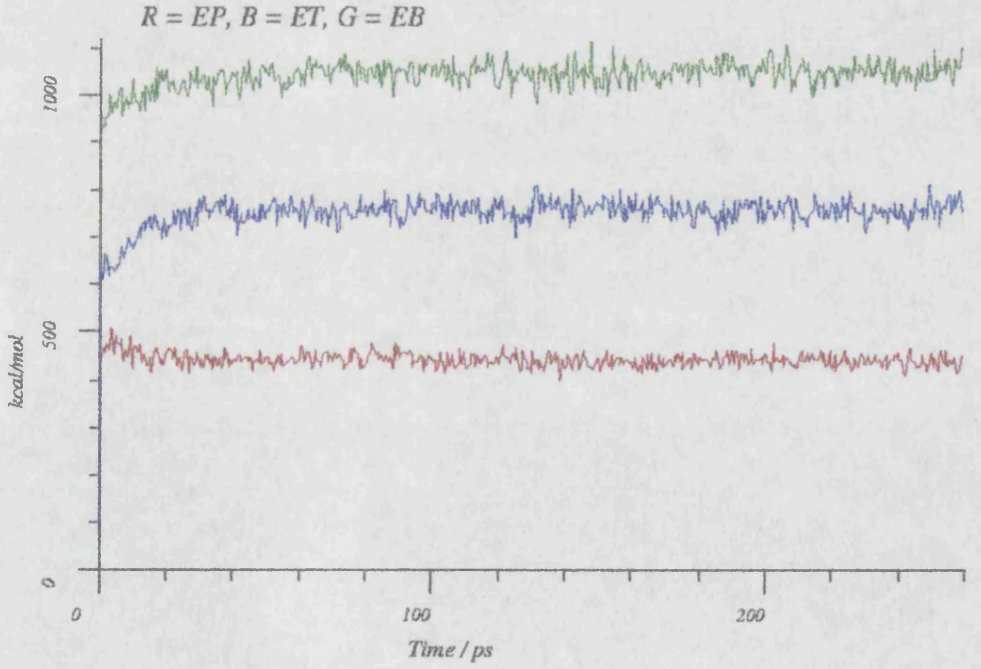
R = EP, B = ET, G = EB
kcal/mol
1000
500
0
0
100
200
Time / ps

Figure 6.1.2

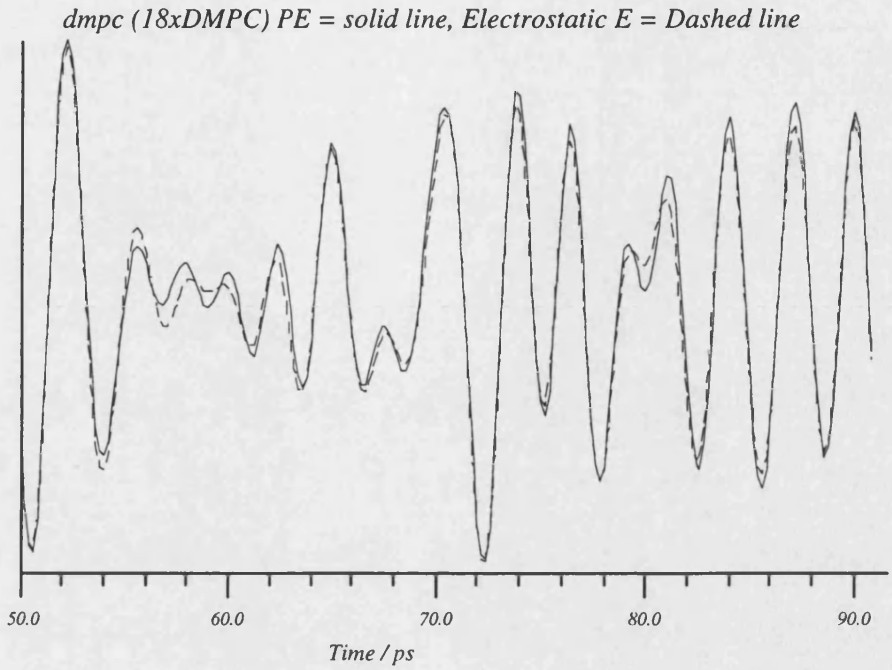

The relationship between E_{est} and PE has been further explored, using fourier transformation and filtering of the energy function with respect to time. The energies of the system are filtered to remove frequencies higher than $20cm^{-1}$. This removes the high frequency "noise" and makes interpretation of the energies easier. The relationship between the PE and E_{est} can be clearly demonstrated from Figure 6.1.2, the superimposition of E_{est} and PE. Clearly the general form of the potential matches that of the electrostatic energy.

Examination of the filtered pressure of the system indicates that there is an anti-correlation between the electrostatic energy and the potential energy of the system. The pressure of the system varies around an average of 78±800bar for the 50-260ps sampled range. This suggests that the correlation time for the pressure will be extremely large, in the order of nanoseconds. The variation of the pressure increases as the unit cell vectors are reduced, another indication that the electrostatics of the system are dominating the potential energy. The scaling of the cell vectors and the corresponding contraction of the system causes a large increase in the coulombic interaction, increasing the energy and causing the pressure to increase. This motion can be thought of as a "phonon" vibration in the unit cell. This is an artifact of the coarse nature of the pressure algorithm used. It should however be noted that

pressure has a large correlation time even in NVE ensemble trajectories. The pressure is "isotropic" in the plane of the bilayer (P_y = 119.3bar P_z = 120.7bar). The pressure component in the bilayer normal direction is 78.0bar. Phospholipid bilayers, whilst not being isotropic in all three directions, have been observed to exhibit some two dimensional "isotropy".[2] However this comparison is not significant due to the large standard deviation for these pressures.

6.1.2. Density Profiles

The distribution of density along the bilayer normal can be seen from density profile plots. Figure 6.1.3a contains the density distribution over the first ps of the trajectory and Figure 6.1.3b contains the density distribution over the final 10ps of the sampled trajectory. These illustrate that the PC head group of the DMPC molecule is of highest density, 1.0g/mol, and the acyl chains are approximately 0.4g/mol. This is less dense than that expected for liquid paraffin (0.775g/mol), which is a consequence of the free volume available to each lipid acyl chain in the initial coordinates of the model. This is further illustrated by the relative densities of the DMPC moieties. Clearly the glycerol and PC are much denser than the acyl chains. This model is consistent with electron density maps from X-ray studies.[3-5] The density of the acyl chain region increases to reach a value of approximately 0.7g/mol. The acyl chain density decreases near the centre of the hydrophobic region. Interdigitation of the two monolayers is observed at about 4Å either side of the centre of the bilayer. The density of the Sn2 chain decreases near the centre of the bilayer, but the Sn1 chain increases in density. This is a consequence of the turn in the Sn1 Chain (C23) of the DMPC(A) crystal structure. The Sn2 chain penetrating further into the other monolayer. The density of the PC and glycerol moieties is "smeared" compared with the starting conformation, indicating translation along the bilayer normal during the trajectory. This may be an artifact of the pressure scaling. The contraction of the system in the bilayer normal direction brings the charged PC groups into close proximity across the periodic system. This is in contrast to experimental systems, in which the PC interactions are shielded by the inter-lamella water.

Figure 6.1.3a

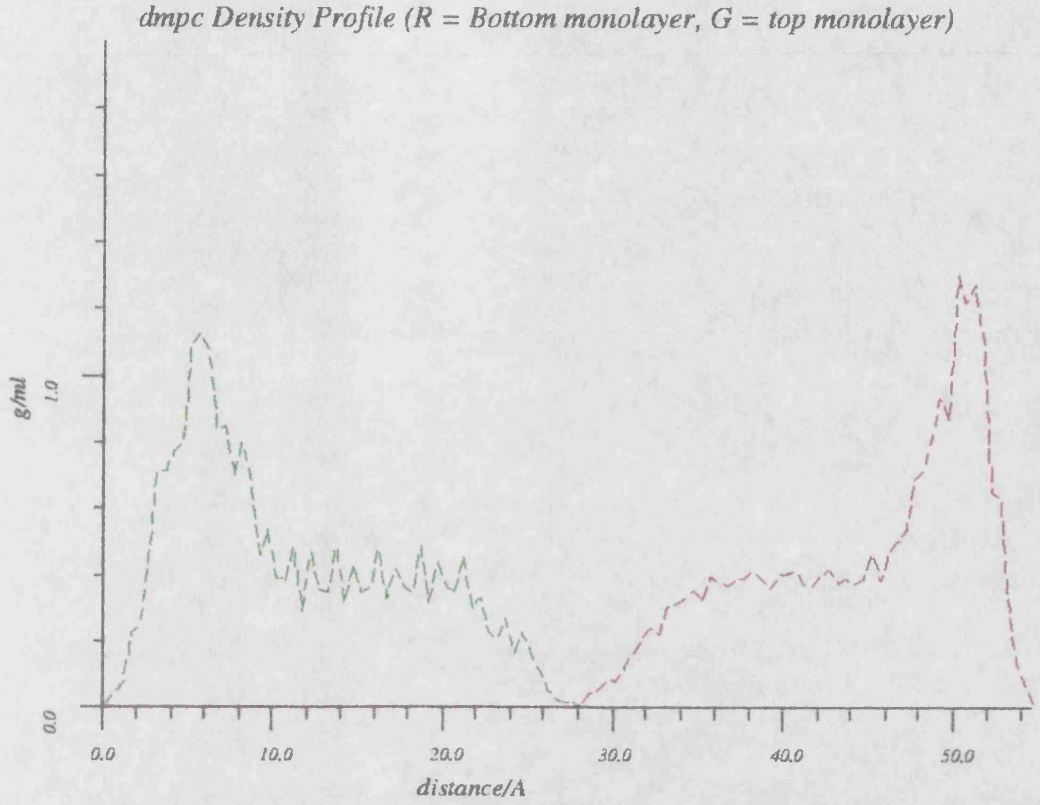
dmpc Density Profile (R = Bottom monolayer, G = top monolayer)
g/ml
1.0
0.0
0.0
10.0
20.0
30.0
40.0
50.0
distance/A

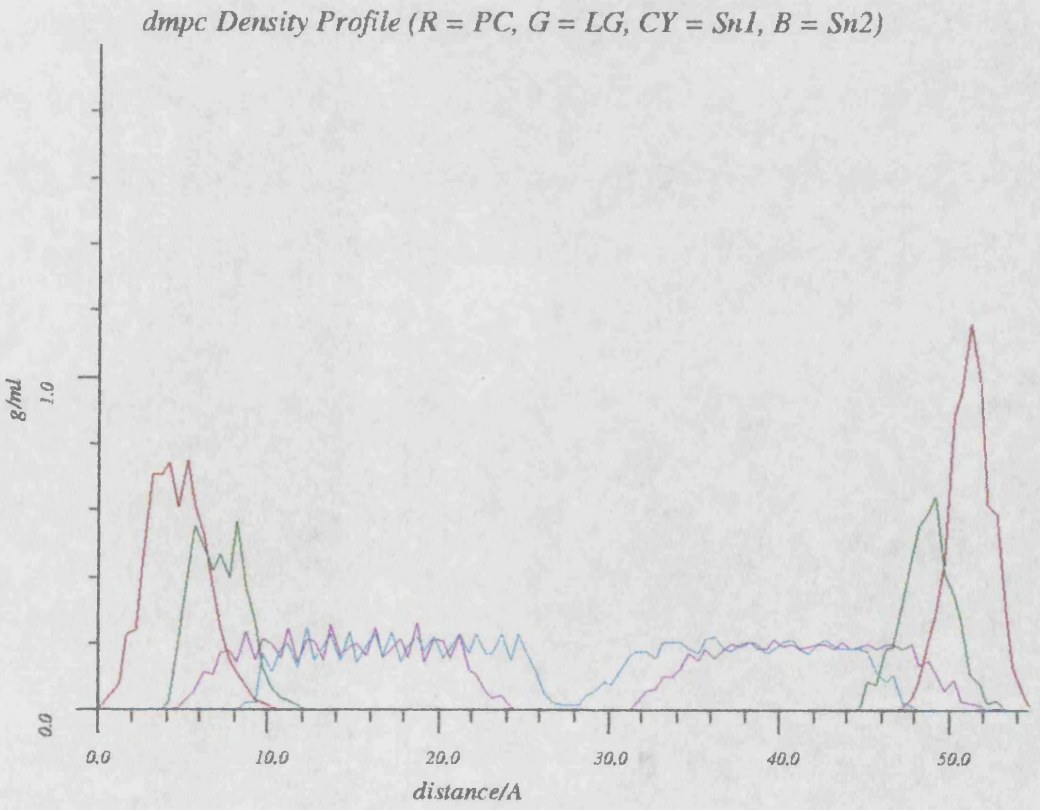
dmpc Density Profile (R = PC, G = LG, CY = Sn1, B = Sn2)
g/ml
1.0
0.0
0.0
10.0
20.0
30.0
40.0
50.0
distance/A

Figure 6.1.3b

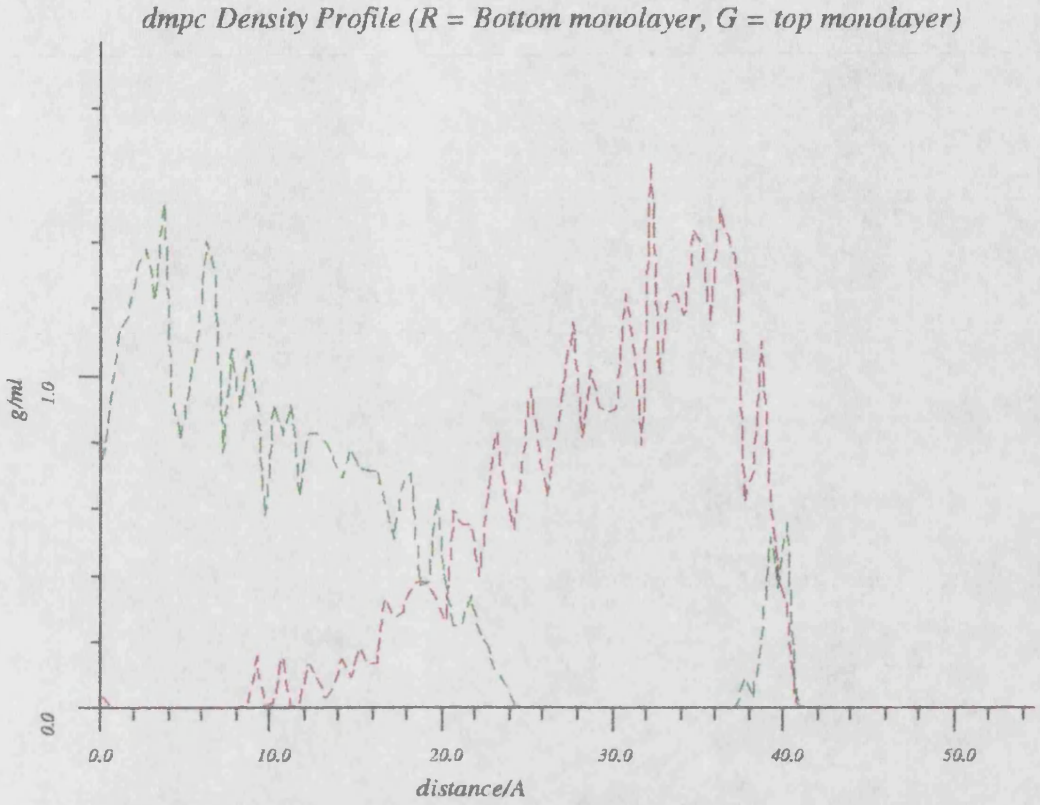
dmpc Density Profile (R = Bottom monolayer, G = top monolayer)
g/ml
1.0
0.0
0.0
10.0
20.0
30.0
40.0
50.0
distance/A

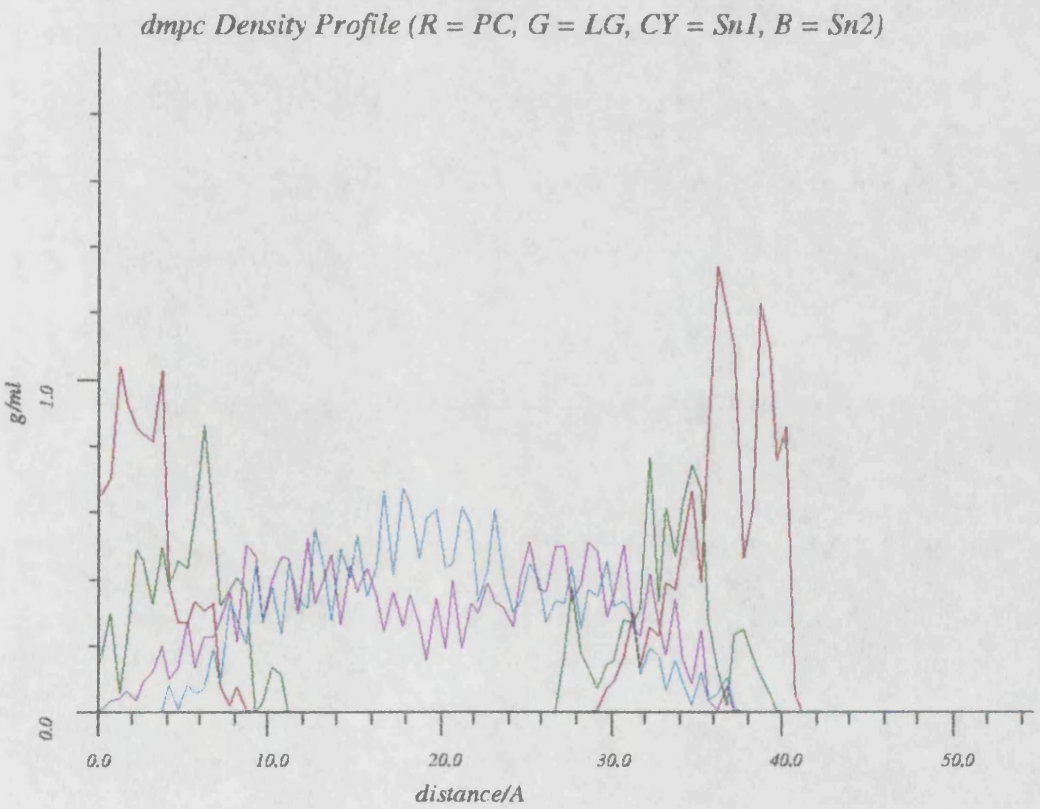
dmpc Density Profile (R = PC, G = LG, CY = Sn1, B = Sn2)
g/ml
1.0
0.0
0.0
10.0
20.0
30.0
40.0
50.0
distance/A

6.1.3. Non-Bonded Internals

In order to examine the dynamics of the DMPC molecule a series of internal geometries have been defined (Chapter 5).

From an analysis of the internal non-bonded angles (Chapter 5), the conformational freedom of the DMPC molecule can be probed. In Table 6.1.2 it can be seen that the majority of conformational freedom can be assigned to variation of the angle C21-C6-C35. This "scissor" action is consistent with the variation in the distance between the two terminal carbons. This angle varies considerably in the first 40ps of the simulation, as each molecule adjusts to the position of other molecules within each bilayer. This results in a range of values for the angles, although the variation of each angle once at equilibrium is relatively small. This cooperativity of lipid molecules is a general feature of such systems.

Table 6.1.2

Non-Bonded Angles dmpc			
	Av	SD	SDav
θ_1	96.2	7.7	24.5
θ_2	21.6	3.4	8.8
θ_3	111.5	7.7	26.5
θ_4	105.1	7.7	25.6

where θ is the average angle, and SD is the average standard deviation and SDav is the standard deviation of the average values.

From the internal non-bonded distances defined (Table 6.1.3), it is clear that there is not significant conformational freedom in the DMPC molecule. There is however some variation in the conformation of individual molecules in the bilayer, although the variation of that conformation is small across the trajectory. This can be seen from the standard deviation for the non-bonded distances within DMPC. The majority of conformational freedom appears to be in the motion of the head group relative to the glycerol backbone and in the "scissor" action of the acyl chains. A comparison between the relative variation of the Sn1 and Sn2 chains (C6-C21 and C6-C35) indicates that there is more conformation freedom in the Sn1 chain relative to the Sn2 chain. This is opposite to that generally observed in phospholipids. However the conformation of DMPC(A) contains a turn at C23 of the Sn1 chain. This is in contrast to the conformation of most phospholipids in which the turn is in the Sn2 chain. Hence there is

Table 6.1.3

Non-bond Distances (Å) dmpc			
Atoms	D	SD	SDav
N P	5.1	0.2	0.2
N C6	6.4	0.4	1.0
C6 C21	18.2	0.3	0.3
C6 C35	15.8	0.5	0.9
C8 C21	16.4	0.2	0.1
C22 C35	15.7	0.2	0.2
C21 C35	6.9	0.9	2.4

where D is the average non-bonded distance, SD the average standard deviation for that distance and SDav is the standard deviation of the averages.

more conformational similarity between the Sn1 chain of DMPC(A) to the Sn2 chain of most phospholipids.

There is no significant shortening of the acyl chains over the trajectory, only a small variation in length of the Sn1 and Sn2 chains (1.0%,1.3% respectively) being observed. This indicates little, if any, torsional freedom in the acyl chains.

6.1.4. Torsion Angles

The values of all torsions defined (See Chpt 5) in all bilayer DMPC molecules have been calculated across the sampled trajectory. The distribution of torsion values has been examined, and their ensemble average calculated. As indicated by the non-bonded angles and distances, the acyl chains exist in only the trans conformation. There is only small variation in the torsion angles of the Sn1 and Sn2 chains (SD $< 10,^{\circ}$ Table 6.1.4). There is therefore no gauche population. Increased torsional freedom is observed in torsions around the phosphate group and those in the glycerol backbone (SD $\approx 20^{\circ}$). Whilst the variation in individual torsions is small there is a range of different values in all molecules in the bilayer. This suggests that each molecule adjusts its conformation in response to its neighbouring molecules through flexibility of these torsions rather than those in the acyl chain.

Table 6.1.4

SD of Torsions dmpc					
	SD	avSD		SD	avSD
ϕ_1	6.0	0.3	ϕ_2	6.0	0.5
ϕ_3	31.5	13.3	ϕ_4	25.2	16.2
ϕ_5	18.6	10.2	ϕ_6	18.1	10.0
ϕ_7	5.6	0.5	ϕ_8	5.5	0.5
ϕ_9	19.9	7.8	ϕ_{10}	8.3	1.0
ϕ_{11}	21.1	7.7	ϕ_{12}	5.7	0.3
ϕ_{13}	5.5	0.3	ϕ_{14}	5.5	0.3
ϕ_{15}	5.3	0.3	ϕ_{16}	5.3	0.4
ϕ_{17}	5.2	0.3	ϕ_{18}	5.3	0.4
ϕ_{19}	5.3	0.3	ϕ_{20}	5.3	0.3
ϕ_{21}	5.4	0.2	ϕ_{22}	5.5	0.1
ϕ_{23}	22.8	15.2	ϕ_{24}	9.0	1.9
ϕ_{25}	28.2	18.9	ϕ_{26}	5.6	0.4
ϕ_{27}	5.4	0.3	ϕ_{28}	5.4	0.4
ϕ_{29}	5.3	0.4	ϕ_{30}	5.3	0.4
ϕ_{31}	5.3	0.3	ϕ_{32}	5.3	0.3
ϕ_{33}	5.3	0.3	ϕ_{34}	5.4	0.2
ϕ_{35}	5.4	0.2	ϕ_{36}	5.5	0.2

where SD is the standard deviation of the average torsion values and avSD is the average standard deviation or all molecules.

6.1.5. Segmental Order Parameters

The segmental order parameters of the acyl chains have been calculated for the sampled trajectory, with respect to the bilayer normal. These indicate the order of the system. Figure 6.1.4 shows the ensemble average order parameters of the Sn1 and Sn2 chains. These reflect the variation in orientation of the acyl chains with respect to the bilayer normal rather than the torsional disorder, or liquid like disorder measured in experimental systems. They do however show some similarity to the experimental results and may indicate the effect of orientation on the results. The Sn2 chain is more ordered than the Sn1 chain. This is

specific to the DMPC(A) conformation. The chain with no turn at the second carbon segment is generally the more ordered in the order parameter profile. The Sn1 chain shows the characteristic low order at the C2 position caused by its turn. The general form and value of the order parameter of the two chains does not match that of the experiment.

6.1.6. Average Temperatures

In an attempt to probe the reasons for the lack of conformational freedom in the acyl chain region of the bilayer model, the distribution of atomic temperatures has been calculated. Figure 6.1.5 shows the ensemble average temperature of the acyl chains, glycerol and PC moieties. The PC and glycerol groups are on average of higher temperature (314.1±16.2K and 313.9±10.5K respectively). than the two acyl chains (Sn1 306.9±8.3K and Sn2 307.3±8.7K). This may be due to the increased coulombic interactions in the head group relative to the acyl chains. Phospholipids are by nature amphiphilic and therefore can be rationalised as a two component molecule. Hence they have a densely charged head group component (hydrophilic) and a relatively charge diffuse acyl chain component (hydrophobic).

Table 6.1.5

Average Temperatures (K) dmpc		
	T	SD
PC	313.9	10.5
GL	314.1	16.2
Sn1	306.9	8.3
Sn2	307.3	8.7

This temperature differential within a molecule is not unexpected as, temperature factors from X-ray crystallographical studies of proteins indicate a temperature variation with sequence. The extent of temperature variation observed in this simulation is however surprising.

Figure 6.1.4

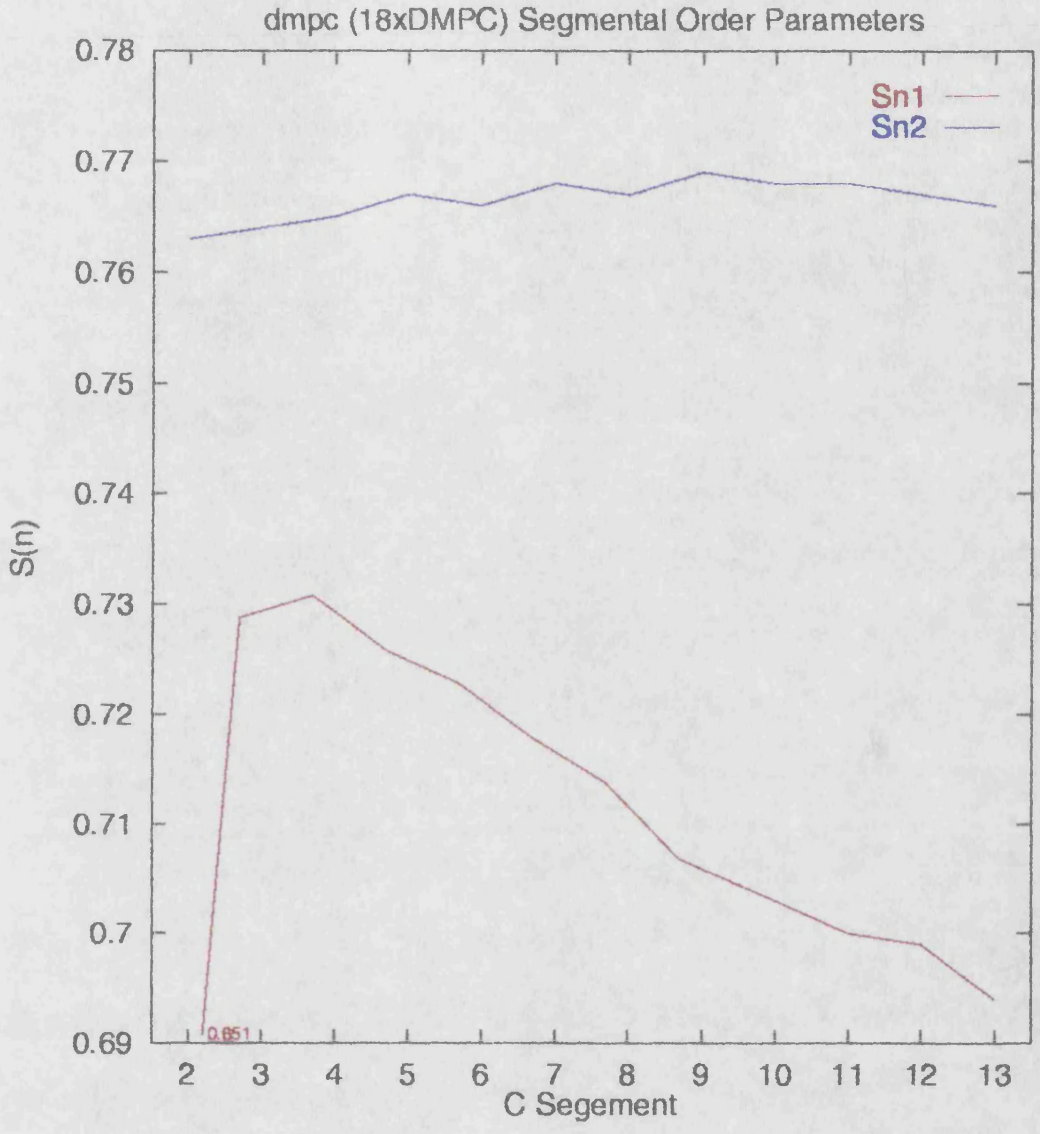

Figure 6.1.5

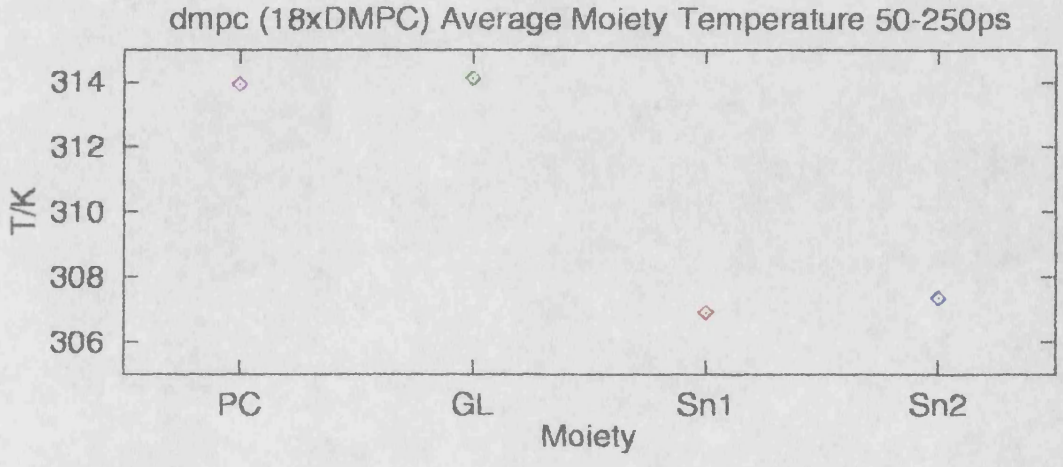

6.2. System II dmpc_i (18xDMPC)

In an attempt to investigate the effect of interdigitation of the acyl chains in these phospholipids bilayers, a bilayer of 18 DMPC molecules in the crystal structure A conformation was constructed. The two monolayers were then interdigitated, translating the upper monolayer along the bilayer normal (7Å), but being careful not to introduce van der Waals overlap.

These coordinates were then minimised and used as the starting configuration to sample 100ps of molecular dynamics trajectory from the NPT ensemble (Table 4.4).

6.2.1. Thermodynamics and Energetics

Figure 6.2.1 shows the extracted thermodynamics and energies from the trajectory. The volume of the system decreases rapidly over the first 2ps of the trajectory due to the reaction of the unit cell vectors to the high pressure of the initial configuration. The bilayer normal unit cell axis increases from 38.7Å to 48.3Å in 10ps. This becomes dominated by the contraction of the other two axes, resulting in decreased volume. The bilayer normal then reaches an average value of 48.0±0.1Å. The other two axes are, A 26.1±0.1Å and C 24.1±0.1Å. These give an average volume of the unit cell of 30556±237Å.

The temperature of the system is constrained, resulting in an ensemble average of 309.3±3.8K. The kinetic energy of the system was therefore also constrained, KE 1957.9±23.8kcal/mol. The potential energy of the system is dominated by the electrostatic energy. The form of the potential is exactly matched by that of the electrostatics. The system, although reaching equilibrium in terms of the volume of the system, still has considerable variation in the potential and electrostatic energies. The internal energies of the system mirror the trend in the non-interdigitated model. The bond and theta energies increase from the starting configuration, but the torsional energy is decreased.

Table 6.2.1

Energy Components (kcal/mol) dmpc_i			
	Av	SD	%SD
E_b	765	21	2.7
E_θ	1037	21	2.0
E_ϕ	416	20	4.8
E_{rep}	4034	50	1.2
E_{dsp}	-5813	76	1.0
E_{est}	-1316	259	19.7

The internal energies are very similar to those of the non-interdigitated bilayer. The dispersion and repulsion energies are increased due to the interdigitation of the acyl chains, increasing the interaction between adjacent chains. The reduced inter-phosphate distance is reflected in a decreased electrostatic energy. The system has not however reached equilibrium in terms of the electrostatic energy, which is indicated by a high standard deviation.

Figure 6.2.1

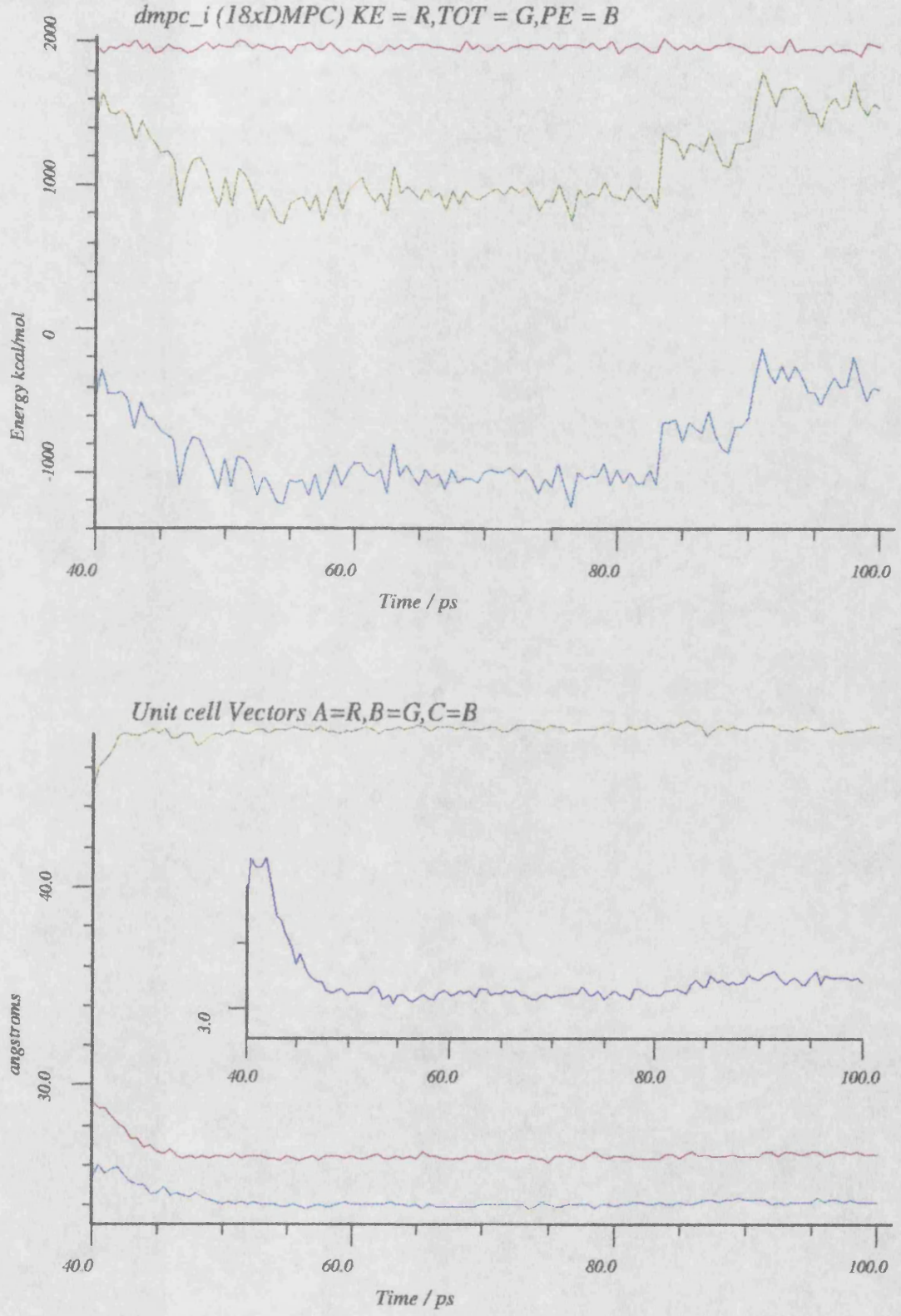
dmpc_i (18xDMPC) KE = R,TOT = G,PE = B
Energy kcal/mol
2000
1000
0
-1000
40.0
60.0
80.0
100.0
Time / ps
Unit cell Vectors A=R,B=G,C=B
angstroms
40.0
30.0
3.0
40.0
60.0
80.0
100.0
40.0
60.0
80.0
100.0
Time / ps

Figure 6.2.1b

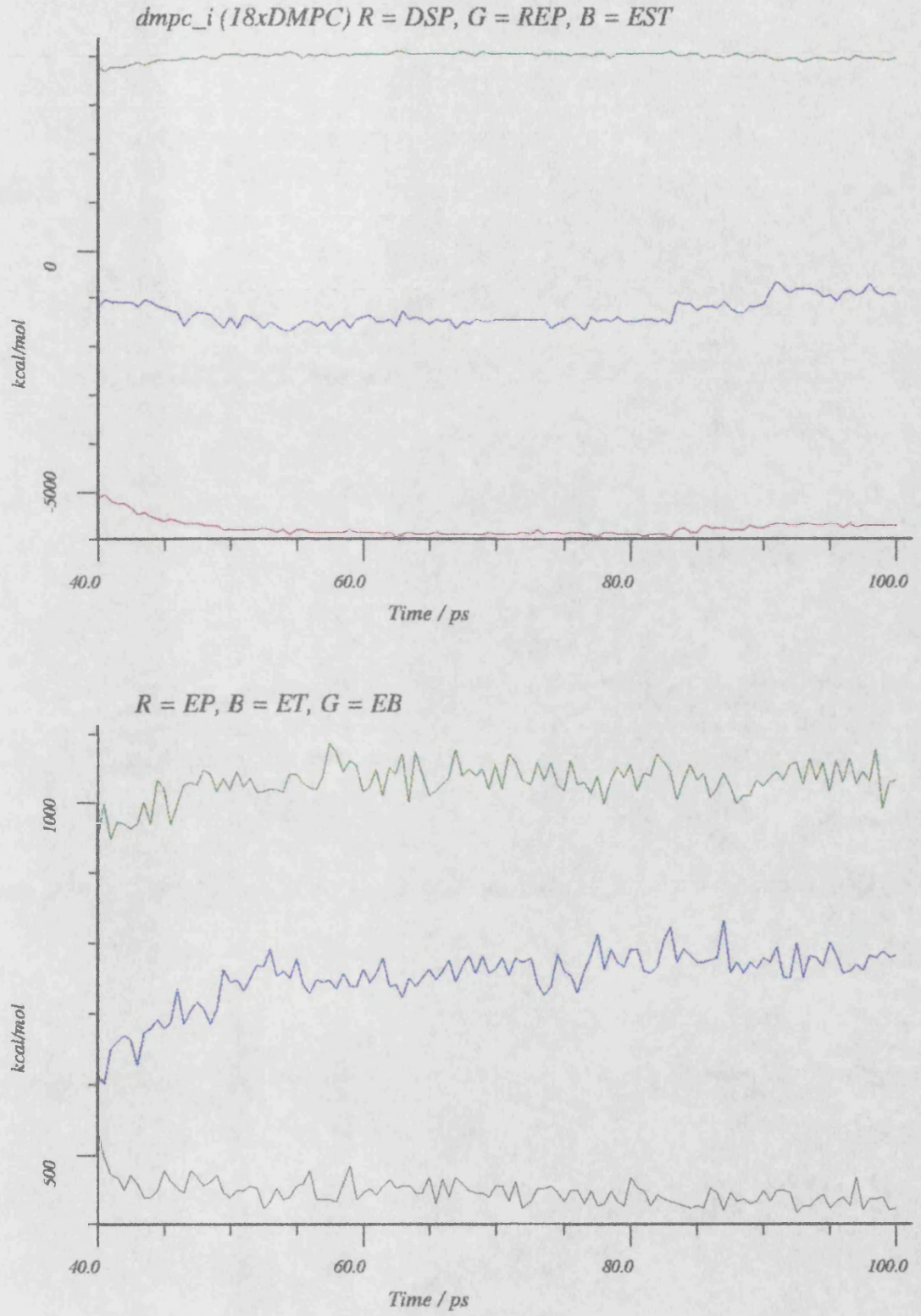
dmpc_i (18xDMPC) R = DSP, G = REP, B = EST
0
-5000
kcal/mol
40.0
60.0
80.0
100.0
Time / ps
R = EP, B = ET, G = EB
1000
500
kcal/mol
40.0
60.0
80.0
100.0
Time / ps

The pressure of the two systems is similar although comparison between the pressure of the two models is difficult, because the standard deviation is an order of magnitude larger than the pressure. The variation in pressure at each step is large when sampling a relatively small system.

6.2.2. Density Profile

Figure 6.2.2(a,b) shows the density distribution along the bilayer normal in the first 1000 steps and last 1000 steps respectively. For reasons of computational efficiency the coordinates are stored relative to the centre of the bilayer normal. Hence where a molecule or part of a molecule crosses the unit cell axis its coordinates appear on the other side of the unit cell. For this reason most bilayer model coordinates have been translated into the positive quadrant, removing this artifact of the calculation from the results. However this system's coordinates are not all in the positive quadrant. The PC separation is observed to decrease from 33.1Å to 26.6Å across the hydrophobic region. The density of the acyl chains increases from 0.34g/ml to 0.54g/ml over the trajectory. This is still lower than that expected in the liquid paraffin (0.775g/ml). The bilayer normal unit cell vector increases from an initial value of 38.7Å to 48.0Å over the trajectory, introducing a vacuum between the bilayers. This is surprising, because the decrease in potential energy of the system caused by interdigitation overwhelms the increased repulsive energy.

The density of the head group region is increased from 1.1g/ml to 1.6g/ml. This reflects the contraction of the system in the bilayer plane.

Figure 6.2.2a

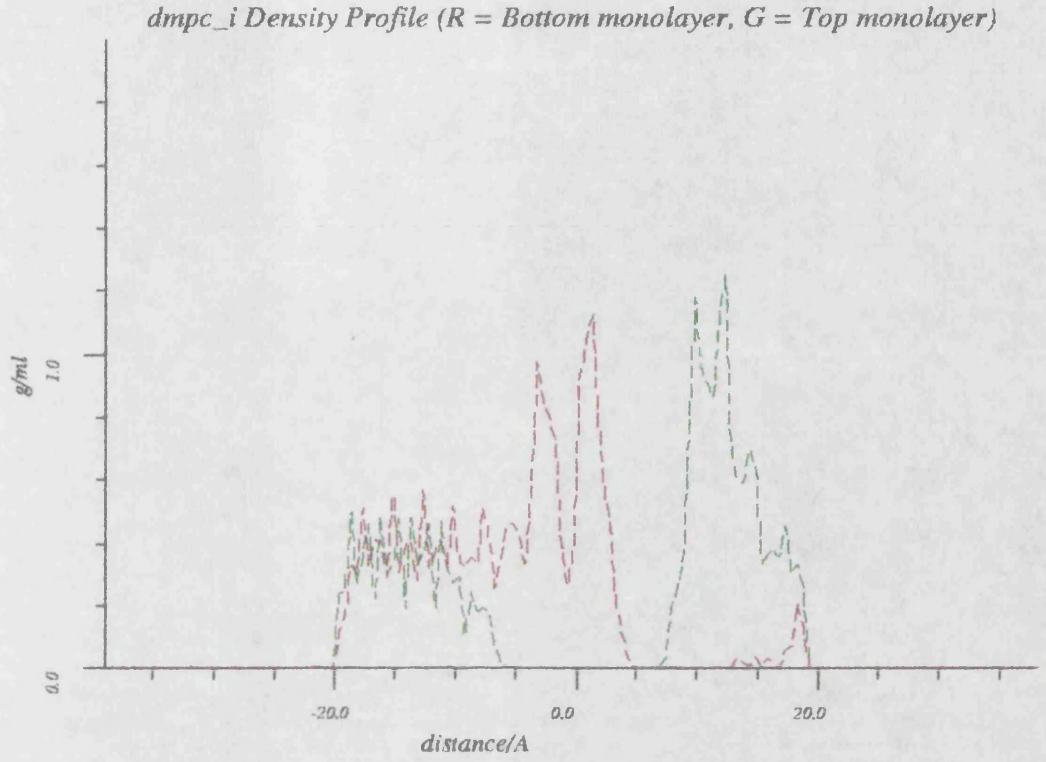
dmpc_i Density Profile (R = Bottom monolayer, G = Top monolayer)
g/ml
1.0
0.0
-20.0
0.0
20.0
distance/A

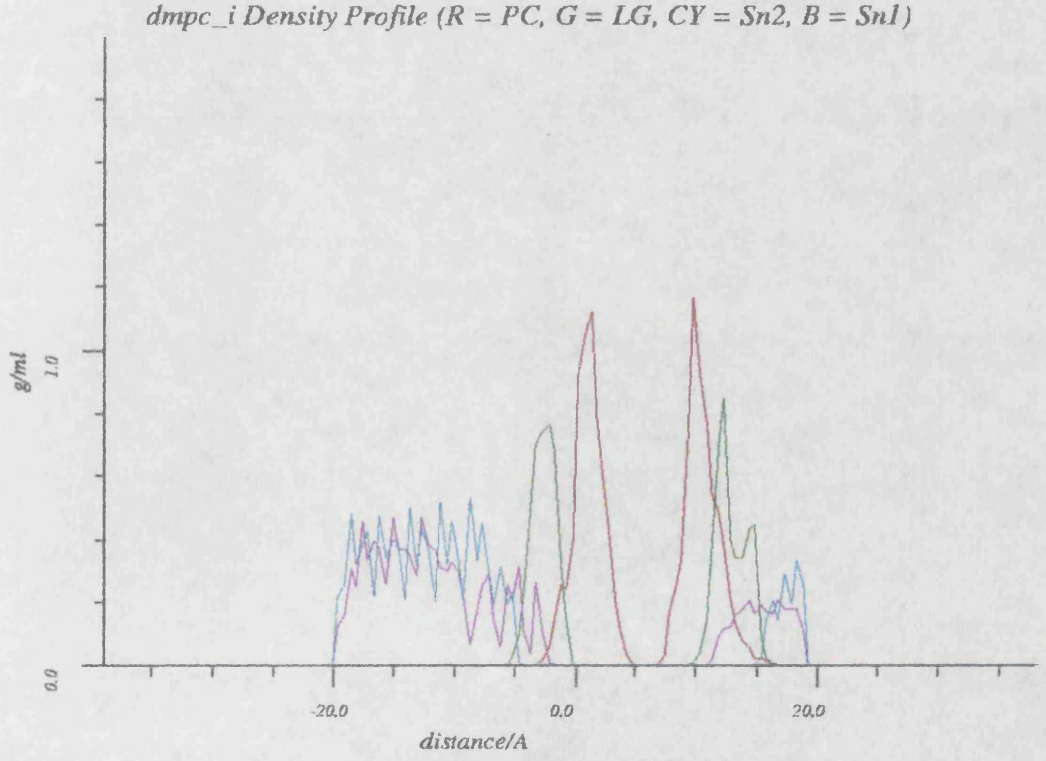
dmpc_i Density Profile (R = PC, G = LG, CY = Sn2, B = Sn1)
g/ml
1.0
0.0
-20.0
0.0
20.0
distance/A

Figure 6.2.2b

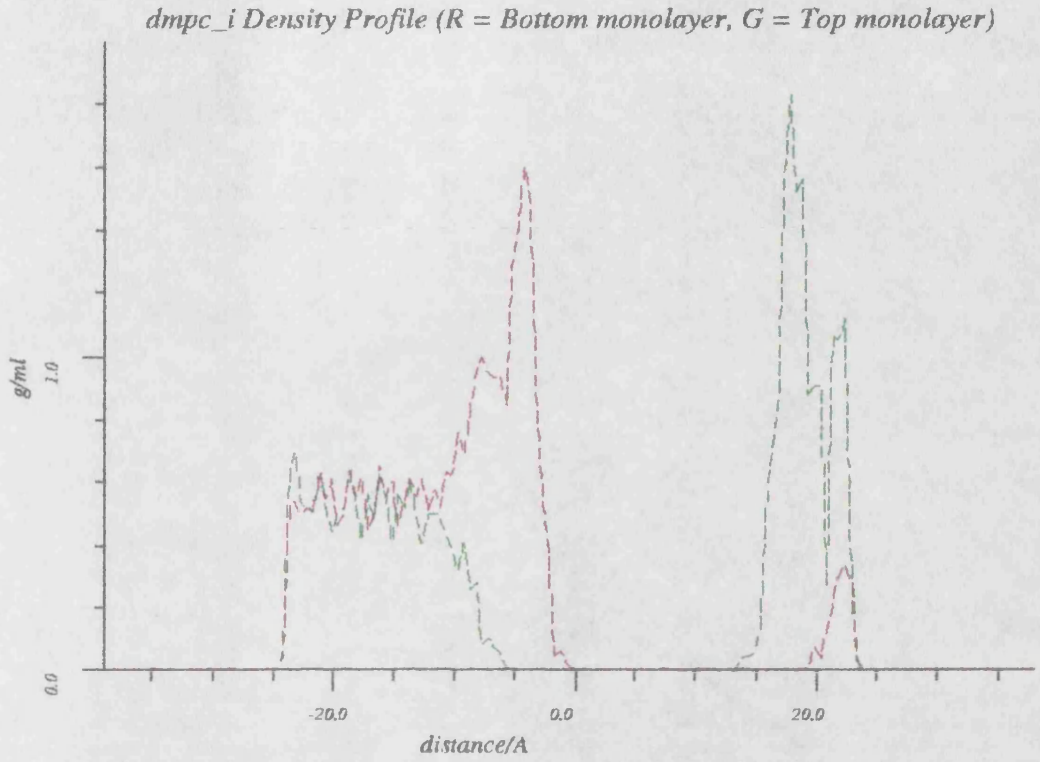
dmpc_i Density Profile (R = Bottom monolayer, G = Top monolayer)
g/ml
1.0
0.0
-20.0
0.0
20.0
distance/A

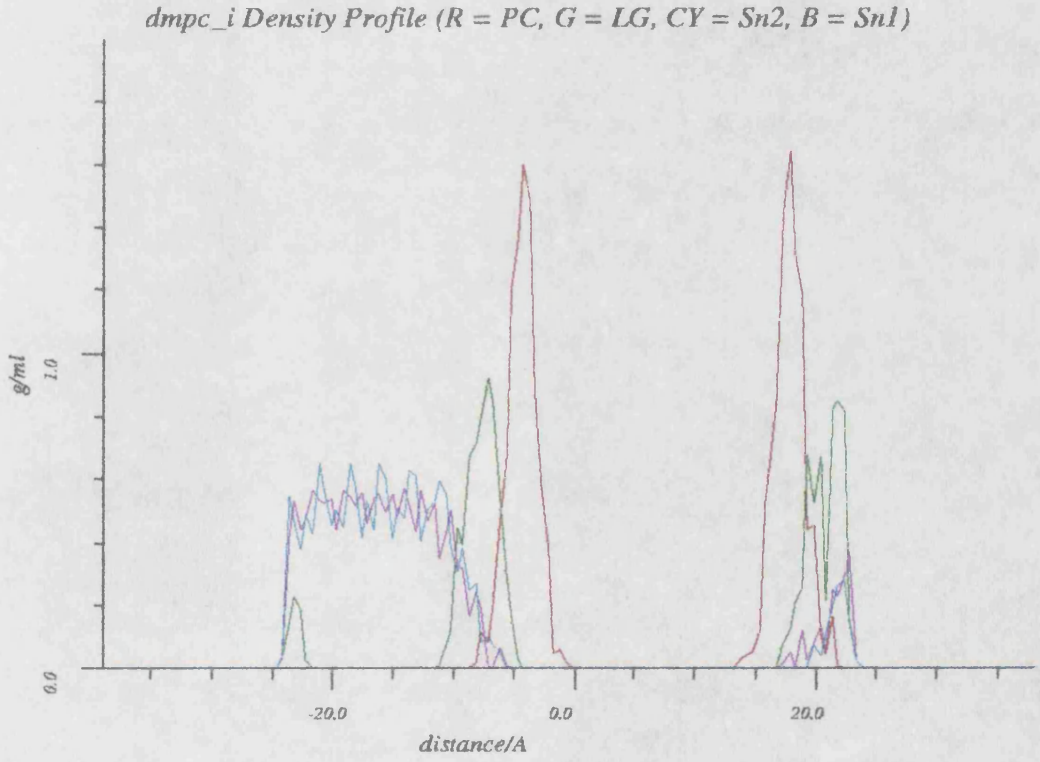
dmpc_i Density Profile (R = PC, G = LG, CY = Sn2, B = Sn1)
g/ml
1.0
0.0
-20.0
0.0
20.0
distance/A

6.2.3. Interdigitation

Although the system has obviously not reached equilibrium, further computational effort on this system, given its lack of torsional freedom and unphysical configuration after 100ps (acyl chains from one monolayer having interdigitated into the hydrophilic region of its opposing monolayer), was seen as unproductive. However it can be seen that introducing significant interdigitation can lead to the collapse of the bilayer system and a fully interdigitated bilayer. This is interesting in itself and may justify further investigation given current interest in the effect of alcohol on phospholipid bilayers. A fully interdigitated structure is rapidly imposed on the introduction of even trace amounts of alcohol into the hydrophobic region of phospholipid membranes.[6-10] This may have exciting implications for a number of biochemical processes, for example the action of anaesthetics.

References

1. Lemon AP, 1992. BUILDER, Molecular Graphics Unit, Bath UK
2. Cevc G and Marsh D, in *Phospholipid Bilayers*, Wiley-interscience, 1987.
3. Nagle JF, Wiener MC, and Suter RM, *Biophysical J*, vol. 55, pp. 315-325, 1989.
4. Marsh D, in *Handbook of Lipid Bilayers Crc Press*, 1991.
5. Scherer JR, *Biophysical J*, vol. 55, pp. 957-964, 1989.
6. Rowe ES, *Biochemistry*, vol. 22, no. 14, pp. 3299-3305, 1983.
7. McIntosh TJ, McDaniel RV, and Simon SA, *Biochimica et Biophysica Acta*, vol. 731, pp. 97-108, 1983.
8. McIntosh TJ, McDaniel RV, and Simon SA, *Biochimica et Biophysica Acta*, vol. 731, pp. 109-114, 1983.
9. Simon DA and McIntosh TJ, *Biochimica et Biophysica Acta*, vol. 773, pp. 169-172, 1984.
10. Tamura K, Kaminoh Y, Kamaya H, and Ueda I, *Biochimica et Biophysica Acta*, vol. 1066, pp. 219-224, 1991.

7. DLPC Bilayer Models

7.1. System III dlpc (16xDLPC)

The bilayer model dlpc consisting of 16 DLPC molecules was constructed from the crystal structure conformation of DLPE.[1] The crystal structure of DLPE is a hexagonally packed bilayer (See Table 4.2). The resulting coordinates were then minimised and used as the starting configuration for sampling the molecular dynamics trajectory (See Table 4.4).

The molecular dynamics trajectory was sampled from the NVT ensemble (See Table 4.4) for 350ps using a time step of 1fs, and storing coordinates and velocities every 10fs. The bilayer normal is orientated along the A axis of the unit cell axis. The first 200ps were sampled from the NVT ensemble using a temperature constraint of 310K. Followed by 100ps of the trajectory was sampled with a temperature constraint of 350K and 50ps at 400K. The increased temperature ensemble sampling was undertaken in order to examine to partitioning of the thermal energy in the system.

7.1.1. Thermodynamics and Energetics

Figure 7.1.1 contains the extracted thermodynamics information. The volume of the unit cell is 14751.03$Å^3$. The temperature of the system, and hence the kinetic energy, was constrained, resulting in an average value of 310.4±4.5K (0-200ps). The standard deviations of the relative energy components (Table 7.1.1) clearly indicate that the electrostatic energy of the system is dominating the potential energy. The form of the potential energy of the system matches that of the electrostatic energy. This is graphically demonstrated in Figure 7.1.2. The PE and E_{est} have been filtered from 0-20cm^{-1} and superimposed.

In this NVT ensemble simulation the pressure of the system shows a large deviation from its average at each step. The pressure 2696±1045bar is non-isotropic, P_x -2971±3108bar, P_y 8054±2675bar and P_z 3000±2711, the large standard deviations indicating a long correlation time. Some correlation was observed from the fourier transformed and filtered variation of the pressure and bilayer normal unit cell vector with time, but the same relationship was not observed for the other two vectors. This suggests that the pressure is more correlated along the bilayer normal direction compared with that in the bilayer plane. This trend agrees with other observed properties, which show a marked difference between their

behaviour in the plane of the bilayer and parallel to the bilayer normal.

Table 7.1.1

Energetics (kcal/mol) dlpc			
	E	SD	%SD
E_{tot}	600.8	106.3	17.7
E_{KE}	1569.2	21.8	1.4
E_{PE}	-968.4	108.1	6.6
E_{dsp}	-4920.2	20.9	0.4
E_{rep}	3478.3	35.2	1.0
E_{est}	-1376.8	107.1	7.8
E_{ϕ}	362.7	11.5	3.2
E_{θ}	886.2	19.4	2.2
E_{b}	615.6	19.0	3.1

All averages and SD over sampled range (40-190ps).

7.1.2. Density Profiles

The distribution of density along the bilayer normal can be seen from density profile plots (Figures 7.1.3a and 7.1.3b). These illustrate the distribution of different subcomponents of the system with respect to the bilayer normal. Figure 7.1.3a contains both the density profile of the two monolayers of the model and the density profile of the PC, glycerol and two lauryl chains in the initial 1ps of the trajectory. It can be seen that the PC head group of the DLPC molecule is of highest density, giving rise to a broad peak of approximately 2.0g/mol, 8Å wide, and the acyl chains are at approximately 0.8g/mol in the starting configuration. This compares well with that expected for the liquid parafin (0.775g/mol) and represents the chain packing density in the crystal structure configuration. Figure 7.1.3b is the density distribution sampled from 248-249ps. The density of both the lauryl chains and head group are maintained across the trajectory. The density of the Sn2 chain decreases near to the centre of the bilayer, a consequence of the turn in the Sn2 Chain (C21) of the DLPC crystal structure. The Sn1 chain penetrates into the other monolayer. There is a "smoothing" effect from the motional averaged density distribution. There is no significant increase in interdigitation of the two monolayers from the starting configuration. The system appears to be stable with respect to the bilayer

Figure 7.1.1a *dlpc (16xDLPC) R = KE, G = TOT, B = PE*

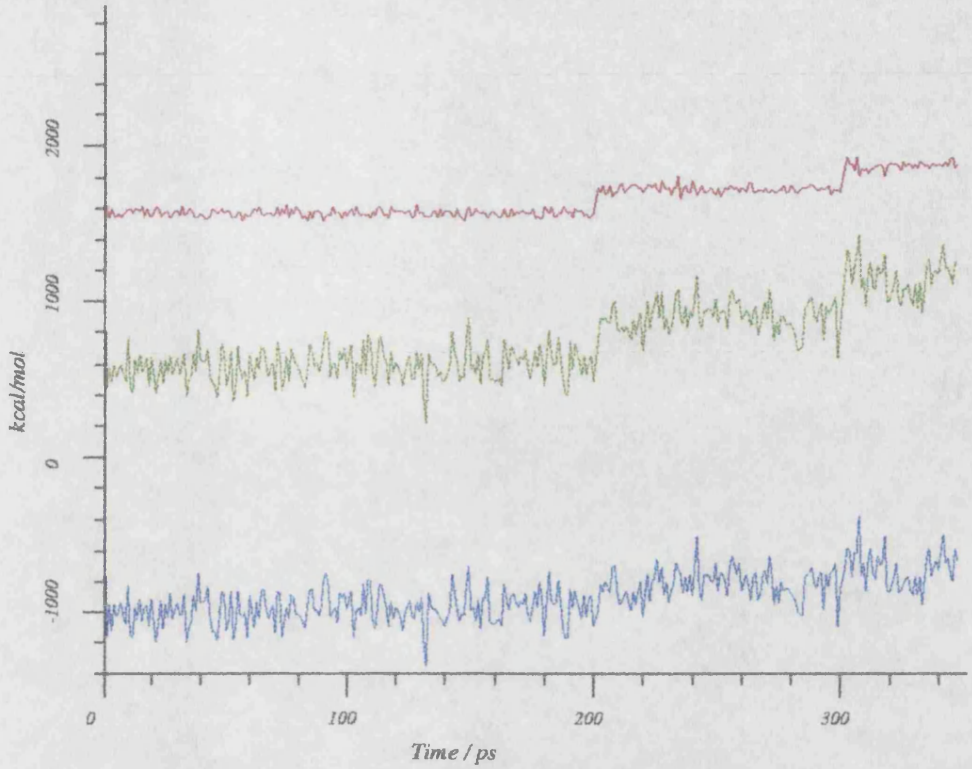

Non-Bond Energy (R = DSP, G = REP, B = EST)

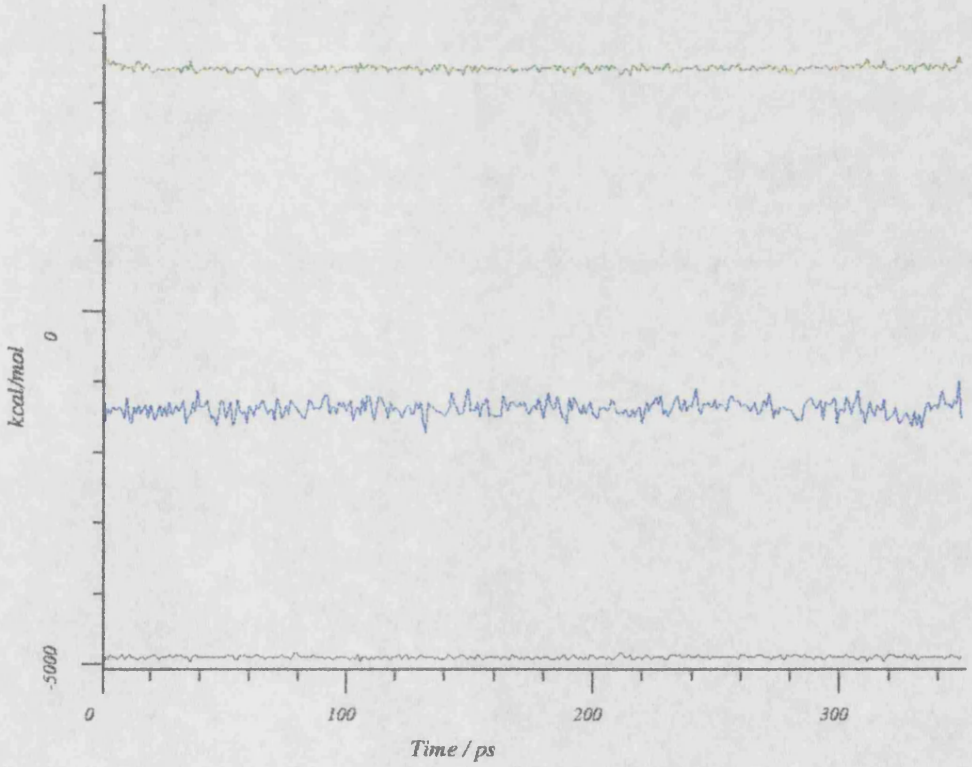

Figure 7.1.1b *dlpc Internal Energy (Bk = EP, G = ET, B = EB)*

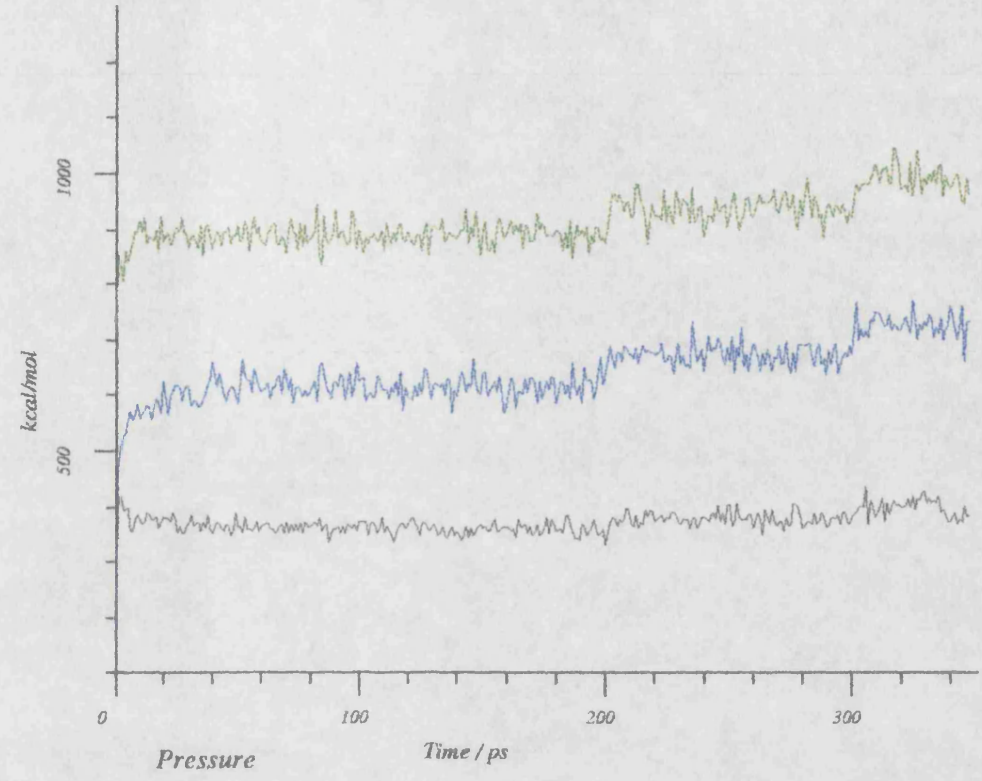

Pressure

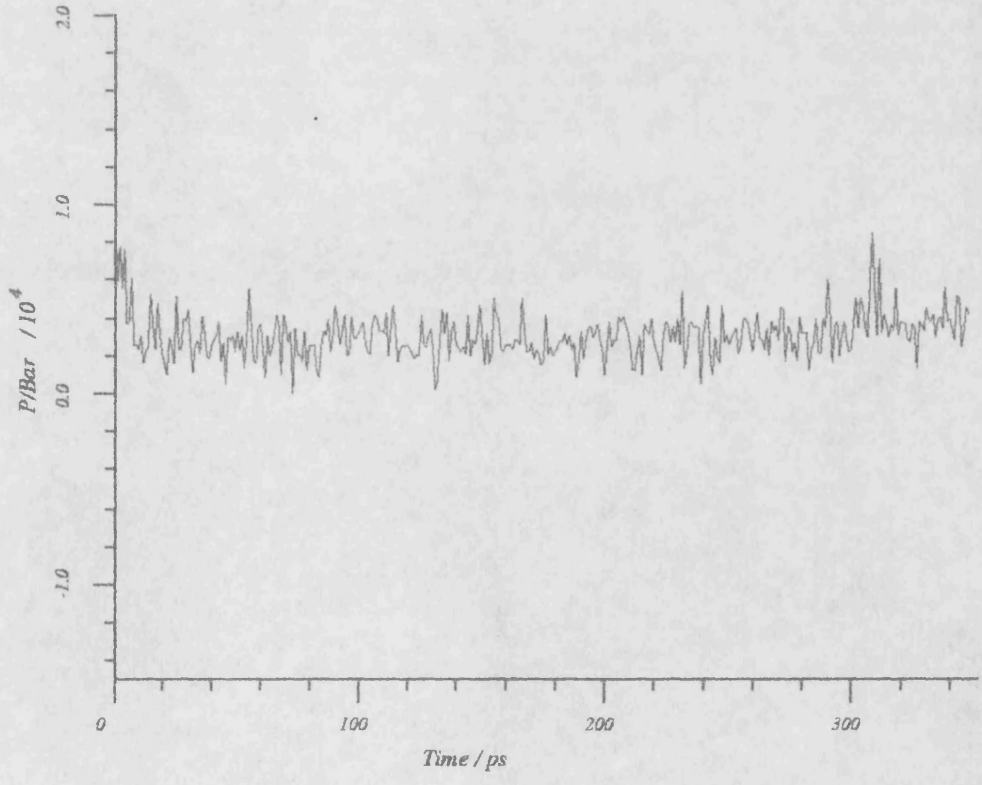

Figure 7.1.2

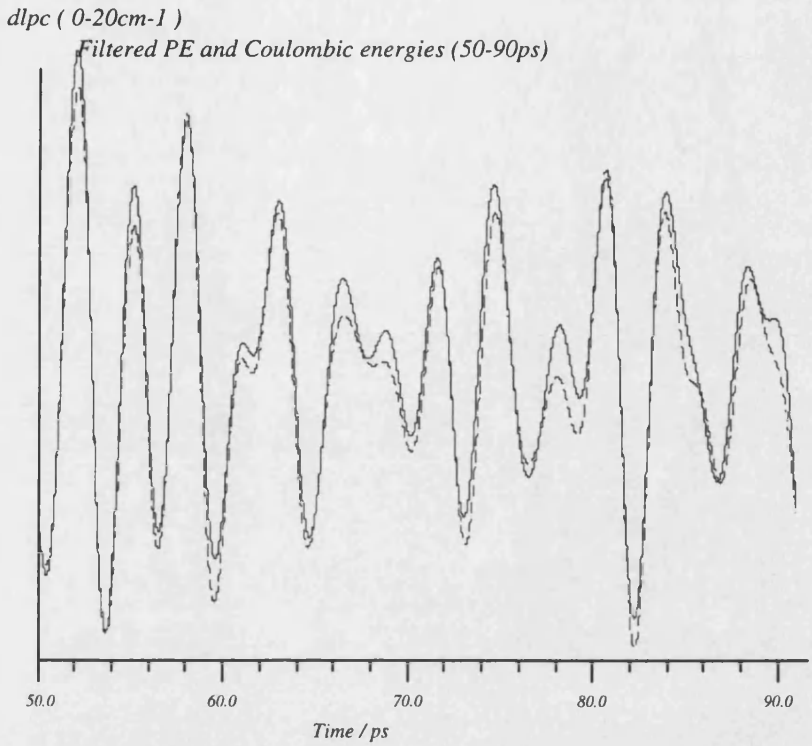

Solid line = PE. Dashes line = Coulombic

The filtered (0-20cm^{-1}) potential and coulombic energies sampled from 50-90ps of the trajectory.

normal across the trajectory.

7.1.3. Non-Bonded Internals

In order to examine the dynamics of the DLPC molecule a series of internal geometries have been defined (Chpt 5).

From the internal non-bonded angles (Chpt 5), the conformational freedom of the DLPC molecule can be probed. In Table 7.1.2 it can be seen that the majority of conformational freedom can be assigned to the angle variation between the central glycerol carbon and the terminal carbon of the Sn1 and Sn2 chains. This "scissor" action is consistent with the variation in the distance between the two terminal carbons. This angle varies considerably in the first 40ps of the simulation. Each molecule adjusts to the position of other molecules within each bilayer. This results in a range of values for the angles, although the variation of each angle once at equilibrium is relatively small. This "cooperativity" of lipid molecules is a general feature of such systems.[2]

Figure 7.1.3a

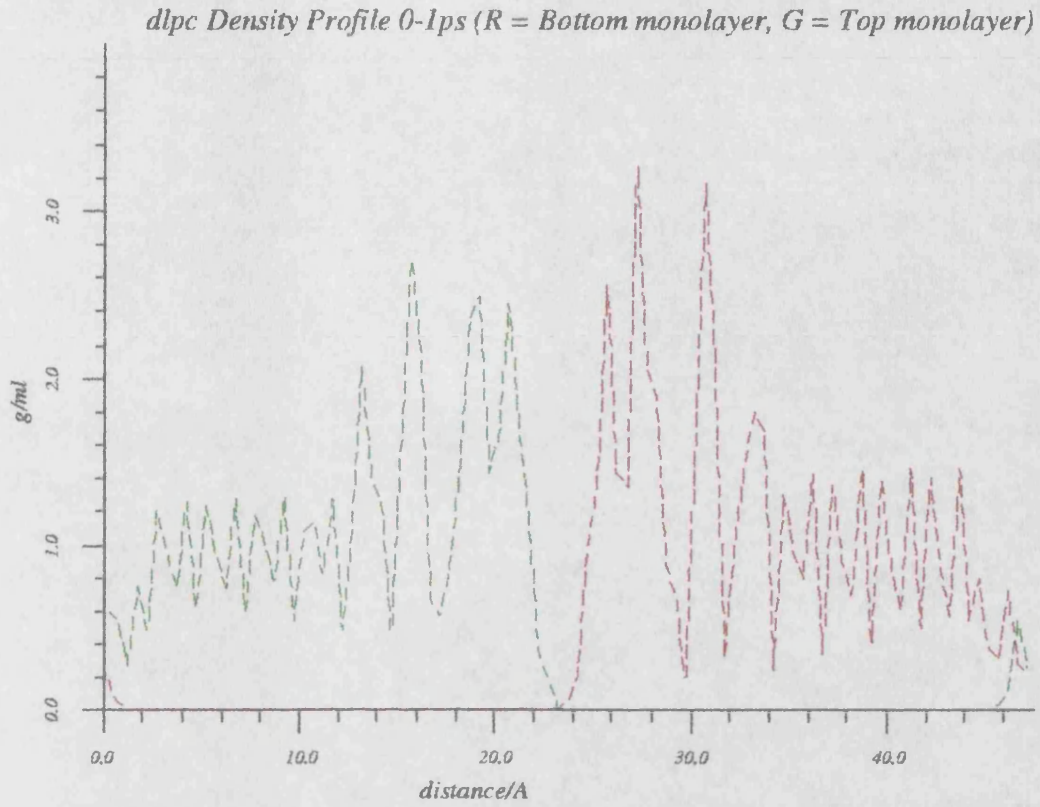
dlpc Density Profile 0-1ps (R = Bottom monolayer, G = Top monolayer)
g/ml
0.0
1.0
2.0
3.0
0.0
10.0
20.0
30.0
40.0
distance/A

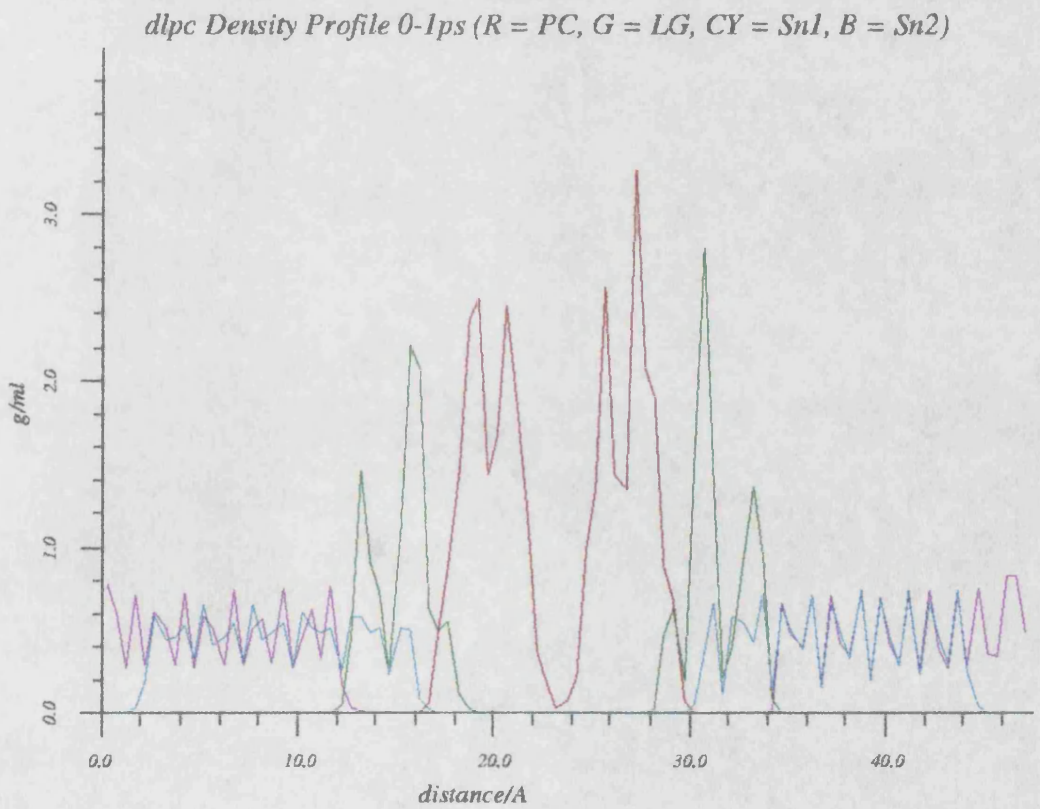
dlpc Density Profile 0-1ps (R = PC, G = LG, CY = Sn1, B = Sn2)
g/ml
0.0
1.0
2.0
3.0
0.0
10.0
20.0
30.0
40.0
distance/A

Figure 7.1.3b

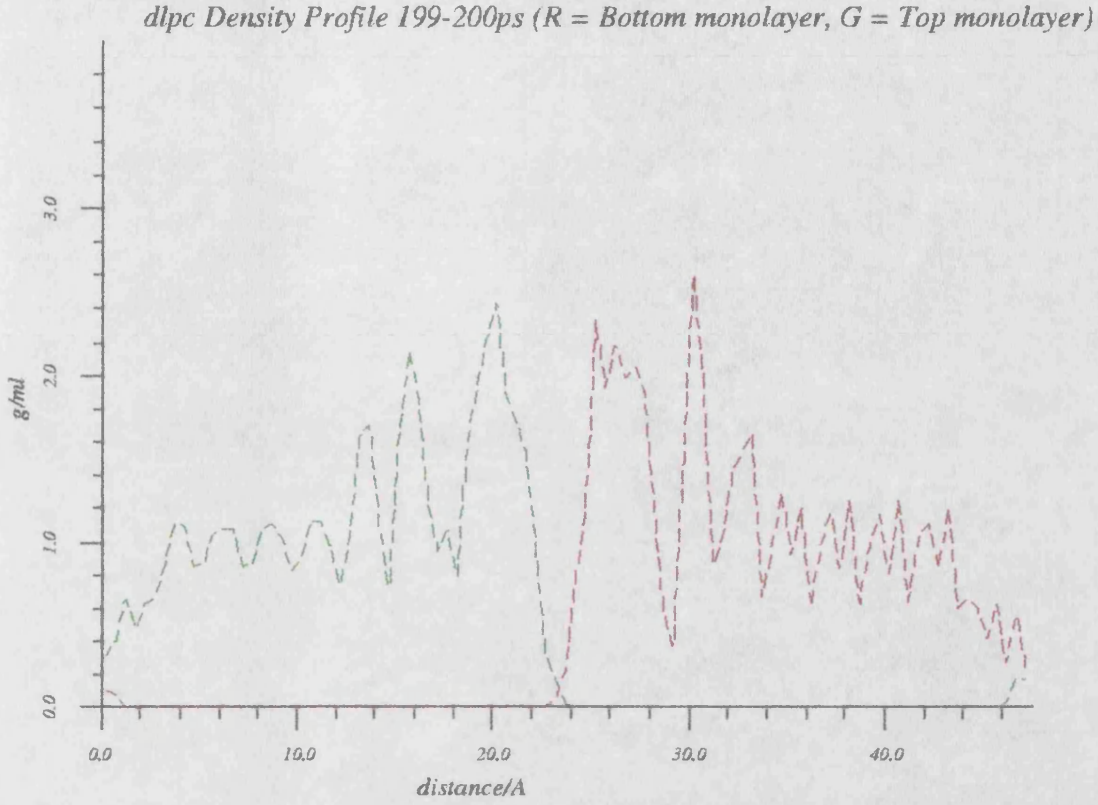
dlpc Density Profile 199-200ps (R = Bottom monolayer, G = Top monolayer)
g/ml
0.0
1.0
2.0
3.0
0.0
10.0
20.0
30.0
40.0
distance/A

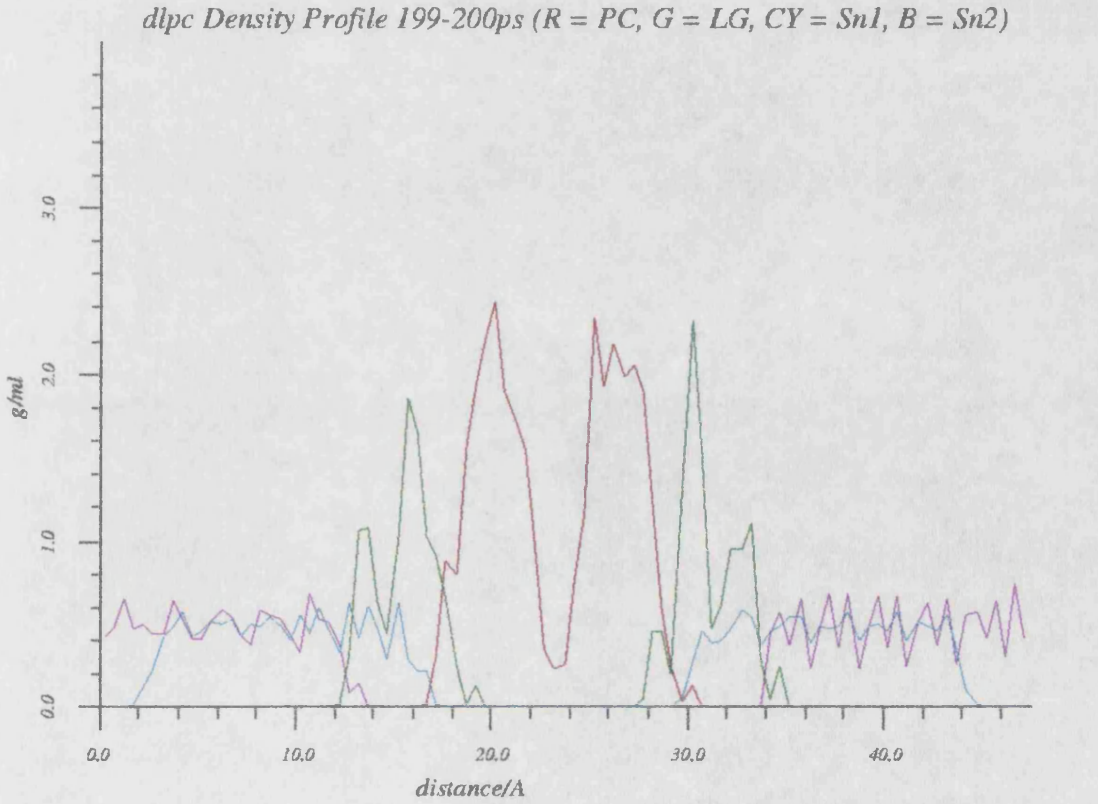
dlpc Density Profile 199-200ps (R = PC, G = LG, CY = Sn1, B = Sn2)
g/ml
0.0
1.0
2.0
3.0
0.0
10.0
20.0
30.0
40.0
distance/A

Table 7.1.2

Non-Bonded Angles dlpc			
	θ	SD	SDav
θ_1	117.8	8.6	5.3
θ_2	16.8	0.8	2.2
θ_3	121.5	7.8	3.9
θ_4	131.7	7.5	3.8

Sampled from 50-200ps, where θ is the average angle, and SD is the average standard deviation and SDav is the standard deviation of the average values.

From the internal non-bonded distances defined, it is clear that there is not significant conformational freedom in the DLPC molecule. There is however some variation in the conformation of individual molecules in the bilayer, although the variation of that conformation is small across the trajectory. This can be seen from the standard deviation for the non-bonded distances within DLPC (Table 7.1.3).

Table 7.1.3

Non-Bonded Distances (Å) dlpc			
	D	SD	AvSD
N P	4.1	0.1	0.1
N C6	6.8	0.3	0.2
C6 C19	17.2	0.1	0.2
C6 C31	13.6	0.3	0.3
C8 C19	14.0	0.0	0.1
C20 C31	13.2	0.1	0.2
C19 C31	5.8	0.3	0.5

Sampled from 50-200ps, where D is the average non-bonded distance, SD the average standard deviation for that distance.

The majority of conformational freedom appears to be in the motion of the head group relative to the glycerol backbone and in the "scissor" action of the acyl chains. A comparison between the relative variation of the Sn1 and Sn2 chains indicates that there is more conformation

freedom in the Sn2 relative to the Sn1 chain. This is generally observed in phospholipids due to the turn in the Sn2 chain at C21.

There is no significant shortening of the acyl chains over the trajectory. Only a small variation in length of the Sn1 and Sn2 chains (0.3%, 0.8% respectively) is observed. This indicates little, if any, torsional freedom in the acyl chains.

7.1.4. Torsion Angles

The values of all torsions defined (See Chpt 5) in all bilayer DLPC molecules has been calculated across the sampled trajectory. The distribution of torsion values has been examined, and their ensemble average calculated. As indicated from the non-bonded angles and distances, the lauryl chains exist in only the trans conformation. There is only a small variation in the torsion angles of the Sn1 and Sn2 chains (SD 4.46°). Increased conformational freedom is observed in the phosphate and glycerol torsion angles (Table 7.1.4).

Almost all of the torsional flexibility in the molecule can be assigned to variation of the head group and backbone torsions. These not only show larger standard deviations, but also exhibit a range of values in the DLPC molecules within the bilayer. The glycerol and PC moieties appear to act as "hinges" to allow for the adjustment of the conformation and configuration of the DLPC molecules relative to each other in this "gel" phase (ie non-fluid hydrophobic region) bilayer model.

7.1.5. Euler Angles

Table 7.1.5 contains the characteristic Euler angles for the glycerol-PC backbone and head group of dlpc. It can be seen that on average the glycerol group is perpendicular to the bilayer normal. This is consistent with experimental results for phospholipid bilayers. The high standard deviation in the E_1 angle is due to adjustment of the configuration of dlpc molecules within the bilayer model. The average standard deviation is only 4.18, indicating some cooperativity between molecules in the bilayer.

7.1.6. Segmental Order Parameters

The segmental order parameters of the acyl chains have been calculated for the sampled trajectory, with respect to the bilayer normal. These indicate the order of the system.

Table 7.1.4

Standard Deviations of Torsions dlpc					
	SD	sdSD		SD	sdSD
ϕ_1	5.2	0.4	ϕ_2	4.8	0.3
ϕ_3	7.8	3.7	ϕ_4	10.2	5.0
ϕ_5	9.5	6.4	ϕ_6	10.8	5.3
ϕ_7	5.2	0.4	ϕ_8	4.9	0.4
ϕ_9	15.6	10.1	ϕ_{10}	7.3	0.8
ϕ_{11}	13.9	4.2	ϕ_{12}	5.0	0.2
ϕ_{13}	4.9	0.1	ϕ_{14}	4.7	0.1
ϕ_{15}	4.8	0.1	ϕ_{16}	4.8	0.1
ϕ_{17}	5.0	0.1	ϕ_{18}	5.1	0.1
ϕ_{19}	5.3	0.2	ϕ_{20}	5.4	0.1
ϕ_{21}	9.5	2.3	ϕ_{22}	5.9	0.5
ϕ_{23}	9.8	1.8	ϕ_{24}	5.2	0.1
ϕ_{25}	4.9	0.2	ϕ_{26}	4.9	0.1
ϕ_{27}	4.8	0.1	ϕ_{28}	4.8	0.1
ϕ_{29}	4.7	0.1	ϕ_{30}	4.8	0.1
ϕ_{31}	5.0	0.1	ϕ_{32}	5.1	0.1

Sampled from 50-200ps. Where AvSD is the average standard deviation for that torsion over all molecules in the bilayer and sdSD is the standard deviation of the average SD.

Table 7.1.5

Euler Angles dlpc			
	Av	SD	AvSD
E_1	90.1	73.2	4.2
E_2	116.0	2.7	3.4
E_3	123.9	1.7	3.0

Sampled from 50-200ps. Where AvSD is the average standard deviation for that angle over all molecules in the bilayer.

Figure 7.1.4a shows the ensemble average order parameters of the Sn1 and Sn2 chains sampled from the 50-200ps at 320K. The general form of the order parameter profile is consistent with measured experimental systems and theoretical studies,[3-7] although they exhibit higher absolute values. Several key features of the experimentally measured order parameters can be observed. There is a characteristic drop in order at the second carbon segment of the Sn2 chain. This is a direct consequence of the re-orientation of the C-H vector with respect to the bilayer normal, brought about by the turn in the Sn2 chain. An order parameter "plateau" is observed. Segments 2-6 are observed to have characteristically higher order parameter values than segments 7-12. This is a general feature of the order parameter profile of all phospholipids.[8] The average order parameter value for Sn1 is 0.943±0.036, and for Sn2 0.952±0.026.

The segmental order parameter profile for the lauryl chains sampled from 300-350ps have been calculated in order to examine the sensitivity of the order parameters in detecting increased conformational freedom. Figure 7.1.4b shows the calculated order parameter profile. The general form of the profiles are the same. There is an overall drop in the order of both the Sn1 and Sn2 chains

7.1.7. Average Temperature

In an attempt to probe the reasons for the lack of conformational freedom in the acyl chain region of the bilayer model, the distribution of atomic temperatures has been calculated. Figure 7.1.5 shows the ensemble average temperature of the acyl chains, glycerol and PC moieties. The PC and glycerol groups are on average of higher temperature than the two lauryl chains (Table 7.1.6). This is due to the increased coulombic interactions in the head group relative to the lauryl chains, brought about by contact with adjacent head groups across the periodic system.

A further 150ps of trajectory was sampled from the NVT ensemble, 200-300ps using a temperature constraint of 350K and 300-350ps at 400K. The average temperature of each moiety is are shown in Table 7.1.6 and Figure 7.1.5.

The acyl chain torsion trajectories have also been sampled and the average standard deviation over all acyl chain torsions for each part of the trajectory calculated. From 200-300ps(350K) the average standard deviation for the acyl chain torsions were 5.12, and

Figure 7.1.4a

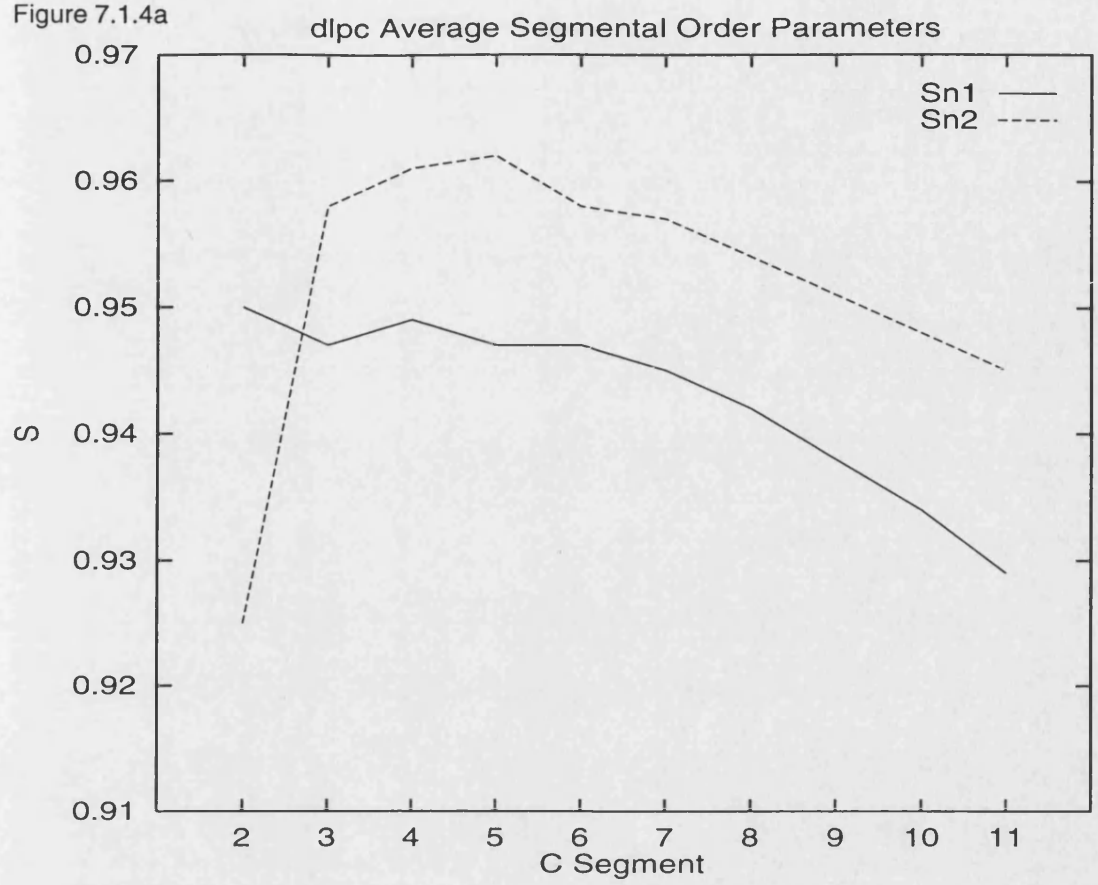

Figure 7.1.4b

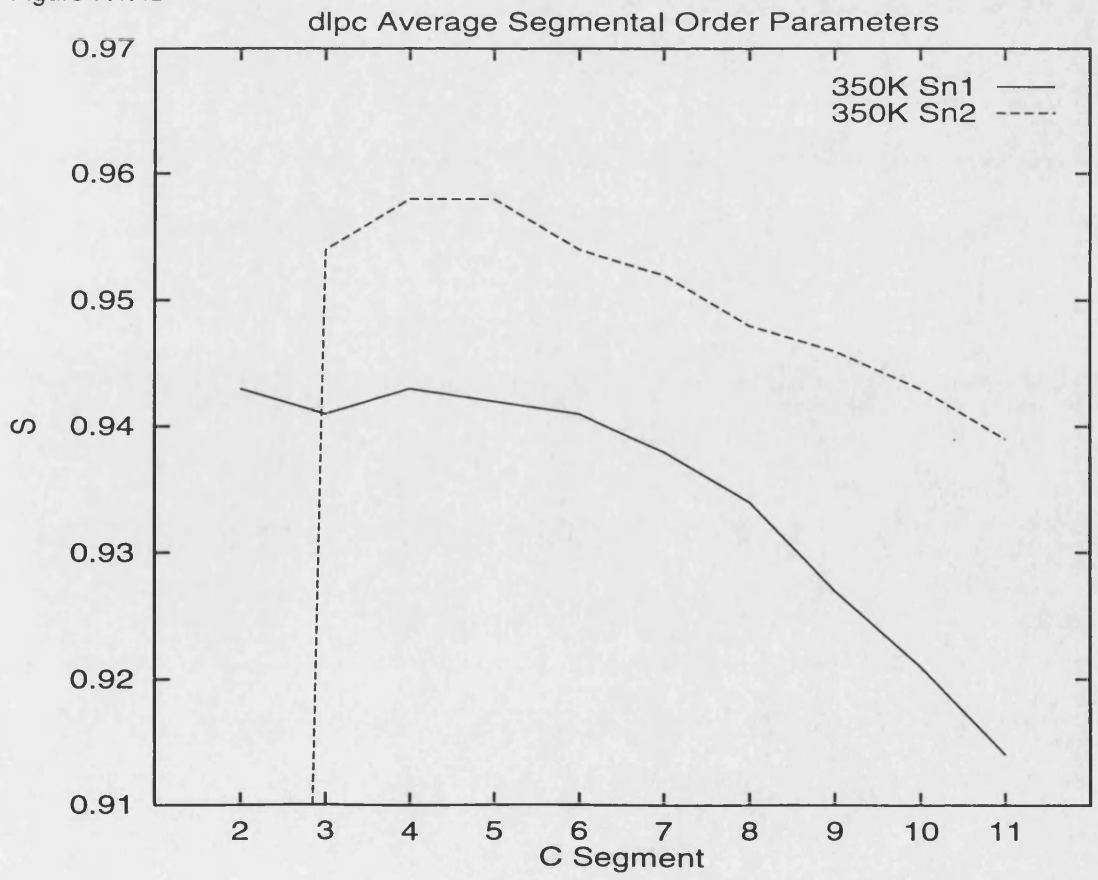

from 300-350ps(400K) they were measured as 5.38. Clearly the partitioning of the temperature in the acyl chains has an effect on their torsion freedom, but this is not sufficient to induce any gauche conformations. There is therefore a more dominant property of these systems that is decreasing the torsional freedom of the acyl chains of these molecules. This cannot simply be a function of the torsion potential, the parameters of which have been determined and validated in several studies.[9-12]

Table 7.1.6

Average Temperatures (K) dlpc								
	T	SD		T	SD		T	SD
PC	329.3	11.2	PC	354.5	12.6	PC	389.2	31.0
GL	315.1	16.4	GL	348.2	17.6	GL	381.9	33.7
Sn1	301.3	9.4	Sn1	333.8	10.4	Sn1	364.1	26.8
Sn2	303.2	9.4	Sn2	333.6	10.6	Sn2	373.9	25.4

In order to explain the observed trend in the segmental order parameter profile for the DLPC acyl chain (Figure 7.1.4a), the average temperature of each carbon segment and hydrogens was calculated from their atomic velocities, averaged over all equivalent segments (Table 7.1.7 and Figure 7.1.6).

Given the standard deviations for the temperature of each segment it is difficult to make a specific interpretation from the segmental temperature. However it can be observed that segments 2-5 are generally of higher temperature compared with segments 6-12. This is surprising as increased atomic velocities within these segments would be expected to give rise to reduced order. The order parameters are a measure of the orientational order of the C-H bonds with respect to the bilayer normal. Clearly in this system, given its lack of fluidity and general conformational freedom, the dominant effect on the order of the system is the orientation of the molecule with respect of the bilayer normal. Hence small adjustments in the configuration of DLPC molecules within the each monolayer have a dominant effect on the order parameter profile. Clearly the effect of this molecular orientation will be insignificant in "fluid" bilayer models, in which the conformational freedom of the lauryl chains would be the most important factor affecting the orientation of the C-H vector. It has been suggested by others working in this field (B.Roux, personal communication) that the segmental order parameter is not a very "sensitive" measure of the "fluidity" of the hydrophobic region, and this result

Table 7.1.7

Average Methylene Temperature (K) dlpc					
Sn1			Sn2		
C Segment	Av	SD	C Segment	Av	SD
2	299.3	35.1	2	311.9	36.6
3	303.6	35.6	3	307.8	35.9
4	303.4	34.9	4	310.9	36.8
5	304.4	35.5	5	307.7	35.6
6	298.7	36.3	6	299.6	33.7
7	295.5	33.1	7	302.5	35.6
8	296.0	34.5	8	300.3	35.4
9	300.9	36.4	9	299.6	35.0
10	296.6	34.5	10	296.4	34.1
11	299.4	34.9	11	301.5	33.8
12	302.9	29.6	12	300.3	35.1

Sampled over 50-200ps.

supports this hypothesis.

7.1.8. Validity of the Model

The density of the starting configuration is the same as that of the crystal structure of DLPE. The smaller head group area allows for a high density of lauryl chain packing in the crystal structure. This has a constrictive effect on the conformational freedom of the lauryl chains, leading to a lack of fluidity. In equivalent PC lipid crystal structures the increased size of the head group gives rise to a reduced chain packing and tilting.[13] It is clear that with the force field used, the crystal structure does not reproduce the bilayer environment, in terms of the fluidity of the hydrophobic region.

One solution to this lack of fluidity may be to reduce the density of the lauryl chain region, while maintaining the spatial configuration and conformation. This can be achieved by rescaling the coordinates of the centre of mass of each molecule in the bilayer model.

Figure 7.1.5

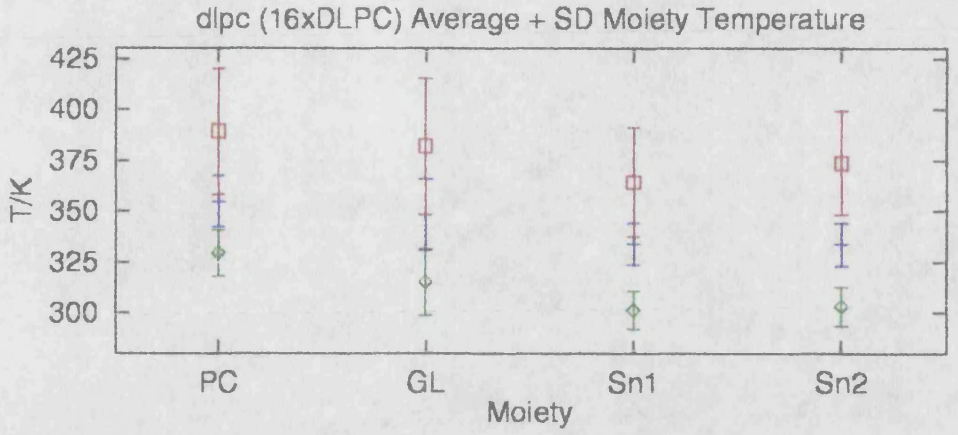

Figure 7.1.6

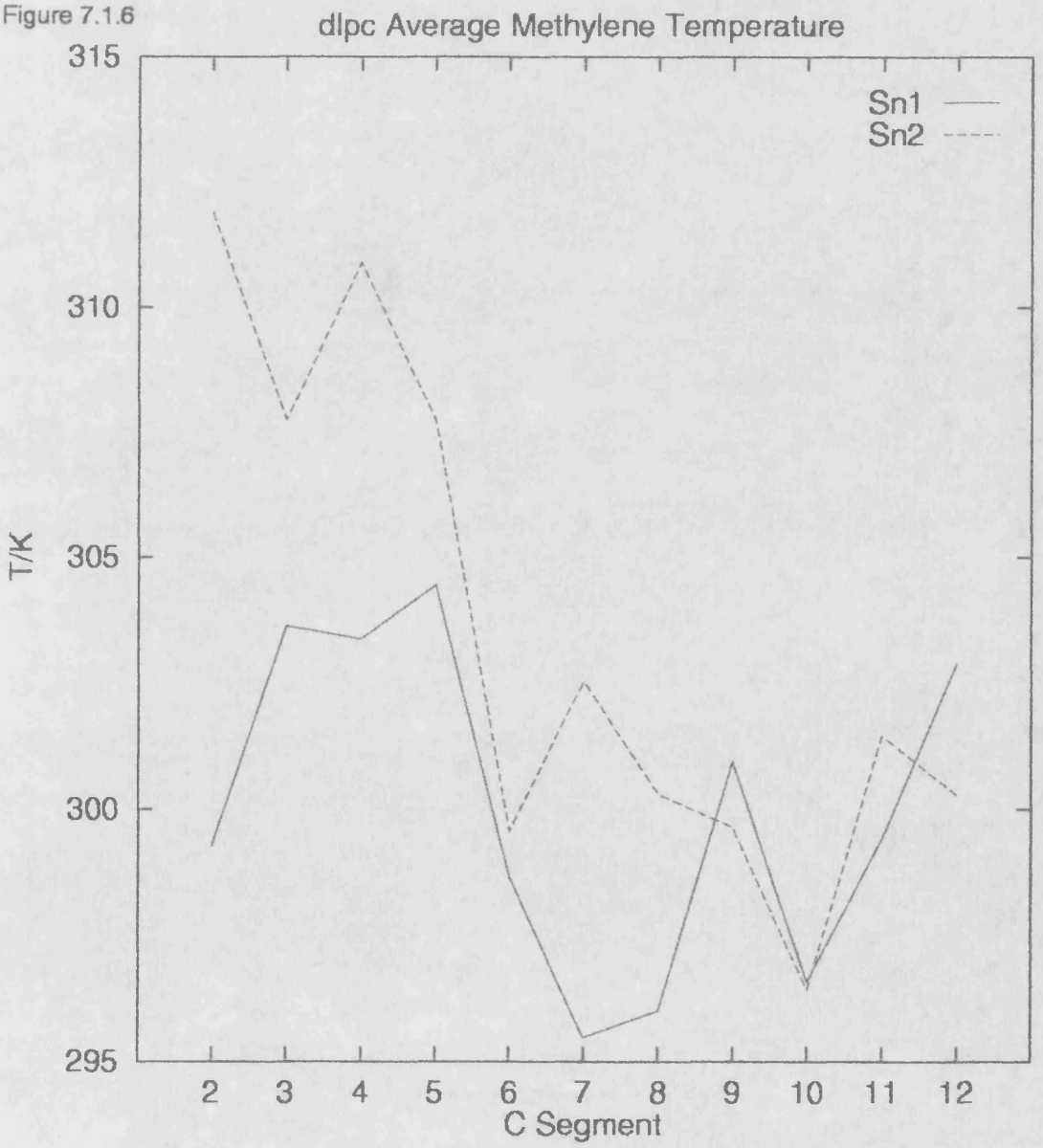

7.2. System II dlpc_y1 (16xDLPC)

The bilayer model dlpc_y1 was constructed from the coordinates of the dlpc model, expanded along all three cell axes. The centres of mass of all molecules in the unit cell were translated such that their spatial arrangement was conserved. Rescale factors of A=1.05, B=1.5 and C=1.5 were used to rescale the positions of the centres of mass of each lipid in the bilayer lattice. The unit cell lengths were also scaled by these values (Table 4.2). These coordinates were then minimised and used as the starting configuration for the molecular dynamics trajectory (Table 4.4).

The molecular dynamics trajectory was sampled from the NPT ensemble, for 300ps. The bilayer normal is orientated along the A unit cell axis. A temperature constraint of 320K was imposed on the simulation, and velocities rescaled every 10fs or whenever the temperature deviated more than ±10K from 320K. This resulted in an ensemble average of 324.2±4.8K.

7.2.1. Thermodynamics and Energetics

Figure 7.2.1a and 7.2.1b contain the extracted thermodynamic information from the trajectory. There is an initial decrease in the volume of the unit cell from 32887Å^3 to 17563 ± 207Å^3 in the first 40ps. This contraction of the system is non-isotropic, the unit cell axis A reduces from 50.1Å to an average of 44.8±0.4Å, B from 23.2Å to an average of 19.0±0.1Å and C from 27.8Å to an average of 20.6±0.1Å.

The standard deviation and sampled ensemble averages of the internal energies (Table 7.2.1) allow comparison of this expanded system with the bilayer model dlpc. The internal energies of the system are reduced in the expanded model compared with the crystal structure. This indicates the removal of strain from the system on expansion. This is most evident in the torsion energy of the expanded system E_ϕ 203.0±11.4 kcal/mol (dlpc_y1) compared with 362.7±11.5 kcal/mol (dlpc). The expansion of the system also reduces the non-bonded interactions as expected. Clearly the major effect on the potential energy of the system can be attributed to the secondary effect of the electrostatic energy under the pressure scaling. The variation of the potential energy in the NVT ensemble trajectory is small compared with that of the NPT.

The pressure and the bilayer normal unit cell axis were filtered to remove their high frequency variation above 20cm^{-1} for the 50-90ps segment of the trajectory. It can be seen from

their superimposed values that the pressure is more sensitive to interactions in the bilayer normal direction. It must however be remembered that in these anhydrous simulations there is vacuum between the PC head groups of the bilayer, which can only be replaced by interaction of the relatively charge dense head groups. This is predominately an electrostatic interaction and therefore is bound to dominate the pressure in that direction.

Table 7.2.1

Energetics (kcal/mol) dlpc_y1			
	E	SD	%SD
E_{tot}	1398.2	236.95	17
E_{KE}	1639.0	24.3	1.5
E_{PE}	-240.8	238.0	99
E_{dsp}	-2828.2	34.7	1.2
E_{rep}	2586.2	33.9	1.3
E_{est}	-1771.6	234.0	13
E_{ϕ}	203.0	11.4	5.6
E_{θ}	938.0	23.5	2.5
E_b	635.6	21.3	3.4
	T/K	SD	%SD
T	324.2	4.8	1.5
	D/Å	SD	%SD
A	44.8	.409	0.9
B	19.0	.126	0.7
C	20.6	.136	0.7
	$V/Å^3$	SD	%SD
V	17563	206.9	1.2
	P/bar	SD	%SD
P	87.6	1183.4	1350
P_x	2.8	2819.5	10^5
P_y	-2.1	2217.6	10^5
P_z	-0.9	2282.0	10^5

Sampled from 50-300ps of the nPT ensemble.

7.2.2. Density Profiles

Figure 7.2.3a illustrates the density distribution of the various subcomponents of the bilayer with respect to the bilayer normal sampled from the first ps of the trajectory. The expansion of the dlpc model leads to a general decrease in density. The lauryl chains region of the bilayer has a density of approximately 0.4g/ml, lower than the liquid paraffin density (0.775g/ml). There is a corresponding reduction in the density of the glycerol and PC moieties. There is clearly more conformational freedom even in the first ps of the trajectory, illustrated by the "smoothness" of the profile. There is approximately a 7Å gap between the peak density of the two PC groups, indicating the vacuum between the two adjacent monolayers in the initial bilayer model.

Figure 7.2.3b is the density profile sampled from 299-300ps of the trajectory. The contraction of the system under the constant pressure constraint increases the density of the lauryl chains to approximately 0.8g/ml, which compares well with the density of the liquid paraffin. The density of the glycerol and PC moieties are both increased and their peak width reduced indicating increased order in the head group region. This is consistent with the popular model of a crystalline hydrophilic head group region and a fluid hydrophobic region. The density distribution of the Sn1 and Sn2 lauryl chains occupy the same region of the bilayer normal after 300ps of the trajectory, indicating reorientation of the DLPC molecule.

7.2.3. Non-Bonded Internals

From the non-bonded angles (Table 7.2.2) in dlpc_y1 it can be seen that the expanded system allows for increased flexibility in the head group region. The angle θ_1 although exhibiting a smaller range of values, each has a larger standard deviation. The resulting PC orientation agrees well with experiment, orientated parallel to the bilayer plane. The reduced range of conformations is due to the increased free volume of each molecule in the bilayer, allowing the head group to explore more conformational space while the unit cell is contracted under the constant pressure constraint. This can be thought of as a simple packing problem in which the increased free volume allows more conformational adjustment of the molecules achieving more efficient packing.

The characteristic "scissor" angle (θ_2) is on average larger and exhibits both a larger range of values and standard deviation of each value. This is reflected in the non-bonded distances between the terminal carbons of the lauryl chains (Table 7.2.3). The orientation of the

Figure 7.2.1a

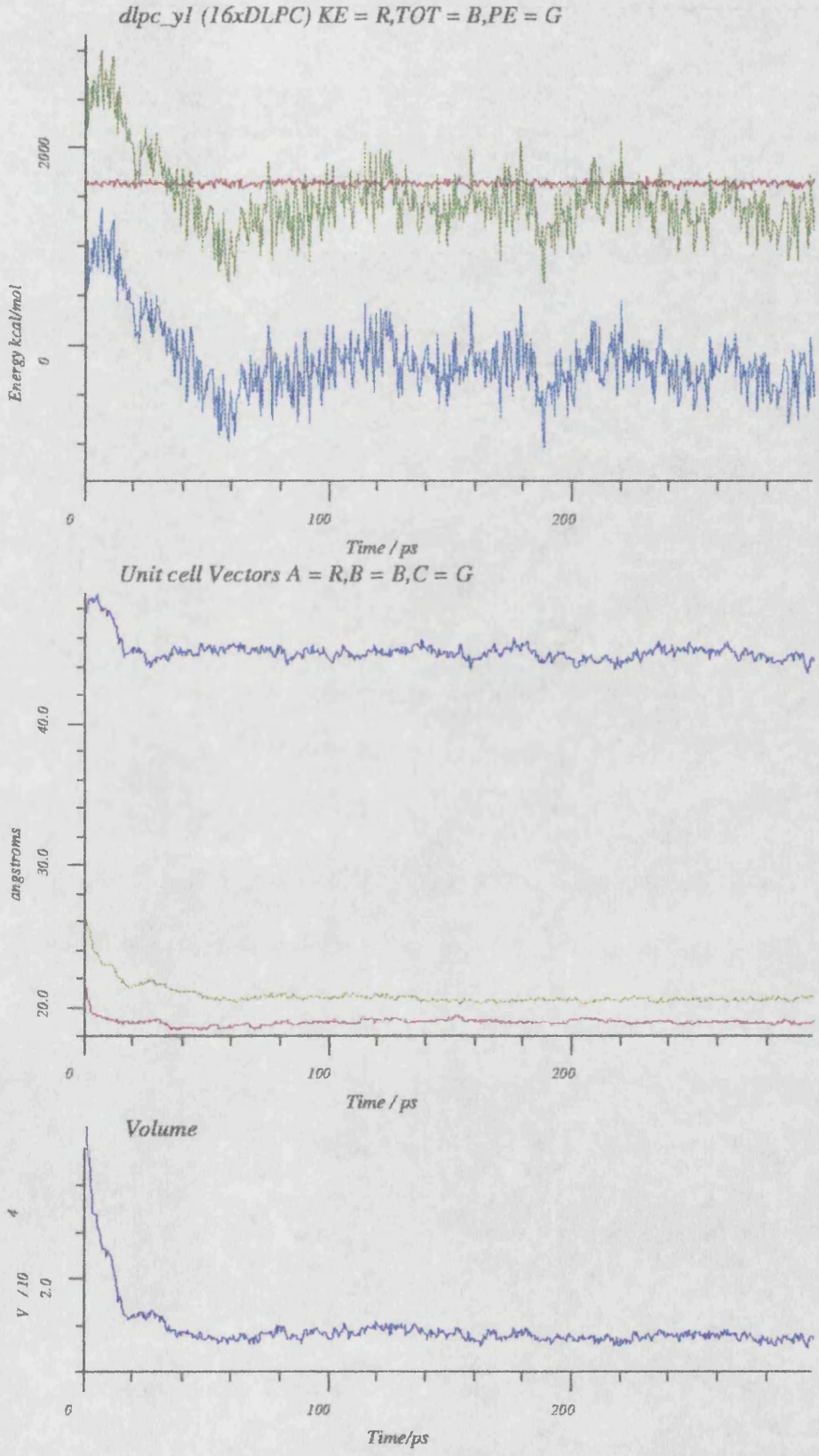
dlpc_y1 (16xDLPC) KE = R,TOT = B,PE = G
Energy kcal/mol
2000
0
0
100
200
Time / ps
Unit cell Vectors A = R,B = B,C = G
angstroms
40.0
30.0
20.0
0
100
200
Time / ps
Volume
V / 10
4
2.0
0
100
200
Time/ps

Figure 7.2.1b

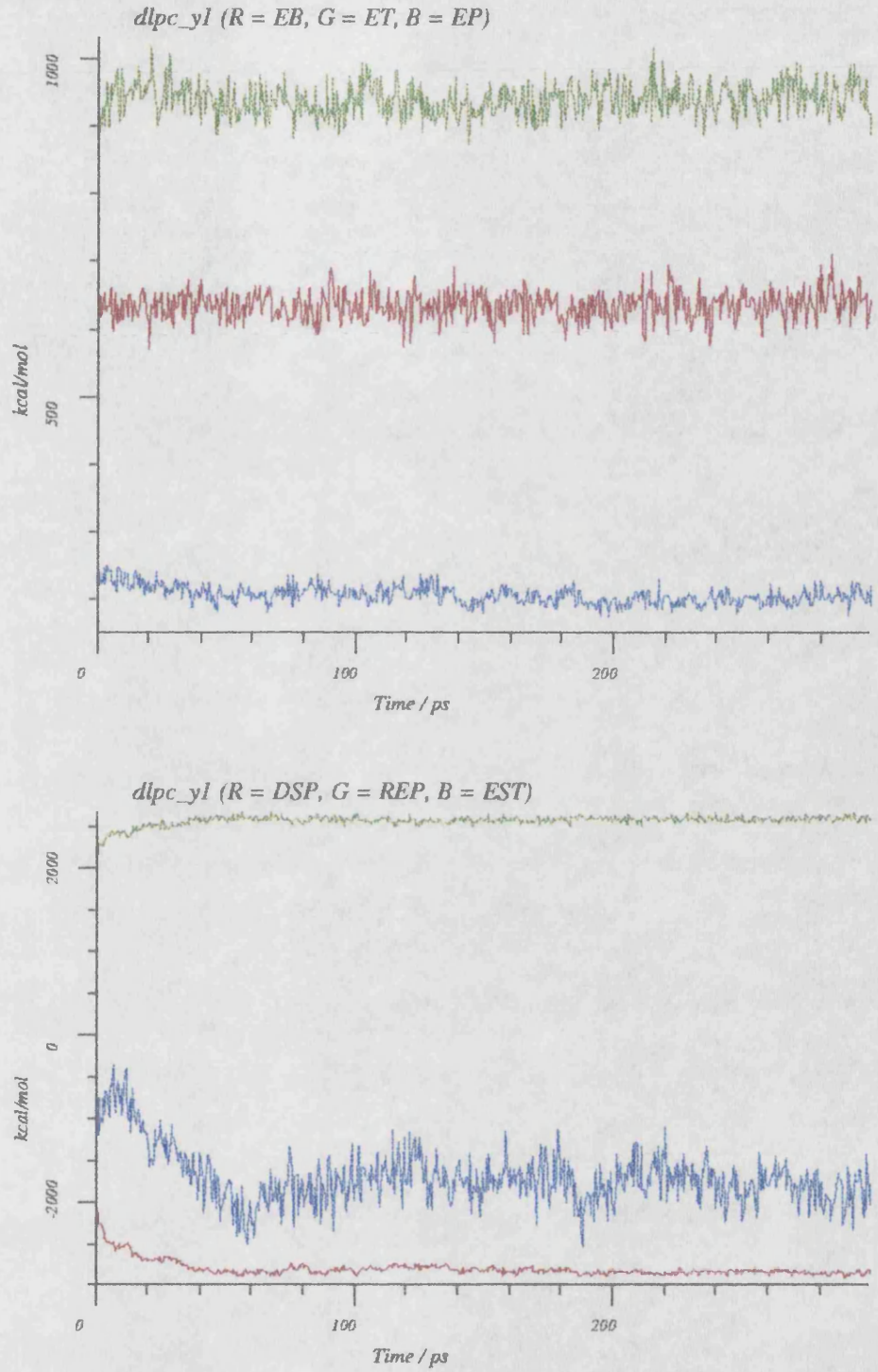
dlpc_y1 (R = EB, G = ET, B = EP)
1000
500
kcal/mol
0
100
200
Time / ps
dlpc_y1 (R = DSP, G = REP, B = EST)
2000
0
-2000
kcal/mol
0
100
200
Time / ps

Figure 7.2.2

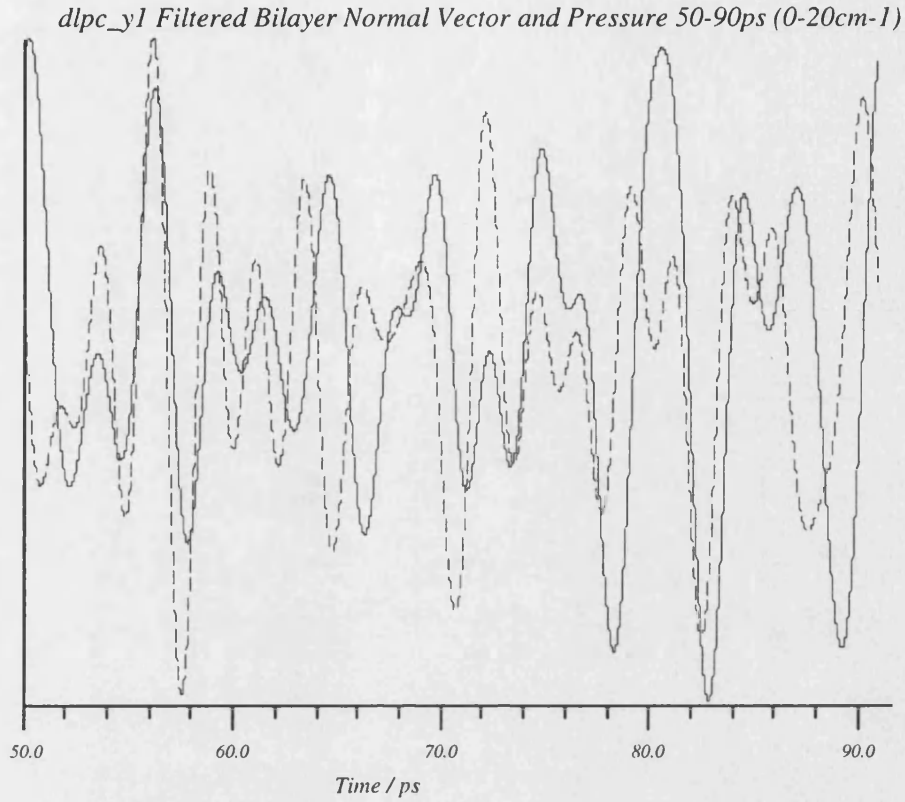

solid line = A, dashed line = Pressure

Table 7.2.2

Non-Bonded Angles dlpc_y1				
	Av	SD	AvSD	sdSD
θ_1	96.0	3.8	8.6	1.4
θ_2	24.8	5.7	5.4	2.0
θ_3	120.4	7.6	9.7	1.4
θ_4	129.9	8.0	9.0	1.5

Sampled over 50-300ps. AvSD is the average standard deviation of each angle in all the molecules of the system, and sdSD is the standard deviation of these standard deviations.

lauryl chains with respect to the head group is conserved in the expanded model, although they exhibit increased flexibility. The length of the two lauryl chains are equivalent despite the

turn at C21 of the Sn2 chain.
Table 7.2.3

Non-Bonded Distances (Å) dlpc_y1			
	D	SD	AvSD
N P	4.9	0.1	0.3
N C6	6.4	0.2	0.4
C6 C19	15.3	0.3	0.7
C6 C31	15.2	0.4	0.6
C8 C19	13.5	0.2	0.5
C20 C31	13.5	0.2	0.5
C19 C31	6.7	1.4	1.4

Sampled from 50-300ps. AvSD is the average standard deviation for that distance in all molecules in the system.

7.2.4. Euler Angles

The characteristic Euler angles (Table 7.2.4) are conserved in the expanded bilayer model. However the orientation of the glycerol backbone, whilst still being on average perpendicular to the bilayer normal, exhibits a smaller range of values. The average standard deviation of this angle (E_1) has increased from 4.2 to 12.2, indicating increased configurational freedom.

Table 7.2.4

Euler Angles dlpc_y1			
	Av	SD	AvSD
E_2	90.1	48.2	12.2
E_3	112.2	0.4	3.9
E_4	123.7	0.2	3.9

Sampled from 50-200ps. Where AvSD is the average standard deviation for that angle over all molecules in the bilayer.

Figure 7.2.3a

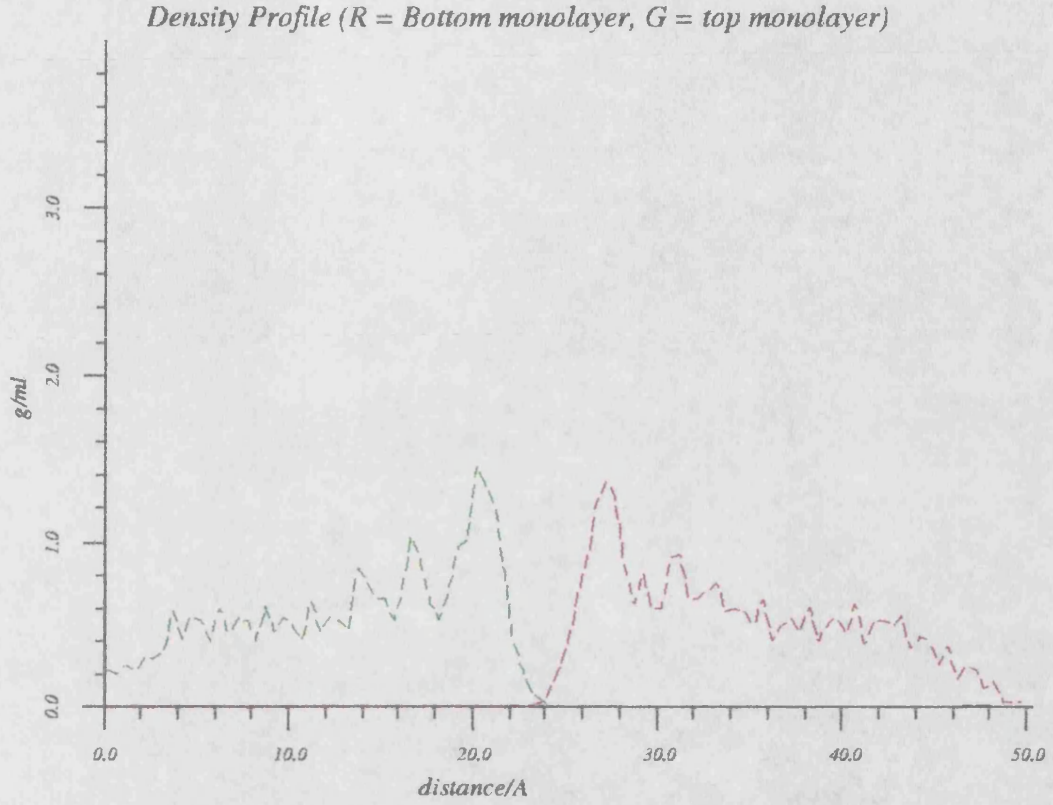
Density Profile (R = Bottom monolayer, G = top monolayer)
g/ml
0.0
1.0
2.0
3.0
0.0
10.0
20.0
30.0
40.0
50.0
distance/A

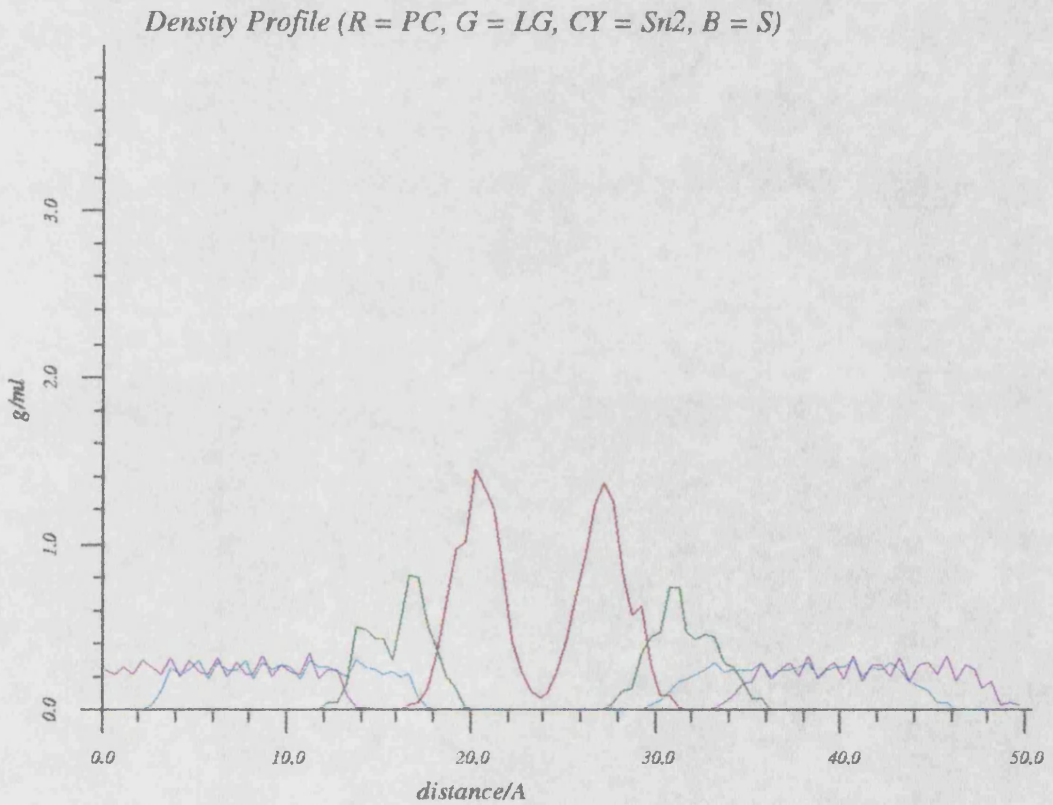
Density Profile (R = PC, G = LG, CY = Sn2, B = S)
g/ml
0.0
1.0
2.0
3.0
0.0
10.0
20.0
30.0
40.0
50.0
distance/A

Figure 7.2.3b

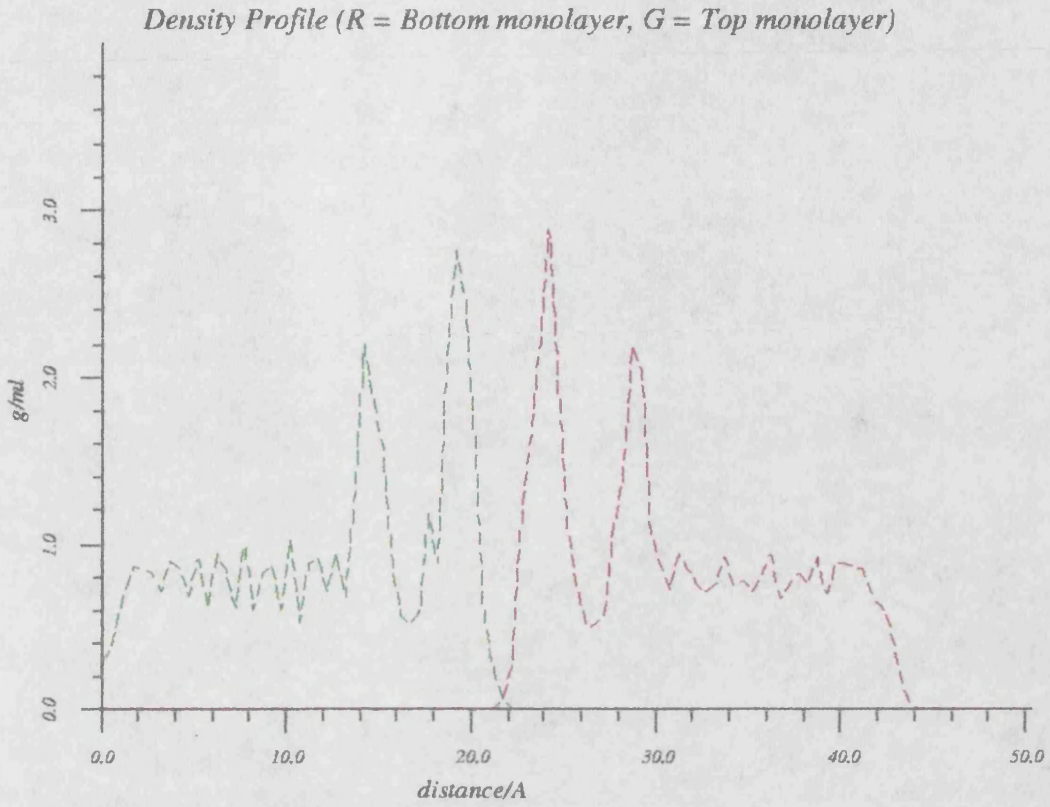
Density Profile (R = Bottom monolayer, G = Top monolayer)
g/ml
0.0
1.0
2.0
3.0
0.0
10.0
20.0
30.0
40.0
50.0
distance/A

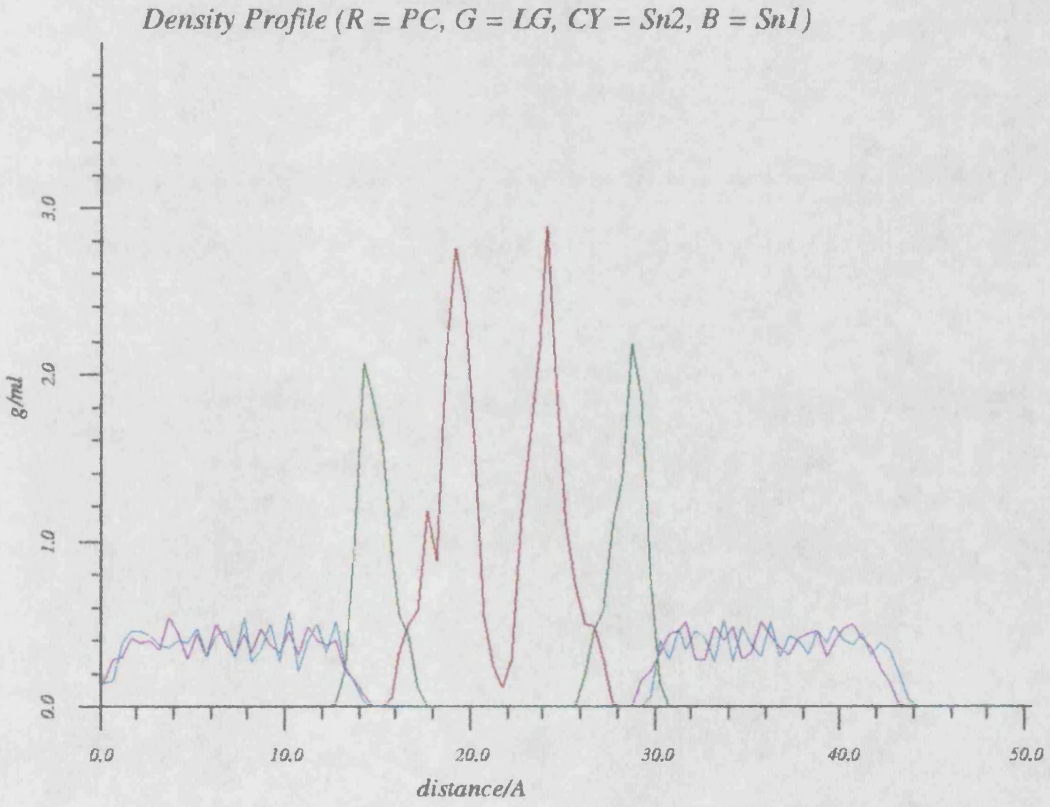
Density Profile (R = PC, G = LG, CY = Sn2, B = Sn1)
g/ml
0.0
1.0
2.0
3.0
0.0
10.0
20.0
30.0
40.0
50.0
distance/A

7.2.5. Torsions

There is on average more conformational freedom in the expanded bilayer model The average standard deviation for the lauryl chains has increased from 4.56 in dlpc to 33.85 in the expanded dlpc_y1 model (Table 7.2.5). This increase in the torsional freedom is sufficient to observe a gauche population in the lauryl chains (Table 7.2.6 and Table 7.2.7). In Table 7.2.7 it can be observed that there is some small variation in the torsional population for the different molecules in the bilayer model, which is a reflection of changes in the free volume of individual chains in the bilayer. Each acyl chain exhibits on average approximately 5% gauche conformations in the sampled trajectory. The Sn2 chain exhibits on average less gauche conformers than the Sn1 lauryl chain. This is in contrast to the experimental results from NMR,[13] in which the Sn2 chain exhibits less order than the Sn1 chain. A change in its orientation with respect to the bilayer normal may be the cause.

Examination of the gauche population in each chain torsion indicates the presence of a plateau region. Torsions ϕ_{15-18} and ϕ_{27-30} exhibit quantitatively less gauche states than the other chain torsions, giving rise to decreased fluidity and hence increased order.

Table 7.2.5

Torsion Statistics dlpc_y1					
Torsion	AvSD	sdSD	Torsion	AvSD	sdSD
ϕ_1	53.7	35.2	ϕ_2	99.1	52.1
ϕ_3	57.9	35.1	ϕ_4	117.7	75.8
ϕ_5	70.3	29.9	ϕ_6	59.1	31.8
ϕ_7	23.4	12.5	ϕ_8	21.8	17.5
ϕ_9	42.7	13.4	ϕ_{10}	16.4	2.1
ϕ_{11}	88.1	59.7	ϕ_{12}	30.7	12.5
ϕ_{13}	35.3	12.5	ϕ_{14}	24.1	9.8
ϕ_{15}	26.7	9.1	ϕ_{16}	26.0	11.2
ϕ_{17}	29.5	10.4	ϕ_{18}	27.6	7.3
ϕ_{19}	32.7	11.2	ϕ_{20}	49.3	34.7
ϕ_{21}	21.6	2.7	ϕ_{22}	14.1	1.2
ϕ_{23}	84.5	47.0	ϕ_{24}	28.1	13.1
ϕ_{25}	32.4	8.4	ϕ_{26}	20.6	10.5
ϕ_{27}	30.9	10.1	ϕ_{28}	23.6	10.5
ϕ_{29}	26.1	9.7	ϕ_{30}	26.2	6.0
ϕ_{31}	34.1	11.4	ϕ_{32}	48.3	29.4

Sampled from 50-300ps.

Table 7.2.6

%Trans/Gauche Conformations dlpc_y1							
	%t	%g^-	%g^+		%t	%g^-	%g^+
ϕ_1	31.50	37.84	28.13	ϕ_2	45.12	25.49	15.82
ϕ_3	37.31	11.97	4.86	ϕ_4	9.50	32.20	38.45
ϕ_5	15.75	32.91	35.28	ϕ_6	22.00	13.49	16.84
ϕ_7	2.00	42.84	48.71	ϕ_8	87.94	0.25	6.77
ϕ_9	28.00	21.57	21.93	ϕ_{10}	92.00	0.00	0.02
ϕ_{11}	1.44	29.67	37.24	ϕ_{12}	85.12	4.94	2.56
ϕ_{13}	82.62	4.71	7.07	ϕ_{14}	91.12	1.48	2.90
ϕ_{15}	90.50	1.57	3.50	ϕ_{16}	90.38	2.58	2.81
ϕ_{17}	88.75	2.34	4.54	ϕ_{18}	90.44	2.99	2.49
ϕ_{19}	86.62	3.49	5.24	ϕ_{20}	83.88	5.35	5.57
ϕ_{21}	29.50	2.61	1.56	ϕ_{22}	91.94	0.00	0.00
ϕ_{23}	8.25	24.03	23.55	ϕ_{24}	86.62	5.68	1.74
ϕ_{25}	87.88	2.41	5.09	ϕ_{26}	92.62	0.69	2.66
ϕ_{27}	88.06	3.61	3.74	ϕ_{28}	91.69	0.53	3.78
ϕ_{29}	90.81	1.65	3.34	ϕ_{30}	92.69	1.95	1.50
ϕ_{31}	85.81	6.18	2.96	ϕ_{32}	83.75	4.67	6.60

Sampled from 50-300ps.

7.2.6. Segmental Order Parameters

The segmental order parameter profile for the lauryl chains has been calculated (Figure 7.2.4). The Sn1 and Sn2 lauryl chains show equivalent order profiles. Indeed the characteristic drop in the order parameter for the second carbon segment of the Sn2 chain is almost completely removed, suggesting some reorientation of the Sn2 chain with respect to the glycerol backbone. The location of the lauryl chains with respect to the bilayer normal in the density profiles and their chain lengths also illustrates the equivalence of the two lauryl chains.

The order parameter "plateau" is conserved in this profile, although extended to carbon segment 9. This is due to the enhanced gauche population in the torsions located at the end of both lauryl chains, which are on average 50% more populated than the other lauryl chain

Table 7.2.7

Acyl Chain Gauche states dlpc_y1			
Molecule	%t	$\%g^-$	$\%g^+$
1	85.56	3.24	5.89
2	89.50	1.29	4.37
3	86.28	3.64	5.12
4	92.89	2.30	1.15
5	86.83	5.17	2.65
6	89.72	2.67	3.07
7	86.33	5.47	2.76
8	90.72	2.60	2.10
9	87.39	3.12	4.61
10	90.67	2.59	2.33
11	87.61	2.99	4.16
12	91.78	1.53	2.65
13	89.72	3.73	2.33
14	83.17	4.88	6.73
15	86.39	4.01	4.59
16	88.22	1.29	6.02

Sampled from torsions ϕ_{12}-ϕ_{20} for Sn1, and ϕ_{24}-ϕ_{32} for Sn2.

torsions. There is an overall decrease in the order of the system compared with the crystal structure density model. This can be assigned to the dominance of the fluidity of the acyl chains compared with the orientational effects in more crystalline models. The equivalence of the two chains order profiles, despite the observed increase in gauche conformations of the Sn1 chain compared with the Sn2 chain would suggest that there are two contributions to the order profile. The fluidity of the chain is dominant in the Sn1 chain, decreasing its order parameter values. However in the Sn2 chain the orientation is the dominant effect on the order profile, increasing its order to that of the Sn1 chain. Hence the two chains exhibit equivalent profiles.

Figure 7.2.4

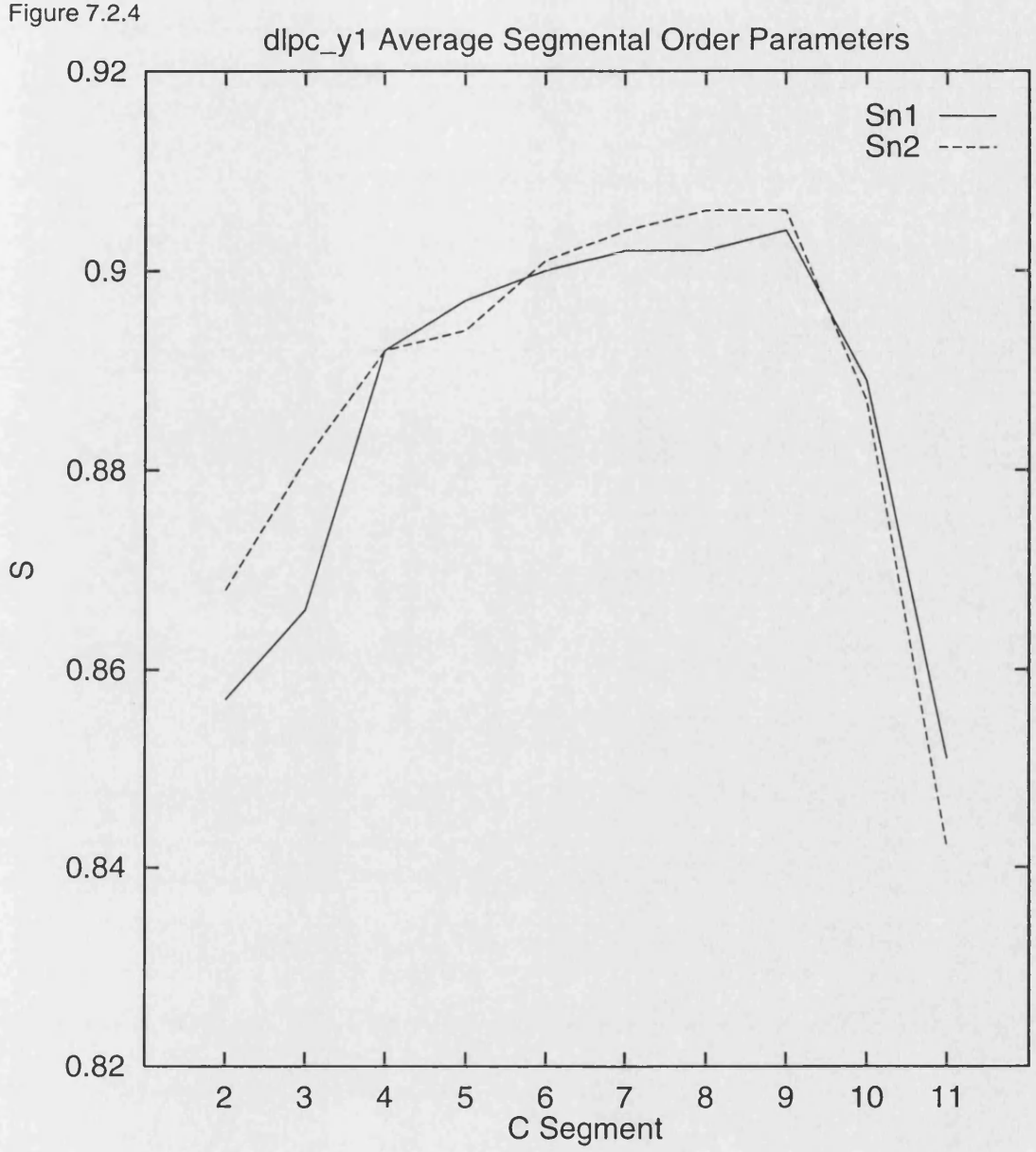
dlpc_y1 Average Segmental Order Parameters
Sn1
Sn2
S
0.92
0.9
0.88
0.86
0.84
0.82
2
3
4
5
6
7
8
9
10
11
C Segment

7.2.7. Thermal Partitioning

The expansion of the system and the increase in conformational freedom exaggerates the partitioning of the temperature between the hydrophilic and hydrophobic moieties (Figure 7.2.5 and Table 7.2.8). The increased flexibility of the head group and glycerol moieties is accompanied by an increase in their temperature. However the lauryl chains are decreased in temperature compared with dlpc. This is the effect of the temperature rescaling, as the increased flexibility of the head group acts as a "heat sink" for the molecule in the initial part of the trajectory. This effect is then exaggerated by the velocity scaling of the temperature constraint. This is due to the increased charge density in the head group, dominating the potential energy of the system and hence the kinetic energy, a small increase in the flexibility of this group results in a relatively larger increase in its atomic velocity. The partitioning is then compounded by the velocity rescaling. The variation of the temperatures of the subcomponents of the system across the trajectory illustrates the partitioning of the thermal energy between the PC head group, glycerol and lauryl chains as a function of time. The temperature differential is maintained throughout the trajectory.

Table 7.2.8

Average Temperature (K) dlpc_y1		
	Av	SD
PC	409.3	15.6
GL	350.5	18.6
Sn1	285.8	10.1
Sn2	287.0	9.3

sampled from 50-300ps.

The average methylene temperatures of each segment (Figure 7.2.7), show an inverse relationship with the segmental order. This conforms to the expected relationship between the temperature and order. An increase in temperature results in a decrease in order. This also supports the molecular orientations effect on the order parameter profile. The shape of the profile is dominated by the presence of gauche conformations and increased torsional flexibility. This is in contrast to the dlpc bilayer model in which the order parameter profile is dominated by the orientational order of the molecules, due to a lack of gauche conformations. This can be seen from the methylene temperatures, which exhibit no correspondence with the

order profile.

Table 7.2.9

Average Methylene Temperatures (K) dlpc_y1					
Sn1			Sn2		
C Segment	Av	SD	C Segment	Av	SD
2	294.0	36.1	2	292.9	34.8
3	293.5	34.5	3	286.3	34.3
4	288.7	34.6	4	287.2	34.0
5	285.7	33.7	5	287.0	34.3
6	281.5	34.7	6	287.0	34.1
7	284.3	33.2	7	285.3	34.2
8	282.3	34.5	8	284.4	33.0
9	281.1	33.3	9	281.3	33.8
10	282.6	33.6	10	283.3	32.6
11	284.4	34.5	11	287.5	32.6
12	296.1	30.0	12	290.6	35.3

Sampled from 50-300ps.

Figure 7.2.5

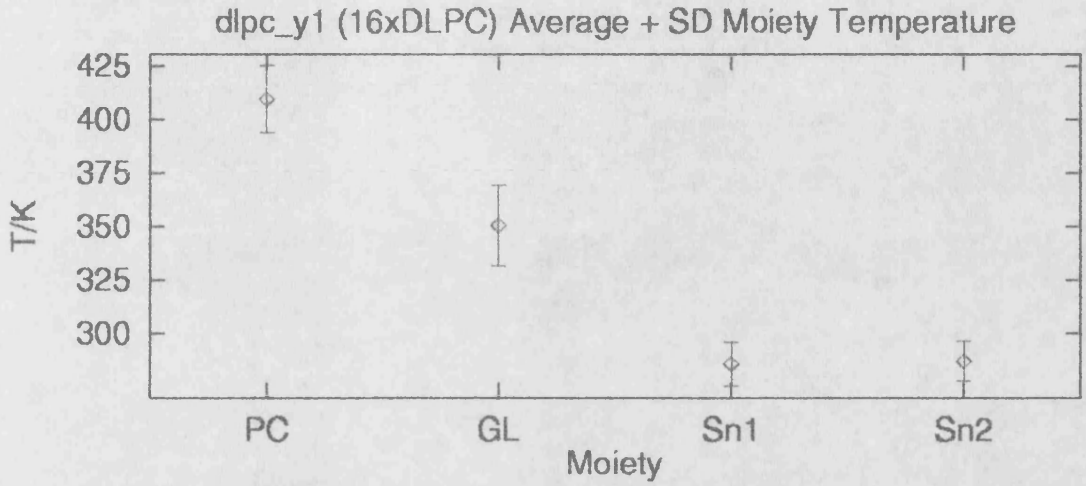

Figure 7.2.6

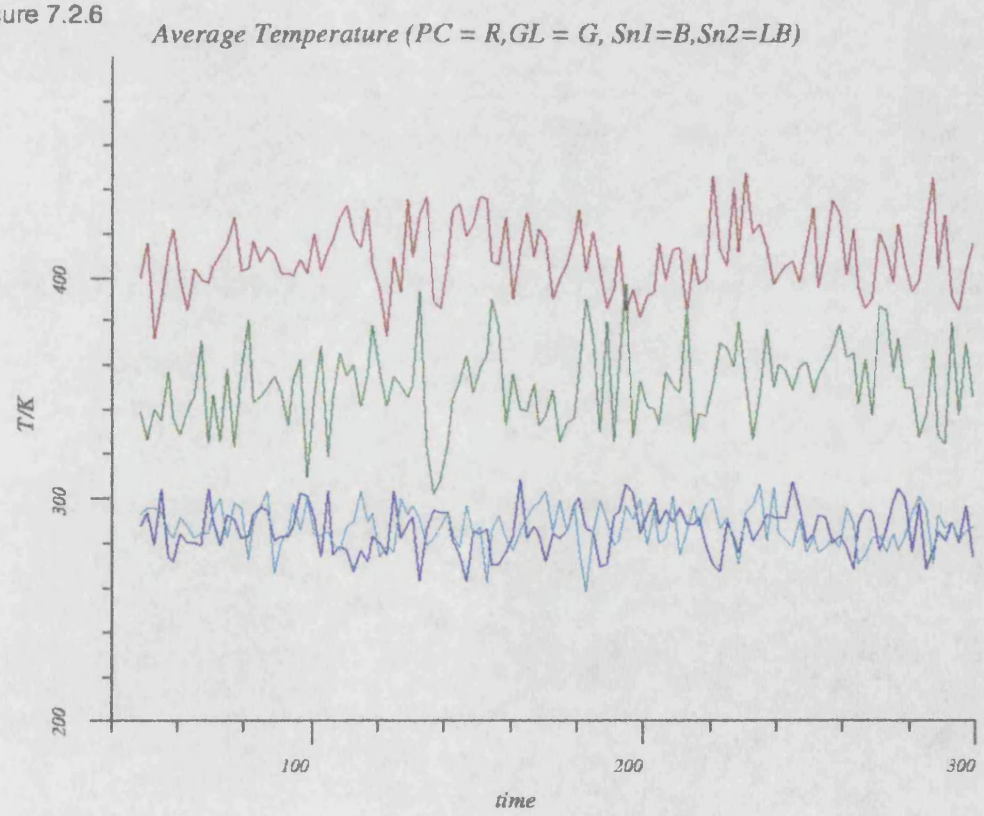

Figure 7.2.7

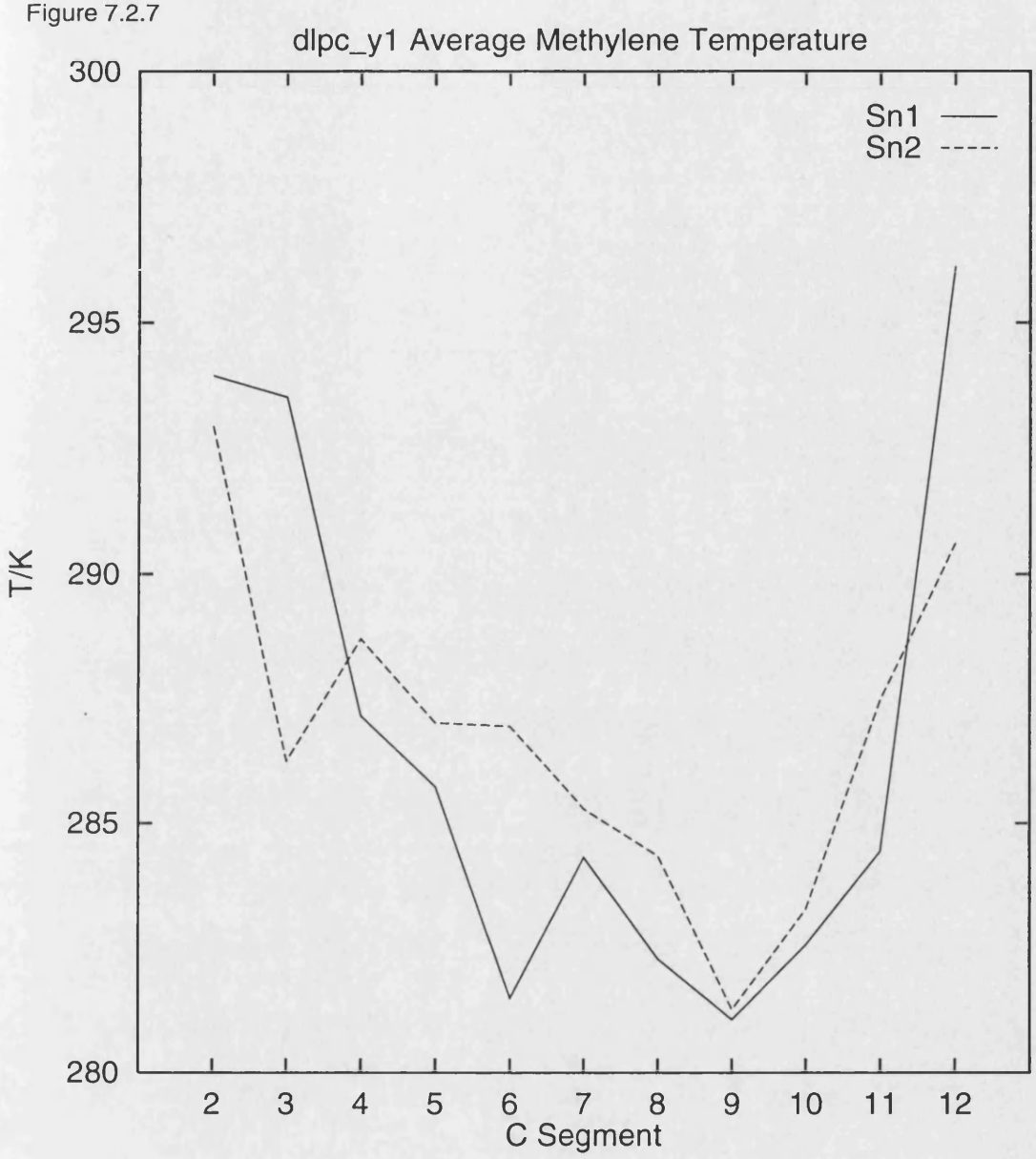
dlpc_y1 Average Methylene Temperature
Sn1
Sn2
T/K
300
295
290
285
280
2
3
4
5
6
7
8
9
10
11
12
C Segment

References

1. Sessions RB. SLICER, Molecular Recognition Centre, Bristol UK
2. Cevc G and Marsh D, in *Phospholipid Bilayers*, Wiley-interscience, 1987.
3. Davies JH, *Biochimica et Biophysica Acta*, vol. 737, pp. 117-171, 1983.
4. Scott HL, *Biochemistry*, vol. 25, no. 20, pp. 6122-6126, 1986.
5. Morrow MR, Singh D, Lu D, and Grant CWM, *Biophysical J*, vol. 64, no. 3, pp. 654-664, 1993.
6. Davies MA, Hubner W, Blume A, and Mendelsohn R, *Biophysical J*, vol. 63, no. 4, pp. 1059-1062, 1992.
7. Fenske DB and Cullis PR, *Biophysical J*, vol. 64, no. 5, pp. 1482-1491, 1993.
8. Knowles PF and Marsh D, *Biochem J*, vol. 274, pp. 625-641, 1991.
9. Ermer O and Lifson S, *J Chem Phys*, vol. 95, no. 13, p. 4121, 1973.
10. Warshel A and Lifson S, *J Chem Phys*, vol. 53, no. 2, p. 582, 1970.
11. Stouch TR, Ward KB, Altieri A, and Hagler AT, *J Comp Chem*, vol. 12, no. 8, pp. 1033-1046, 1991.
12. Stouch TR and Williams DE, *J Comp Chem*, vol. 14, pp. 1066-1076, 1993.
13. Marsh D, in *Handbook of Lipid Bilayers Crc Press*, 1991.

8. Mixed DLPC and Cholesterol Bilayer Models

8.1. System III dlpcchol (8xDLPC+8xCHOL)

The effect of cholesterol on the dynamics and structure of bilayers has been the subject of many studies. Its effect at the molecular level on the structure and dynamics of phospholipid molecules in its association is therefore of fundamental interest. The mixed DLPC and cholesterol bilayer model *dlpcchol* has been constructed from the dlpc model (based on the DLPE crystal structure). Alternate DLPC molecules from each monolayer have been replaced with cholesterol molecules. They are arranged such that no cholesterol molecule is adjacent to another cholesterol either within its monolayer or in the opposing monolayer (see Chpt4). There is a wealth of experimental data for 50% cholesterol bilayer dispersions. At room temperature and pressure they are in the L_α phase region.[1]

The resulting coordinates were then minimised and used as the starting configuration for sampling the molecular dynamics trajectory. The molecular dynamics trajectory was sampled from the NVT ensemble for 300ps using a temperature constraint of 310K. This resulted in an average temperature of 310.2±4.7K. The volume of the unit cell was 15569.3$Å^3$.

8.1.1. Energetics

The relative energetic contributions from both intramolecular and intermolecular interactions have been examined (Table 8.1.1). After about 30ps of the trajectory has been sampled, the potential energy of the system reduces to reach a stable equilibrium value of 308.0±73.8kcal/mol. The kinetic energy is constrained to 1331.5±20.2kcal/mol by the constant temperature algorithm. The intermolecular interactions all reflect this equilibration phase of the trajectory. The contribution of the electrostatic energy is less obvious in this simulation due to the reduction in charge density of the system in the region of the head group on the introduction of cholesterol. The relatively densely charged PC group is replaced with the hydroxyl group of the cholesterol molecule. The sterol ring system also reduces the PC contact distances within the bilayer plane, reducing the contribution of the electrostatic component to the potential energy.

The relative distribution of the internal energies is changed from the starting configuration. E_θ rapidly increases from the starting conformation due to the internal strain in the

cholesterol sterol ring system to reach an ensemble average of 815.5±18.1kcal/mol. The torsional energy decreases from the initial configuration, to reach an ensemble average of 612.1±12.5kcal/mol while the bond energy is increased to reach an average value of 662.2±21.3kcal/mol.

The pressure of the system is negative, reflecting the large negative contribution to the energy by the electrostatic and dispersive contributions at this density. The components of the pressure exhibit a large standard deviation, an indication of the dominance of the pressure by small intermolecular interactions.

8.1.2. Density Profile

The density profiles of the cholesterol doped systems have been calculated, sampling groups of 100 configurations from the trajectory at 50ps intervals to calculate the density profile. Figure 8.1.2 illustrates the average of these profiles and clearly shows the modifying effect of the cholesterol on the density distribution of the bilayer system. The phosphatidylcholine head group region is much less pronounced in the overall density of each monolayer. The PC head groups of each monolayer are in direct contact across the periodic system, indicated by the density of the PC group of the DLPC molecules. The general shape of the profile is more smooth. The cholesterol increases the density of the hydrophobic region near to the centre of the bilayer. This will have a profound effect on the dynamics of the chain segments in this proximity. There is little change in the density of the lauryl chains across the trajectory. The cholesterol modifies the interaction of the lauryl chains disrupting their packing and preventing mixing of the chains. This has the effect of avoiding local density fluctuations and increasing the order of the system below the phase transition in the gel phase(L_{β}). Above the transition temperature the planarity of the sterol ring system introduces order into the hydrophobic region by disrupting the mixing of chain segments.[2]

The cholesterol maintains its position located such that the hydroxyl group occupies the same region of bilayer normal space as the glycerol group. This is in the boundary between the hydrophilic and hydrophobic regions of the bilayer and represents a region of intermediate charge density. The profiles of the two monolayers are not identical, some degree of membrane anisotropy exists between the two monolayers. This is most evident in the structure of the two monolayers density profiles.

Table 8.1.1

Energetics (kcal/mol) dlpcchol		
	E	SD
E_{KE}	1331.6	20.2
E_{tot}	1639.6	71.5
E_{PE}	308.0	73.8
E_{dsp}	-3868.3	33.6
E_{rep}	3108.4	37.8
E_{est}	-967.9	71.6
E_{ϕ}	612.1	12.5
E_{θ}	815.5	18.1
E_b	662.2	21.3
	T/K	SD
T	310.2	4.7
	P/bar	SD
P	-1231.0	722.4
P_x	-295.9	2667.6
P_y	-2021.3	2360.2
P_z	-1361.0	2305.2
	D/Å	SD
A	47.7	0.0
B	16.0	0.0
C	20.4	0.0
	V/Å^3	SD
V	15569.3	0.0

Sampled over 80-300ps.

8.1.3. Non-Bonded internals

The nonbonded internal angles have been sampled from the equilibrium state of the trajectory (Table 8.1.2). These exhibit a larger range of values in the different DLPC molecules within the model bilayer compared to the pure dlpc model although individual molecules do not exhibit significantly different standard deviations for their occupied conformation. This

Figure 8.1.1a

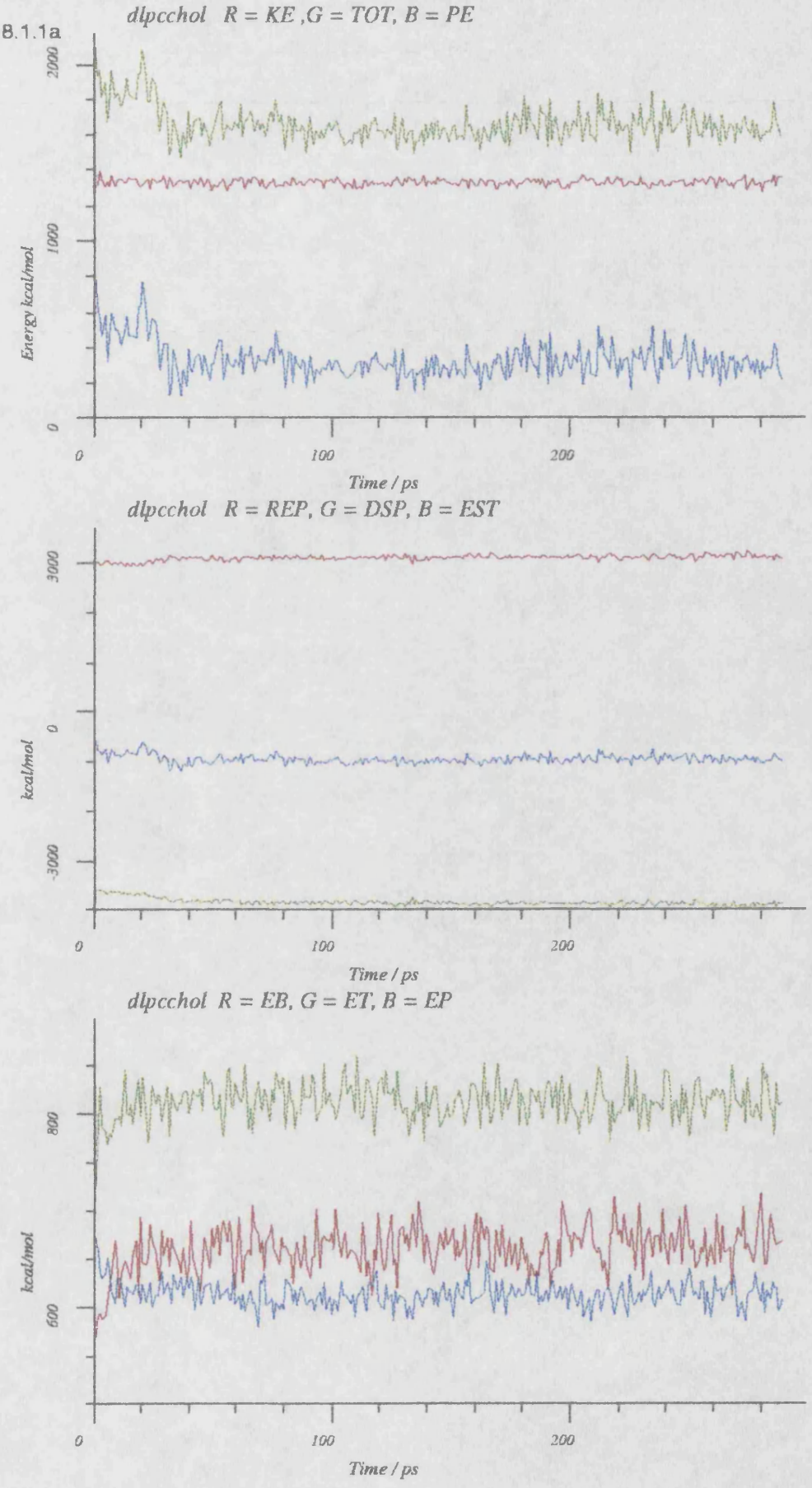
dlpcchol R = KE ,G = TOT, B = PE
Energy kcal/mol
2000
1000
0
0
100
200
Time / ps
dlpcchol R = REP, G = DSP, B = EST
kcal/mol
3000
0
-3000
0
100
200
Time / ps
dlpcchol R = EB, G = ET, B = EP
kcal/mol
800
600
0
100
200
Time / ps

Figure 8.1.2

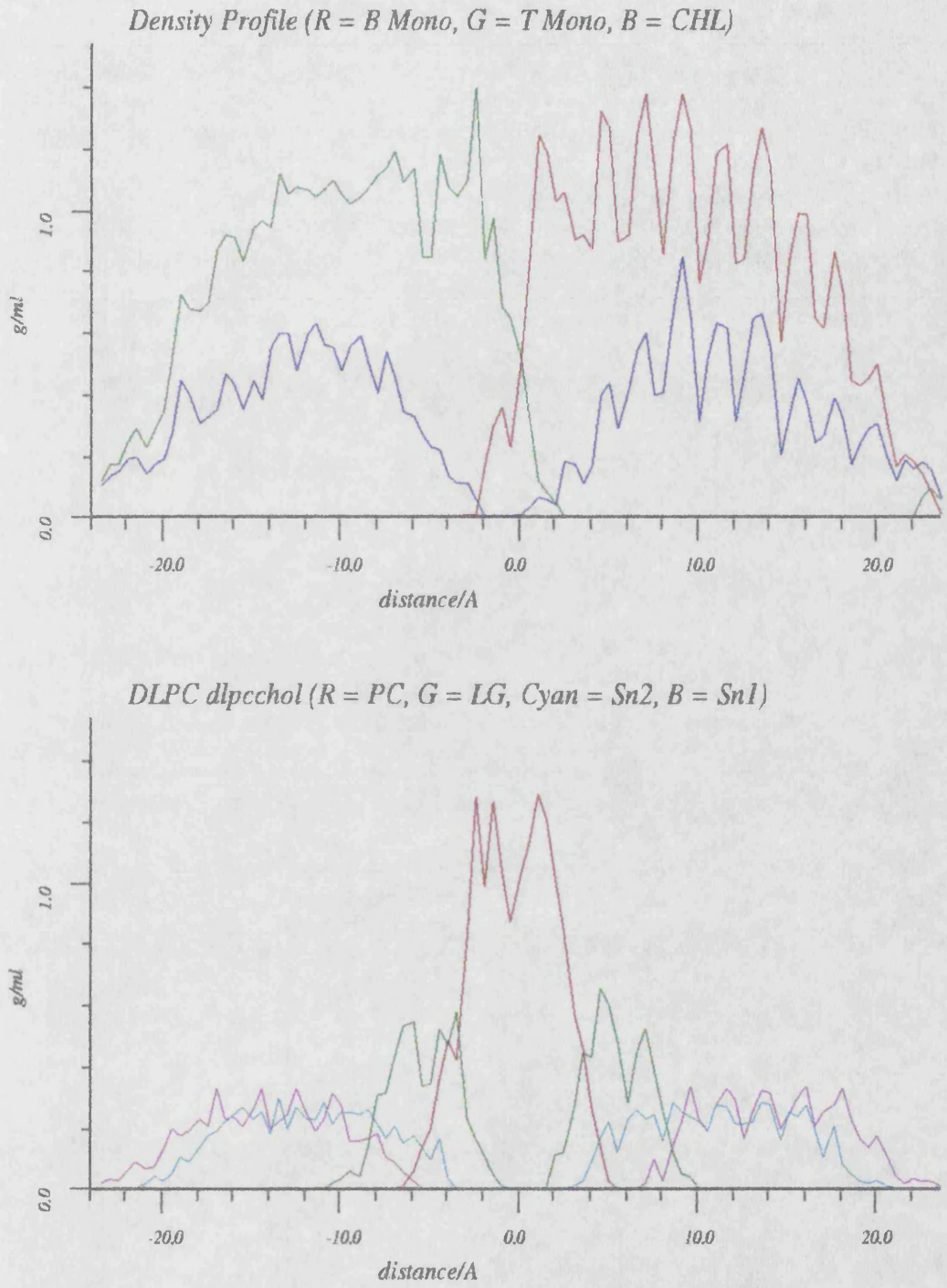
Density Profile (R = B Mono, G = T Mono, B = CHL)
g/ml
1.0
0.0
-20.0
-10.0
0.0
10.0
20.0
distance/A
DLPC dlpcchol (R = PC, G = LG, Cyan = Sn2, B = Sn1)
g/ml
1.0
0.0
-20.0
-10.0
0.0
10.0
20.0
distance/A

indicates that the increased free volume associated with the cholesterol doped bilayer allows for conformational adjustment of the DLPC molecules during the equilibration phase. Once these conformations have been occupied the system remains effectively "locked" in this configuration and conformation. The characteristic "scissor" angle (θ_2) is increased slightly from the dlpc bilayer model, again reflecting the increased free volume in the starting configuration. The head group orientation (θ_1) adopts a similar conformation to the expanded dlpc_y1 model parallel to the bilayer surface. It does however exhibit a larger average standard deviation showing increased flexibility.

The defined internal angle in cholesterol (θ_5) measures the degree of rigidity of the sterol ring system with respect to its saturated chain. This angle does not exhibit significant deviation over the sampled trajectory, the cholesterol molecule maintaining its initial conformation.

Table 8.1.2

Non-Bonded Angles dlpcchol			
	Av	SD	avSD
θ_1	106.0	18.0	4.7
θ_2	18.7	1.7	2.3
θ_3	114.6	18.2	4.4
θ_4	131.0	16.4	4.3
θ_5	165.3	1.9	4.2

Sampled over 80-300ps. Av is the average over all angles, SD is the standard deviation of those averages, and avSD is the average standard deviation of the individual values.

The above trend in the internal angles is also mirrored in the nonbond internal distances (Table 8.1.3). These exhibit a larger range of values for the nonbond distances between the head group, glycerol and the lauryl chains, although the length of the lauryl chains varies little(C8-C19,C20-C31). The average standard deviation for these nonbonded distances is similar to that in the dlpc model indicating conformational restriction in the equilibrium configuration.

Table 8.1.3

Non-Bonded Distances (Å) dlpcchol			
	Av	SD	avSD
N P	4.5	0.3	0.1
N C6	6.7	0.6	0.2
C6 C19	16.6	0.4	0.2
C6 C31	14.0	0.5	0.3
C8 C19	13.9	0.0	0.1
C20 C31	13.2	0.2	0.2
C19 C31	5.6	0.5	0.6

Sampled over 80-300ps. Av is the average over all equivalent distances, SD is the standard deviation of those averages, and avSD is the average standard deviation of the individual values.

8.1.4. Euler Angles

The Euler angles for the glycerol group (Table 8.1.4) are very similar to those of the dlpc model, indicating that the restriction of the DLPE crystal structure packing is the dominant effect on the conformational restriction of the bilayer although the increased free volume present due to the cholesterol does allow some increased configurational freedom.

Table 8.1.4

Euler Angles dlpcchol			
	Av	SD	avSD
1	85.3	62.2	4.8
2	112.6	1.3	3.1
3	122.8	0.5	2.9

Sampled over 80-300ps. Av is the average over all angles, SD is the standard deviation of those averages, and avSD is the average standard deviation of the individual values.

8.1.5. Torsions

The defined torsion angles for both the DLPC and cholesterol molecules have been calculated across the sampled trajectory and their ensemble standard deviations calculated (Table 8.1.5). Comparison of the values obtained from the dlpc model with the same density indicates some important differences in the conformational properties of DLPC in the two models. The cholesterol doped model bilayer shows a small increase in the standard deviation of its acyl chain torsion angles (dlpc 5.0, dlpcchol 5.2). This is due to the small increase in free volume of the system on introduction of the more planar sterol ring system, which while increasing the density profile of the acyl chains with respect to the bilayer normal, provides increased free volume by virtue of its reduced area of cross section.

The location of the cholesterol with respect to the bilayer normal[3] is such that the bulk of its density lies in the region of the lauryl chains. This allows for a large increase in the free volume available to the PC head group resulting in the increased torsional flexibility exhibited in both the PC and glycerol torsions (ϕ_{3-6}, $\phi_{9,11}$ and $\phi_{21,23}$). These torsions control the conformational adjustment of the DLPC molecule in the gel phase allowing it to attain the equilibrium configuration without fluidisation of the acyl chain torsions. There is not enough conformational freedom in the acyl chain torsions to induce any gauche population at this density on introduction of cholesterol. The cholesterol acyl chain torsions also exhibit the same standard deviation for their torsion angles as those in the DLPC molecule.

8.1.6. Segmental Order Parameters

The segmental order parameters for all carbon segments in the two lauryl chains of DLPC in the dlpcchol bilayer system have been calculated across the trajectory relative to the bilayer normal unit cell axis. The resulting order parameter is the average over all equivalent segments and over the sampled trajectory. Figure 8.1.3 shows the resulting segmental order parameter profile. The characteristic drop in the segmental order parameter value at the second carbon segment of the Sn2 chain can be observed. There is an overall drop in the order of the system doped with cholesterol (Sn1 0.80±0.16, Sn2 0.85±0.11). This is in contrast to the expected increase in order in the gel phase bilayer.[2] This may however be a consequence of the lack of gauche conformations in the lauryl chains, giving rise to a dominance of the order parameter values by the orientation of the molecule with respect to the bilayer normal, rather than the fluidisation of the lauryl chains.

Table 8.1.5

Torsion standard deviations dlpcchol			
	avSD		avSD
DLPC			
ϕ_1	6.2	ϕ_2	5.5
ϕ_3	19.9	ϕ_4	18.7
ϕ_5	13.0	ϕ_6	13.1
ϕ_7	5.4	ϕ_8	5.0
ϕ_9	28.3	ϕ_{10}	8.5
ϕ_{11}	27.4	ϕ_{12}	5.3
ϕ_{13}	5.1	ϕ_{14}	5.0
ϕ_{15}	4.9	ϕ_{16}	5.0
ϕ_{17}	5.0	ϕ_{18}	5.2
ϕ_{19}	5.3	ϕ_{20}	5.4
ϕ_{21}	16.0	ϕ_{22}	7.6
ϕ_{23}	17.6	ϕ_{24}	5.7
ϕ_{25}	5.1	ϕ_{26}	5.4
ϕ_{27}	4.9	ϕ_{28}	5.0
ϕ_{29}	5.0	ϕ_{30}	5.2
ϕ_{31}	5.2	ϕ_{32}	5.4
CHOL			
ϕ_1	5.3	ϕ_2	5.2
ϕ_3	5.3	ϕ_4	5.3
ϕ_5	5.3		

Sampled from 50-300ps. The avSD is the average standard deviation of all equivalent torsion angles.

The order profile for the Sn1 chain is flattened with respect to the dlpc model. This is a direct consequence of the increased density in the upper segments of the lauryl chain from the sterol ring system. This results in the removal of the order parameter plateau in the Sn2 chain which shows increased order over the first 7 carbon segments before the order reduces in proximity to the terminal segment. The cholesterol acyl chain exhibits order parameters

equivalent in magnitude to the Sn2 chain although the profile is less smooth. This may indicate that the Sn2 chain and the cholesterol are orientationally similar, whereas the Sn1 chain is angled to the bilayer normal resulting in a flattened profile of reduced order.

Figure 8.1.3

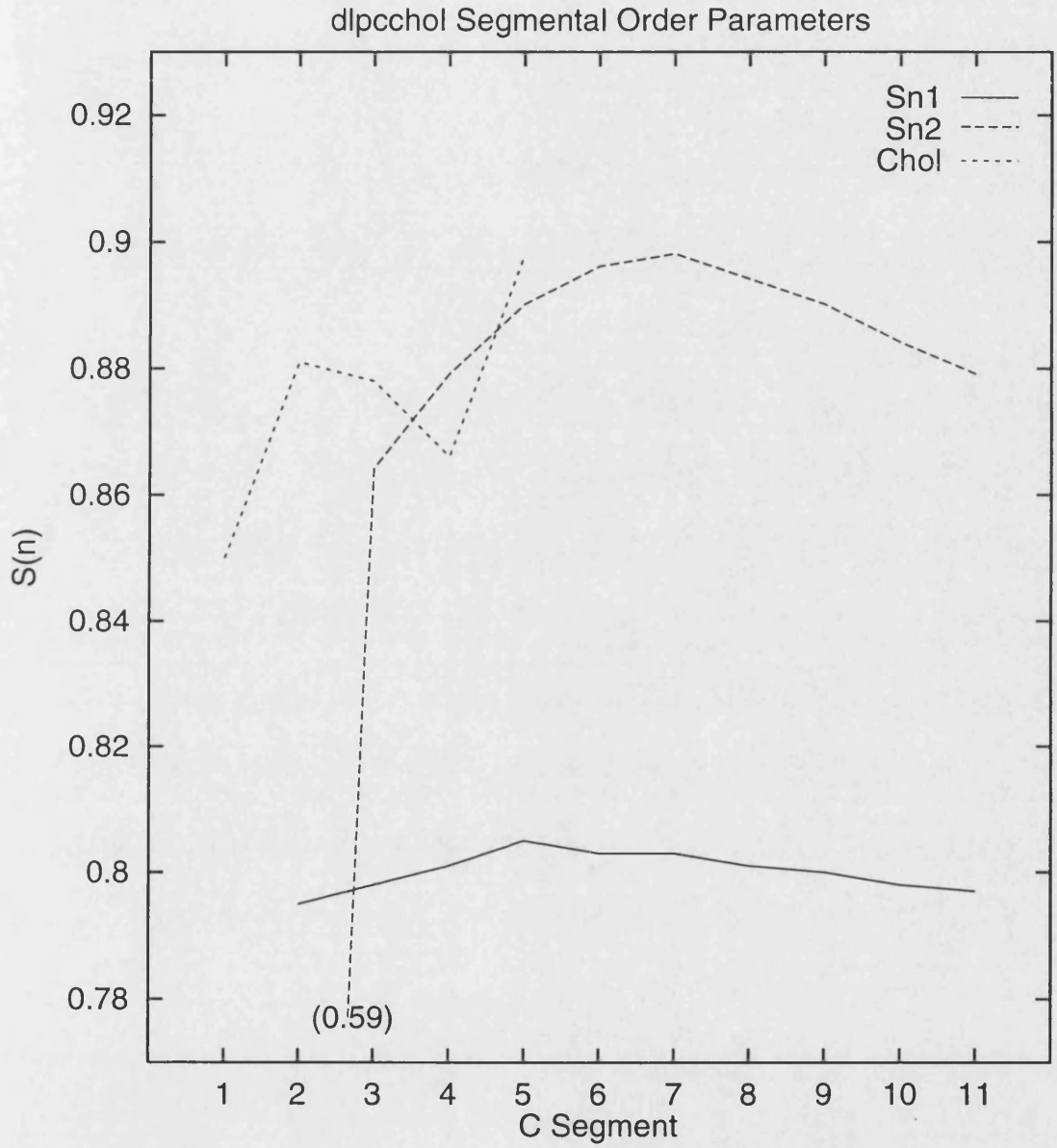

8.1.7. Thermal Partitioning

The partitioning of the thermal energy of the system in this two component model has been examined by calculating the temperature of the subcomponents of the system. The temperature of the cholesterol molecules and subcomponents of the DLPC molecule (PC, glycerol

and lauryl chains) have been calculated from their atomic velocities at each time step across the sampled trajectory (Table 8.1.5 & Figure 8.1.4).

Comparing the ensemble average temperatures of the DLPC moieties in the dlpc and dlpcchol models, both trajectories being sampled from the NVT ensemble using identical temperature baths of 310K, it is clear that the thermal partitioning in the cholesterol doped system is significantly different from that in the single component bilayer. The cholesterol appears to reduce the partitioning of the atomic temperature into the subcomponents of the DLPC molecule. The average temperature of the PC head group is reduced from 329.3K in dlpc to 319.2K in dlpcchol, while the lauryl chains are increased in temperature from 301.3K and 303.2K for the Sn1 and Sn2 chains respectively in the dlpc model to 307.4K and 310.8K in dlpcchol. The glycerol temperature is relatively uneffected; it is 315.1K in dlpc and 315.3K in dlpcchol. The standard deviation for all these temperatures are increased indicating an increase in heat capacity of the system on addition of the cholesterol.

The origins of this change in thermal partitioning lie in the modification of the electrostatic interactions of these groups on addition of the cholesterol. There is an increased separation of the PC head groups in the plane of the bilayer, reducing the electrostatic interactions and allowing increased conformational freedom in the head group of the DLPC molecule. This increased motion reduces the effect of cross periodic interactions reducing the atomic forces and hence velocities of the head group atoms. The rigidity of the sterol system in the plane of the acyl chains prevents the cooperativity of the chains increasing their interaction leading to increased atomic velocities. The environment of the glycerol group is relatively unchanged, the hydroxyl group of the cholesterol is very similar in charge density to that of glycerol. Hence the glycerol group experiences relatively similar interactions. Table 8.1.7 shows the average methylene temperatures for the carbon segments in the lauryl Sn1 and Sn2 chains of DLPC. These reflect the inverse of the segmental order parameter profile. As expected increased temperature results in decreased order within the profile. The methylene temperature profile for the cholesterol doped model (Figure 8.1.5) exhibits a much flatter shape and increased absolute temperatures resulting in a flatter and generally lower order profile. The application of the methylene temperature profile to explain the order parameter profile is of limited use in the gel phase state simulations where the order is orientational in nature.

Table 8.1.6

Average Moiety Temperature (K) dlpcchol		
	Av	SD
PC	319.2	16.2
GL	315.3	23.4
Sn1	307.4	14.5
Sn2	310.8	14.9
DLPC	312.4	7.3
CHOL	307.2	9.0

Sampled over 80-300ps.

Table 8.1.7

Average Methylene Temperature (K) dlpcchol					
Sn1			Sn2		
C Segment	Av	SD	C Segment	Av	SD
2	310.9	51.0	2	308.8	51.0
3	309.7	50.7	3	314.3	52.1
4	306.4	50.8	4	310.3	51.3
5	307.8	50.2	5	312.2	51.8
6	307.2	51.2	6	310.2	52.1
7	306.8	50.5	7	307.9	51.1
8	303.1	50.0	8	311.5	51.2
9	307.7	52.2	9	309.6	52.3
10	307.9	51.4	10	308.1	50.6
11	309.3	50.6	11	311.5	51.4
12	305.4	44.1	12	313.8	43.8

Sampled over 50-300ps.

Figure 8.1.4

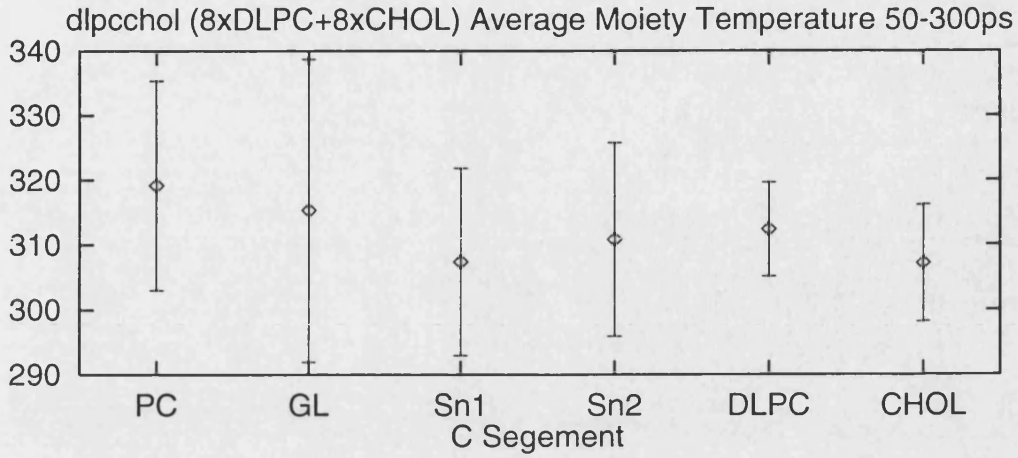

Figure 8.1.5

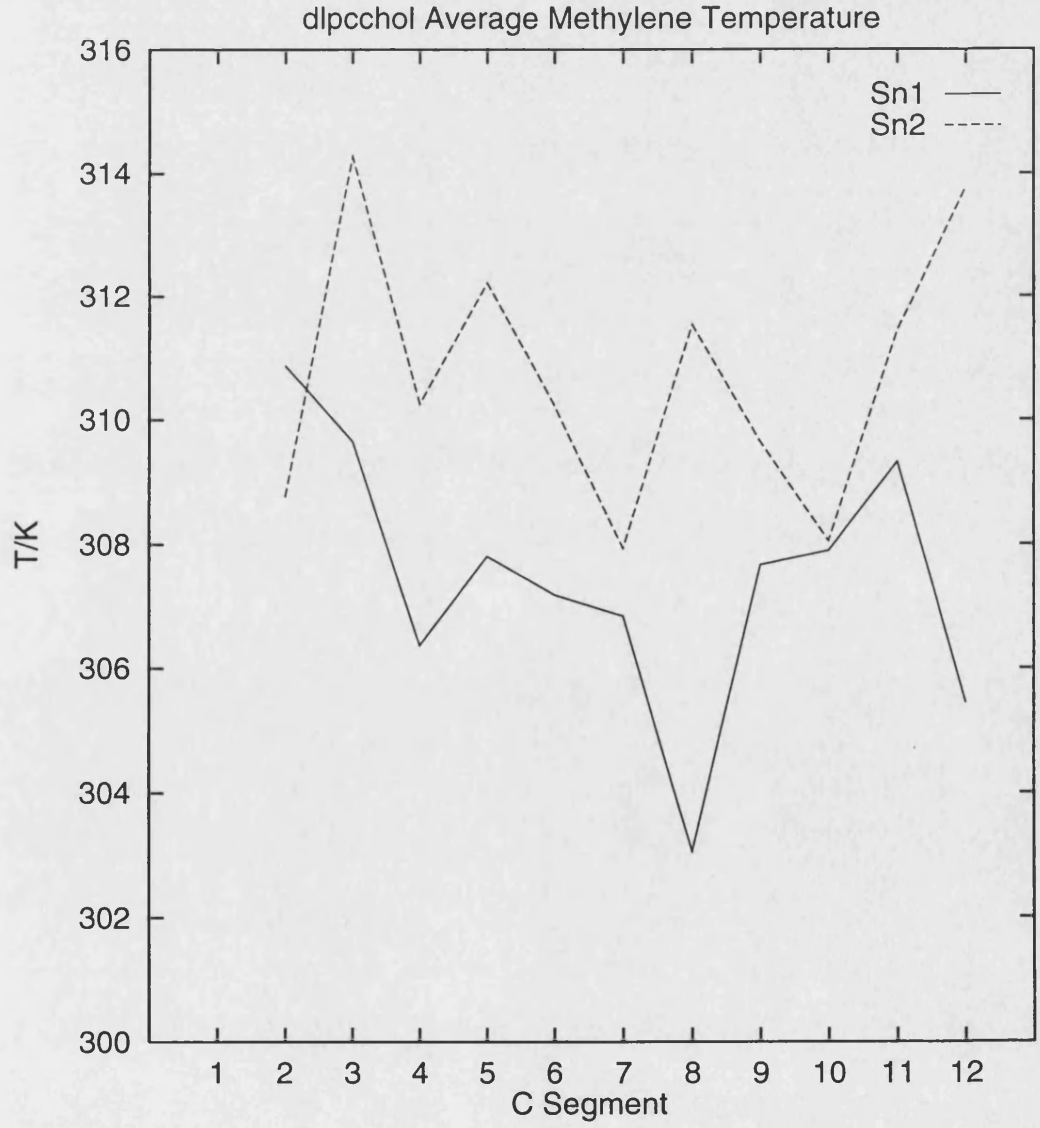

8.2. System IV dlpcchol_s (8xDLPC+8xCHOL)

From the encouraging results of rescaling the coordinates of the centers of mass of the molecules within the bilayer in the dlpc model it was decided to apply this method to the cholesterol doped system. The bilayer model *dlpcchol_s* was constructed from the dlpcchol bilayer coordinates, expanded along all three cell axes. The centres of mass coordinates of all molecules in the unit cell are translated such that their spatial arrangement is conserved. Rescale factors of A=1.05, B=1.5 and C=1.5 were used in order to rescale the positions of the centre of mass of all molecules in the bilayer lattice. The unit cell lengths are also rescaled expanding the volume of the system from 15569.3Å^3 to 23540.8Å^3 and increasing the free volume between each molecule in the bilayer plane.

The resulting coordinates were then minimised and used as the starting coordinates to sample the molecular dynamics trajectory (Table 4.4). The molecular dynamics trajectory was sampled from the NPT ensemble, for 300ps using a temperature constraint of 320K and pressure constraint of 1bar. The bilayer normal is orientated along the A unit cell axis. The ensemble average temperature was 321.8±5.0K.

8.2.1. Energetics

Table 8.2.1 and Figures 8.2.1a and 8.2.1b show the extracted ensemble average and variation of each characteristic energy and thermodynamic quantity of the system across the trajectory. The volume of the system is reduced rapidly over the first 30ps of the trajectory under the constant pressure algorithm. The volume being decreased from 23540.8Å^3 to around the ensemble average of 14711.0Å^3 in 30ps. The volume does not however stabilise until 80ps of trajectory has been sampled. This volume change is not isotropic the bilayer normal unitcell axis A, is reduced by 13.0%, B by 16.7% and C by 16.1%, reflecting the relative rescaling of the coordinates. This change in volume of the system is not smooth, there is a significant change in the volume at 70ps, indicating change in either the configuration or conformation of the system resulting in a relatively large volume change. The sampled trajectory was taken from 80-300ps in the trajectory, the system having stablised with respect to volume changes brought about by the pressure scaling algorithm. The pressure of the system exhibits similar standard deviations to the NVT ensemble trajectory, again indicating the problem of pressure scaling in such a relatively small system in which the pressure is so sensitive to

small intermolecular contacts.

Table 8.2.1

Energetics (kcal/mol) dlpcchol_s		
	E	SD
E_{KE}	1381.0	21.7
E_{tot}	2069.2	103.0
E_{PE}	688.2	104.8
E_{dsp}	-2749.1	22.1
E_{rep}	2690.4	29.6
E_{est}	-988.4	103.9
E_{ϕ}	232.1	8.6
E_{θ}	855.5	20.4
E_b	682.8	22.8
	T/K	SD
T	321.8	5.0
	P/bar	SD
P	96.2	916.1
P_x	-23.1	3101.1
P_y	24.6	2555.8
P_z	-9.6	2560.5
	D/Å	SD
A	43.8	0.7
B	16.5	0.3
C	20.3	0.2
	V/Å^3	SD
V	14711.0	169.2

Sampled from 80-300ps.

Figure 8.2.1a

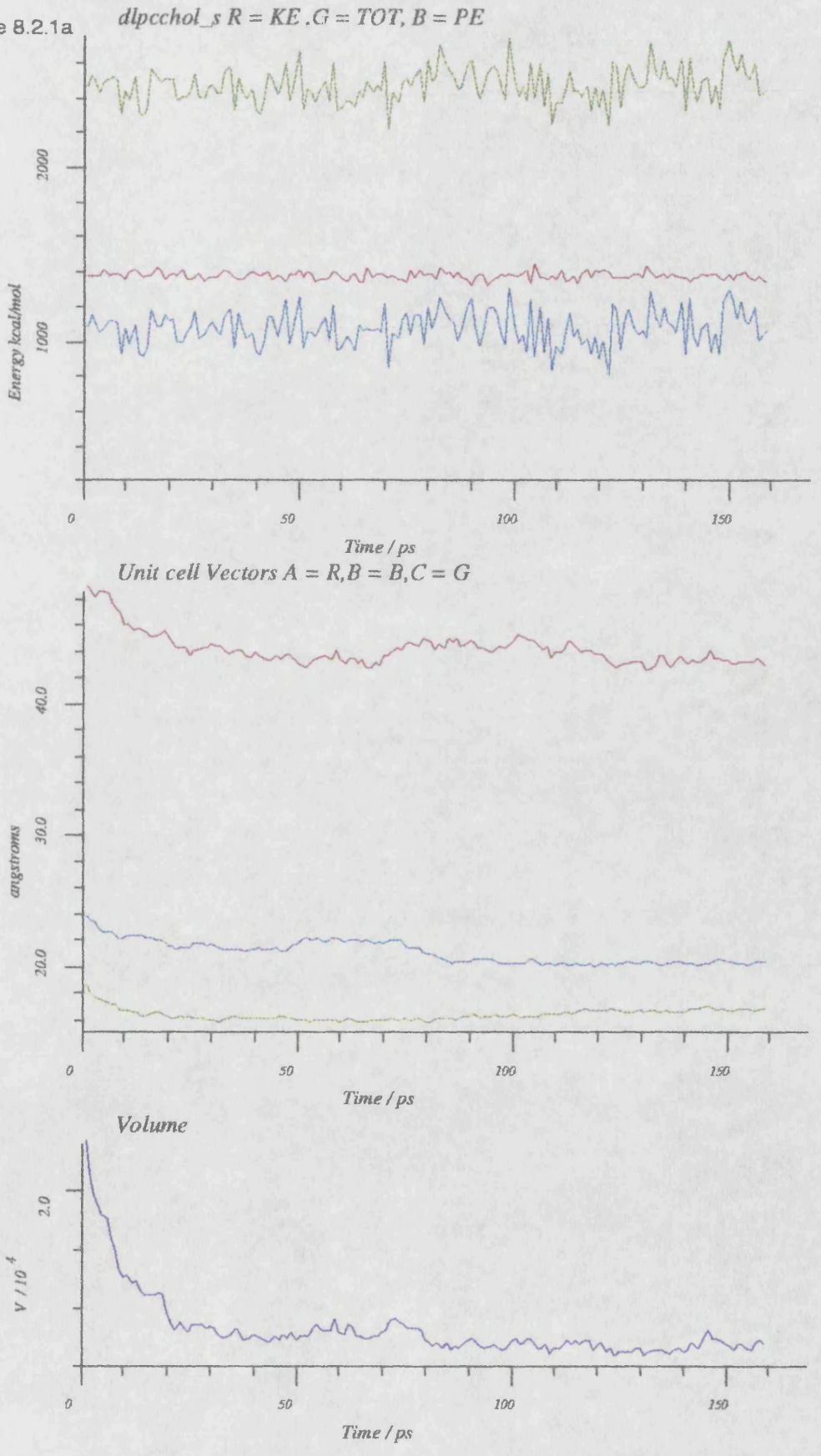
dlpcchol_s R = KE .G = TOT, B = PE
Energy kcal/mol
2000
1000
0
50
100
150
Time / ps
Unit cell Vectors A = R,B = B,C = G
angstroms
40.0
30.0
20.0
0
50
100
150
Time / ps
Volume
V / 10^4
2.0
0
50
100
150
Time / ps

Figure 8.2.1b

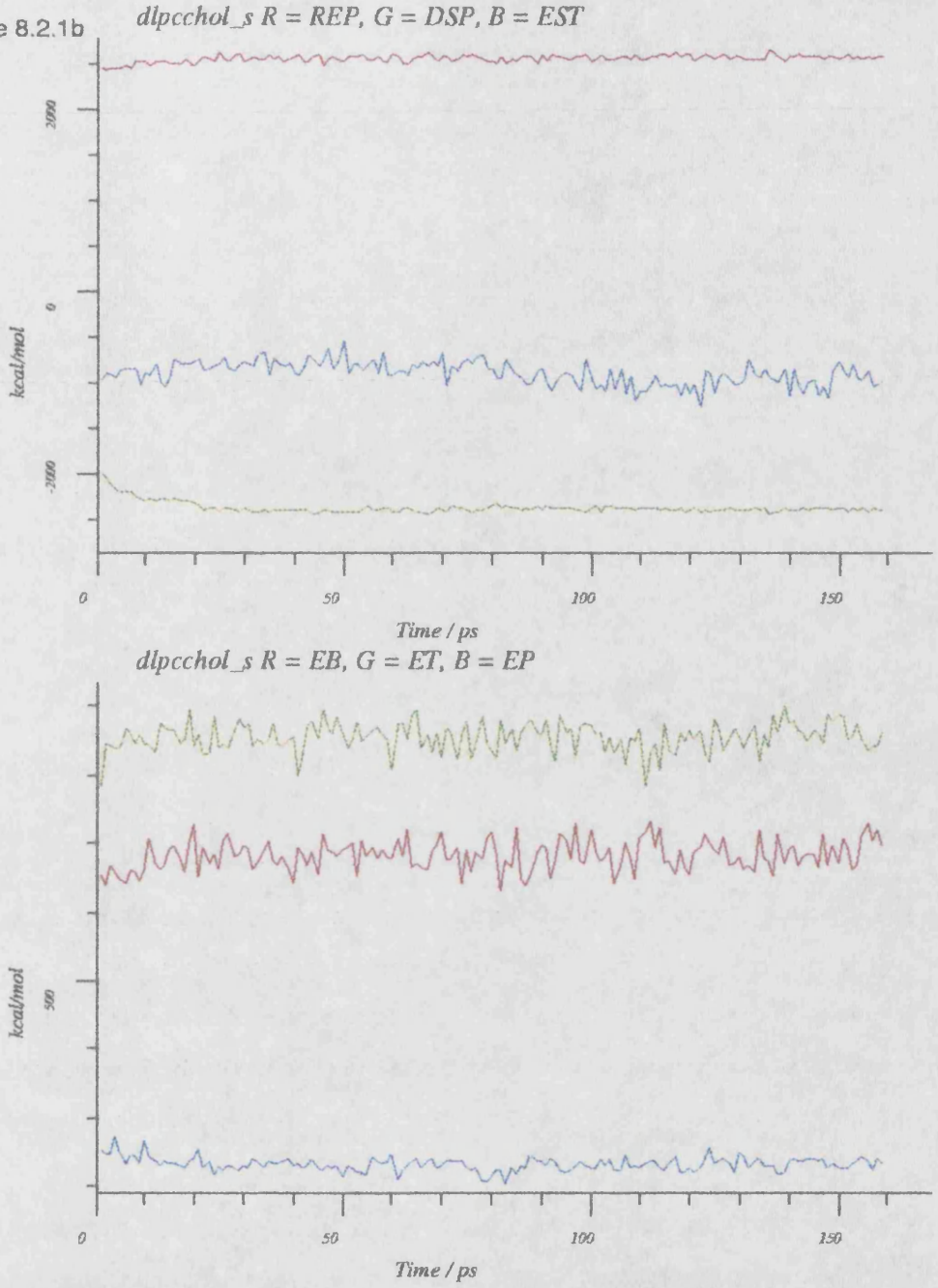

8.2.2. Density Profiles

The density profiles of various defined groups of atoms in the cholesterol doped and expanded bilayer model dlpcchol_s have been calculated from the 50-160ps part of the sampled trajectory (Figure 8.2.2). The resulting profiles are the ensemble average using every tenth step from the trajectory. The inequivalence of the Sn1 and Sn2 lauryl chains in the bilayer normal space is removed, the two chains now occupying the same region of bilayer normal space. There is an increase in the density of the cholesterol in the centre of the bilayer.

This is accompanied by an increase in the resolution of the density of the subcomponents of the DLPC molecule. This is surprising given that the increased free volume in the starting configuration of the bilayer model might be expected to give rise to increased trans-bilayer motion and a broadening of the density profile.

The density distribution of the cholesterol hydroxyl group indicates some considerable movement of the cholesterol molecule in the bilayer normal direction giving rise to significant density between opposing head group regions. However the majority of density is located in the glycerol region of bilayer normal space. This suggests that the cholesterol acts as a molecular damper between interacting DLPC molecules, preventing localised lateral motions of lipid molecules within the bilayer plane whilst itself having some freedom in the bilayer normal direction. Hence the DLPC molecule exhibits intensified density peaks while the cholesterol is broadened.

8.2.3. Non-Bonded Internals

The characteristic non-bond angles for the DLPC molecule have been calculated across the sampled trajectory (Table 8.2.2). These can be used to probe the dynamics of the DLPC molecule in the cholesterol doped system. All the defined internal angles from the DLPC molecule show increased flexibility with respect to both the dlpc and dlpc_y1 models. In addition the expanded dlpcchol_s bilayer model shows an increased range and average standard deviation of values. However the head group orientation (θ_1) changes, and is angled away from the surface of the bilayer to an average angle of 125.6°. The rigidity of the sterol ring system is maintained whilst some increase in its flexibility is observed through increased standard deviation in the θ_5 angle.

The above trend in these angles is reproduced in the non-bonded internal distances. The more extended head group conformation is reflected in an increase in the N-P and N-C6 distances. There is a shortening of the acyl chain lengths indicating increased conformational freedom and the presence of non-trans conformations in the acyl chains. The distance between the two terminal methyl carbon segments in DLPC is not however increased significantly indicating that the configuration of the two chains relative to one another is conserved.

Figure 8.2.2

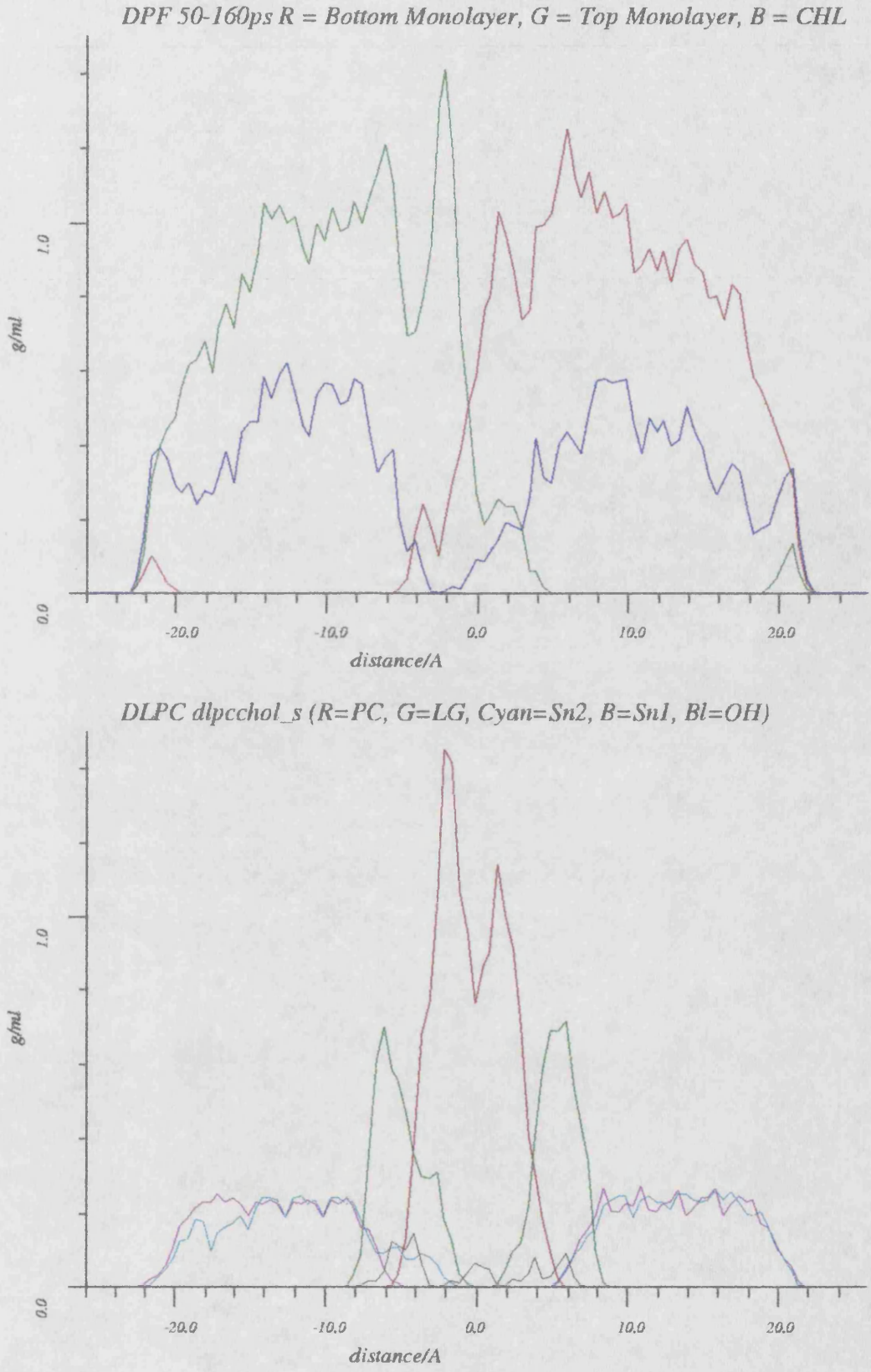
DPF 50-160ps R = Bottom Monolayer, G = Top Monolayer, B = CHL
g/ml
1.0
0.0
-20.0
-10.0
0.0
10.0
20.0
distance/A
DLPC dlpcchol_s (R=PC, G=LG, Cyan=Sn2, B=Sn1, Bl=OH)
g/ml
1.0
0.0
-20.0
-10.0
0.0
10.0
20.0
distance/A

Table 8.2.2

Non-Bond Angles dlpcchol_s			
	Av	SD	avSD
θ_1	125.6	20.4	7.8
θ_2	23.6	3.0	5.0
θ_3	122.3	20.2	6.5
θ_4	137.9	21.5	6.3
θ_5	167.4	5.7	6.5

Sampled over 80-300ps. Av is the average over all angles, SD is the standard deviation of those averages, and avSD is the average standard deviation of the individual values.

Table 8.2.3

Non-Bond Distances (Å) dlpcchol_s			
	Av	SD	avSD
N P	4.8	0.4	0.2
N C6	6.2	1.4	0.3
C6 C19	15.2	1.0	0.7
C6 C31	14.8	0.8	0.6
C8 C19	13.6	0.3	0.5
C20 C31	13.1	0.3	0.4
C19 C31	6.6	0.7	1.3

Sampled over 80-300ps. Av is the average over all equivalent distances, SD is the standard deviation of those averages, and avSD is the average standard deviation of the individual values.

8.2.4. Euler Angles

The characteristic Euler angles for the glycerol group (Table 8.2.4) have been calculated across the sampled trajectory. They are almost identical to those for the dlpcchol model. The first Euler angle shows a decreased range of values within the system although each value exhibits a larger average standard deviation, indicating increased flexibility in a narrower range of conformations.

Table 8.2.4

Euler Angles dlpcchol_s			
	Av	SD	AvSD
1	87.3	48.2	8.6
2	113.4	1.5	3.7
3	124.4	0.7	3.5

Sampled over 80-300ps. Av is the average over all angles, SD is the standard deviation of those averages, and avSD is the average standard deviation of the individual values.

8.2.5. Torsions

The defined torsion angles for both DLPC and cholesterol molecules have been calculated across the sampled trajectory and their ensemble averages and standard deviations calculated (Table 8.2.5). The average standard deviation of all acyl chain torsion angles from the DLPC molecule in the expanded cholesterol doped bilayer is increased from 5.2 in dlpcchol to 22.2 in the dlpcchol_s bilayer. This increase in torsional flexibility is brought about by the increase in the free volume available to each acyl chain within the expanded bilayer model. This torsional flexibility is sufficient to induce conformational transition in the acyl chain torsions resulting in a significant gauche population.

The value of each calculated acyl chain torsion angle was then ranked as either gauche(±), or trans using a ±30° accuracy. This was then used to calculate both the distribution of gauche torsions in the acyl chains and their distribution within the bilayer system (Table 8.2.6 and 8.2.7). From the percentage of trans and gauche conformations averaged over the sampled trajectory (Table 8.2.6) there is clearly a relationship between the carbon segment number and the gauche conformations formed. The first torsion angle in the lauryl chains (ϕ_{11} and ϕ_{23}) is g^+ in the Sn1 chain and g^- in the Sn2 chain reflecting the turn in the Sn2 chain. The torsion angles in the Sn1 chain undergo a smooth transition from from g^+ at the carbonyl end of the chain to g^- at carbon segment 4. Torsion angles then change smoothly from gauche state to gauche state through the trans intermediate over every 3 carbon segments. On average there are 90.94% trans, 1.51% g^- and 4.05% g^+ conformations in the Sn1 chain; the first torsion angle in the Sn2 chain is g^-; subsequent torsions favour the g^+ conformation. The last three torsions are evenly distributed between the two gauche states. On average there are 82.85% trans, 5.32% g^- and 7.03% g^+ conformations in the acyl chain torsions of

Sn2. Clearly the Sn2 chain is on average more disordered than the Sn1 chain, a result which agrees well with experiment.

The percentage conformations in specific molecules within the system (Table 8.2.7) indicates that there is considerable variation in the distribution of these gauche states through the system. This suggests that the formation and distribution of gauche states is a function of the variation in microdensity of the system. Measurement of the variation in microdensity is difficult and of little meaning in such a small system. One can however measure the ensemble average density and conformational distribution which may help in the interpretation of these results.

The increased torsional flexibility in the DLPC molecule is also observed in the acyl chain region of the cholesterol. This results in the formation of significant gauche conformers primarily in the $\phi_{4,5}$ torsion angles.

8.2.6. Segmental Order Parameters

The segmental order parameters of the acyl chains have been calculated for the sampled trajectory, with respect to the bilayer normal (Figure 8.2.3). The formation of gauche conformational states in the acyl chain torsion angles gives rise to an increase in the calculated order parameters for this system (Sn1 0.91±0.04, Sn2 0.88±0.06). One might however reasonably expect an increase in the conformational disorder to result in a decreased order parameter. The presence of gauche conformers results in the removal of the dominance of the orientational order especially in the Sn1 chain. Hence the chain may now occupy a larger range of orientations with respect to the bilayer normal, resulting on average in a larger order parameter. Any increase in the conformational disorder will now result in a decrease in the order parameter due specifically to the presence of gauche conformations and not its orientation. This hypothesis is further validated by the drop in the order parameter for the cholesterol acyl chain brought about by the presence of gauche conformational states. The cholesterol will not be so effected by the orientational disorder because of the planarity of the sterol ring system. The order parameter profile for the Sn1 and Sn2 chains are now equivalent and show some evidence of the order parameter plateau between carbons 4-8.

Table 8.2.5

Torsion standard deviations dlpcchol_s					
	AvSD	sdSD		AvSD	sdSD
DLPC					
ϕ_1	16.0	15.3	ϕ_2	26.0	17.9
ϕ_3	29.7	12.2	ϕ_4	40.9	23.2
ϕ_5	28.2	18.6	ϕ_6	23.7	17.2
ϕ_7	13.3	5.7	ϕ_8	12.0	3.2
ϕ_9	35.7	14.3	ϕ_{10}	13.8	2.3
ϕ_{11}	44.8	16.4	ϕ_{12}	23.6	15.9
ϕ_{13}	11.9	0.5	ϕ_{14}	20.7	14.8
ϕ_{15}	11.7	0.7	ϕ_{16}	16.9	12.1
ϕ_{17}	18.8	8.6	ϕ_{18}	17.4	10.5
ϕ_{19}	30.7	14.4	ϕ_{20}	26.4	12.8
ϕ_{21}	22.6	4.6	ϕ_{22}	12.3	0.9
ϕ_{23}	31.4	7.5	ϕ_{24}	24.0	14.6
ϕ_{25}	20.7	12.4	ϕ_{26}	18.8	9.2
ϕ_{27}	21.2	16.7	ϕ_{28}	19.1	8.3
ϕ_{29}	31.6	16.8	ϕ_{30}	23.1	10.0
ϕ_{31}	36.6	18.3	ϕ_{32}	26.0	16.1
CHOL					
ϕ_1	8.2	0.5	ϕ_2	17.1	5.2
ϕ_3	17.8	8.6	ϕ_4	23.1	15.2
ϕ_5	35.9	13.5			

Sampled from 100-300ps. AvSD is the average standard deviation of all equivalent torsion angles, sdSD is the standard deviation of those AvSD for each molecules and indicates the range of flexibility in the bilayer model.

8.2.7. Thermal Partitioning

The temperature of the cholesterol molecules and subcomponents of the DLPC molecule (PC, glycerol and lauryl chains) have been calculated from their atomic velocities at each time step across the sampled trajectory (Table 8.2.8 & Figure 8.2.4). Comparing the

Table 8.2.6

%Trans/Gauche Conformations dlpcchol_s							
	%t	%g^-	%g^+		%t	%g^-	%g^+
DLPC							
ϕ_1	41.00	12.39	45.51	ϕ_2	57.00	14.55	16.86
ϕ_3	52.00	8.22	1.20	ϕ_4	14.50	42.14	23.17
ϕ_5	19.62	22.72	7.29	ϕ_6	2.88	14.70	17.07
ϕ_7	0.38	12.46	81.89	ϕ_8	93.50	0.06	0.00
ϕ_9	50.12	4.24	16.89	ϕ_{10}	94.62	0.00	0.00
ϕ_{11}	5.88	19.79	32.87	ϕ_{12}	87.25	0.85	7.66
ϕ_{13}	96.62	0.00	1.21	ϕ_{14}	90.50	5.84	0.26
ϕ_{15}	96.50	0.29	0.00	ϕ_{16}	89.75	1.80	5.29
ϕ_{17}	95.12	0.47	1.10	ϕ_{18}	94.75	2.06	0.00
ϕ_{19}	87.00	0.71	8.16	ϕ_{20}	81.00	1.65	12.78
ϕ_{21}	14.38	6.32	4.16	ϕ_{22}	89.50	0.00	0.00
ϕ_{23}	11.50	24.60	17.34	ϕ_{24}	70.62	18.18	2.81
ϕ_{25}	84.38	0.00	11.34	ϕ_{26}	93.62	2.12	0.29
ϕ_{27}	78.00	0.00	18.41	ϕ_{28}	93.25	0.22	1.55
ϕ_{29}	68.75	9.90	16.18	ϕ_{30}	92.75	2.94	0.59
ϕ_{31}	83.12	6.62	5.69	ϕ_{32}	81.12	7.91	6.39
CHOL							
ϕ_1	0.00	0.00	99.87	ϕ_2	77.75	1.20	0.00
ϕ_3	92.38	0.77	0.97	ϕ_4	86.88	1.33	7.02
ϕ_5	35.00	0.00	56.91				

Sampled from 80-90ps and averaged for all 8 DLPC and 8 Cholesterol molecules. %t is the percentage trans (180±30°), %g^- is the percentage negative gauche (-60±30°) and %g^+ is the percentage positive gauche (+60±30°).

ensemble average temperatures of the DLPC moieties in the dlpcchol and dlpcchol_s models it can be observed that the modifying effect of the cholesterol on the thermal partitioning has been removed on expansion of the system. The temperature differential between the head group, glycerol and lauryl chains is again maintained, similar to that observed in the dlpc

Table 8.2.7

Acyl Chain %Trans/Gauche dlpcchol_s			
Mol	%t	$\%g^-$	$\%g^+$
1	93.22	1.77	2.00
2	79.11	3.19	12.42
3	84.44	2.94	7.56
4	87.61	3.17	5.67
5	90.56	5.14	0.84
6	94.28	1.49	1.41
7	78.22	2.30	13.27
8	87.72	7.37	1.17

Sampled from ϕ_{12}-ϕ_{20} and ϕ_{24}-ϕ_{32} from 80-300ps.

system.

The standard deviation of the atomic temperature of the subcomponents of the DLPC molecule are almost identical to those of the unexpanded system. These are a measure of the heat capacity of the system. The origin of the increased partitioning of the velocities between the subcomponents of the molecule must therefore be due specifically to the increase in the free volume of the configuration. This may be compounded by the reduced effect of the cholesterol interaction brought about by this increased free volume. The fact that the same trend was observed in the pure dlpc and dlpc_y1 models suggests that the effect of the increased free volume is dominant over the modifying effect of cholesterol. It has been experimentally observed that cholesterol reduces the fluidity of the acyl chain region above the phase transition and increases fluidity below it. The percentage gauche states are increased from 7.13% in dlpc_y1 to 8.96% in dlpcchol_s suggesting that the system is in the gel phase and that the cholesterol has a disordering effect on the system in terms of the conformational disorder.

The average methylene temperatures have also been calculated. These show almost exactly the same standard deviation in the two cholesterol doped models (dlpcchol 50.5K, and dlpcchol_s 51.0K). The methylene temperature profile shows the inverse relationship to the order parameter profile as expected. However there is a drop in the average methylene temperature of carbon segments 10 and 11 which does not give rise to a corresponding increase

Figure 8.2.3

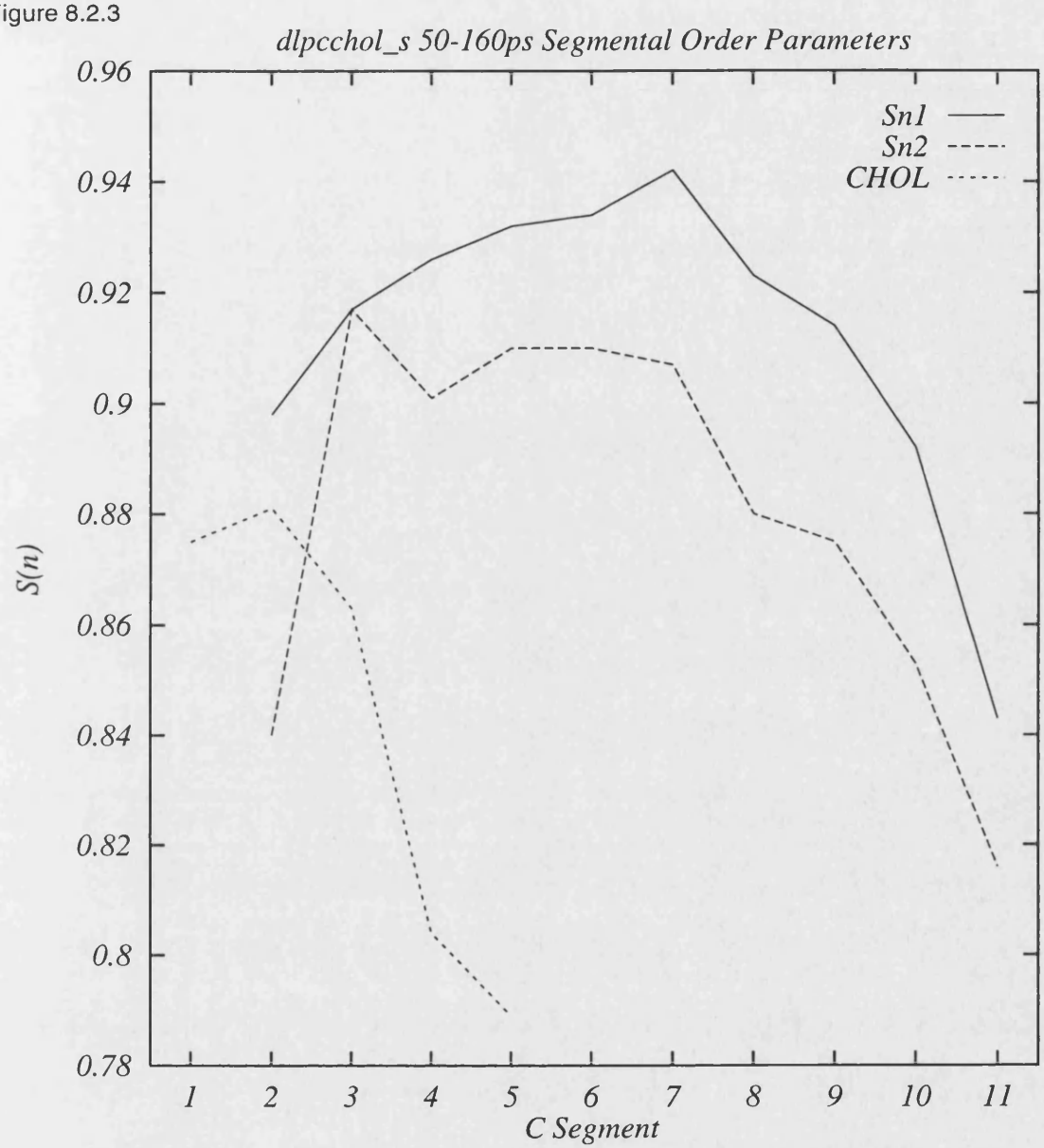

in the order parameter at these segments. This may be due to reorientation of these methylenes brought about by the presence of the combination of two pairs of g^+ turns either side of a g^- conformation in the lower portion of the Sn2 lauryl chain. Clearly great caution must be taken in interpreting the results of the order parameter profile given its sensitivity to small changes in orientation in such a small system.

Table 8.2.8

Average Moiety Temperature (K) dlpcchol_s		
	Av	SD
PC	369.7	20.5
GL	352.7	22.1
Sn1	314.9	15.0
Sn2	310.9	12.7
DLPC	331.9	7.7
CHOL	308.2	9.5

Sampled over 80-300ps.

Table 8.2.9

Average Methylene Temperature (K) dlpcchol_s					
Sn1			Sn2		
C Segment	Av	SD	C Segment	Av	SD
2	317.6	51.6	2	317.0	52.3
3	310.4	51.0	3	312.7	51.5
4	310.6	52.6	4	308.3	51.1
5	309.8	51.4	5	311.5	50.9
6	308.7	50.6	6	310.9	50.0
7	311.4	52.2	7	310.9	51.9
8	312.5	52.2	8	313.6	52.0
9	313.8	52.8	9	311.1	50.4
10	312.7	52.7	10	303.8	50.6
11	313.9	52.5	11	307.6	51.5
12	325.0	45.8	12	316.5	45.0

Sampled over 80-300ps.

8.2.8. Radial Distribution Function

The pairwise radial distribution for oxygen, phosphorus and nitrogen atoms in the system has been calculated from the 90-160ps portion of the trajectory (Figure 8.2.6). A resolution of 0.2Å and radial search distance of 10.0Å was used. This can be used to look for

Figure 8.2.4

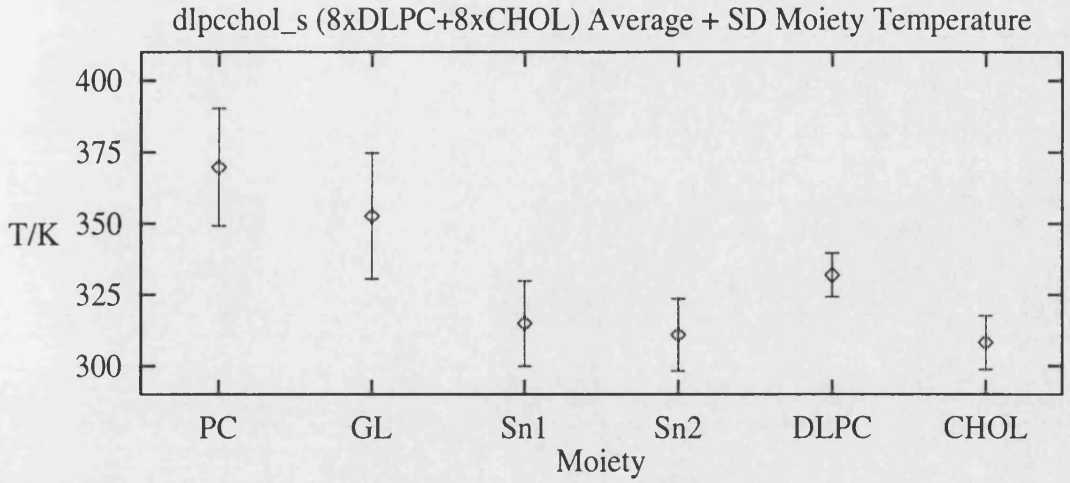

Figure 8.2.5

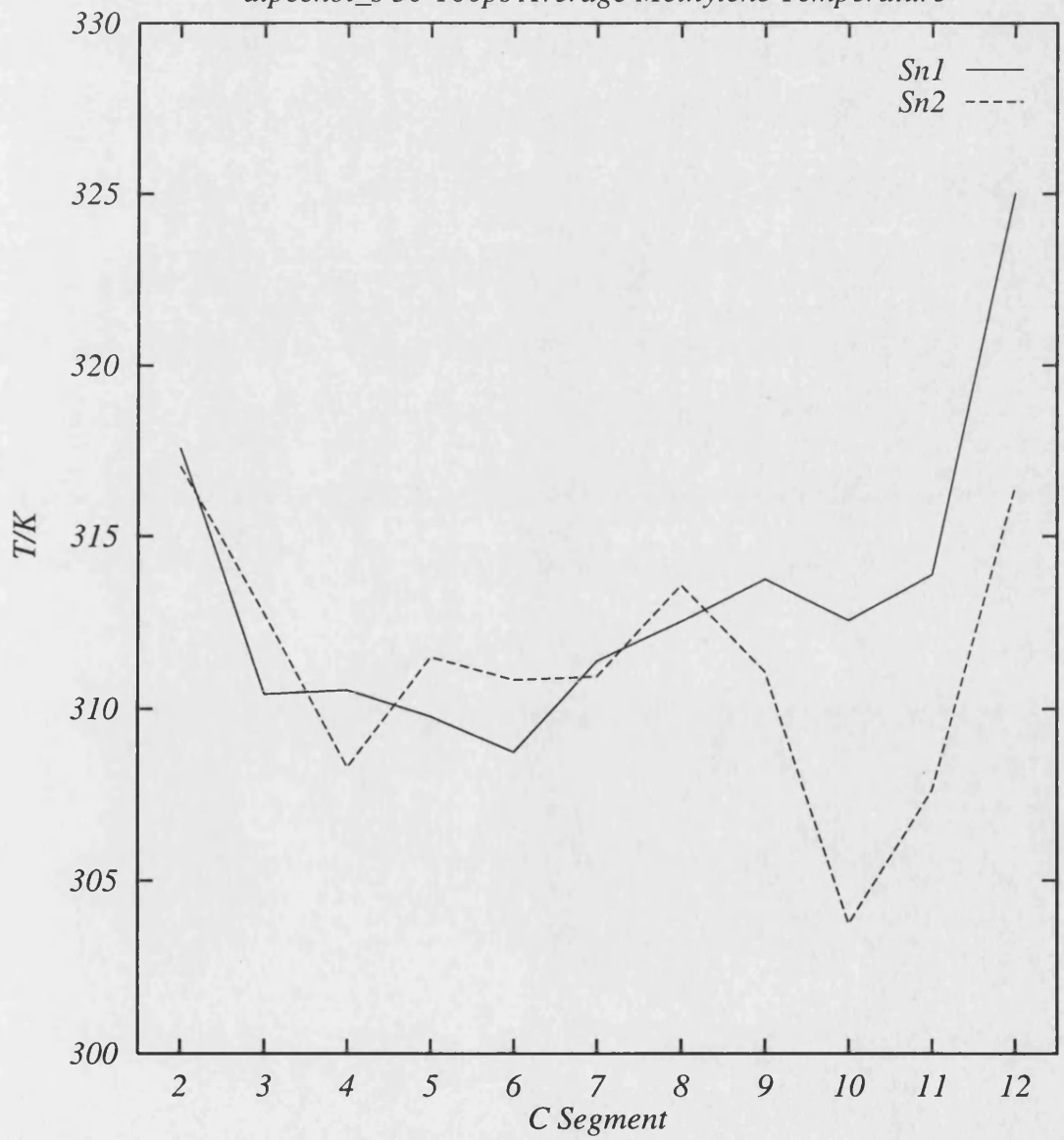

characteristic non-bonded distances between these atoms in the coordinate system.

Examining Figure 8.2.6 certain peaks in the radial distribution can be assigned to characteristic non-bonded distances in the DLPC molecule. There is a large peak around 1.5Å which can be assigned to the separation of oxygen and phosphorus atoms in the phosphate group (1.45Å-1.65Å). The broader peak around 2.6Å can be assigned to two internal non-bonded distances.

(a) oxygen separation in the lauryl fatty acid chains (2.3Å-2.5Å).

(b) non-bonded distance between phosphate oxygens (2.5Å-2.6Å).

The less obvious broad peaks at approximately 4.4Å and 7.6Å are due to the N-P and inter-molecular choline contacts respectively. Both peaks are broadened by the flexibility of the head group and the variation of the configuration across the trajectory. Indeed the 7.6Å peak agrees well with experimentally observed inter-lipid separations in the orthorhombic pack. This structure contains characteristic distances of 4.9Å and 7.6Å, suggesting that the coordinate system is in a distorted orthorhombic structure.[4-6]

The excess molecule function displayed in the dashed line represents the integral of the radial distribution function which is greater than 1.0. This is the excess radial density measured. This allows one to examine the radial distribution for hydration shells and other characteristic non-bonded inter-molecular order. In this radial distribution there is little evidence for significant hydrogen bonding between the cholesterol hydroxy group and either the carbonyl or phosphate oxygens, the only hydrogen bondable groups in this coordinate system. Any cholesterol DLPC hydrogen bonding would be masked by the peak around 2.5Å, given that the expected hydrogen bond would be in that range. There is only a small peak in the excess molecule function suggesting little hydrogen bonding.

Figure 8.2.6

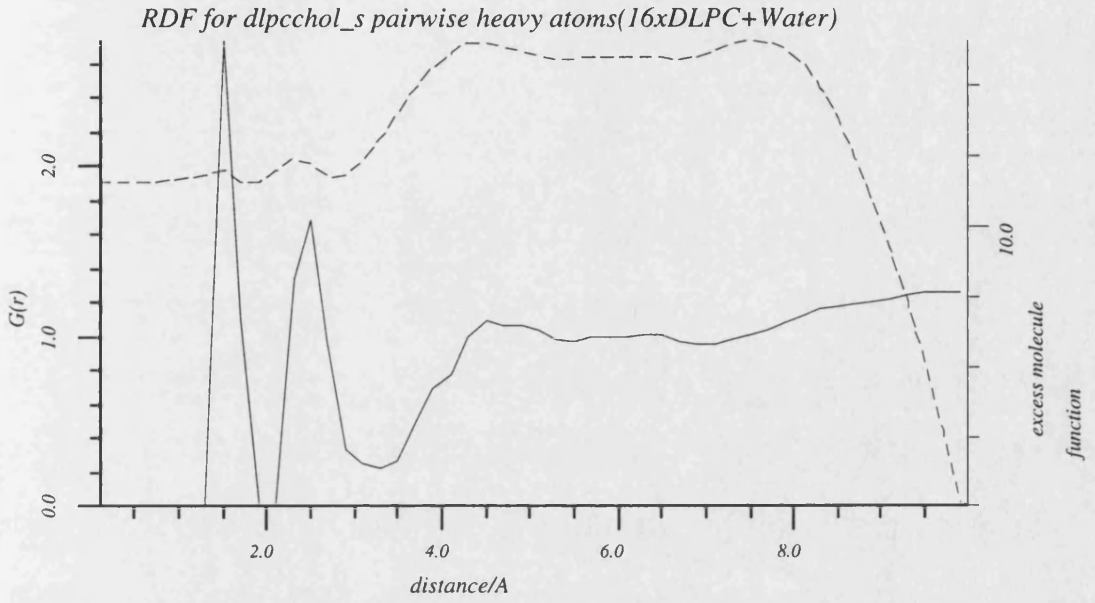

Sampled from 90-160ps using a resolution of 0.2Å and range of 10.0Å. Atoms O,N and P distances only.

8.2.9. Hydrogen Bonding

In order to explicitly examine the trajectory for any possible hydrogen bonding between the cholesterol hydroxy group and the DLPC molecule a distance defined hydrogen bond search was undertaken. The cholesterol hydroxyl group is the only hydrogen bond donor in the coordinate system and there are only eight available acceptor atoms, the four phosphate oxygens and the four glycerol oxygens. Figure 8.2.7 illustrates the obtained results.

It can be seen that the only atom with significant hydrogen bonding to the cholesterol hydroxyl group is a single nonesterified oxygen from the phosphate group of the DLPC molecule. These atoms on average make between 0.6-1.0 hydrogen bonds and on average have at least some interaction of a hydrogen bonded nature. The esterified oxygens of the phosphate group make no significant hydrogen bonds, only occasionally making a transient

bond. The glycerol oxygens are in general too far from the hydroxyl end of the cholesterol to make hydrogen bonding contact, although two of the Sn2 esterified oxygens do on average make 0.0-0.2 hydrogen bonds. This suggests that the more mobile Sn2 chain comes into closer contact to the cholesterol hydroxyl group. With the absence of any aqueous interaction the cholesterol is attracted into the phosphate region of the DLPC bilayer hydrogen bonding through electrostatic interaction.

References

1. Lunt GG and Harrison R, in *Biological Membranes*, Blackie & Son Glasgow, 1980.

2. Ipsen JH, Mouritsen OG, and Bloom M, *Biophysical J*, vol. 57, pp. 405-412, 1990.

3. Worcester DL and Franks NP, *J Mol Biol*, vol. 100, pp. 359-378, 1976.

4. Small DM, *J Lipid Research*, vol. 25, pp. 1490-1500, 1984.

5. Nagle JF, Wiener MC, and Suter RM, *Biophysical J*, vol. 55, pp. 315-325, 1989.

6. Ruocco MJ and Shipley G, *Biochimica et Biophysica Acta*, vol. 684, pp. 59-66, 1982.

Figure 8.2.7

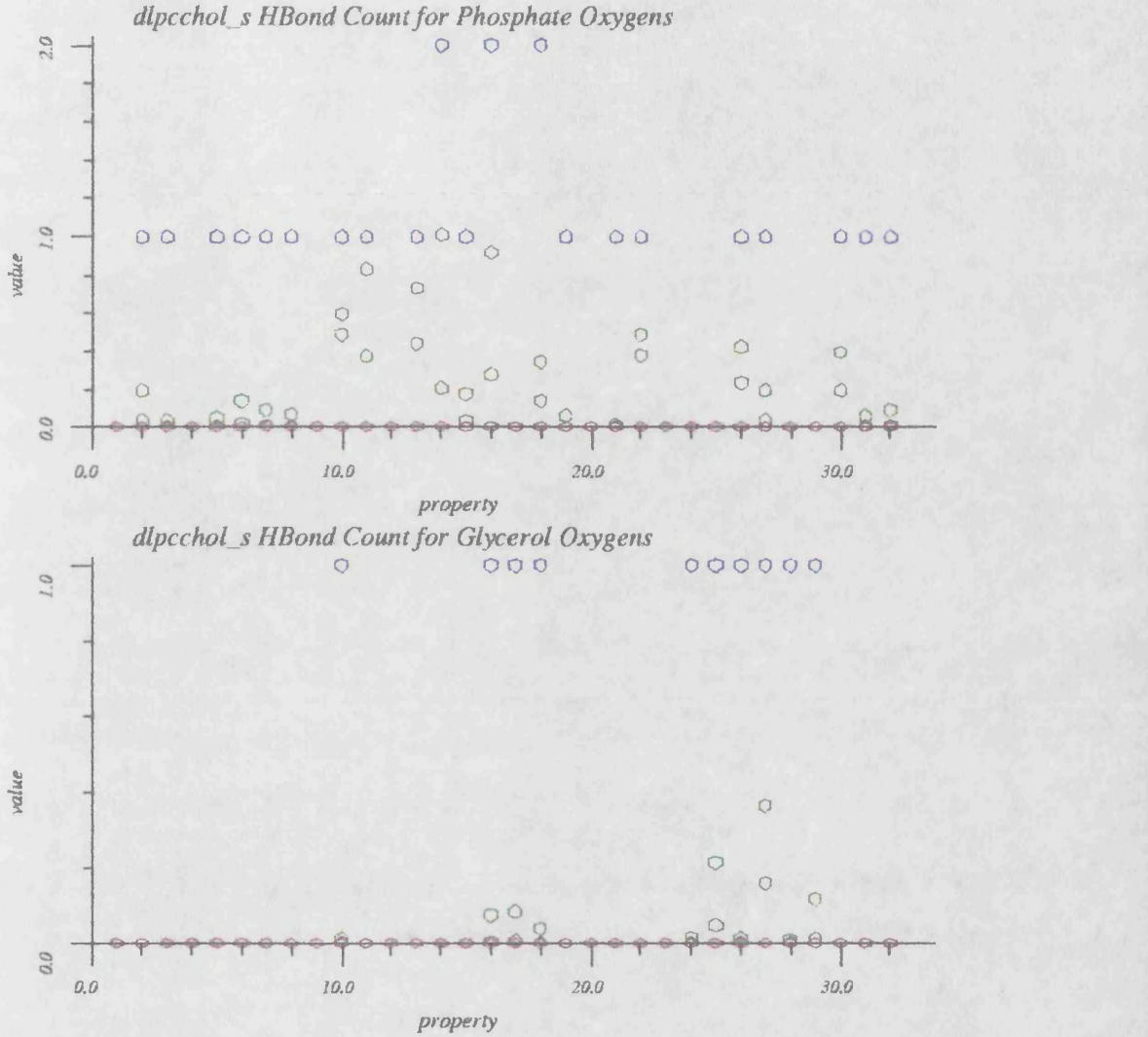

Sampled from 90-160ps. The property number refers to the atom index of the hydrogen bond acceptor.

Top: 1-8 is the first esterified phosphate oxygen, and 25-32 the second. 9-24 are the nonesterified oxygens of the phosphate group.

Bottom: 1-8, and 25-32 are the esterified oxygens of the glycerol group. 9-24 are the carbonyl oxygens.

Black is the average number of hydrogen bonds found, Green the standard deviation, Red the minimum and Blue the maximum.

9. Hydrated Bilayer Models

9.1. System VIII dlpc_wat (16xDLPC+Water)

Most experimental membrane systems are studied in an aqueous environment in which various states of hydration of the lipid head groups are observed. In fact many lipid systems exhibit phase behaviour dependent on their degree of hydration. The bilayer model dlpc_wat was constructed from the non-expanded bilayer model dlpc (See Chapter 4). Waters are removed from the hydrophobic core of the bilayer (defined as the volume enclosed by the first CH_2 of the lauryl chains[1]). This results in the coordinate system (*dlpc_wat*) consisting of a DLPC bilayer sandwiched between two aqueous layers (25%molwt H_2O), such that under the imposed periodic boundary conditions one monolayer does not interact with its periodic image, except through secondary water interactions.

The resulting coordinates were then minimised and used as the starting configuration for sampling the molecular dynamics trajectory from the NPT ensemble using pressure and temperature constraints of 1.0bar and 310K respectively. 300ps of trajectory was sampled.

9.1.1. Energetics

Table 9.1.1 and Figures 9.1.1a and 9.1.1b show the extracted ensemble average and standard deviation of each characteristic energy and thermodynamic quantity of the system across the trajectory. The volume of the system does not reach equilibrium under the constant pressure ensemble increasing from 22419.5Å^3 to 40955.7Å^3 across the trajectory. This expansion is not isotropic, the unit cell axes expanding non-uniformly (A 68.2-112.6Å, B 16.1-17.4Å and C 20.3-21.8Å). Interactions in the bilayer normal direction are dominant in the pressure calculation.

9.1.2. Density Profile

Figure 9.1.2 shows the density profile of the system in the bilayer normal direction. This illustrates the effect of the expansion of the system in the bilayer normal direction on the distribution of both the DLPC bilayer and the aqueous layer above and below the lipids. The figure represents snap shots of the expansion of the system taken at 50ps intervals, sampling 100 configurations. The density and stability of the DLPC bilayer is maintained across the

Table 9.1.1

Energetics (kcal/mol) dlpc_wat		
	E	SD
E_{KE}	2093.2	27.5
E_{tot}	313.4	126.4
E_{PE}	-1779.9	129.0
E_{rep}	3800.6	55.0
E_{dsp}	-5051.4	47.7
E_{est}	-2338.2	141.7
E_b	676.7	24.3
E_θ	839.4	24.9
E_ϕ	312.7	13.3
	P/bar	SD
P	17.6	392.2
P_x	69.1	969.6
P_y	-21.6	921.5
P_z	-1.1	882.3
	D/Å	SD
A	99.4	8.5
B	16.9	0.1
C	21.1	0.3
	V/Å^3	SD
V	35570.1	3268.2

Sampled over 80-300ps.

trajectory, the density of the acyl chains being increased from approximately 0.5gml^{-1} to 0.7gml^{-1} over the first 50ps of the trajectory. This acyl chain density is sufficient to prevent the water from penetrating the hydrophobic region. Waters are observed to penetrate down to the first methyl of the lauryl chains locating around the glycerol region.

The density of the aqueous layer however is not well maintained and the rapid expansion of the system in the bilayer normal direction leads to the formation of vacuum between the periodic images of the semi-hydrated bilayer. This leads to a low water density in the head

Figure 9.1.1a

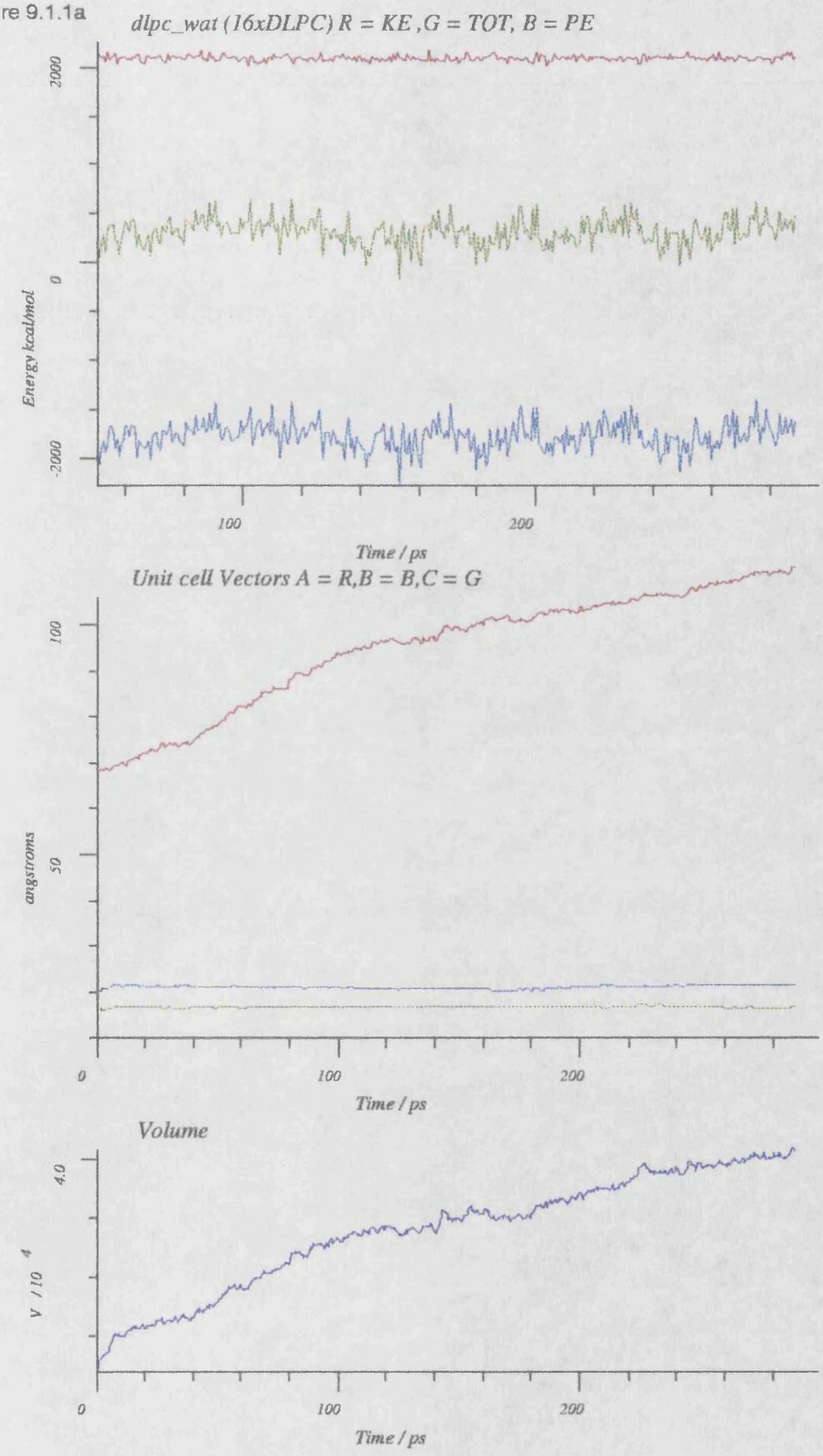
dlpc_wat (16xDLPC) R = KE ,G = TOT, B = PE
2000
0
-2000
Energy kcal/mol
100
200
Time / ps
Unit cell Vectors A = R,B = B,C = G
100
50
angstroms
0
100
200
Time / ps
Volume
4.0
V / 10 4
0
100
200
Time / ps

Figure 9.1.1b

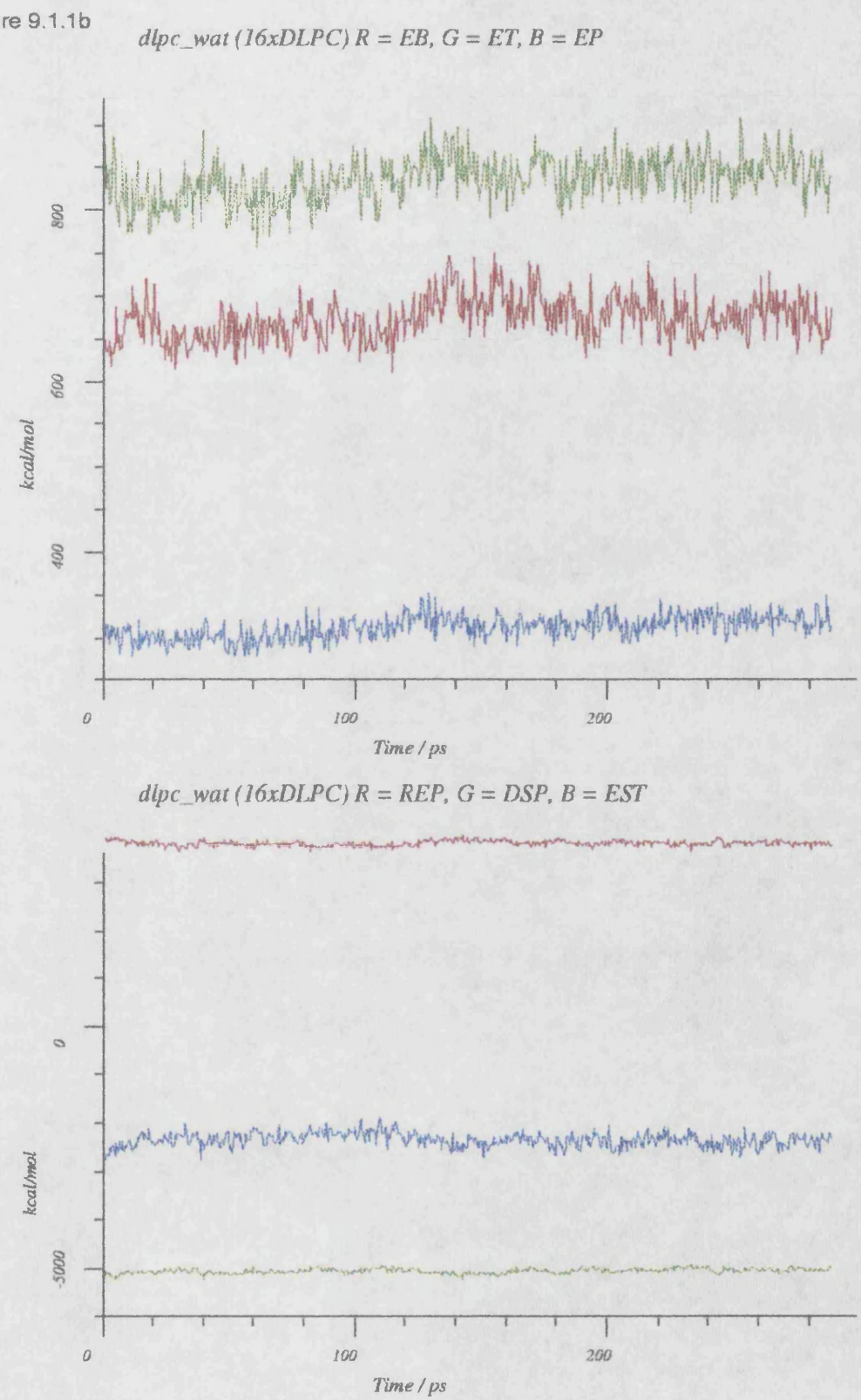
dlpc_wat (16xDLPC) R = EB, G = ET, B = EP
800
600
400
kcal/mol
0
100
200
Time / ps
dlpc_wat (16xDLPC) R = REP, G = DSP, B = EST
0
-5000
kcal/mol
0
100
200
Time / ps

group region. The liquid bilayer and its hydration shell are therefore in equilibrium with a water vapour phase. Hydrated waters are maintained in the liquid state around the head group of the DLPC molecules through hydrogen bonding interactions. Waters which break free from this interaction form the gaseous phase. This therefore no longer represents a physical model of an aqueous phase bilayer system. It can however be used to yield some information about the hydration of the DLPC molecule.

9.1.3. Euler Angles

Hydration of the DLPC molecule will clearly be a function of the conformation and dynamics of the PC head group. The characteristic Euler angles (Table 9.1.2) show an average orientation of the PC head group parallel to the surface of the bilayer. The orientation of individual molecules in the bilayer model varies considerably although once they have occupied their "equilibrium" state they only exhibit an average standard deviation of 4.7°. This indicates a bilayer surface model in which there is a range of orientations of the PC head group which are on average parallel to the surface, although there is considerable disorder.

9.1.4. Thermal Partitioning

Clearly there is some reason for the rapid expansion of the system along the bilayer normal direction. In order to examine the state of thermal equilibrium of the system the average temperature of the subcomponents of the system have been calculated from their atomic velocities across the trajectory. Table 9.1.3 and Figure 9.1.3 show the average temperature of the DLPC moieties (PC, glycerol and the two lauryl chains) and the aqueous layer. The temperature of the aqueous phase (506.7K) is higher than that of the lipid phase. The Sn1 and Sn2 lauryl chains of the DLPC molecules have average temperatures of 216.4K and 218.9K respectively, while the glycerol backbone and PC head group have average temperatures of 278.2K and 310.7K respectively. The standard deviations of these temperatures are almost identical with those observed for the dlpc bilayer model.

These temperature differences between the subcomponents of the bilayer and the aqueous layer lead to a system in which there are several phases present.

(a) Solid phase lauryl chains forming the hydrophobic region of the bilayer of relatively high density and low temperature.

(b) Fluid phase PC head group region of the DLPC bilayer of intermediate temperature

Figure 9.1.2

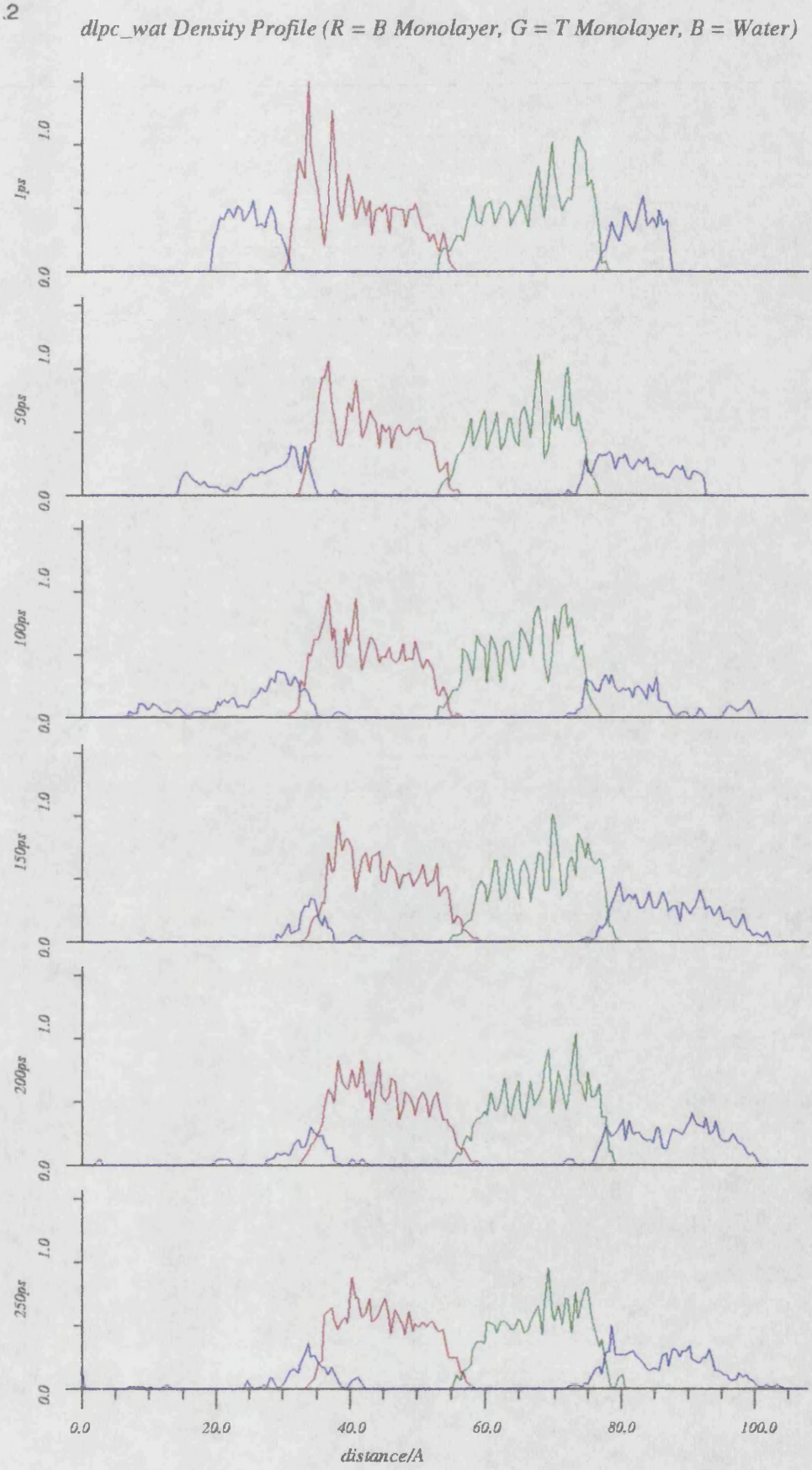
dlpc_wat Density Profile (R = B Monolayer, G = T Monolayer, B = Water)
1ps
50ps
100ps
150ps
200ps
250ps
1.0
0.0
0.0
20.0
40.0
60.0
80.0
100.0
distance/A

Table 9.1.2

Euler Angles dlpc_wat			
	Av	SD	avSD
1	93.1	72.6	4.7
2	113.9	2.1	3.3
3	123.2	1.9	3.0

Sampled over 80-300ps. Av is the average over all angles, SD is the standard deviation of those averages, and avSD is the average standard deviation of the individual values.

and with some translational motion. The hydrating water surrounding the PC head group region is also in the liquid state.

(c) Gaseous waters in equilibrium with the liquid phase waters in proximity with the PC head groups.

The temperature differential between the aqueous and lipid phases can be examined as a function of time. Figure 9.1.4a shows the temperature of the subcomponents of the system over the first picosecond of the trajectory. Clearly the temperature difference is a function of the starting coordinates. Strain is introduced into the water structure relative to the pre-relaxed bilayer structure, causing an increase in the atomic velocities of the water atoms relative to the bilayer atoms. The velocity rescaling then rescales all velocities by the same rescale factor causing the cooling of the lipids relative to the water and compounding the effect. There is no evidence of significant coupling between the temperature of the water and lipid phases. This is a direct result of the lack of equilibrium of the system.

This temperature difference is maintained across the trajectory as illustrated in figure 9.1.4b. There is some readjustment of the velocities, but on average the imbalance is maintained.

9.1.5. Radial Distribution Functions

In order to study the hydration of the DLPC molecule by the surrounding water, pairwise radial distribution functions for the water oxygen atoms relative to the hydrogen bond acceptor atoms in the DLPC molecule have been calculated. These include the oxygens of the phosphate group and the oxygens of the glycerol backbone (Figures 9.1.5a-f). In order to probe the structure of the water the pairwise radial distribution function for the water in the system has

Table 9.1.3

Average Moiety Temperature (K) dlpc_wat		
	Av	SD
PC	310.7	12.4
GL	278.2	17.3
Sn1	216.4	11.3
Sn2	218.9	10.5
WAT	506.7	24.4

Sampled over 10-300ps.

Figure 9.1.3

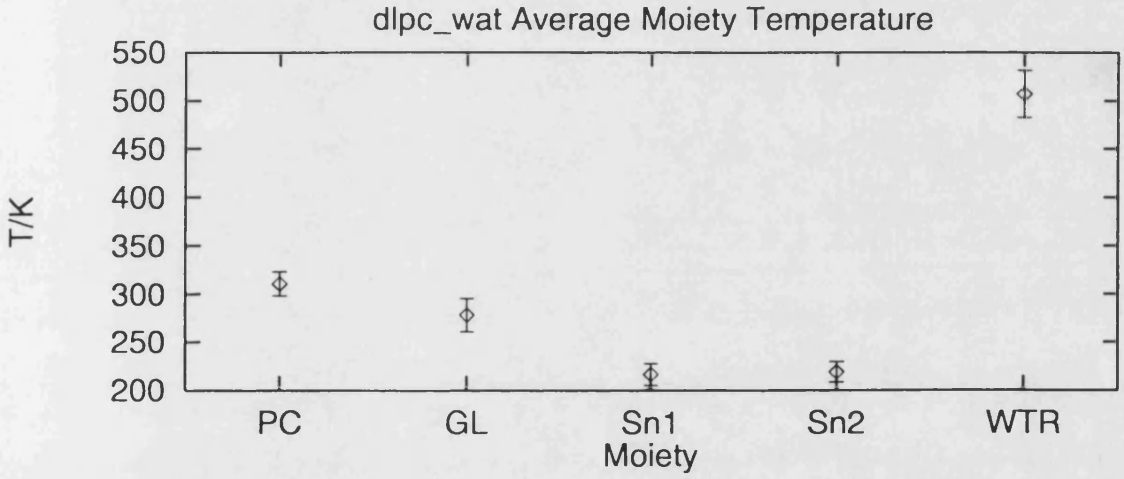

been calculated. As the system is not pure water none of these radial distributions will normalise to 1.0.

From the radial distribution function of the glycerol oxygens one can follow the penetration of the water molecules into the glycerol region forming a broad hydration shell 2-6Å around the glycerol oxygens. Even after 300ps of trajectory has been sampled the exchange of water molecules into the glycerol region is not at equilibrium, which is not surprising given the expansion of the bilayer normal unit cell axis.

Figure 9.1.4a

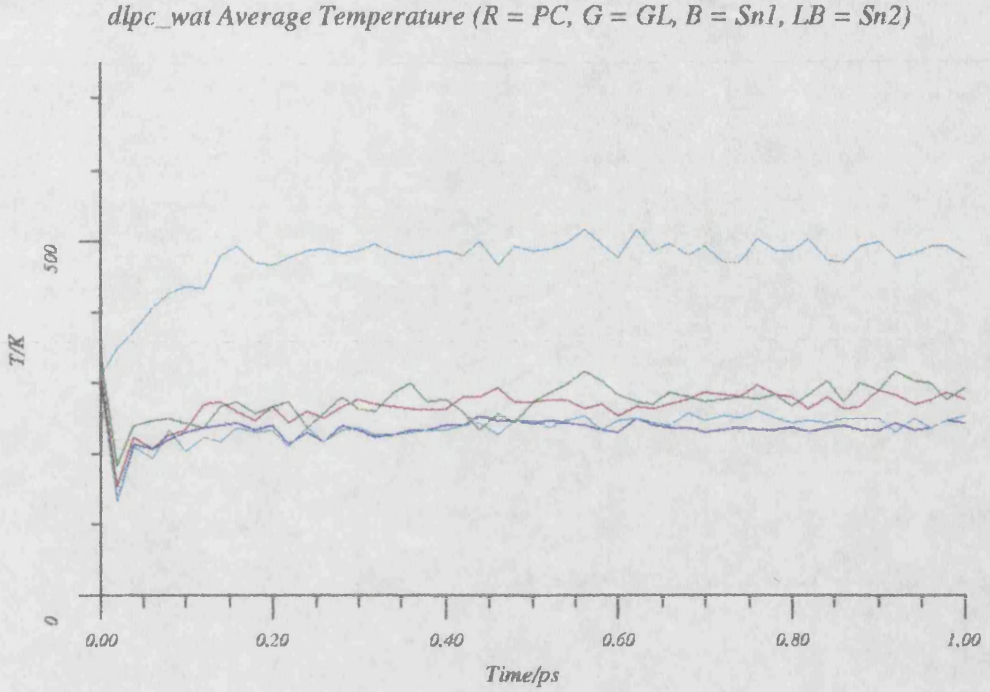

Figure 9.1.4b

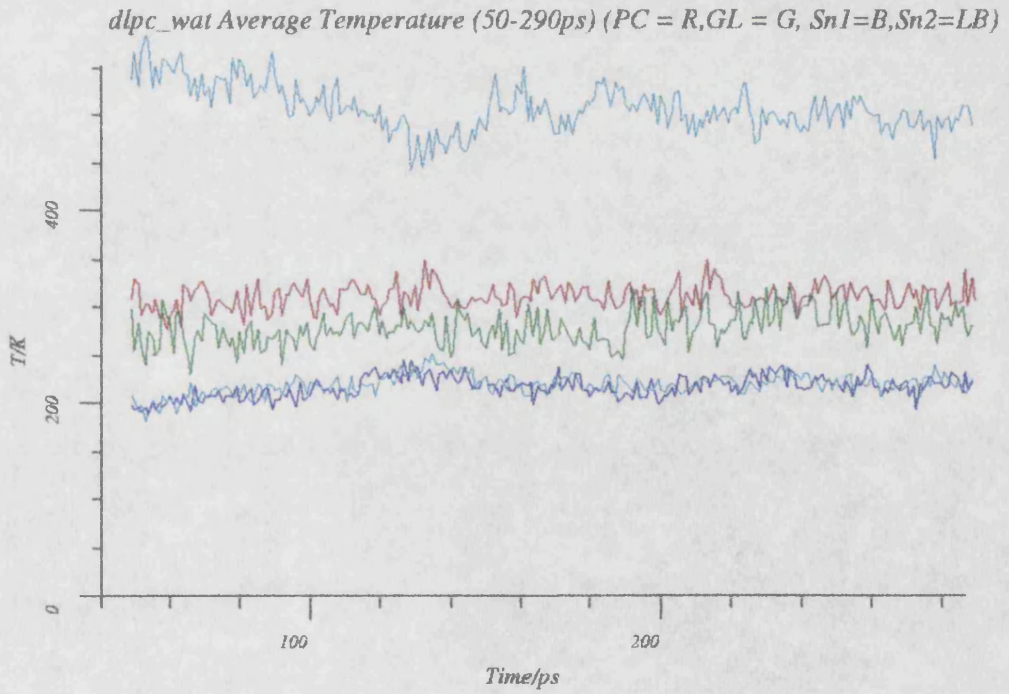

Examination of the radial distribution of water oxygen atoms relative to the phosphate oxygens indicates the presence of two hydration shells around the phosphate group. The first hydration shell is at approximately 2.5Å, the expected first hydrogen bonded shell. However there is also a broad peak at approximately 5Å forming a second hydration shell and evidence of longer range order. This is a consequence of the long range effect of the larger charges on the phosphate and choline groups of the phosphatidyl choline moiety.

The radial distribution function for the water oxygens of the system reflect the expansion of the system, reducing in intensity as the density of the system falls. The principle peak in the radial distribution function for water is longer than the equivalent peak in the phosphate radial distribution. This indicates stronger binding of water to the phosphate than to itself. This can be rationalised on the basis of the pure electrostatic nature of this representation of hydrogen bonding.

9.1.6. Hydrogen Bonding

In order to examine the trajectory for any evidence of hydrogen bonding between waters and the hydrogen bond acceptor atoms in the DLPC molecule a hydrogen bond search was performed on the trajectory, hydrogen bonds being assigned on the basis of a distance only criteria. This searches for water hydrogens that are closer than 2.5Å from one of the eight possible hydrogen bond acceptor atoms, the four phosphate oxygens and the four glycerol oxygens in each DLPC molecule. Figure 8.1.6 shows the hydrogen bonding information.

The esterified oxygens of the phosphate group make on average less than one hydrogen bond with the water molecules surrounding them. They do however form some transient bonds as indicated by the maximum hydrogen bonds formed. The non-esterified oxygens form on average between one and two hydrogen bonds up to a maximum of six. The two oxygens are not equivalent in their hydrogen bonding behaviour indicating some polarisation of the phosphate group with respect to the bilayer normal direction and hence penetrating waters. Clearly there is significant binding of waters through hydrogen bonding interactions with the phosphate group, as indicated by the radial distribution functions.

There is some evidence of hydrogen bonding to some of the glycerol oxygens, but no differentiation between the hydrogen bonding to the esterified and non-esterified oxygens of the glycerol. Some on average form between 0.0-0.5 hydrogen bonds, but most appear not to significantly hydrogen bond. This may be a function of the lack of penetration of water into the

Figure 9.1.5a

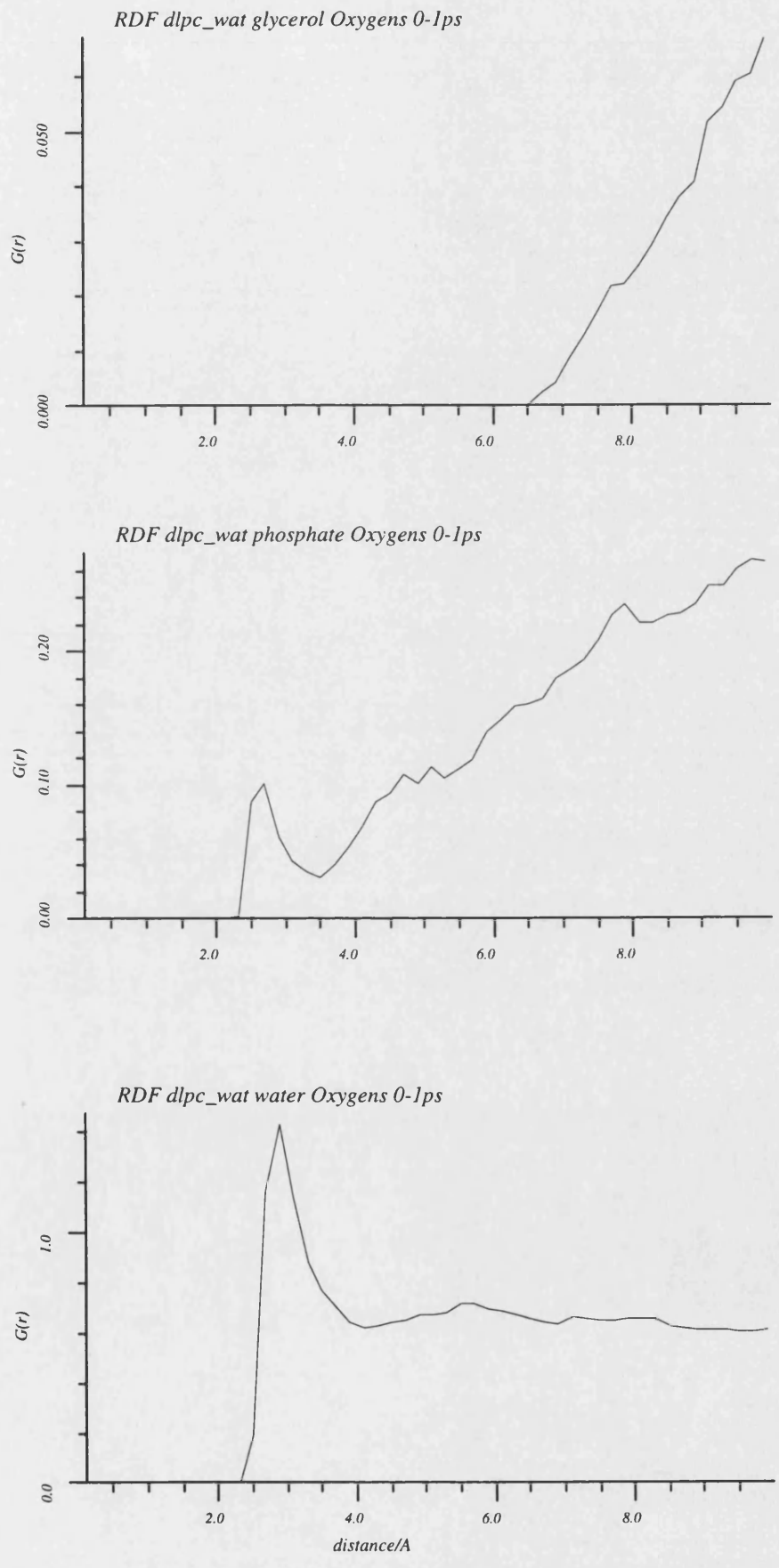
RDF dlpc_wat glycerol Oxygens 0-1ps
G(r)
0.050
0.000
2.0
4.0
6.0
8.0
RDF dlpc_wat phosphate Oxygens 0-1ps
G(r)
0.20
0.10
0.00
2.0
4.0
6.0
8.0
RDF dlpc_wat water Oxygens 0-1ps
G(r)
1.0
0.0
2.0
4.0
6.0
8.0
distance/A

Figure 9.1.5b

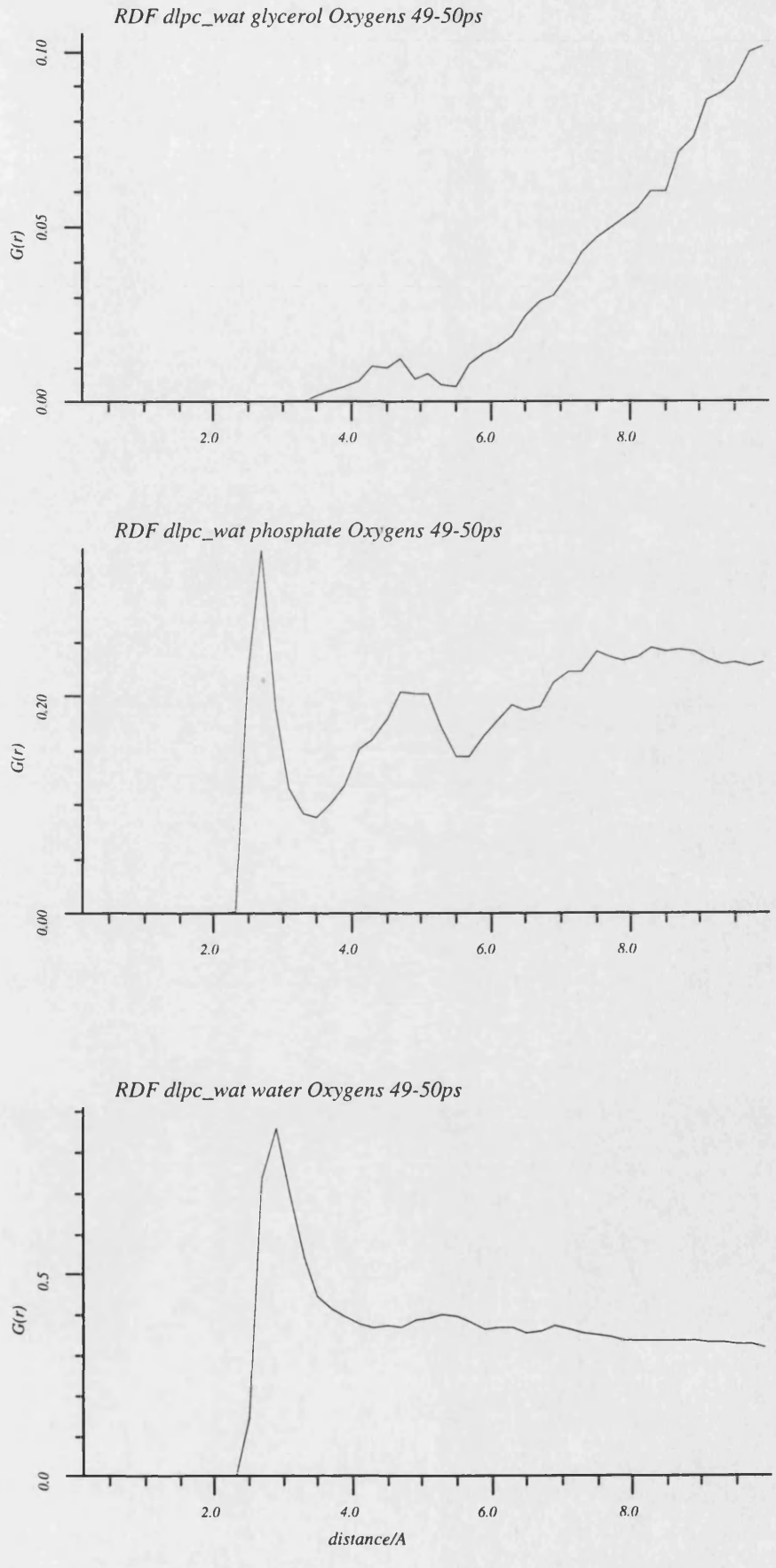
RDF dlpc_wat glycerol Oxygens 49-50ps
G(r)
0.00
0.05
0.10
2.0
4.0
6.0
8.0
RDF dlpc_wat phosphate Oxygens 49-50ps
G(r)
0.00
0.20
2.0
4.0
6.0
8.0
RDF dlpc_wat water Oxygens 49-50ps
G(r)
0.0
0.5
2.0
4.0
6.0
8.0
distance/A

Figure 9.1.5c

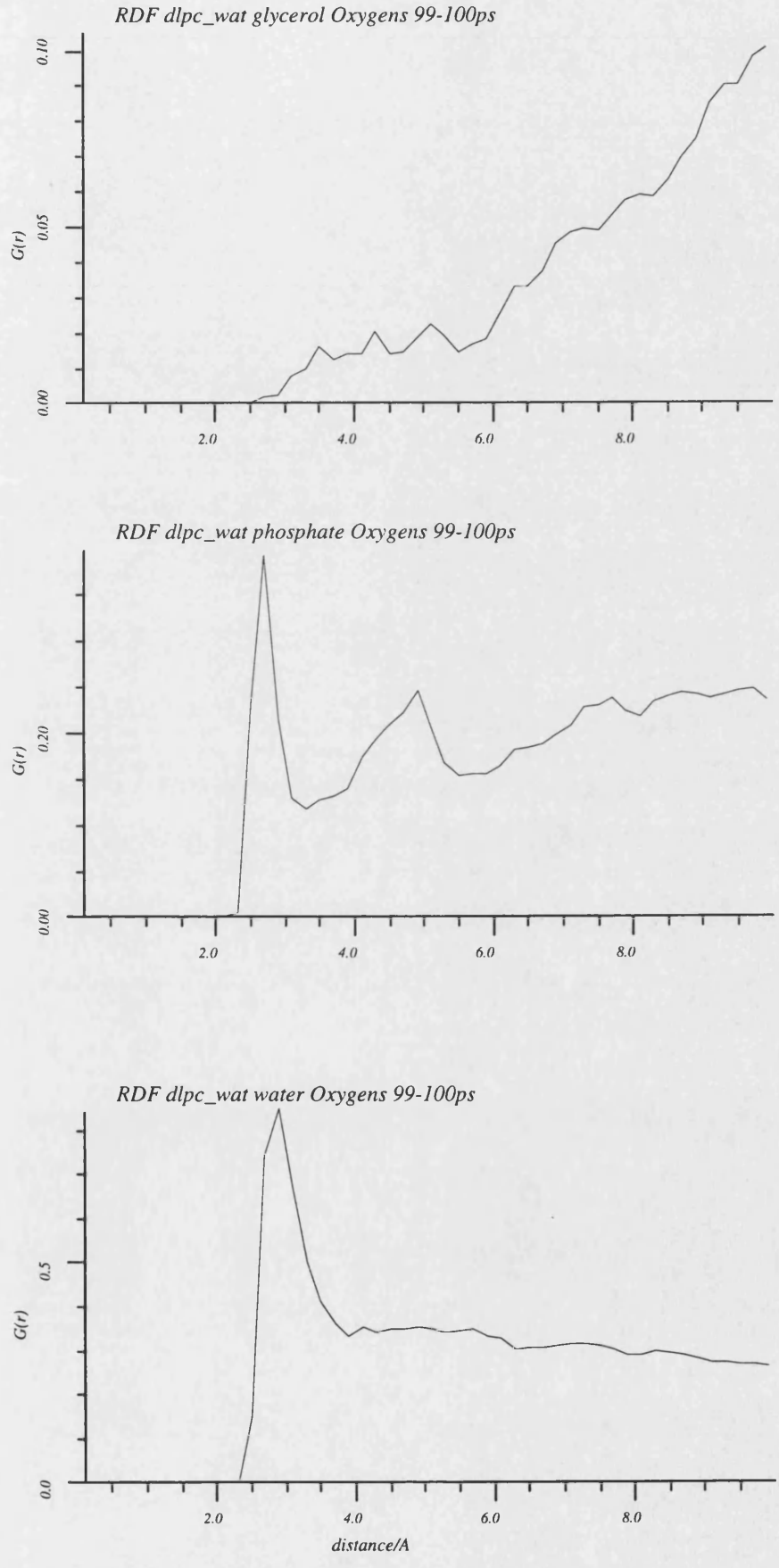
RDF dlpc_wat glycerol Oxygens 99-100ps
G(r)
0.00
0.05
0.10
2.0
4.0
6.0
8.0
RDF dlpc_wat phosphate Oxygens 99-100ps
G(r)
0.00
0.20
2.0
4.0
6.0
8.0
RDF dlpc_wat water Oxygens 99-100ps
G(r)
0.0
0.5
2.0
4.0
6.0
8.0
distance/A

Figure 9.1.5d

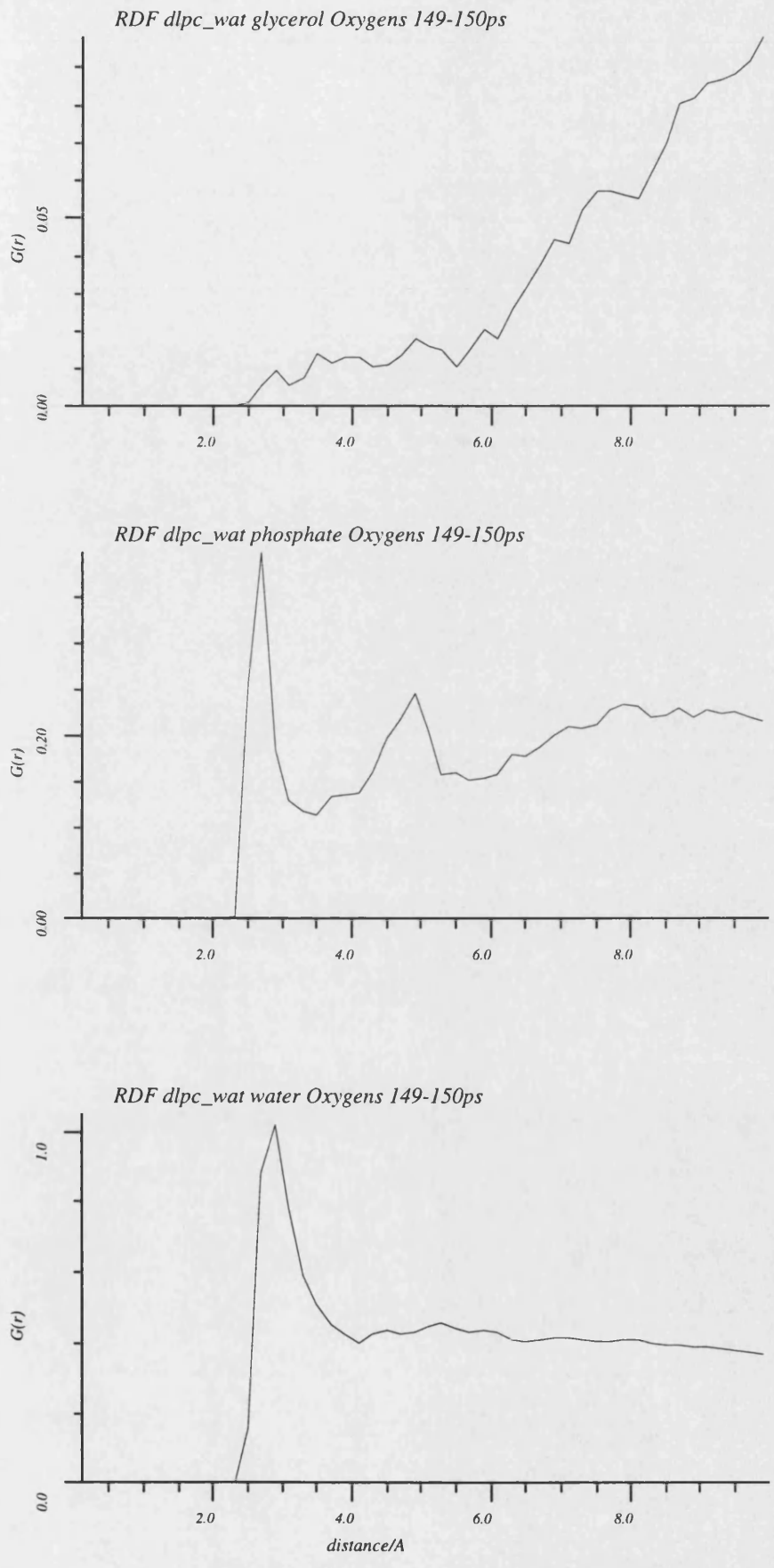
RDF dlpc_wat glycerol Oxygens 149-150ps
G(r)
0.00
0.05
2.0
4.0
6.0
8.0
RDF dlpc_wat phosphate Oxygens 149-150ps
G(r)
0.00
0.20
2.0
4.0
6.0
8.0
RDF dlpc_wat water Oxygens 149-150ps
G(r)
0.0
1.0
2.0
4.0
6.0
8.0
distance/A

Figure 9.1.5e

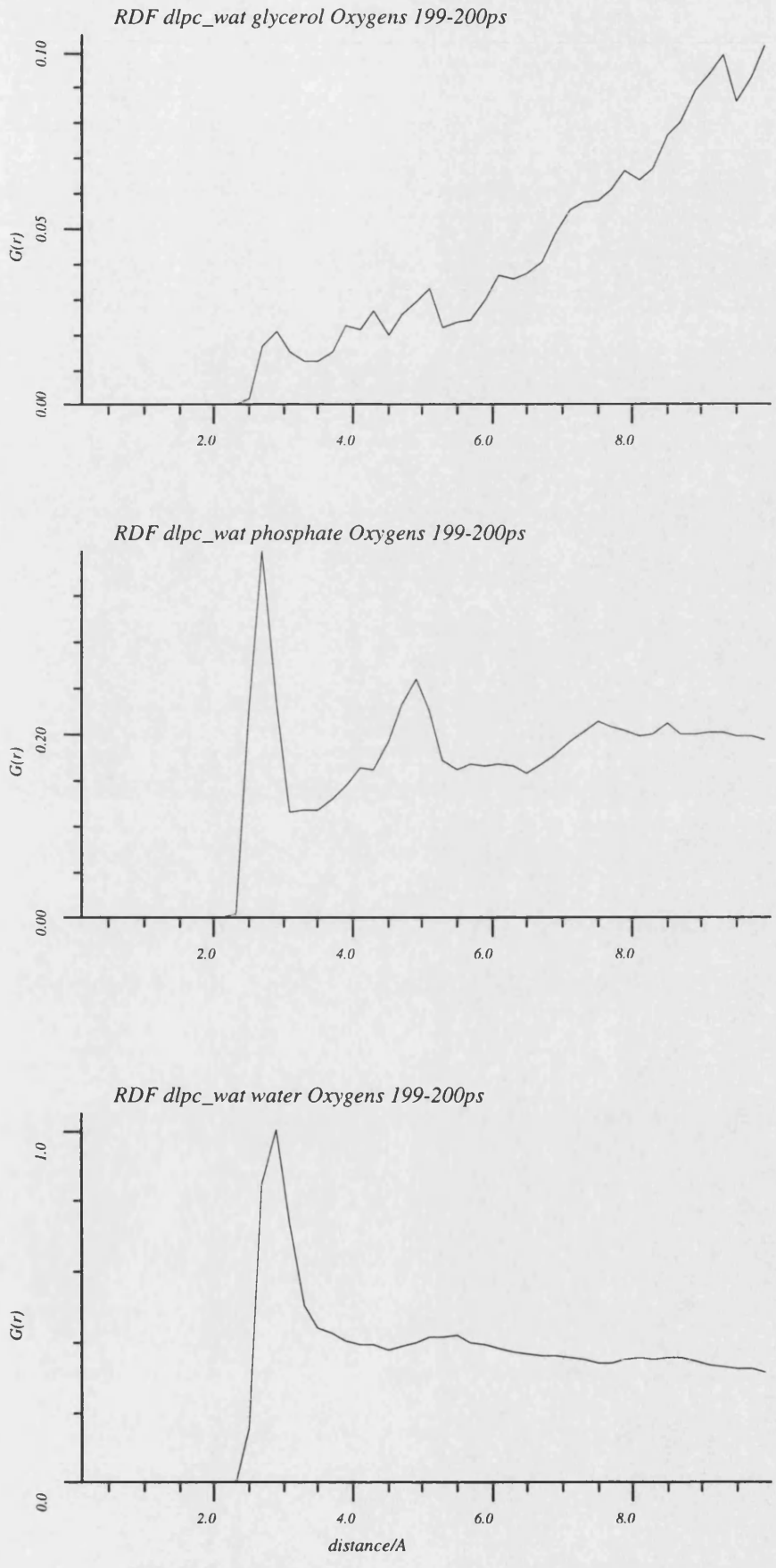
RDF dlpc_wat glycerol Oxygens 199-200ps
G(r)
0.00
0.05
0.10
2.0
4.0
6.0
8.0
RDF dlpc_wat phosphate Oxygens 199-200ps
G(r)
0.00
0.20
2.0
4.0
6.0
8.0
RDF dlpc_wat water Oxygens 199-200ps
G(r)
0.0
1.0
2.0
4.0
6.0
8.0
distance/A

Figure 9.1.5f

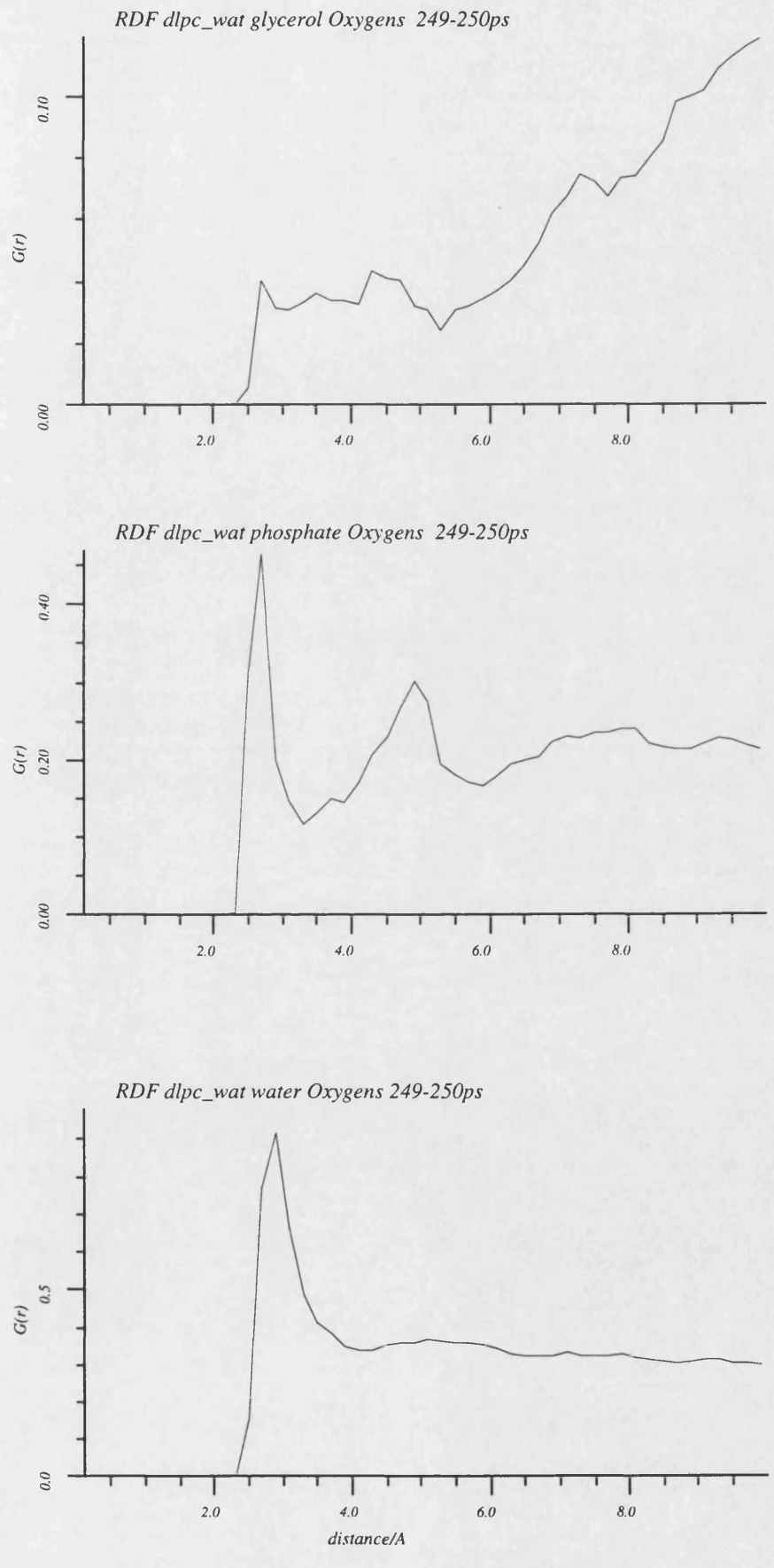
RDF dlpc_wat glycerol Oxygens 249-250ps
G(r)
0.00
0.10
2.0
4.0
6.0
8.0
RDF dlpc_wat phosphate Oxygens 249-250ps
G(r)
0.00
0.20
0.40
2.0
4.0
6.0
8.0
RDF dlpc_wat water Oxygens 249-250ps
G(r)
0.0
0.5
2.0
4.0
6.0
8.0
distance/A

Figure 9.1.5g

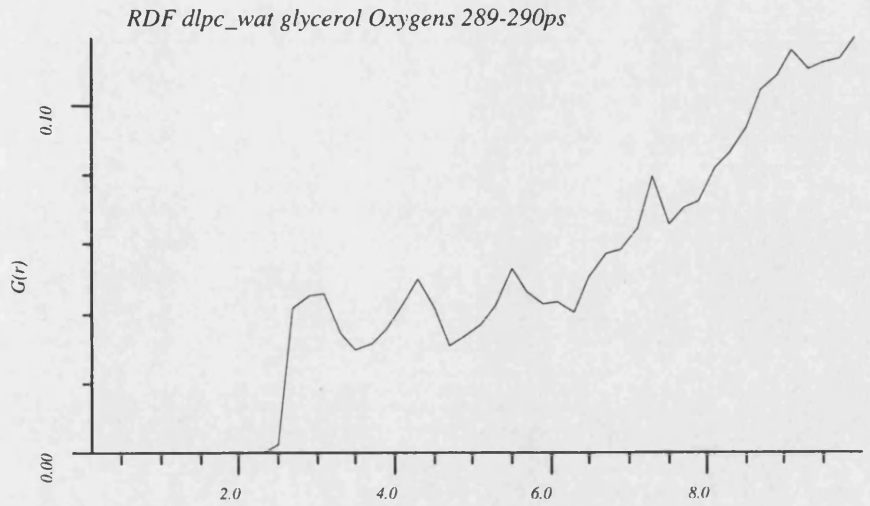
RDF dlpc_wat glycerol Oxygens 289-290ps
G(r)
0.00
0.10
2.0
4.0
6.0
8.0

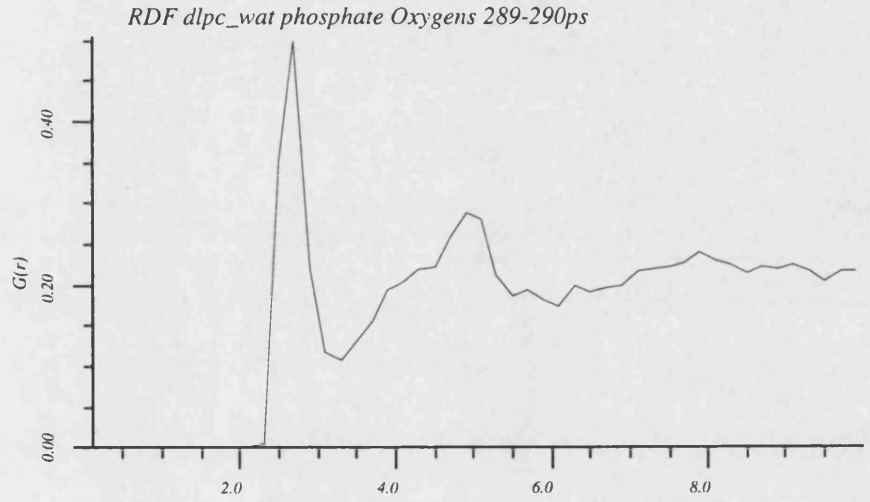
RDF dlpc_wat phosphate Oxygens 289-290ps
G(r)
0.00
0.20
0.40
2.0
4.0
6.0
8.0

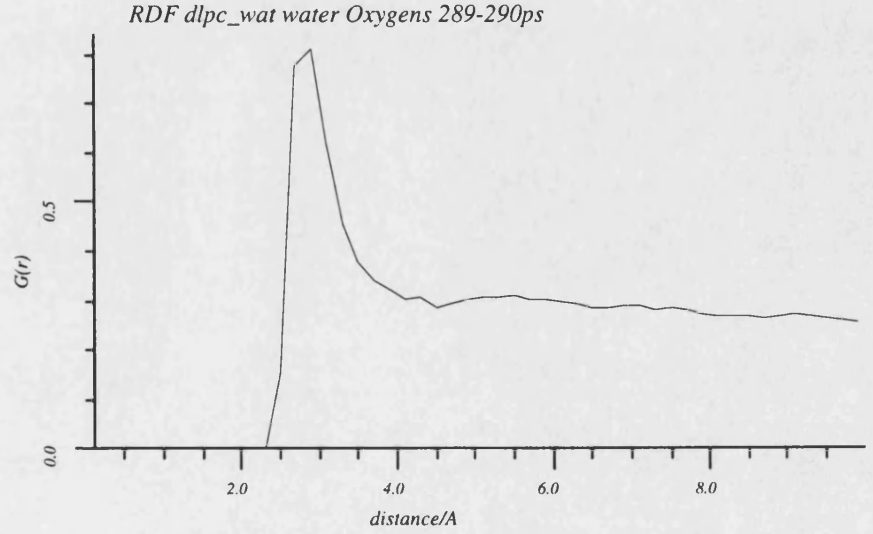
RDF dlpc_wat water Oxygens 289-290ps
G(r)
0.0
0.5
2.0
4.0
6.0
8.0
distance/A

glycerol region over the first 200ps of the trajectory, although one would expect to see more evidence of hydrogen bonding interactions even at this low penetration. There is generally less hydrogen bonding than in the phosphate group. This also reflects the lack of peaks in the radial distribution functions for the glycerol oxygens.

9.1.7. Electrostatic Potential

The electrostatic potential for an ion of single positive charge travelling across the membrane barrier from one side to the other is represented in Figure 9.1.7. This is a measure of the degree of motional polarisation of the waters at the interface. Waters in equilibrium with the bulk should have no contribution to the electrostatic potential of the membrane. This also allows one to measure the membrane potential and to identify the membrane boundary from the motional polarisation of the hydrating waters.[2-4]

Examination of the calculated electrostatic potential in Figure 9.1.7 shows the vapour - liquid boundary to be at approximately 30Å from the edge of the unit cell in the bilayer normal direction. The boundary between the liquid water and DLPC bilayer is less obvious but is estimated to be at 41Å. There is therefore 11Å of liquid water interacting with the bilayer. This can be rationalised on the basis of the 8Å nonbond cut used, secondary water interactions propagating the effect of the bilayer surface over 11Å of bilayer normal space. The net electrostatic potential ($\Delta\Phi$) is the difference in electrostatic potential between the bilayer (50Å) and centre of the liquid water (35.5Å) 0.38V. This agrees well with experimental results from similar bilayer systems[5] both in terms of the sign and magnitude of $\Delta\Phi$.

9.2. wat_dlpc_y2 (16xDLPC+Water)

From the results of the hydrated model dlpc_wat (9.1) it was decided that a model in which a reduced density DLPC bilayer is hydrated with less strained waters may provide a more physical model. It was hoped that this would provide fluidity of the acyl chain region and allow the presence of both bulk liquid water and hydrating waters in the head group region of the DLPC bilayer. From the results of the expanded DLPC bilayer model *dlpc_y1* (7.2) in which some fluidity of the lauryl chains of the membrane lipids was observed, it was decided to use this starting structure for the DLPC bilayer and to hydrate this model in order to provide the aqueous environment. This was achieved using the "soak" module from INSIGHT (56.4%molwt H_2O). The resulting structure was then minimised in order to remove the strain from the solvating water (see Chapter4).

The resulting coordinates (*wat_dlpc_y2*) were then used to sample the molecular dynamics trajectory from the NPT ensemble using pressure and temperature constraints of 1.0bar and 320K respectively. 300ps of molecular dynamics trajectory was sampled. An ensemble average temperature of 326.2±3.3K was observed.

9.2.1. Thermodynamics and Energetics

The relative energetic contributions from both intermolecular and intramolecular interactions have been examined (Table 9.2.1 and Figures 9.2.1a and 9.2.1b). The energetics of the system are dominated by the water interactions. The presence of the hydrating waters reduces the dominance of the potential energy by a few inter head group contacts. The shielding effect of the hydrating waters reduces the standard deviation of the pressure, removing the hard inter-lipid contacts across the periodic boundary system. The volume of the system is reduced to an ensemble average of 41777$Å^3$ over the first 30ps of the trajectory. This contraction of the system is nonisotropic the bilayer normal unit cell axis increasing (A 81.2→91.3±3.4Å), while the in bilayer plane axes reduce (B 23.3→19.5±0.5Å, and C 27.8→23.7±0.9Å). This results in a relatively stable volume of the system with respect to the constant pressure algorithm. The area per head group in the hydrated model is increased from 48.9$Å^2$ in the anhydrous model to 56.2$Å^2$. This is due to the increased volume of the PC head group and hydrating waters.

Figure 9.1.6

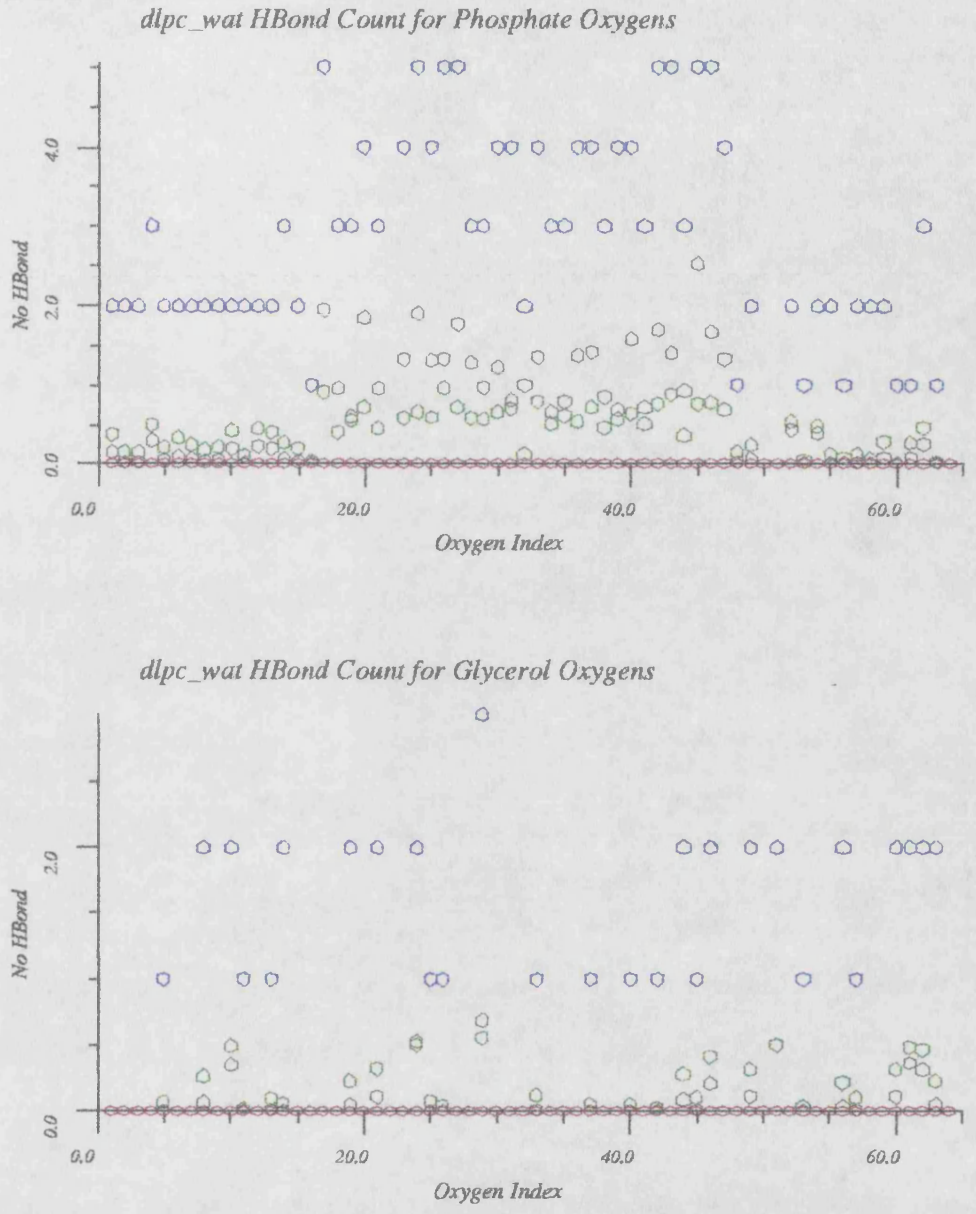

Sampled from 199-290ps. The property number refers to the atom index of the hydrogen bond acceptor.

Top: 1-16 is the first esterified phosphate oxygen, and 49-64 the second. 17-48 are the nonesterified oxygens of the phosphate group.

Bottom: 1-16, and 33-48 are the esterified oxygens of the glycerol group. 17-32 and 49-64 are the carbonyl oxygens.

Black is the average number of hydrogen bonds found, Green the standard deviation, Red the minimum and Blue the maximum.

Figure 9.1.7

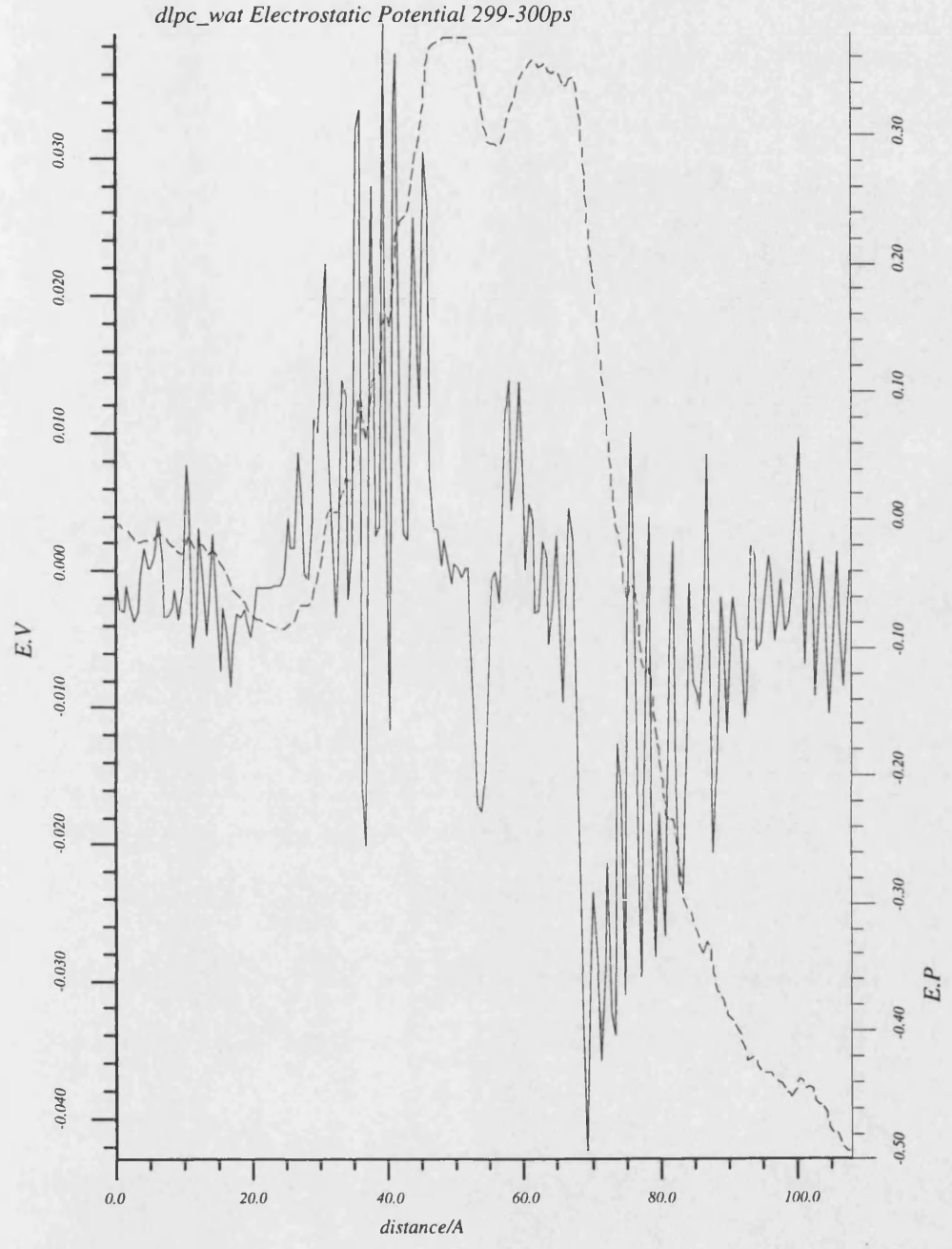
dlpc_wat Electrostatic Potential 299-300ps
E.V
E.P
distance/A
0.030
0.020
0.010
0.000
-0.010
-0.020
-0.030
-0.040
0.30
0.20
0.10
0.00
-0.10
-0.20
-0.30
-0.40
-0.50
0.0
20.0
40.0
60.0
80.0
100.0

Table 9.2.1

Energetics (kcal/mol) wat_dlpc_y2		
	Av	SD
E_{KE}	3734.4	37.0
E_{tot}	-1809.7	159.3
E_{PE}	-5544.1	164.0
E_{est}	-8781.5	181.4
E_{dsp}	-5310.2	45.1
E_{rep}	5847.9	67.8
E_b	1332.1	36.6
E_θ	1280.8	31.3
E_ϕ	181.8	10.1
Unit cell	Å	
A	93.0	1.7
B	19.3	0.2
C	23.3	0.4
Volume	$Å^3$	
V	41776.6	372.2
Pressure	bar	
P	101.3	378.4
P_x	18.2	1275.9
P_y	-19.5	1153.1
P_z	-48.7	1150.3
Temperature	K	
T	326.2	3.3

Sampled over 100-300ps.

9.2.2. Density Profile

Figure 9.2.2a is the density profile of the system along the bilayer normal unit cell axis. These are the average density profiles of a series of 100 sampled configurations taken at 50ps intervals along the trajectory. In the initial picosecond of the trajectory the acyl chains are at the density of the expanded dlpc_y1 model, less than 0.6g/ml. The aqueous layer

Figure 9.2.1a

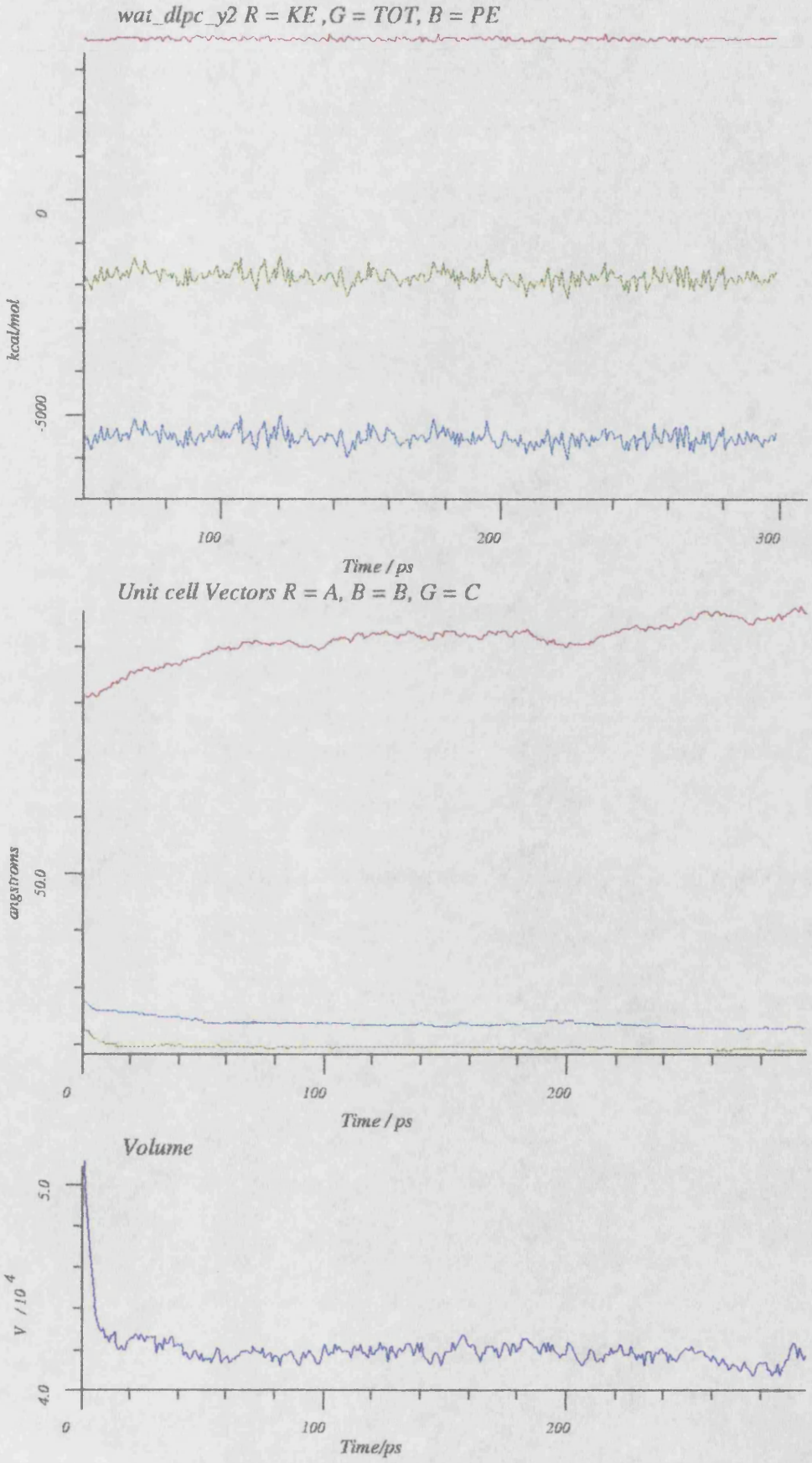
wat_dlpc_y2 R = KE ,G = TOT, B = PE
0
-5000
kcal/mol
100
200
300
Time / ps
Unit cell Vectors R = A, B = B, G = C
angstroms
50.0
0
100
200
Time / ps
Volume
5.0
4.0
V / 10^4
0
100
200
Time/ps

Figure 9.2.1b

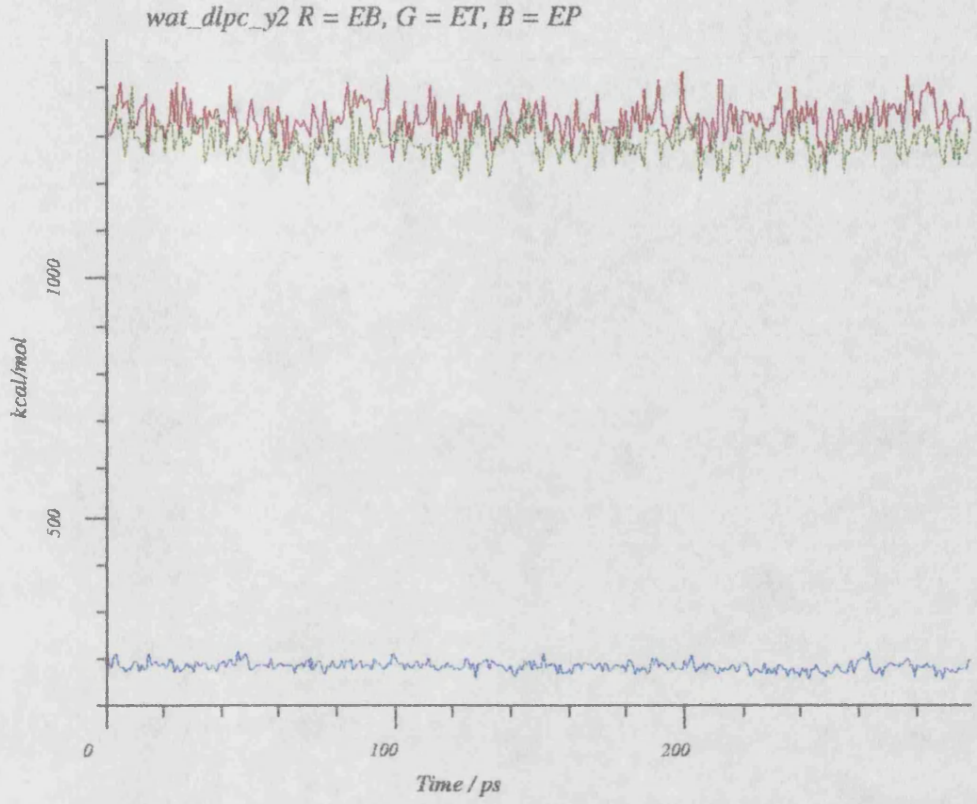
wat_dlpc_y2 R = EB, G = ET, B = EP
kcal/mol
1000
500
0
100
200
Time / ps

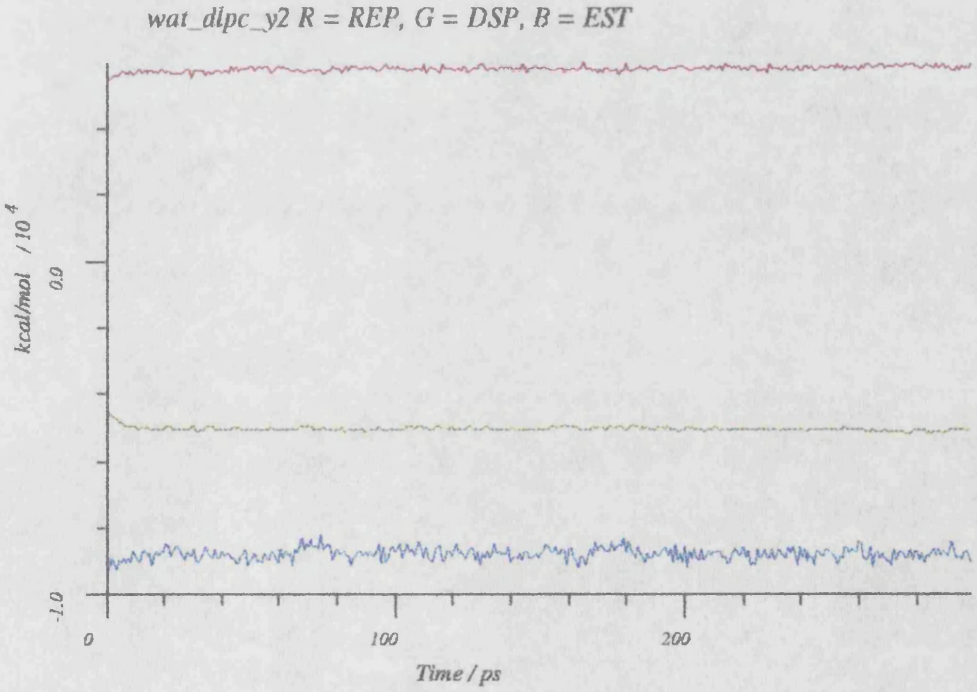
wat_dlpc_y2 R = REP, G = DSP, B = EST
kcal/mol / 10^4
0.0
-1.0
0
100
200
Time / ps

above and below the bilayer is at a density of approximately 1.0g/ml and penetrates into the glycerol region of the DLPC molecules. As the trajectory is sampled the low density of the lauryl chains allows water to penetrate into the hydrophobic core of the bilayer. This is followed by an increase in the density of the acyl chain region over the 50-200ps portion of the trajectory expelling waters from the lauryl chain region. Waters are found to locate around the glycerol region penetrating to the first methylene group of the lauryl chains. This results in the water penetration observed in the experimental results.

Figure 9.2.2b shows the density of the subcomponents of the system as a function of the bilayer normal, averaged from the 250-300ps sample of the trajectory. There is an aggregation of water density around the phosphate and glycerol region of the DLPC molecules. This can be assigned to the hydration of these polar regions and the formation of hydrogen bonded shells. The penetration of the water into the hydrophobic core of the bilayer matches almost exactly the location of the density of the glycerol atoms. Although the average density of the water in the system is near that of bulk water there is a density gradient from the edge of the unit cell to the membrane boundary. This is caused by the hydration of the PC and glycerol at the bilayer surface attracting water density away from the bulk water phase. The density of the Sn1 and Sn2 chains occupy the same region of bilayer normal space with the same density.

9.2.3. Non-Bonded Internals

The nonbonded internal angles have been sampled from the equilibrium state of the trajectory (Table 9.2.2). Comparing the characteristic nonbonded angles from this hydrated model with those of the anhydrous trajectory (Table 7.2.2) it can be seen that their average values are consistent within 5°. However there is an increase in the standard deviation of these averages, indicating a wider range of values are occupied. The average standard deviation of each angle is also increased by approximately 20% indicating an increase in molecular flexibility for the system in the hydrated model. The characteristic "scissor" angle (θ_2) exhibits a larger standard deviation and average value.

The nonbonded distances (Table 9.2.3) defined within the DLPC molecule (see Chapter 5) indicate an extension of the head group conformation into the surrounding solvent. The N-P and N-C6 distances are increased, while the chain lengths are reduced due to the presence of gauche torsions within the lauryl chains. The average standard deviation for all the defined internals is increased in the hydrated model which suggests that the increased electrostatic

Figure 9.2.2a *wat_dlpc_y2 DPF (1-300ps) g/ml (R = B Monol, G = T Monol, B = Water)*

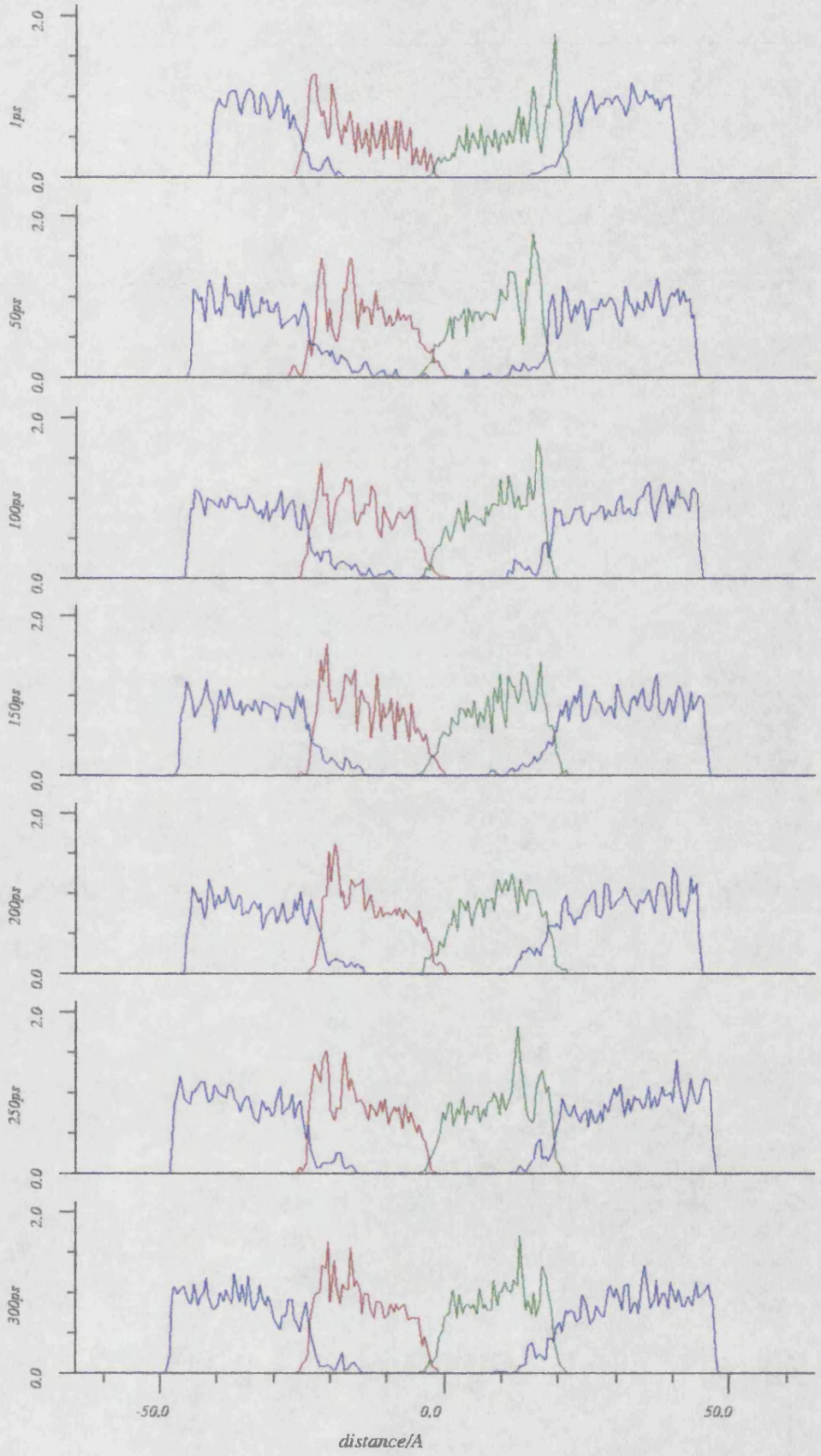

Figure 9.2.2b

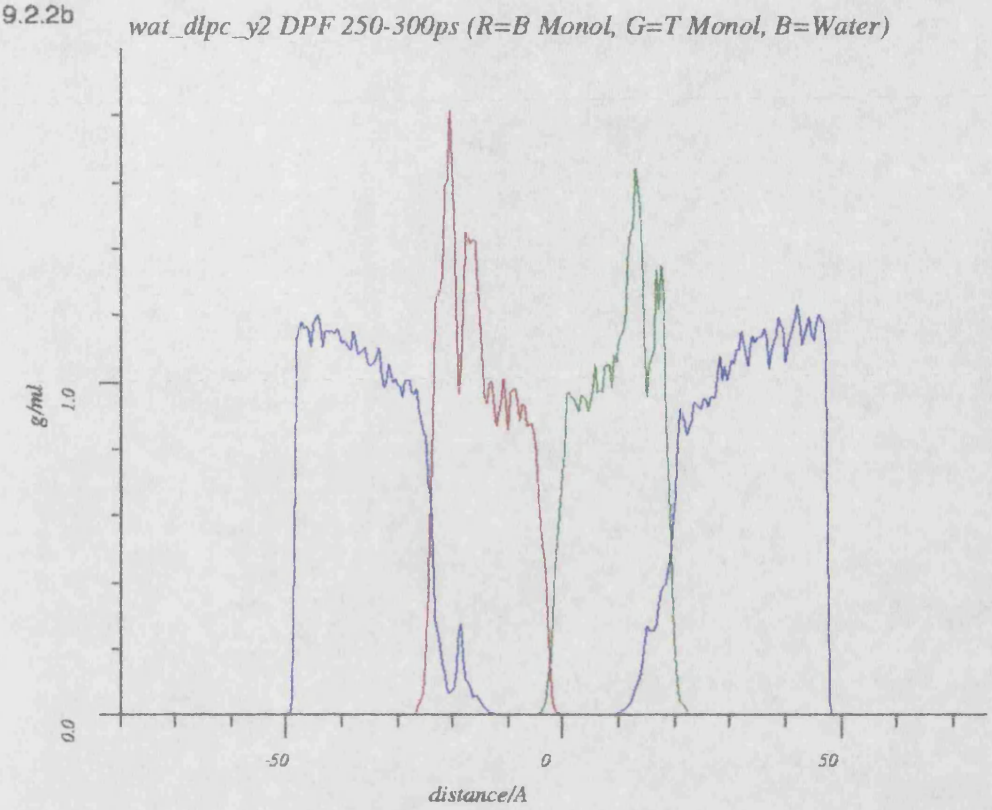
wat_dlpc_y2 DPF 250-300ps (R=B Monol, G=T Monol, B=Water)
g/ml
1.0
0.0
-50
0
50
distance/A

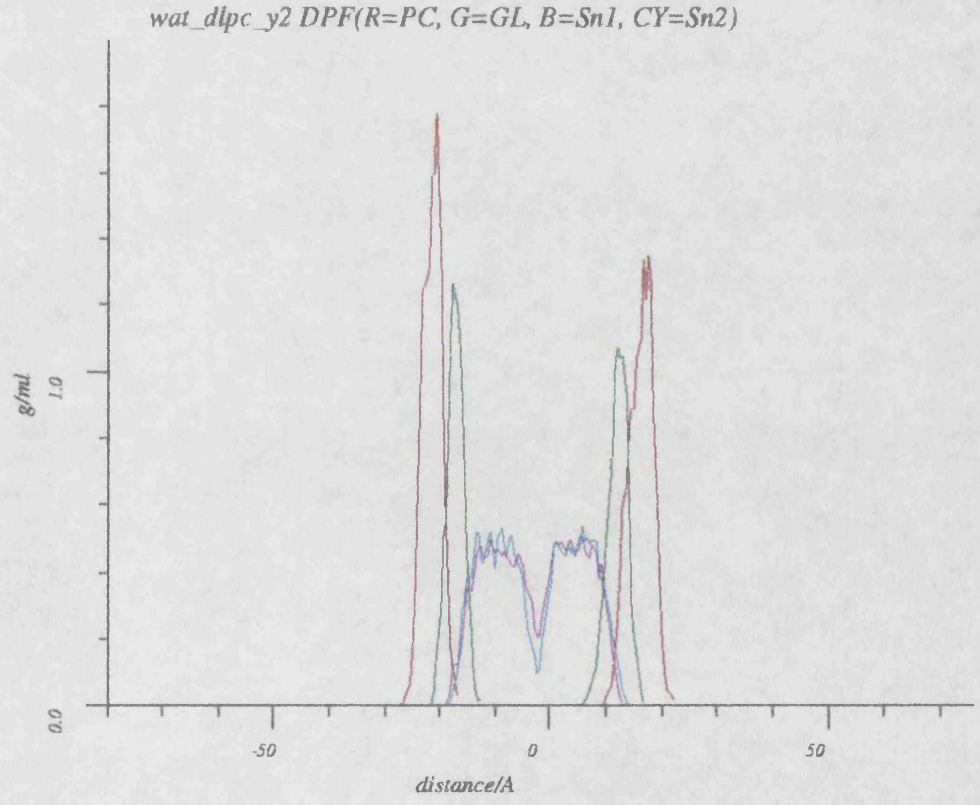
wat_dlpc_y2 DPF(R=PC, G=GL, B=Sn1, CY=Sn2)
g/ml
1.0
0.0
-50
0
50
distance/A

shielding from the hydrating waters increases the flexibility of the DLPC molecule.
Table 9.2.2

Non-Bond Angles wat_dlpc_y2			
	θ	SD	SDav
θ_1	100.9	10.8	9.8
θ_2	28.7	7.8	7.4
θ_3	115.8	22.9	11.1
θ_4	130.3	16.1	10.4

Sampled over 80-300ps. Where θ is the average angle, and SD is the average standard deviation and SDav is the standard deviation of the average values.

Table 9.2.3

Non-Bond Distances (Å) wat_dlpc_y2			
	D	SD	SDav
N P	5.1	0.1	0.3
N C6	6.8	0.5	0.5
C6 C19	15.2	1.2	0.9
C6 C31	14.9	0.6	0.7
C8 C19	13.3	0.6	0.6
C20 C31	13.4	0.4	0.5
C19 C31	7.6	2.0	1.8

Sampled over 100-300ps. Where D is the average non-bonded distance, SD the average standard deviation for that distance and SDav is the standard deviation of the average values.

9.2.4. Euler Angles

The characteristic Euler angles (Table 9.2.4) are consistent with both the dlpc and dlpc_y1 bilayer models. They do however exhibit decreased average standard deviations when compared with the dlpc_y1 model. This indicates more stability for the orientation of the principle axis of the DLPC molecule with respect to the bilayer normal in the hydrated model. This is most evident in the first Euler angle (E_2) which reflects the orientation of the PC head group relative to the bilayer normal. This can again be rationalised on the basis of increased

electrostatic shielding of the head group interactions stablising the orientation of the molecule with respect to the bilayer normal.

Table 9.2.4

Euler Angles wat_dlpc_y2			
	Av	SD	avSD
1	87.2	49.8	8.9
2	112.2	0.8	3.6
3	123.6	0.8	3.6

Sampled over 100-300ps.

9.2.5. Torsions

The hydrated model exhibits on average a lower standard deviation for its acyl chain torsion angles (Table 9.2.5) compared with the anhydrous model (dlpc_y1 33.9, wat_dlpc_y2 25.6). This is however still sufficient to observe gauche torsion angles in the lauryl chains (Tables 9.2.6 and 9.2.7). Comparing the percentage gauche torsions in the dlpc_y1 and wat_dlpc_y2 models for both the Sn1 and Sn2 chains:

dlpc_y1: Sn1 %t=87.70, %g^-=3.27, %g^+=4.08

Sn2 %t=88.88, %g^-=3.04, %g^+=3.49

wat_dlpc_y2: Sn1 %t=89.90, %g^-=3.69, %g^+=2.73

Sn2 %t=82.66, %g^-=8.26, %g^+=5.47

It can be seen that the hydrated model exhibits increased gauche conformations in the Sn2 chain relative to the anhydrous model. This is a direct consequence of the increased area per head group, which is experimentally observed to increase on the gel to liquid crystalline phase change. The Sn1 chains in the two models are very similar in terms of gauche conformations, but a small increase in the percentage g^- from the g^+ can be seen.

It can be seen from table 9.2.7 that there is significant variation in the distribution of each conformation across the DLPC molecules of the system, reflecting the local environment of each molecule. On average there is however an increase in the formation of gauche torsion angles, favouring the g^- over the g^+ conformers. The %g^- increases from 3.35% in the dlpc_y1 to 5.98% in the wat_dlpc_y2 model, and the %g^+ increases from 3.78% to 4.10%.

There is therefore an observable increase in fluidity in the hydrated model in comparison to the anhydrous state. This should have an effect on the relative order parameter for these two models.

Table 9.2.5

Torsion Standard Deviations wat_dlpc_y2					
	SD	sdSD		SD	sdSD
ϕ_1	20.8	16.2	ϕ_2	70.6	45.3
ϕ_3	38.0	8.3	ϕ_4	89.4	43.0
ϕ_5	45.7	22.8	ϕ_6	37.2	12.9
ϕ_7	26.7	21.4	ϕ_8	15.0	10.6
ϕ_9	43.5	12.8	ϕ_{10}	15.1	2.3
ϕ_{11}	61.7	22.2	ϕ_{12}	20.1	9.9
ϕ_{13}	28.4	14.5	ϕ_{14}	15.7	6.4
ϕ_{15}	28.2	14.0	ϕ_{16}	19.0	11.0
ϕ_{17}	30.5	15.9	ϕ_{18}	25.0	15.9
ϕ_{19}	30.0	11.3	ϕ_{20}	34.2	19.8
ϕ_{21}	21.3	5.3	ϕ_{22}	13.0	1.3
ϕ_{23}	37.8	18.0	ϕ_{24}	26.6	15.5
ϕ_{25}	20.5	16.2	ϕ_{26}	25.5	27.1
ϕ_{27}	21.1	13.5	ϕ_{28}	22.2	13.1
ϕ_{29}	17.7	9.5	ϕ_{30}	20.3	12.7
ϕ_{31}	26.6	15.0	ϕ_{32}	29.6	18.2

Sampled over 80-300ps.

9.2.6. Segmental Order Parameters

The segmental order parameter profile for the lauryl chains has been calculated (Figure 9.2.3). The observed equivalence of the Sn1 and Sn2 order parameters in the dlpc_y1 model is removed. The orientation of the molecule is maintained with respect to the bilayer normal, indicated from the Euler angles. There is therefore no reorientation of the molecule which causes the equivalence in the order parameters. The upper segments of the lauryl chains exhibit the reverse relationship between the order of the Sn1 and Sn2 chains in comparison with the lower segments. This reflects the relationship between gauche states in torsion

Table 9.2.6

%Trans/Gauche Conformations wat_dlpc_y2							
	%t	%g^-	%g^+		%t	%g^-	%g^+
ϕ_1	37.00	24.64	36.98	ϕ_2	53.62	12.80	24.39
ϕ_3	57.81	1.77	1.79	ϕ_4	13.75	48.27	17.90
ϕ_5	13.19	38.39	29.56	ϕ_6	41.38	7.29	12.88
ϕ_7	23.31	49.07	24.79	ϕ_8	73.12	11.37	12.27
ϕ_9	41.56	14.62	4.43	ϕ_{10}	92.44	0.00	0.00
ϕ_{11}	8.19	37.23	8.48	ϕ_{12}	91.00	0.00	4.34
ϕ_{13}	90.62	5.17	0.98	ϕ_{14}	91.81	2.33	1.59
ϕ_{15}	83.62	1.78	10.42	ϕ_{16}	94.38	0.00	2.24
ϕ_{17}	95.81	0.00	1.05	ϕ_{18}	92.56	0.21	3.69
ϕ_{19}	87.38	9.31	0.00	ϕ_{20}	81.88	14.39	0.27
ϕ_{21}	32.62	2.17	1.43	ϕ_{22}	93.31	0.00	0.00
ϕ_{23}	3.81	20.38	25.31	ϕ_{24}	45.88	29.26	17.97
ϕ_{25}	88.75	1.16	5.83	ϕ_{26}	68.75	27.34	0.00
ϕ_{27}	85.50	5.84	5.88	ϕ_{28}	84.69	0.04	11.65
ϕ_{29}	95.75	0.00	1.71	ϕ_{30}	86.19	10.59	0.29
ϕ_{31}	97.31	0.12	0.00	ϕ_{32}	91.12	0.00	5.95

Sampled over 80-300ps. These are the average of all equivalent torsions in all molecules in the system.

angles from these regions of the two lauryl chains.

The average of the calculated order parameters is reduced from approximately 0.89 in the dlpc_y1 model to 0.78 in the hydrated model, reflecting the increased fluidity and resulting in decreased order. The average order parameter in both chains is Sn1 0.78±0.15 and Sn2 0.79±0.12. The shape of the two curves does however question the sensitivity of these calculated order parameters to conformational and configurational changes.

9.2.7. Thermal Partitioning

In order to examine the distribution of thermal energy in this nonhomogeneous system the temperature of the subcomponents of the system have been calculated from their atomic

Table 9.2.7

%Trans/Gauche Conformations in Acyl Chains wat_dlpc_y2			
Mol	%t	$\%g^-$	$\%g^+$
1	87.39	4.99	5.17
2	79.56	7.75	8.36
3	93.33	0.00	3.07
4	92.17	0.00	5.22
5	88.06	0.00	8.15
6	87.06	4.56	2.79
7	95.33	0.48	2.04
8	79.72	10.89	5.42
9	98.33	0.00	0.00
10	80.83	5.01	10.53
11	85.22	10.77	0.24
12	87.11	10.59	0.16
13	92.94	5.27	0.00
14	70.33	16.75	7.02
15	84.00	8.68	1.96
16	79.06	9.87	5.54

Sampled from torsions ϕ_{12}-ϕ_{20} for Sn1, and ϕ_{24}-ϕ_{32} for Sn2 (50-300ps).

velocities (Table 9.2.8 and Figures 9.2.4a&b). Once again the increased conformational freedom of the DLPC molecule is accompanied by an increase in the partitioning of thermal energy within the molecule. The acyl chains are on average still below the gel-to-liquid-crystal phase transition temperature for the molecule. The temperature of the aqueous layer in comparison with the lipid layer is still higher, although the removal of strain from the initial coordinates has reduced the temperature differential. The temperature difference in the system is a function of the charge density of each subcomponent. The temperature difference is maintained across the trajectory.

The methylene temperatures show an inverse correlation with the segmental order parameter profile (Table 9.2.9). It should be noted that the relationship between the order of the Sn1 and Sn2 chains is also mirrored by their average methylene temperatures (Figure 9.2.5).

Figure 9.2.3

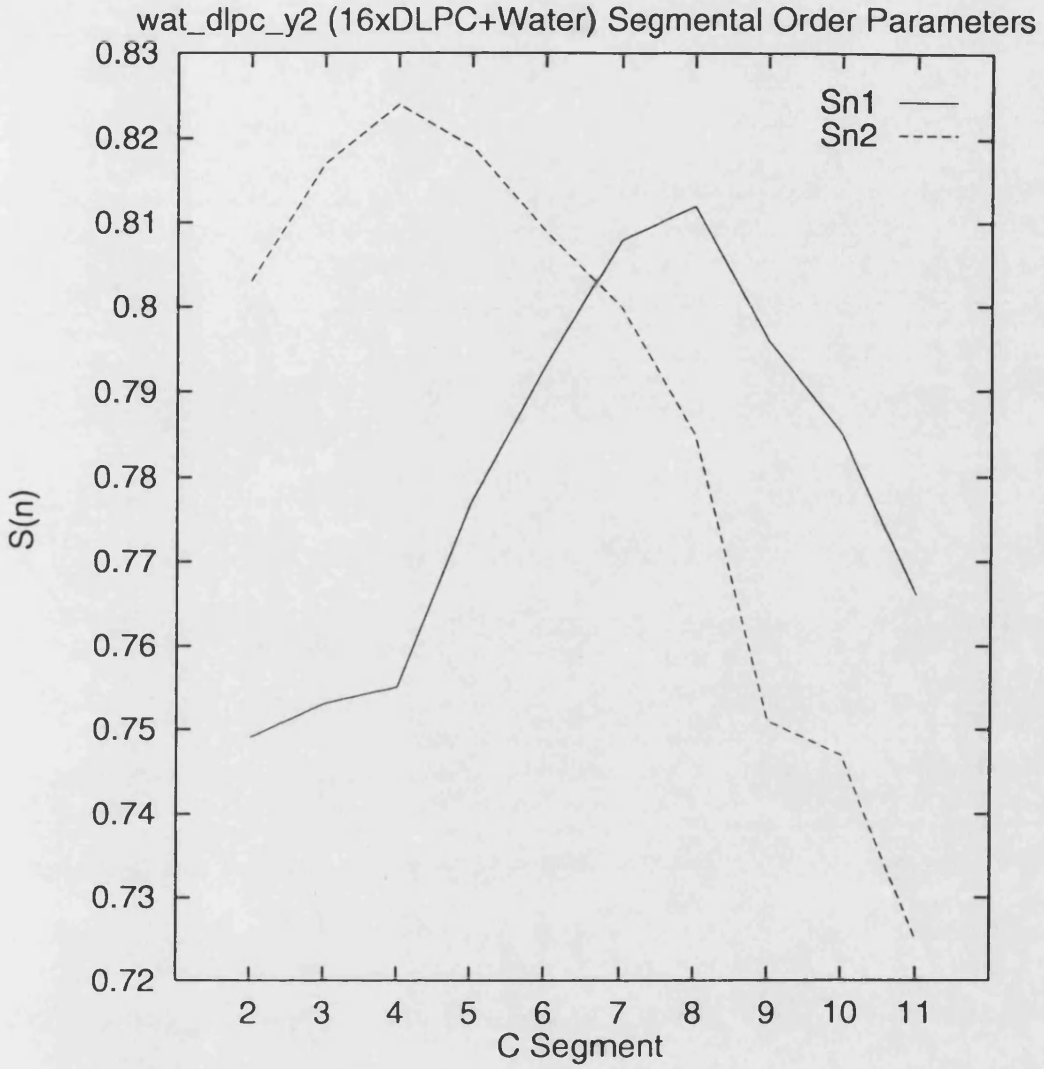

Sampled over 80-300ps.

9.2.8. Radial Distribution Functions

In order to study the hydration of the DLPC molecule by the surrounding water, pairwise radial distribution functions for the water oxygen atoms relative to the hydrogen bond acceptor atoms in the DLPC molecule have been calculated. These include the oxygens of the phosphate group and the oxygens of the glycerol backbone (Figures 9.2.6). In order to probe the structure of the water the pairwise radial distribution function for the water in the system has been calculated. As the system is not pure water none of these radial distributions will normalise to 1.0. Each graph contains the radial distribution calculated from 100 configurations

Table 9.2.8

Average Temperature (K) wat_dlpc_y2		
	Av	SD
PC	328.0	13.9
GL	279.1	15.4
SN1	205.7	7.8
SN2	210.4	9.0
WAT	389.7	5.8

Sampled over 1-300ps.

Table 9.2.9

Average Methylene Temperature (K) wat_dlpc_y2					
Sn1			Sn2		
C Segment	Av	SD	C Segment	Av	SD
2	217.9	27.3	2	221.7	28.5
3	211.4	26.7	3	213.9	26.2
4	211.0	25.2	4	210.9	27.8
5	210.2	26.6	5	207.4	25.4
6	206.6	26.5	6	207.4	25.8
7	203.3	25.9	7	204.3	25.3
8	200.2	25.2	8	205.4	26.9
9	202.5	25.8	9	203.8	25.6
10	200.6	26.4	10	204.0	26.2
11	203.1	25.6	11	202.9	25.2
12	208.5	23.2	12	211.6	27.0

Sampled over 230-280ps.

taken at 50ps intervals across the trajectory and the ensemble average distribution from 200-300ps (thick black).

From the radial distribution function of the glycerol oxygens one can follow the penetration of the water molecules into the glycerol region. In contrast to the dlpc_wat model the penetration of water into the the glycerol region does appear to reach equilibrium after 250ps. There are two clear hydration shells formed, a peak at approximately 2.7Å equivalent in radius

Figure 9.2.4a

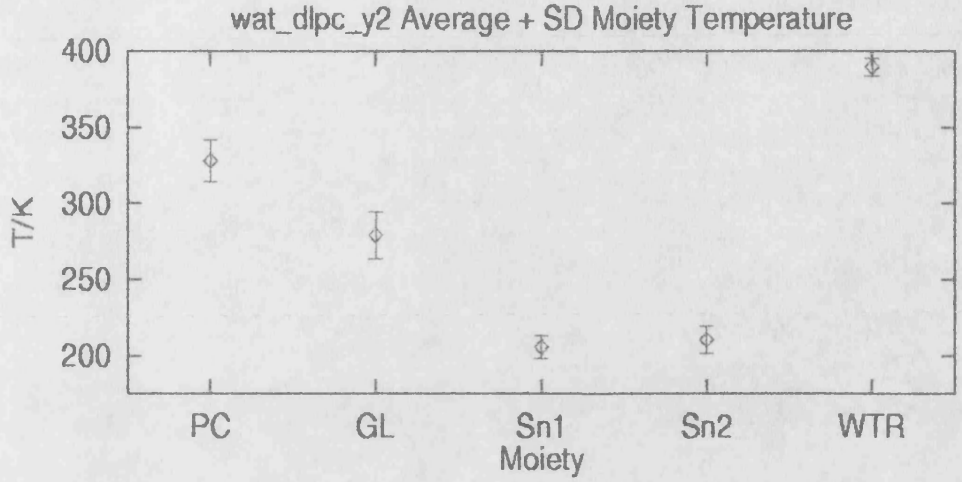

Figure 9.2.4b

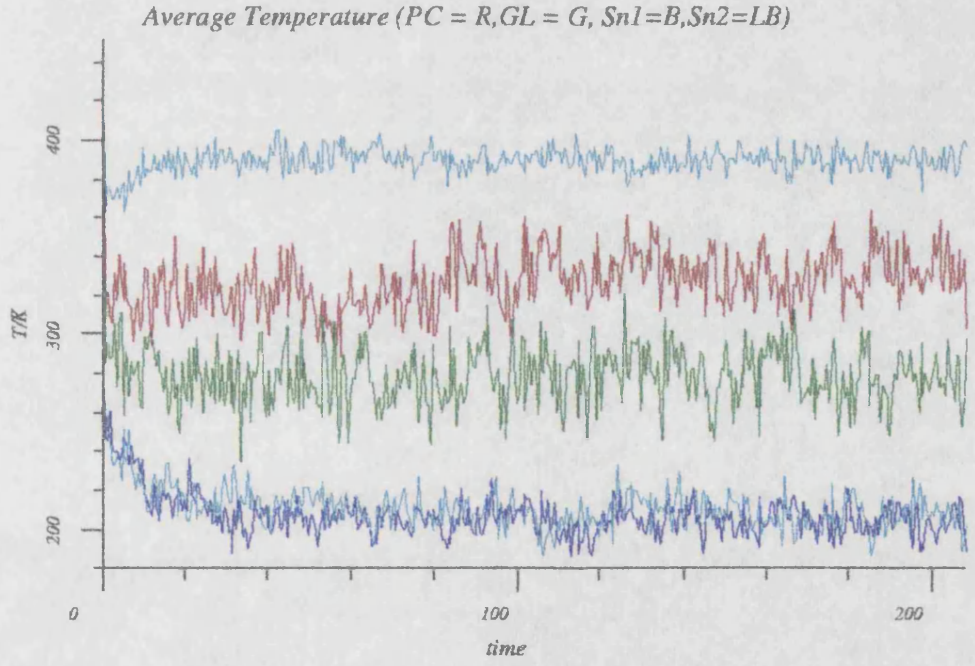

to the first hydration shell of water and a broad peak around 2.9-3.9Å. This suggests that the nature of the electrostatic environment of the glycerol oxygens is equivalent to that of the water oxygen. The second hydration shell is however at shorter range than in the water radial distribution.

Figure 9.2.5

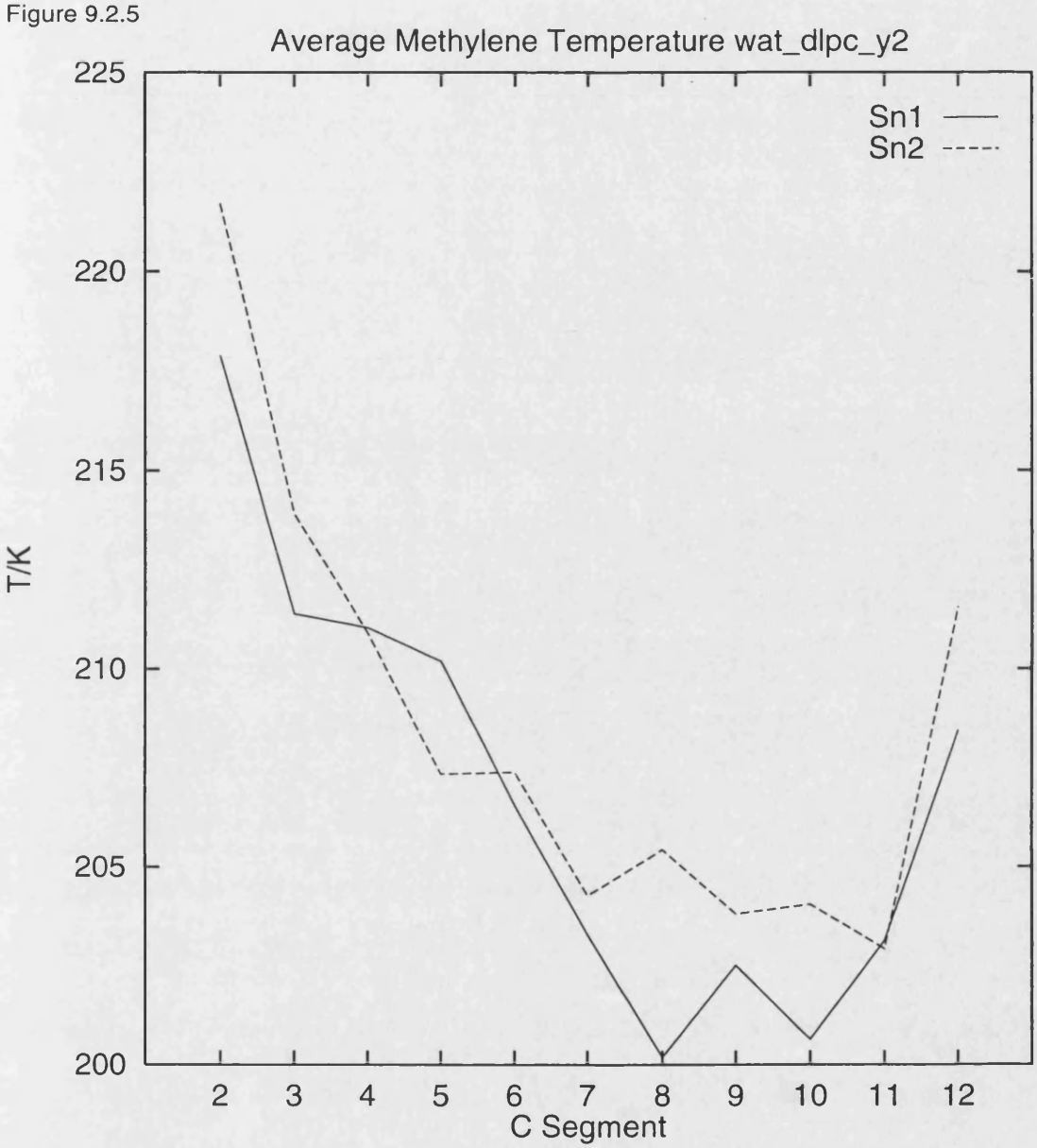

Examination of the radial distribution of water oxygen atoms relative to the phosphate oxygens clearly shows the presence of two hydration shells around the phosphate group. The first hydration shell is a sharp peak at 2.6Å. The second peak broad peak is at approximately 5Å. There is also evidence of long range order. The increased charge density around the phosphate group causes increased binding of the water oxygens and results in a shorter range hydration shell.

The radial distribution function for the water oxygens of the system normalises to approximately 0.9, reflecting the effect of the DLPC molecules on the density of the water in the system. The principle peak in the radial distribution function for water is longer than the equivalent peak in the phosphate radial distribution. This indicates stronger binding of water to the phosphate than to itself. This can be rationalised on the basis of the pure electrostatic nature of this representation of hydrogen bonding. There is also evidence of a broad secondary peak around 5.4Å. The system appears to have little long range order above 6.5Å.

9.2.9. Hydrogen Bonding

In order to examine the trajectory for any evidence of hydrogen bonding between waters and the hydrogen bond acceptor atoms in the DLPC molecule a hydrogen bond search was performed on the trajectory, hydrogen bonds being assigned on the basis of a distance-only criterion. This searches for water hydrogens that are closer than 2.5Å from one of the eight possible hydrogen bond acceptor atoms, the four phosphate oxygens and the four glycerol oxygens. Figure 9.2.8 shows the hydrogen bonding information results.

Comparing the results from the *wat_dlpc_y2* trajectory with those of *dlpc_wat* there is on average more hydrogen bonding to the esterified oxygens of the wat_dlpc_y2 model making on average 1.8 hydrogen bonds compared to only 1.6 in dlpc_wat. This is due to the increase in density of water around the head group region and lack of expansion of the system in the bilayer normal direction. There is an increase in the hydrogen bonding to the two carbonyl oxygens. There is considerable variation in the hydrogen bonding to these atoms, but some on average make up to 0.5 hydrogen bonds. Only transient hydrogen bonding is observed with the esterified oxygens of the glycerol group.

Figure 9.2.6

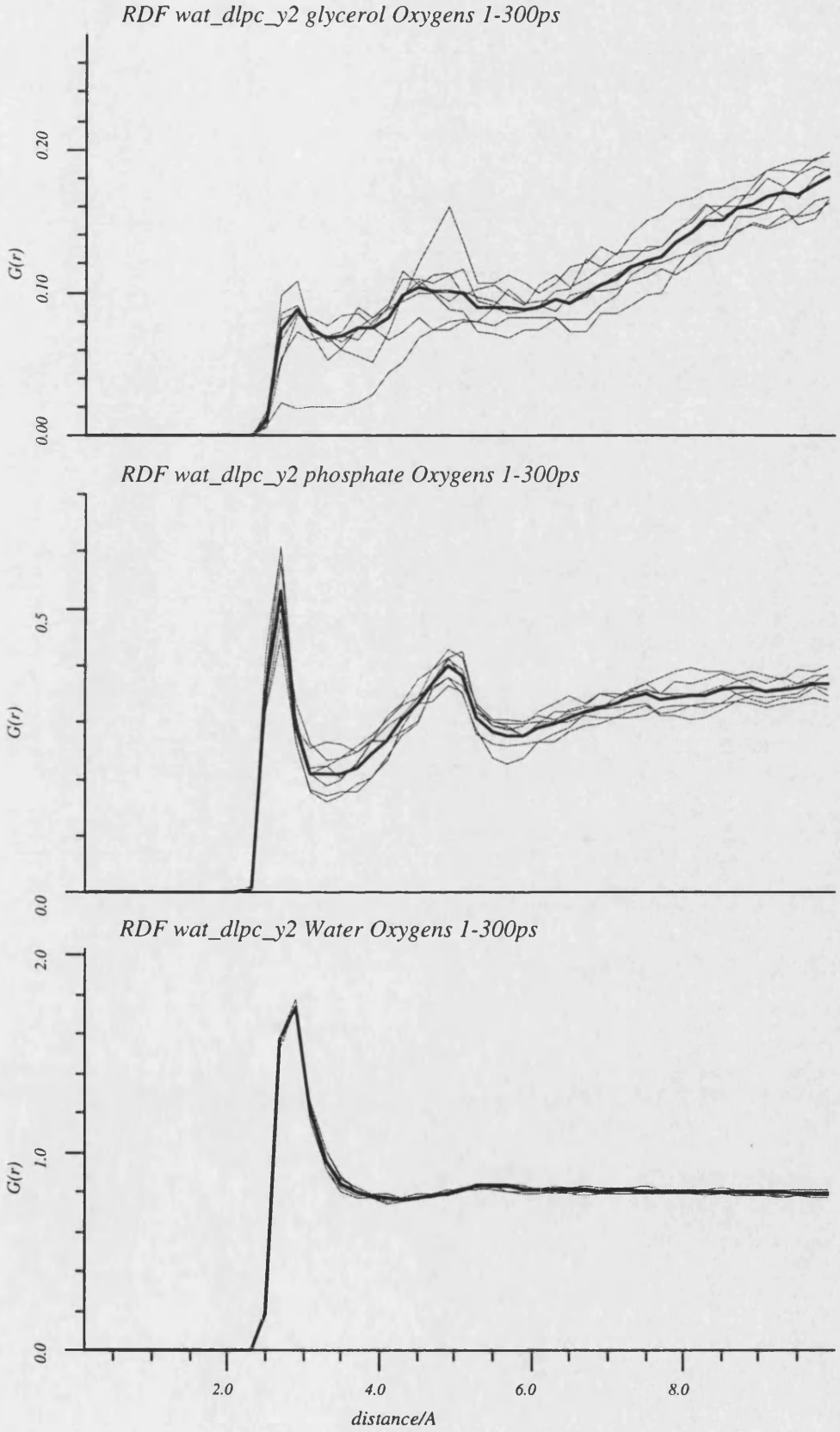
RDF wat_dlpc_y2 glycerol Oxygens 1-300ps
G(r)
0.00
0.10
0.20
RDF wat_dlpc_y2 phosphate Oxygens 1-300ps
G(r)
0.0
0.5
RDF wat_dlpc_y2 Water Oxygens 1-300ps
G(r)
0.0
1.0
2.0
2.0
4.0
6.0
8.0
distance/A

Figure 9.2.7

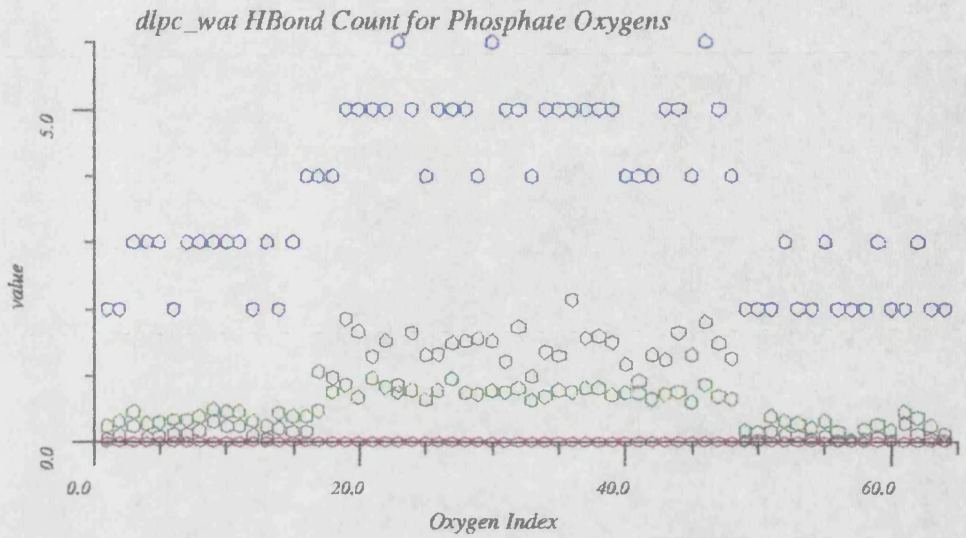

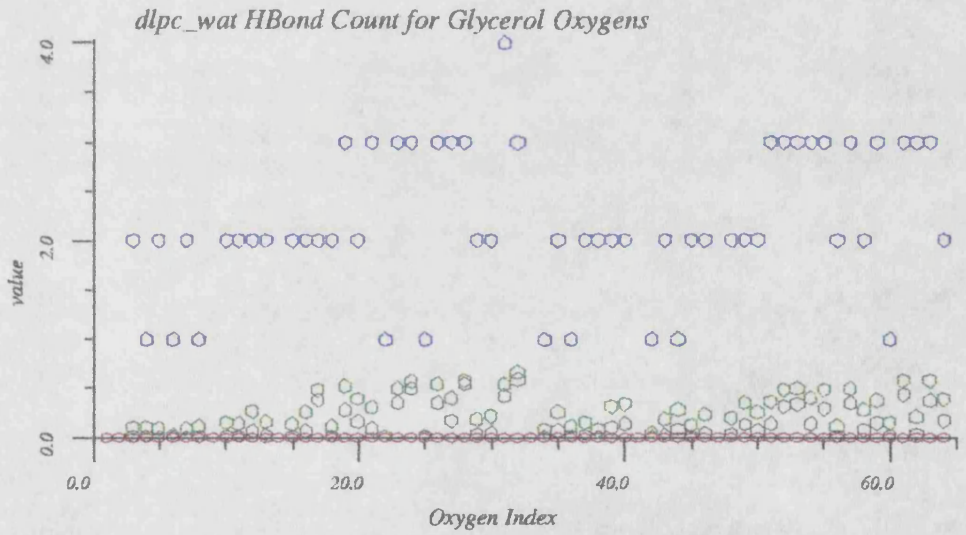

Sampled from 200-300ps. The property number refers to the atom index of the hydrogen bond acceptor.

Top: 1-16 is the first esterified phosphate oxygen, and 49-64 the second. 17-48 are the nonesterified oxygens of the phosphate group.

Bottom: 1-16, and 33-48 are the esterified oxygens of the glycerol group. 17-32 and 49-64 are the carbonyl oxygens.

Black is the average number of hydrogen bonds found, Green the standard deviation, Red the minimum and Blue the maximum.

9.2.10. Electrostatic Potential

The electrostatic potential for an ion of single positive charge travelling across the membrane barrier from one side to the other is represented in Figure 9.2.8. This is a measure of the degree of motional polarisation of the waters at the interface. Waters in equilibrium with the bulk have no contribution to the electrostatic potential of the membrane. This also allows one to measure the membrane potential and to identify the membrane boundary from the motional polarisation of the hydrating waters.[2-4]

Examination of the calculated electrostatic potential in Figure 9.2.8 elucidates the vapour - liquid boundary to be at approximately 31Å from the centre of the unit cell in the bilayer normal direction. The boundary between the liquid water and DLPC bilayer well defined compared to the *dlpc_wat* bilayer results, being at 18Å from the centre of the unit cell bilayer normal axis. The effect of the bilayer surface extends over 17Å from the bilayer water interface despite the increased number of hydrating waters. This indicates stronger propagation of the polarisation of hydrating water molecules by the phosphatidylcholine head groups of the bilayer. The net electrostatic potential ($\Delta\Phi$) is the difference in electrostatic potential between the bilayer (18Å) and centre of the liquid water (31Å) 0.11V. This agrees well with experimental results from similar bilayer systems[5-7] both in terms of the sign and magnitude of $\Delta\Phi$. This is smaller than the corresponding value for the *dlpc_wat* model.

Figure 9.2.8

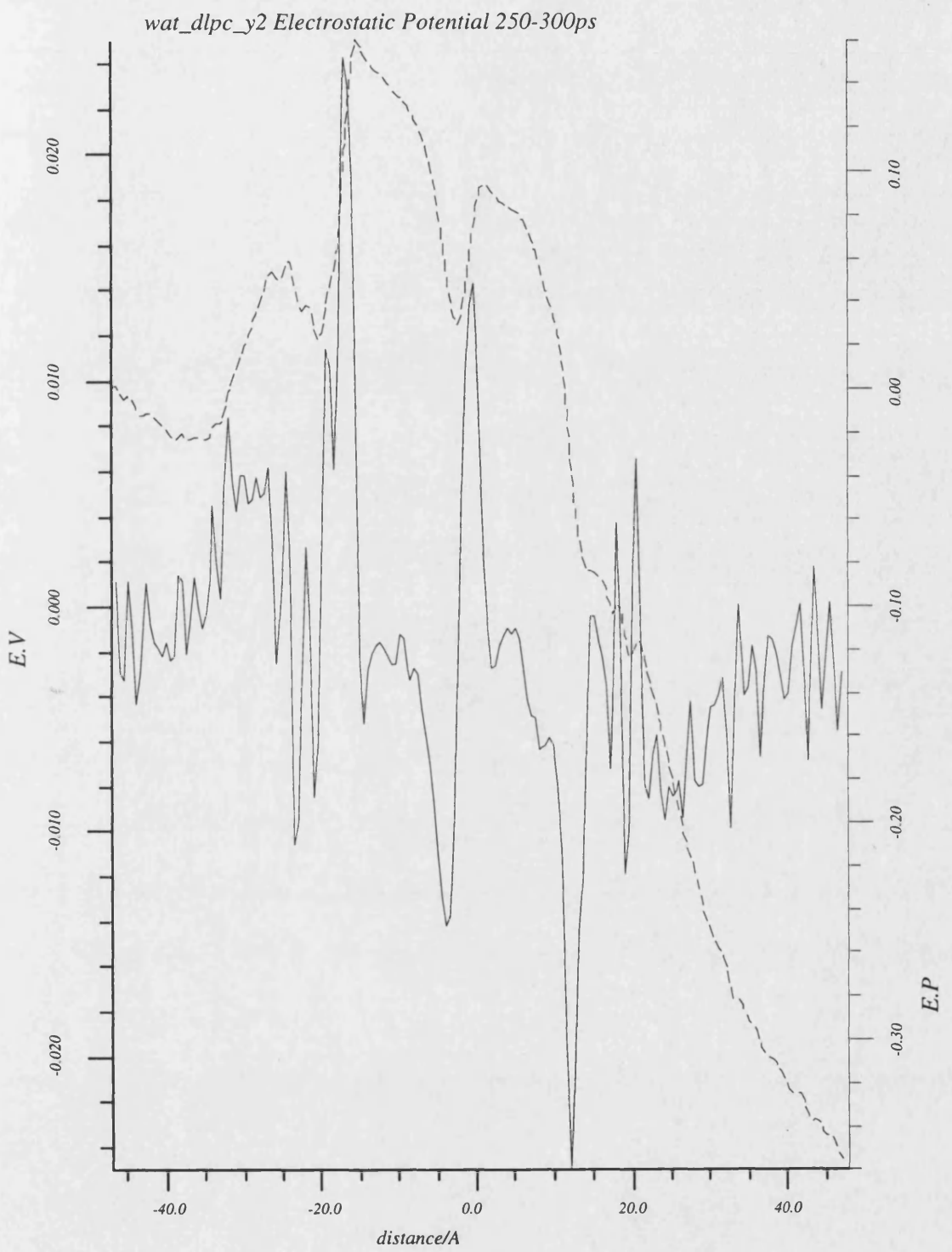
wat_dlpc_y2 Electrostatic Potential 250-300ps
E.V
E.P
distance/A
0.020
0.010
0.000
-0.010
-0.020
0.10
0.00
-0.10
-0.20
-0.30
-40.0
-20.0
0.0
20.0
40.0

9.3. System IX wat_dlpcchol (8xDLPC+8xCHOL+Water)

The model *wat_dlpcchol* is based on the cholesterol doped bilayer *dlpcchol_s.* The results of the anhydrous simulation show fluidisation of the lauryl chains. It was hoped that the addition of an aqueous environment would improve the simulation in terms of its representation of key features of the experimental system. The bilayer coordinates were those of the minimised dlpcchol_s system. Waters were added by hydrating the unit cell with waters sampled from a Monti-Carlo simulation (41.6%molwt H_2O), removing waters in the hydrophobic region of the bilayer, defined as the region below the first carbon of the lauryl chains. The resulting model was then minimised to remove strain from the water and lipid phases.

The resulting structure was then used to sample the molecular dynamics trajectory of the system from the NPT ensemble using temperature and pressure constraints of 320K and 1.0bar respectively.

9.3.1. Energetics

The system took approximately 100ps to reach equilibrium in terms of the constant pressure scaling. The volume of the system was reduced from 31061.0Å^3 to approximately 26000Å^3 after 100ps, giving an ensemble average volume of 26055.1Å^3. This volume change is non-isotropic. The bilayer normal unit cell vector was increased from 65.24Å to approximately 82Å in the first 30ps of the trajectory and reached an ensemble average of 80.64Å. The in-plane unit cell vectors both decrease from 19.20Å and 24.48Å to their ensemble average values of 15.45Å and 19.64Å respectively. This corresponds to a decrease in area per head group from 58.75Å^2 to 37.93Å^2. It should however be noted that these area per head groups are the average of both the smaller cholesterol and the DLPC molecules present.

The standard deviation for the pressure of the system (wat_dlpcchol: 465.5bar) is larger than the equivalent standard deviation in the hydrated pure lipid system (wat_dlpcchol_y2: 378.4bar), which suggests that this system is more sensitive to intermolecular contacts. This can be rationalised from the lack of shielding between the sterol ring system of the cholesterol and the adjacent lipid chains. In the hydrated lipid model the large surface area of the PC head group and the shielding of this group by hydrating waters reduces the effect of interactions between adjacent lauryl chains, reducing their effect on the pressure of the system. Hence there is a lower standard deviation for the pressure of the pure lipid system.

Table 9.3.1

Energetics (kcal/mol) wat_dlpcchol		
	Av	SD
E_{KE}	2325.1	29.9
E_{tot}	355.4	105.6
E_{PE}	-1969.7	109.6
E_{dsp}	-3692.8	30.6
E_{rep}	3925.0	51.2
E_{est}	-4142.2	121.7
E_{ϕ}	205.7	7.7
E_{θ}	891.6	24.3
E_b	904.3	29.3
	Pressure/bar	SD
P	96.1	465.5
P_x	-21.3	1824.1
P_y	-5.4	1522.6
P_z	-19.8	1515.4
	Unit cell/Å	SD
A	80.6	1.0
B	16.2	0.2
C	19.9	0.1
	Volume/$Å^3$	SD
V	26053.4	343.1
	Temperature/K	SD
T	325.4	4.2

Sampled over 100-300ps.

9.3.2. Density Profiles

The distribution of density in the unit cell with respect to the bilayer normal has been calculated using 1000 sampled configurations at 10ps intervals across the trajectory, from 160-220ps (Figure 9.3.2). This can be used to examine the variation in distribution of material across the sampled trajectory after equilibrium has been achieved in terms of the volume of

Figure 9.3.1a

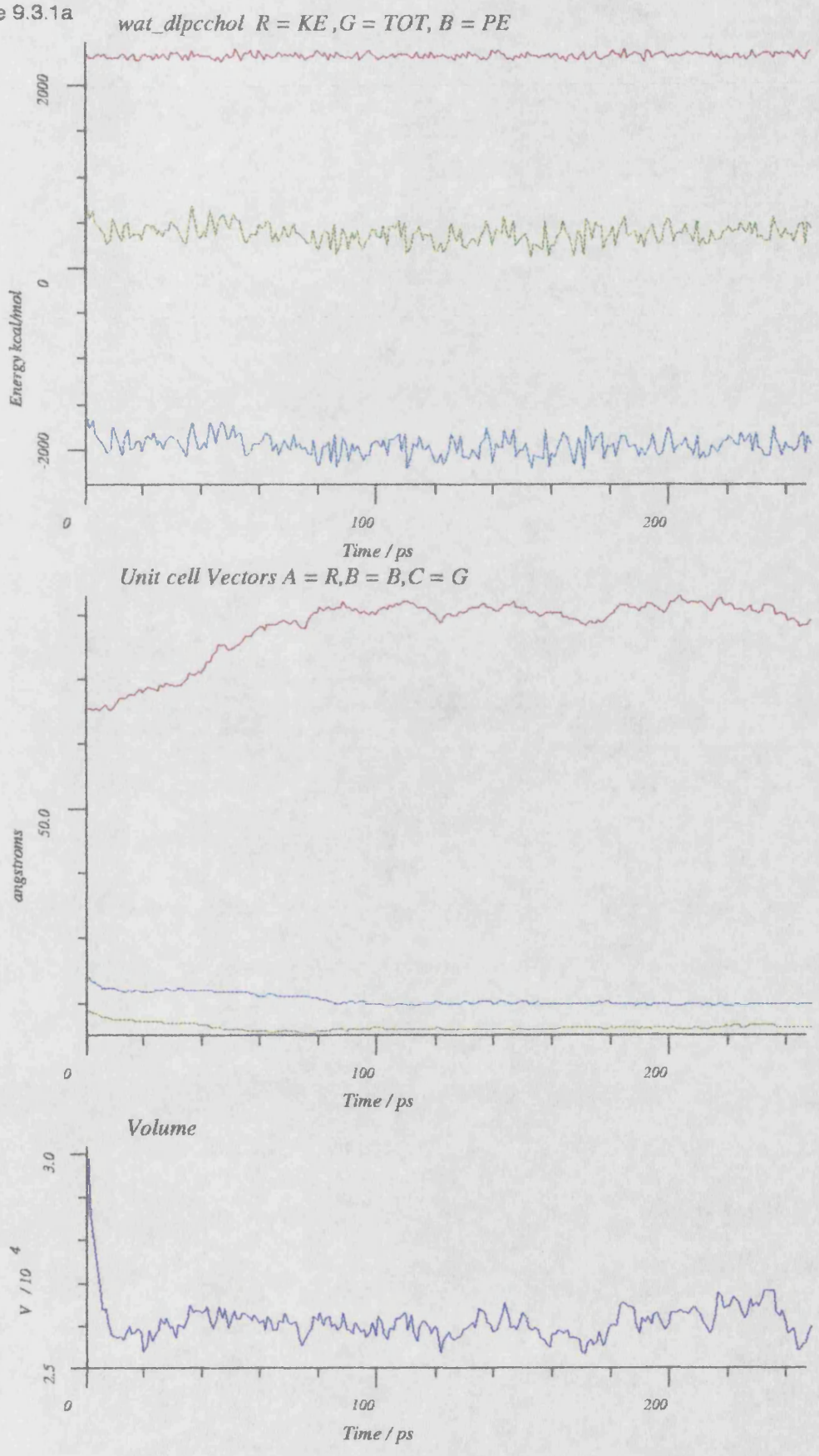
wat_dlpcchol R = KE ,G = TOT, B = PE
2000
0
-2000
Energy kcal/mol
0
100
200
Time / ps
Unit cell Vectors A = R,B = B,C = G
50.0
angstroms
0
100
200
Time / ps
Volume
3.0
2.5
V / 10 4
0
100
200
Time / ps

Figure 9.3.1b

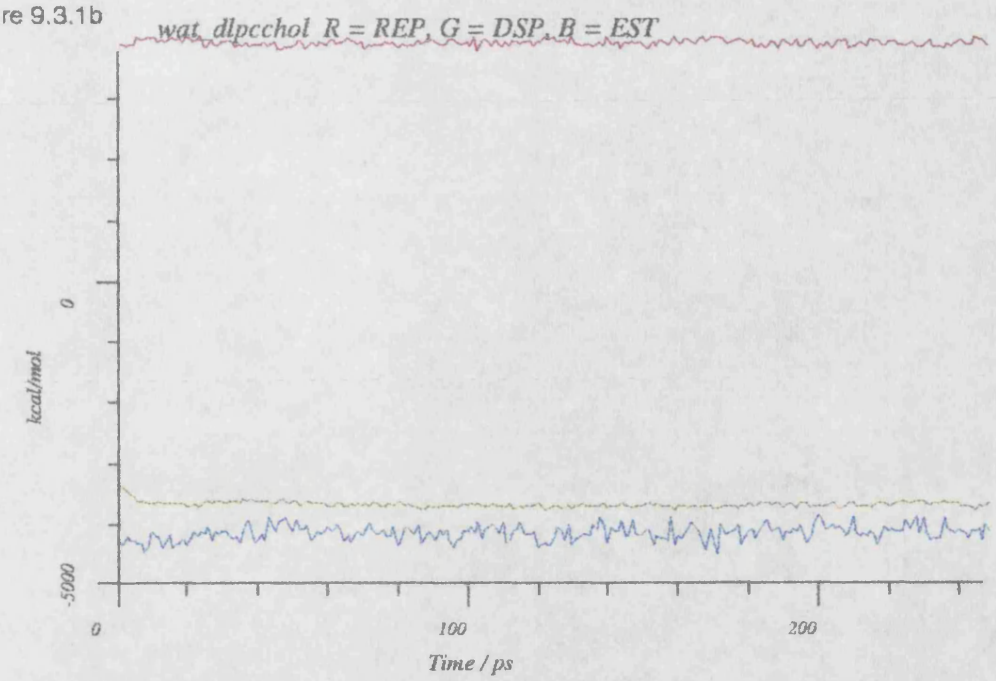
wat_dlpcchol R = REP, G = DSP, B = EST
kcal/mol
0
-5000
0
100
200
Time / ps

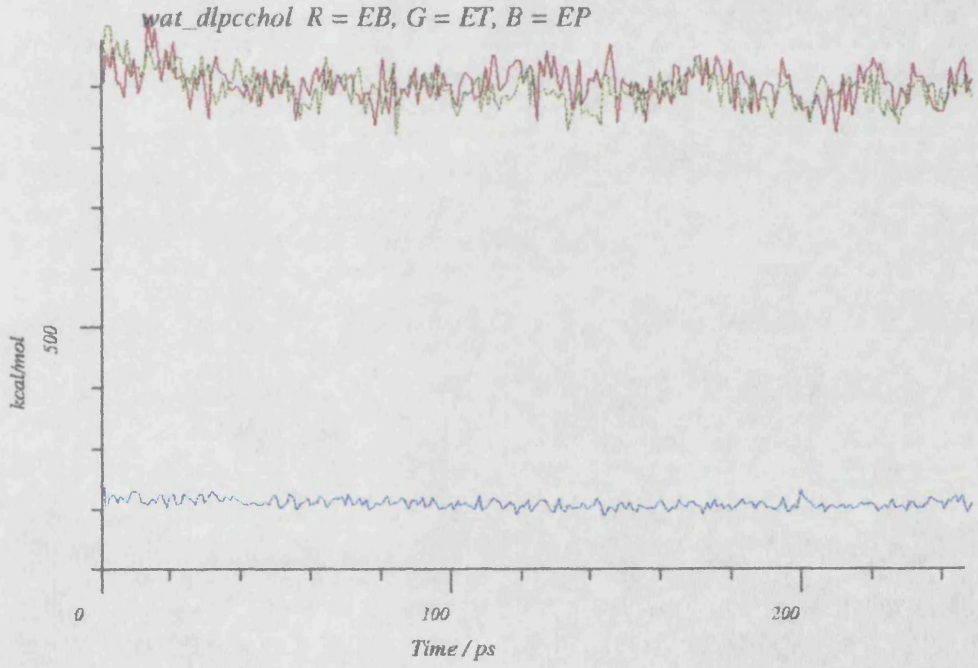
wat_dlpcchol R = EB, G = ET, B = EP
kcal/mol
500
0
100
200
Time / ps

the unit cell. The density of the aqueous phase is maintained across the sampled configurations at approximately 0.9g/ml below the expected density of bulk water. The pressure scaling algorithm gives rise to a low density of the aqueous phase, which may be due to the inhomogenity of this mixed phase system, with the pressure of the lipids dominating the pressure scaling in the bilayer normal direction resulting in a large water phase volume relative to the water pressure. This suggests that the system requires a much longer equilibration time in order to remove these artifacts from the system and couple the pressure of the aqueous and lipid phases correctly.

There is some evidence of interdigitation of the two monolayers, evident from the overlap of the density of the two opposing monolayers. The density of the acyl chain region of the DLPC molecules is maintained, being on average slightly denser than the aqueous phase. The head group region can be clearly distinguished in the density distribution. Water density can be seen to penetrate down into the head group region of the DLPC monolayers, but does not penetrate beyond the first carbon of the lauryl chains. This water density appears to have reached equilibrium.

9.3.3. Non-Bonded Internals

The characteristic non-bonded internals of the system have been calculated across the trajectory. These can be used to elucidate the characteristic motions and conformations of the DLPC molecule in the bilayer environment. Table 9.3.2 contains the ensemble average non-bond angles for the DLPC molecule. All the internal angles defined exhibit reduced standard deviations indicating reduced flexibility in comparison with the wat_dlpc_y2 model. This suggests that the sterol ring system of the cholesterol reduces the fluidity of the DLPC molecule. Comparison of the anhydrous model dlpcchol_s with the hydrated model wat_dlpcchol the hydrated model exhibits less range of conformations, but each conformation is more flexible.

From the ensemble average non-bonded distances (Table 9.2.3) it can be seen that the hydrated model shows reduced conformational freedom in the hydrophobic region of the DLPC molecule. The average length of both lauryl chains is increased, suggesting the presence of less gauche torsion angles. The head group region of the DLPC molecule shows increased flexibility and an extended conformation in comparison with the anhydrous simulation although within a smaller range of values.

Figure 9.3.2

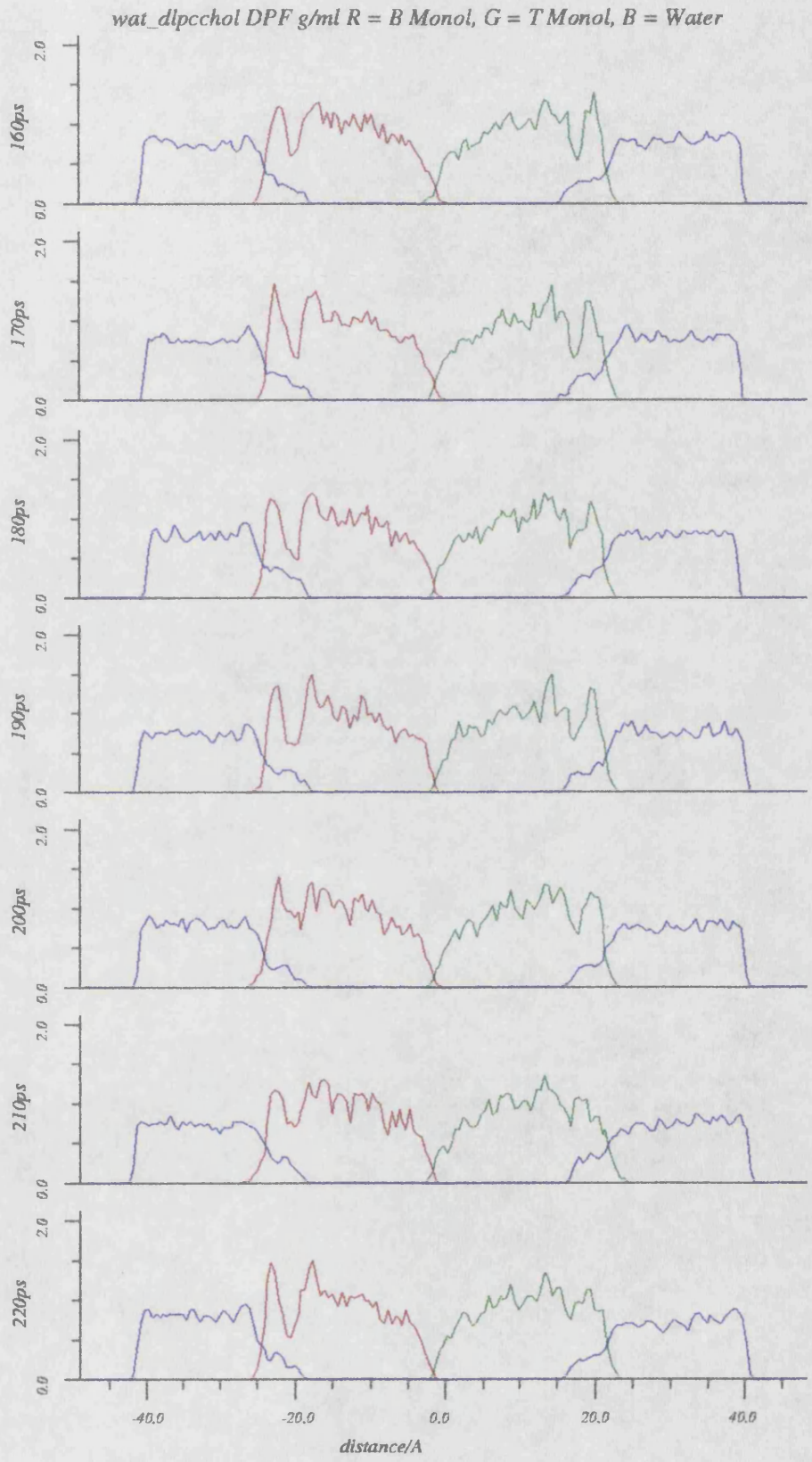
wat_dlpcchol DPF g/ml R = B Monol, G = T Monol, B = Water
160ps
170ps
180ps
190ps
200ps
210ps
220ps
2.0
0.0
-40.0
-20.0
0.0
20.0
40.0
distance/A

Table 9.3.2 ·

Non-Bond Angles wat_dlpcchol			
	Av	SD	avSD
DLPC			
θ_1	95.9	3.1	10.2
θ_2	20.9	1.0	3.9
θ_3	118.1	5.6	9.1
θ_4	118.0	6.0	9.6
CHOL			
θ_1	168.2	3.6	6.3

Sampled over 100-300ps.

Table 9.3.3

Non-Bond Distances (Å) wat_dlpcchol			
	Av	SD	avSD
N P	5.1	0.1	0.3
N C6	6.7	0.2	0.5
C6 C19	15.9	0.4	0.7
C6 C31	15.4	0.4	0.6
C8 C19	13.8	0.1	0.3
C20 C31	13.7	0.2	0.3
C19 C31	5.9	0.3	1.0

Sampled over 100-300ps. Av is the average over all equivalent distances, SD is the standard deviation of those averages, and avSD is the average standard deviation of the individual values.

9.3.4. Euler Angles

The characteristic Euler angles of the glycerol group have been calculated, showing the orientation and dynamics of the DLPC molecule with respect to the bilayer normal. The values of the measured Euler angles are consistent with the anhydrous model in terms of both their average values and variation across the trajectory.

Table 9.3.4

Euler Angles wat_dlpcchol			
	Av	SD	avSD
1	92.9	53.5	11.4
2	111.9	0.5	3.6
3	123.3	0.3	3.7

Sampled over 100-300ps. Av is the average over all angles, SD is the standard deviation of those averages, and avSD is the average standard deviation of the individual values.

9.3.5. Torsions

The defined torsion angles for both DLPC and cholesterol molecules have been calculated across the sampled trajectory and their ensemble averages and standard deviations calculated (Table 9.3.5). The average standard deviation in an acyl chain torsion angle in the hydrated bilayer *wat_dlpcchol* (Sn1 SD = 15.26, Sn2 SD = 16.73) is less than that observed in the anhydrous bilayer *dlpcchol_s* (Sn1 SD = 19.79, Sn2 SD = 24.57). This indicates reduced flexibility in the lauryl chain region of the hydrated bilayer. This reduced flexibility also gives rise to the reduction in the number of gauche torsion angles observed. Table 9.3.6 contains the ensemble average distribution of lauryl chain torsion angles. The average number of observed gauche torsions is reduced in comparison with the anhydrous model:

dlpcchol_s	Sn1	81.25%T	1.51%g^-	4.05%g^+
	Sn2	80.94%T	5.32%g^-	7.03%g^+
wat_dlpcchol	Sn1	96.16%T	1.50%g^-	1.05%g^+
	Sn2	94.13%T	2.02%g^-	1.96%g^+

The decrease in torsional flexibility in the hydrated model gives rise to a decrease in the population of gauche torsions. This reduction in fluidity of the bilayer despite only a relatively small decrease in the surface area per head group of the lipid molecules in the hydrated bilayer (*wat_dlpcchol* 40.3Å^2, *dlpcchol_s* 41.9Å^2) illustrates the sensitivity of the cooperative interactions of the lauryl chains.

Both the standard deviations and relative distribution of gauche/trans conformations in the torsion angles of the cholesterol acyl chain (see Tables 9.3.5 and 9.3.6) indicate that most conformational flexibility lies in the torsion angles ϕ_3 and ϕ_4. In contrast to the DLPC torsion angles the cholesterol torsions increase in flexibility and exhibit an increased g^+ population.

Table 9.3.4

Euler Angles wat_dlpcchol			
	Av	SD	avSD
1	92.9	53.5	11.4
2	111.9	0.5	3.6
3	123.3	0.3	3.7

Sampled over 100-300ps. Av is the average over all angles, SD is the standard deviation of those averages, and avSD is the average standard deviation of the individual values.

9.3.5. Torsions

The defined torsion angles for both DLPC and cholesterol molecules have been calculated across the sampled trajectory and their ensemble averages and standard deviations calculated (Table 9.3.5). The average standard deviation in an acyl chain torsion angle in the hydrated bilayer *wat_dlpcchol* (Sn1 SD = 15.26, Sn2 SD = 16.73) is less than that observed in the anhydrous bilayer *dlpcchol_s* (Sn1 SD = 19.79, Sn2 SD = 24.57). This indicates reduced flexibility in the lauryl chain region of the hydrated bilayer. This reduced flexibility also gives rise to the reduction in the number of gauche torsion angles observed. Table 9.3.6 contains the ensemble average distribution of lauryl chain torsion angles. The average number of observed gauche torsions is reduced in comparison with the anhydrous model:

dlpcchol_s	Sn1	81.25%T	1.51%g^-	4.05%g^+
	Sn2	80.94%T	5.32%g^-	7.03%g^+
wat_dlpcchol	Sn1	96.16%T	1.50%g^-	1.05%g^+
	Sn2	94.13%T	2.02%g^-	1.96%g^+

The decrease in torsional flexibility in the hydrated model gives rise to a decrease in the population of gauche torsions. This reduction in fluidity of the bilayer despite only a relatively small decrease in the surface area per head group of the lipid molecules in the hydrated bilayer (*wat_dlpcchol* 40.3Å^2, *dlpcchol_s* 41.9Å^2) illustrates the sensitivity of the cooperative interactions of the lauryl chains.

Both the standard deviations and relative distribution of gauche/trans conformations in the torsion angles of the cholesterol acyl chain (see Tables 9.3.5 and 9.3.6) indicate that most conformational flexibility lies in the torsion angles ϕ_3 and ϕ_4. In contrast to the DLPC torsion angles the cholesterol torsions increase in flexibility and exhibit an increased g^+ population.

This reflects the fluidity of the DLPC torsion angles in the centre of the bilayer. The cholesterol molecule exhibits increased torsional freedom in the two unstericly hindered torsions $\phi_{3,4}$.

Table 9.3.7 shows the ensemble average distribution of gauche/trans conformations in the lauryl chains of the DLPC molecules in the bilayer. This illustrates the effect of the cholesterol and hydration of the head group on the lauryl chains dynamics. The hydration or change in head group surface area on hydration has a dramatic effect on the distribution of lauryl chain torsion angles. There is a large decrease in the total population of the gauche torsions and a shift from g^+ to g^- conformations.

Table 9.3.5

Torsion Standard Deviations wat_dlpcchol					
	SD	AvSD		SD	AvSD
DLPC					
ϕ_1	32.2	21.8	ϕ_2	78.8	49.3
ϕ_3	34.6	4.9	ϕ_4	141.5	95.6
ϕ_5	42.5	27.4	ϕ_6	33.7	9.8
ϕ_7	25.9	27.1	ϕ_8	13.4	6.1
ϕ_9	33.3	9.5	ϕ_{10}	13.9	1.5
ϕ_{11}	45.7	13.4	ϕ_{12}	18.2	11.2
ϕ_{13}	11.9	2.5	ϕ_{14}	11.6	1.6
ϕ_{15}	10.4	0.4	ϕ_{16}	10.4	0.2
ϕ_{17}	10.5	0.4	ϕ_{18}	13.7	5.8
ϕ_{19}	22.0	10.8	ϕ_{20}	28.6	17.2
ϕ_{21}	21.3	3.2	ϕ_{22}	12.9	1.3
ϕ_{23}	33.2	10.8	ϕ_{24}	30.3	30.1
ϕ_{25}	11.7	2.3	ϕ_{26}	10.5	1.2
ϕ_{27}	10.2	0.5	ϕ_{28}	10.0	0.4
ϕ_{29}	10.8	0.7	ϕ_{30}	13.9	6.5
ϕ_{31}	18.2	8.9	ϕ_{32}	35.0	20.3
CHOL					
ϕ_1	7.7	0.7	ϕ_2	17.1	4.3
ϕ_3	28.2	16.7	ϕ_4	28.7	18.4
ϕ_5	36.5	12.1			

Sampled over 100-300ps.

9.3.6. Segmental Order Parameters

The lack of formation of gauche torsion angles in the lauryl chains of the DLPC molecules increases their order relative to the more fluid *dlpcchol_s* results (Sn1 0.95±0.02, Sn2 0.84±0.03). This is the expected change in the order parameters on a decrease in fluidity of the system. The observed values of the Euler angles indicate that there is more orientational stability of the system, suggesting that re-orientation of the DLPC molecules does not

Table 9.3.6

%Trans/Gauche Conformations wat_dlpcchol							
	%t	%g^-	%g^+		%t	%g^-	%g^+
DLPC							
ϕ_1	41.50	21.08	36.03	ϕ_2	63.38	14.98	11.40
ϕ_3	64.88	1.35	1.28	ϕ_4	30.50	25.32	21.99
ϕ_5	5.12	53.08	20.88	ϕ_6	43.50	3.80	1.65
ϕ_7	4.62	68.97	22.94	ϕ_8	96.75	0.00	0.88
ϕ_9	69.00	2.91	2.39	ϕ_{10}	94.38	0.00	0.00
ϕ_{11}	12.75	14.61	31.17	ϕ_{12}	93.62	3.49	0.04
ϕ_{13}	98.38	0.01	0.19	ϕ_{14}	98.62	0.04	0.17
ϕ_{15}	99.00	0.00	0.00	ϕ_{16}	98.88	0.00	0.00
ϕ_{17}	98.75	0.00	0.00	ϕ_{18}	97.38	0.00	0.87
ϕ_{19}	93.25	1.08	2.96	ϕ_{20}	85.00	7.37	4.18
ϕ_{21}	24.12	2.76	2.37	ϕ_{22}	94.25	0.00	0.00
ϕ_{23}	6.12	26.26	14.60	ϕ_{24}	82.38	6.29	8.43
ϕ_{25}	98.25	0.11	0.03	ϕ_{26}	98.62	0.00	0.02
ϕ_{27}	98.88	0.00	0.00	ϕ_{28}	99.00	0.00	0.00
ϕ_{29}	98.38	0.00	0.00	ϕ_{30}	97.38	0.18	0.84
ϕ_{31}	95.38	0.68	1.77	ϕ_{32}	78.88	10.96	6.53
CHOL							
ϕ_1	0.00	0.00	99.80	ϕ_2	76.00	0.63	0.00
ϕ_3	82.75	0.77	12.60	ϕ_4	75.75	0.44	20.16
ϕ_5	36.38	0.00	58.46				

Sampled over 100-300ps and averaged for all 8 DLPC and 8 Cholesterol molecules. %t is the percentage trans (180±30°), %g^- is the percentage negative gauche (-60±30°) and %g^+ is the percentage positive gauche (+60±30°).

affect their order parameter values. The order parameter profile for the two acyl chains are equivalent, except for the characteristic turn at C2 of the Sn2 chain. There is evidence of the order parameter plateau from segments 3-8 in the lauryl chains. The cholesterol acyl chain exhibits higher absolute values for the upper segments, although the more fluid lower segments give order parameters in the same order as the *dlpcchol_s* simulation. The general

Table 9.3.7

Acyl Chain %Trans/Gauche Conformations wat_dlpcchol			
DLPC			
Mol	%t	$\%g^-$	$\%g^+$
1	92.61	2.90	2.62
2	98.06	0.04	0.36
3	93.67	2.88	1.31
4	91.89	4.65	0.80
5	95.89	1.72	0.84
6	97.17	0.05	1.27
7	92.67	0.73	4.36
8	98.06	0.46	0.00

Sampled from ϕ_{12}-ϕ_{20} and ϕ_{24}-ϕ_{32} from 80-300ps.

form of the order parameter profile shows similarity to that observed in the expanded pure DLPC simulation (*dlpc_y1*).

9.3.7. Thermal Partitioning

From the results of previous simulations of muti-component systems, it is expected that the partitioning of thermal energy in the system will not be uniform. Table 9.3.8 and Figure 9.2.4a contain the ensemble average temperatures of the different components of the system (Cholesterol, PC, Glycerol, Lauryl chains, and water). Clearly the system has not reached thermal equilibrium. The waters are on average more than 200K higher in temperature than the bilayer.

Figures 9.3.4b and 9.3.4c illustrate the temperatures of the subcomponents of the system with time from the starting configuration across the trajectory. The aqueous layer is on average at a higher temperature than either the lipid or cholesterol. The partitioning of thermal energy into the DLPC molecule is also not homogeneous: the PC group is on average at a higher temperature than either the glycerol or lauryl chains, which are well below their gel-to-liquid-crystalline transition temperature. This temperature differential is maintained across the trajectory and shows no indication of moving towards equilibrium. This suggests that there is little coupling between the aqueous and lipid phases in the system, even through collisions of

Figure 9.3.3

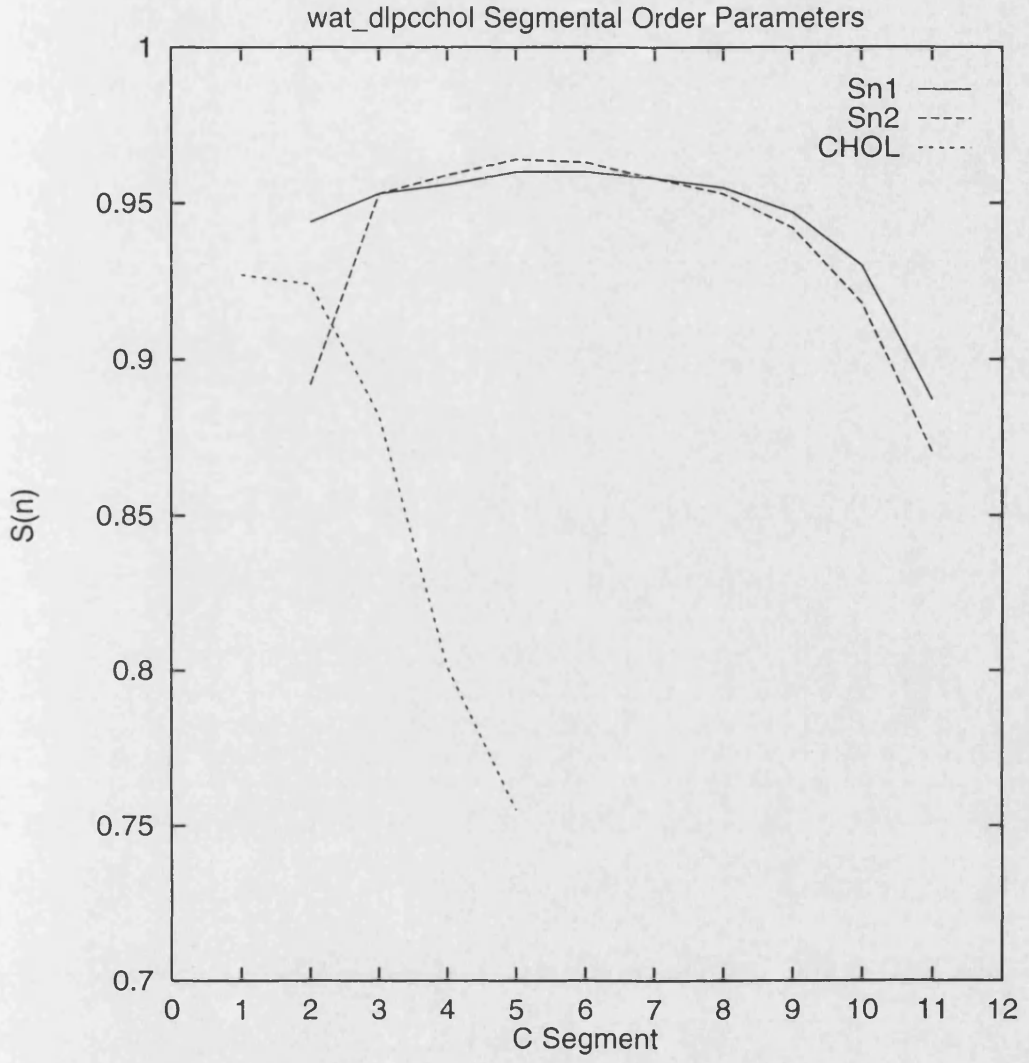

Sampled over 100-300ps.

waters and lipid. This maybe a consequence of the hydrating waters buffering the thermal exchange between the lipid and aqueous phases and preventing efficient transfer of kinetic energy between the two subsystems.

Figure 9.3.5 shows the ensemble average methylene temperature calculated from their atomic velocities and averaged across the sampled trajectory. These can be used to examine the effect of the thermal gradient in the lauryl chains on the calculated order parameter profile. Segments in close contact to the glycerol backbone are on average of higher temperature than the central carbon segments and exhibit lower relative order parameters. The terminal

segments also exhibit lower order parameters and (as expected) on average are at a higher temperature than the central carbon segments which form the order parameter plateau. Segments 2 and 3 are on average of higher temperature than the terminal carbon segments, but exhibit higher relative order (with the exception of the segment 2 of the Sn2 chain). The temperature gradient can therefore not be the only effect on the order, and some orientational component must be operating through reorientation of the DLPC molecules relative to the bilayer normal. The temperature of the terminal segment is at a higher temperature relative to the rest of the chain, the order parameters are not given. This is due to the methylene rotor effect giving low order parameters due to rotational averaging of the hydrogen positions relative to the bilayer normal.

Table 9.3.8

Average Temperature (K) wat_dlpcchol		
	Av	SD
PC	344.3	20.7
GL	287.2	24.9
Sn1	214.7	16.0
Sn2	216.3	15.1
LIP	256.0	9.5
CHL	204.8	11.3
WTR	461.3	15.1

Sampled over 100-300ps.

9.3.8. Radial Distribution Functions

The pairwise radial distribution functions for water oxygen atoms around hydrogen bond acceptor atoms in the system has been calculated. These include

1. The carbonyl oxygens and esterified oxygens of the glycerol and lauryl chains
2. The phosphate oxygens of the DLPC molecules
3. The total pairwise radial distribution for water oxygens
4. The cholesterol hydroxyl oxygen
5. The total pairwise radial distribution function for all O,N and P atoms in the system.

See Figure 9.3.6.

Table 9.3.9

Average Methylene Temperature (K) wat_dlpcchol					
Sn1			Sn2		
C Segment	Av	SD	C Segment	Av	SD
2	219.6	38.3	2	221.1	39.2
3	212.8	37.1	3	214.6	36.0
4	209.0	36.3	4	213.2	37.0
5	207.7	36.2	5	210.4	36.4
6	206.7	35.9	6	208.3	36.2
7	204.8	35.4	7	206.7	35.8
8	205.0	35.3	8	206.8	35.3
9	204.7	35.2	9	203.7	35.4
10	207.2	35.7	10	203.3	35.4
11	209.7	36.2	11	206.6	35.9
12	217.7	33.7	12	214.2	32.8

Sampled over 100-300ps.

Comparing the radial distribution function for water oxygens relative to the glycerol oxygens from the *wat_dlpc_2* and *wat_dlpcchol* simulations, the presence of the cholesterol appears to have no effect on the radial distribution of waters around the glycerol region, even allowing for the increased free volume around the head groups. This indicates that the polarisation of water molecules around the glycerol oxygens has reached saturation for the given degree of penetration. There is a peak at 2.9Å corresponding to the first hydration shell of the carbonyl oxygens and a broad peak centred on 5.0Å indicating longer range ordering. The peaks are of both the same height and positions as the average peaks for the *wat_dlpc_y1* results.

Comparing the radial distribution function for water oxygens relative to phosphate oxygens in *wat_dlpc_y2* and *wat_dlpcchol*, the first peak is identical in both distributions in terms of both height and position, indicating strong polarisation of the first water hydration shell in both simulations. The second peak appears to be two overlapping peaks in close proximity giving rise to the one broad peak. This is also indicated by the lack of symmetry in the *wat_dlpc_y2* distribution. This can be assigned to the presence of the two esterified oxygens of the phosphate group with lower partial charge (-0.48 compared with -0.75) and therefore

Figure 9.3.4a

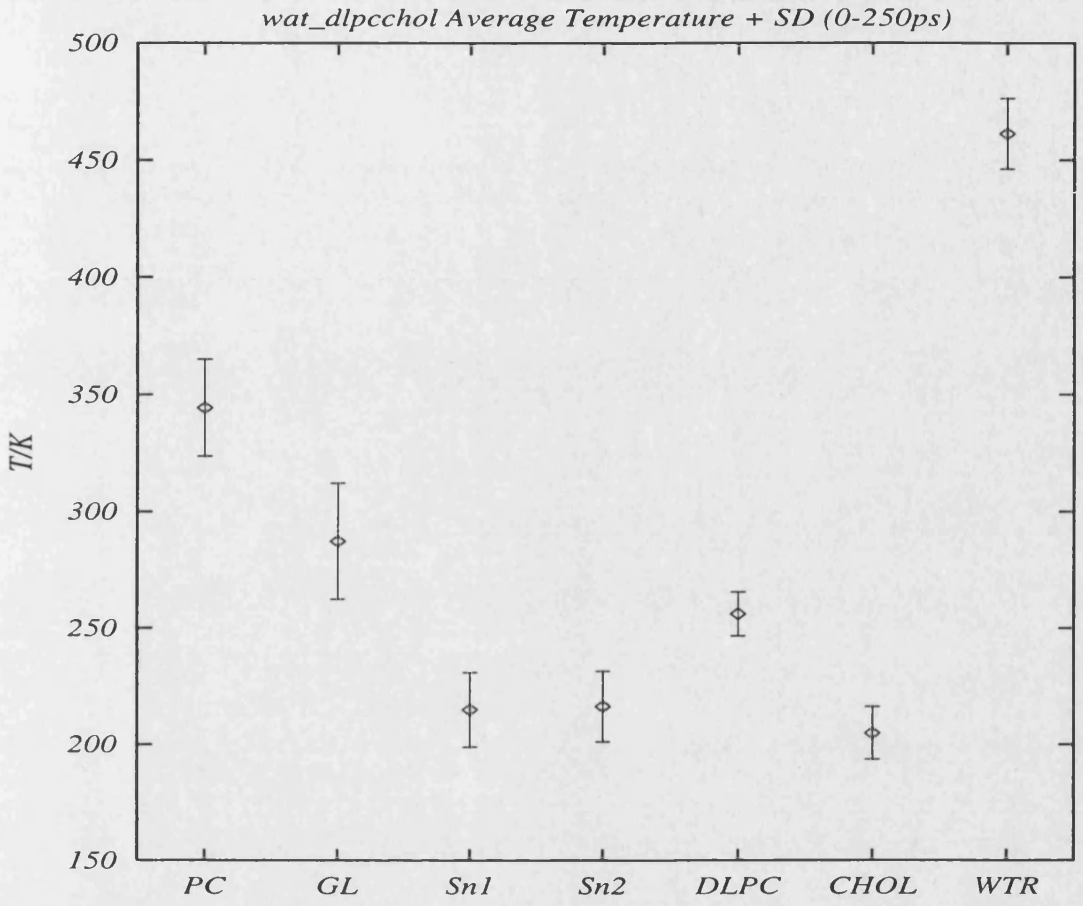

Sampled over 100-300ps.

weaker ordering effect on the second hydration shell. This gives rise to the two broad peaks observed. The first peak is however sharp as steric constraints around the esterified oxygens prevent waters for hydrogen bonding significantly to these atoms and the first hydration shell is negligible compared with the dominant peak from the unesterified oxygens. The distribution in the cholesterol doped simulation appears to normalise to a constant value indicating less long range ordering of the water atoms. This is a direct result of the lower density of phosphate groups at the bilayer surface. This is due to the reduced magnitude of electrostatic field associated with the head group region.

The pairwised radial distribution function for water oxygens in the system contains a peak at 2.7Å, which arises from the first hydration shell of the water structure and a broad peak at 5.4Å the second hydration shell. The bulk density is clearly below that of liquid water,

Figure 9.3.4b&c

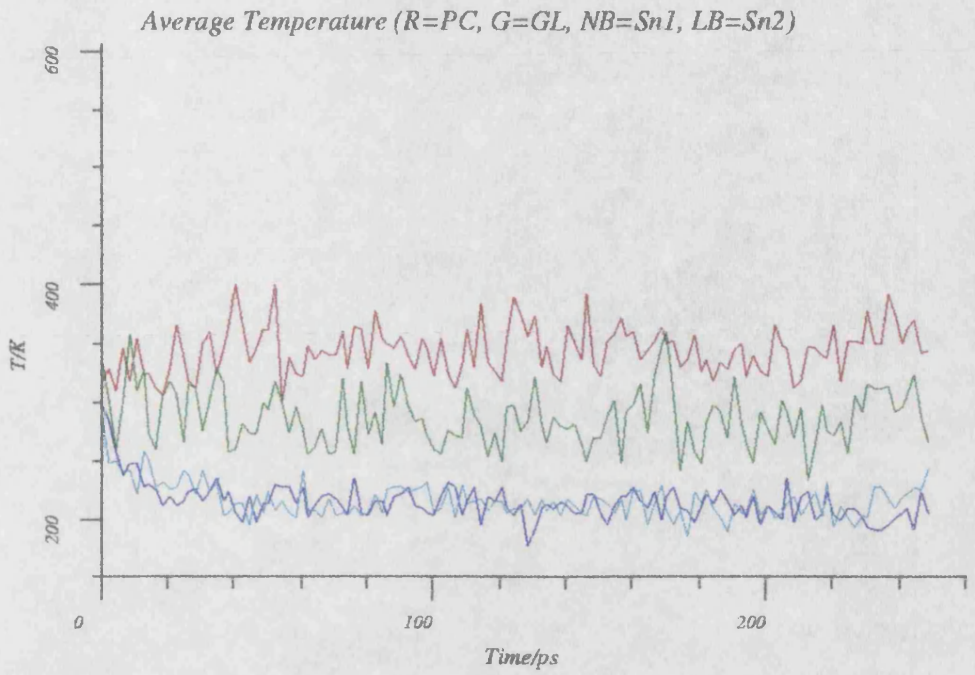

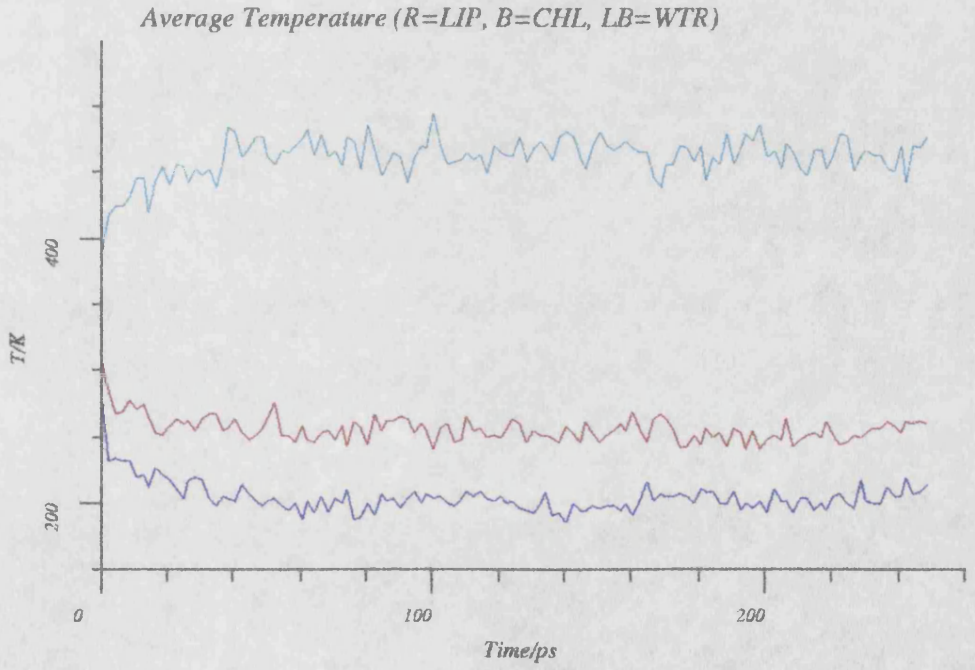

normalising to only 0.72 instead of 1.0.

The radial distribution function for water oxygens around the cholesterol oxygen exhibits a peak at 2.6Å, similar in position to the first hydration shell of the phosphate group. This suggests strong hydrogen bonding between the water and cholesterol hydroxy group. There is no

Figure 9.3.5

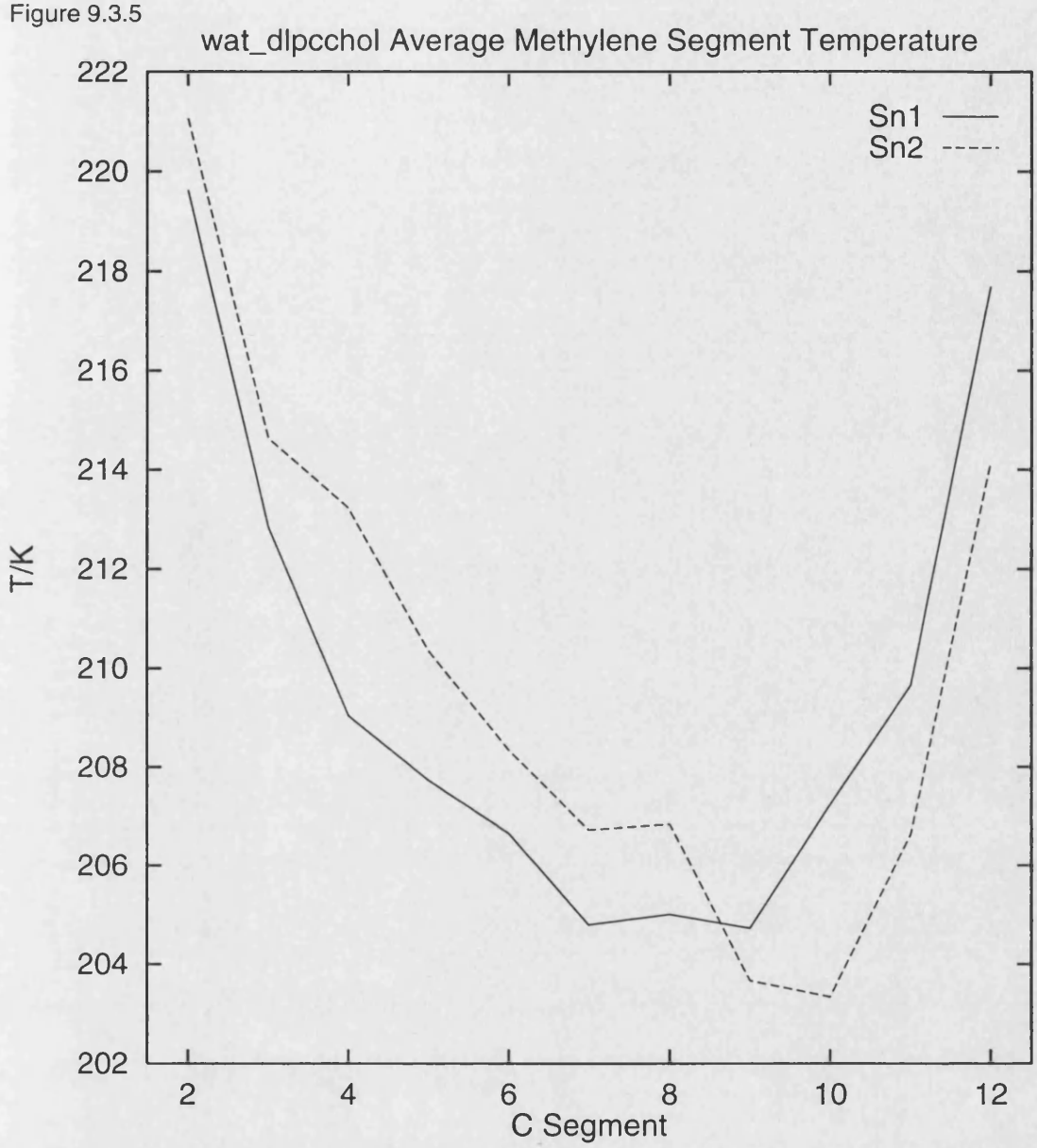

indication from the radial distribution whether this is a hydrogen bond from the water hydrogen to the cholesterol oxygen or from the cholesterol hydroxyl group hydrogen to the water oxygen. The charge on the cholesterol oxygen is only -0.38 in comparison with the water oxygen charge of -0.82, which suggests that hydrogen bonding between the cholesterol hydrogen and water oxygen would be more energetically favoured.

The total pairwise radial distribution of all O, N and P atoms in the lipid phase can be used to elucidate any long range ordering of the lipid molecules. The first peak at 1.4Å is the oxygen-phosphorus separation in the phosphate group and the second peak at 2.4Å can be assigned to the non-bonded distance between phosphate oxygen atoms. The broad peak at

approximately 4.7Å can be assigned to the average separation between the glycerol oxygens, choline nitrogen and phosphate groups. There is however no evidence of significant long range ordering resulting from any regular packing arrangement, which is not surprising given the relatively small size of this system.

9.3.9. Hydrogen Bonding

A distance search was used to assign hydrogen bonds between the cholesterol hydroxyl hydrogen and the DLPC hydrogen bond acceptors, and the water hydrogens and the DLPC hydrogen bond acceptors. In addition a search was performed for hydrogen bonds between the cholesterol acceptor and donor atoms, and water acceptor and donor atoms. Figures 9.3.7a and 9.3.7b show graphically the results of this search.

Figure 9.3.7a shows the hydrogen bonds founds between the water hydrogens and various hydrogen bond acceptor atoms in the bilayer. Examination of the distribution of hydrogen bonds made with the phosphate oxygens reflects the same distribution found in the *wat_dlpc_y1* simulation results. The esterified oxygens only form on average less than 0.3 hydrogens bonds, whilst the nonesterified oxygens form on average approximately 2.0 hydrogen bonds with water hydrogens. This provides validation for the sharpness of the first peak of the radial distribution function for waters around the phosphate oxygens. The standard deviation of the number of hydrogen bonds formed is however greater than the average, indicating the presence of transient and exchanging hydrogen bonds.

There is little evidence for significant hydrogen bonding between the water hydrogens and the glycerol esterified oxygens which form on average less than 0.1 hydrogen bonds each. The carbonyl oxygens of the lauryl chains however form on average approximately 0.4 hydrogen bonds each up to a maximum of 4.0. This is steric in nature, the carbonyl oxygens being more accessible than the esterified oxygens to water molecules. The standard deviation of approximately 0.5 indicates that this hydrogen bonding is transient in nature being broken and reformed many times, as is the nature of hydrogen bonding between solvent and solute.

There are only on average less than 0.3 hydrogen bonds formed between the cholesterol hydroxyl oxygen and the water hydrogens, although some cholesterols never form hydrogen bonds of this nature across the sampled trajectory. Clearly this interaction is not energetically favoured. In addition the cholesterol hydroxy group is thought to be located in the region of the glycerol backbone. Hence the lack of water penetration precludes significant hydrogen

Figure 9.3.6

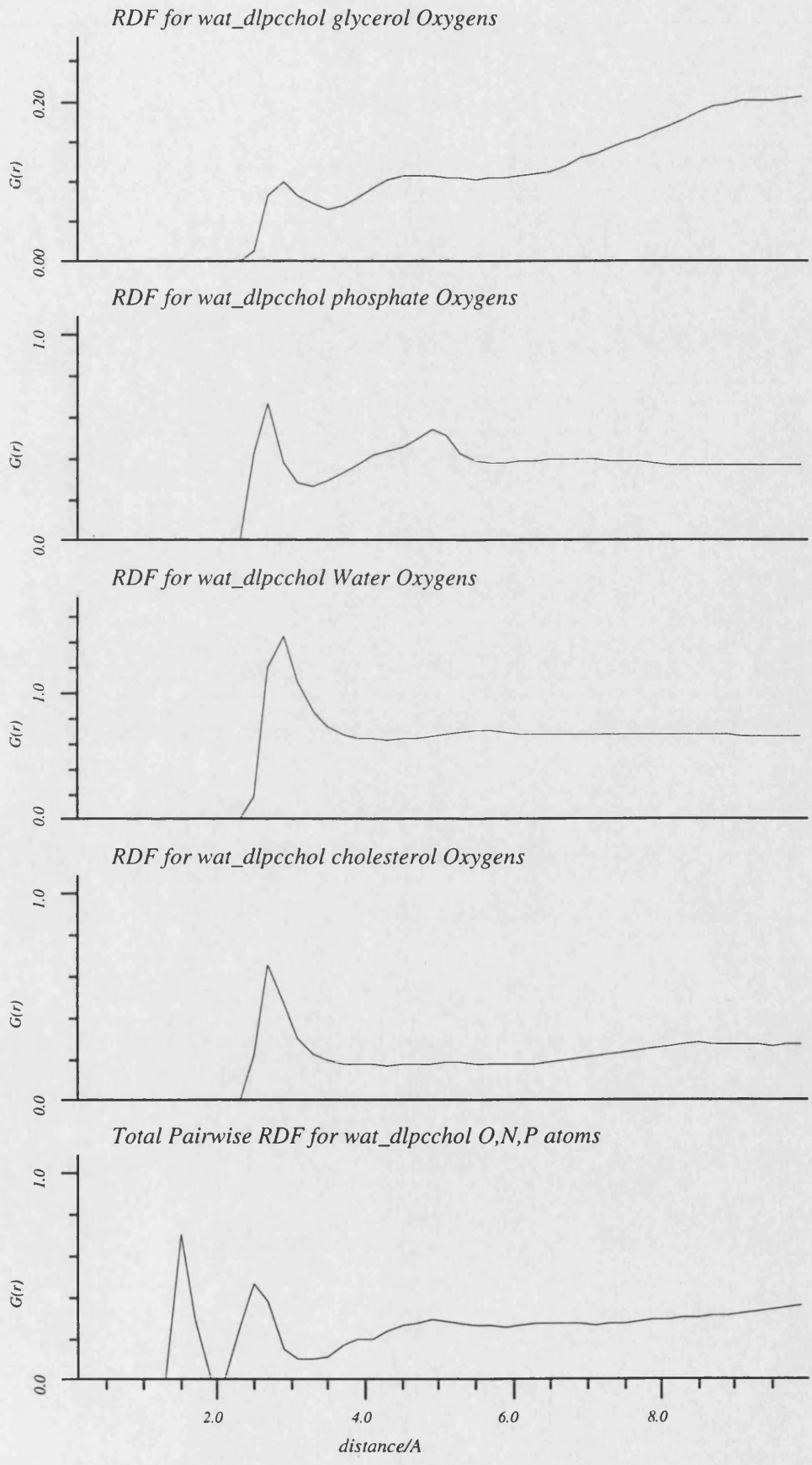
RDF for wat_dlpcchol glycerol Oxygens
G(r)
0.00
0.20
RDF for wat_dlpcchol phosphate Oxygens
G(r)
0.0
1.0
RDF for wat_dlpcchol Water Oxygens
G(r)
0.0
1.0
RDF for wat_dlpcchol cholesterol Oxygens
G(r)
0.0
1.0
Total Pairwise RDF for wat_dlpcchol O,N,P atoms
G(r)
0.0
1.0
2.0
4.0
6.0
8.0
distance/A

bonding with the water hydrogens.

Figure 9.3.7b shows the hydrogen bonds found between the cholesterol hydroxy hydrogens and hydrogen bond acceptor atoms in the DLPC molecule and water. Examination of the hydrogen bond distribution for the phosphate oxygen acceptor atoms indicates there is no significant hydrogen bonding between the esterified oxygens of the phosphate and the cholesterol hydrogens. There is however one DLPC molecule which on average forms one hydrogen bond between the phosphate nonesterified oxygen and the cholesterol hydroxy hydrogen. This suggests that one cholesterol molecule has moved along the bilayer normal into the upper region of the glycerol backbone to form this hydrogen bond with the phosphate oxygen, or that the DLPC molecule has adopted a head group conformation such that the phosphate oxygen is within hydrogen bonding distance of the cholesterol hydrogen. A combination of these two reasons is more realistic and even close examination of the trajectory on a graphics system failed to identify any such interaction.

No hydrogen bonding was observed between the esterified oxygens of the glycerol backbone and the cholesterol hydrogens. Only transient hydrogen bonds were observed between the cholesterol hydrogen and the carbonyl oxygens. This suggests that the cholesterol hydroxy group was in fact located nearer to the phosphate group in the bilayer normal direction, explaining the increased interaction.

Examination of the hydrogen bond distribution for water oxygen acceptor atoms and cholesterol hydroxy hydrogen donor atoms illustrates that on average there is significant hydrogen bonding. This does however vary between molecules in the system from 0.8 to less than 0.1 hydrogen bonds, suggesting a dependency on the local environment of the cholesterol molecule. There is however on average more hydrogen bonding than between the water donor and cholesterol acceptor atoms, supporting the previous hypothesis that this hydrogen bond pair is energetically favoured on electrostatic grounds.

9.3.10. Electrostatic Potential

The electrostatic potential for an ion of single positive charge travelling across the membrane barrier from one side to the other is represented in Figure 9.3.8. This is a measure of the degree of motional polarisation of the waters at the interface. Waters in equilibrium with the bulk have no contribution to the electrostatic potential of the membrane. This also allows one to measure the membrane potential and to identify the membrane boundary from the

Figure 9.3.7a

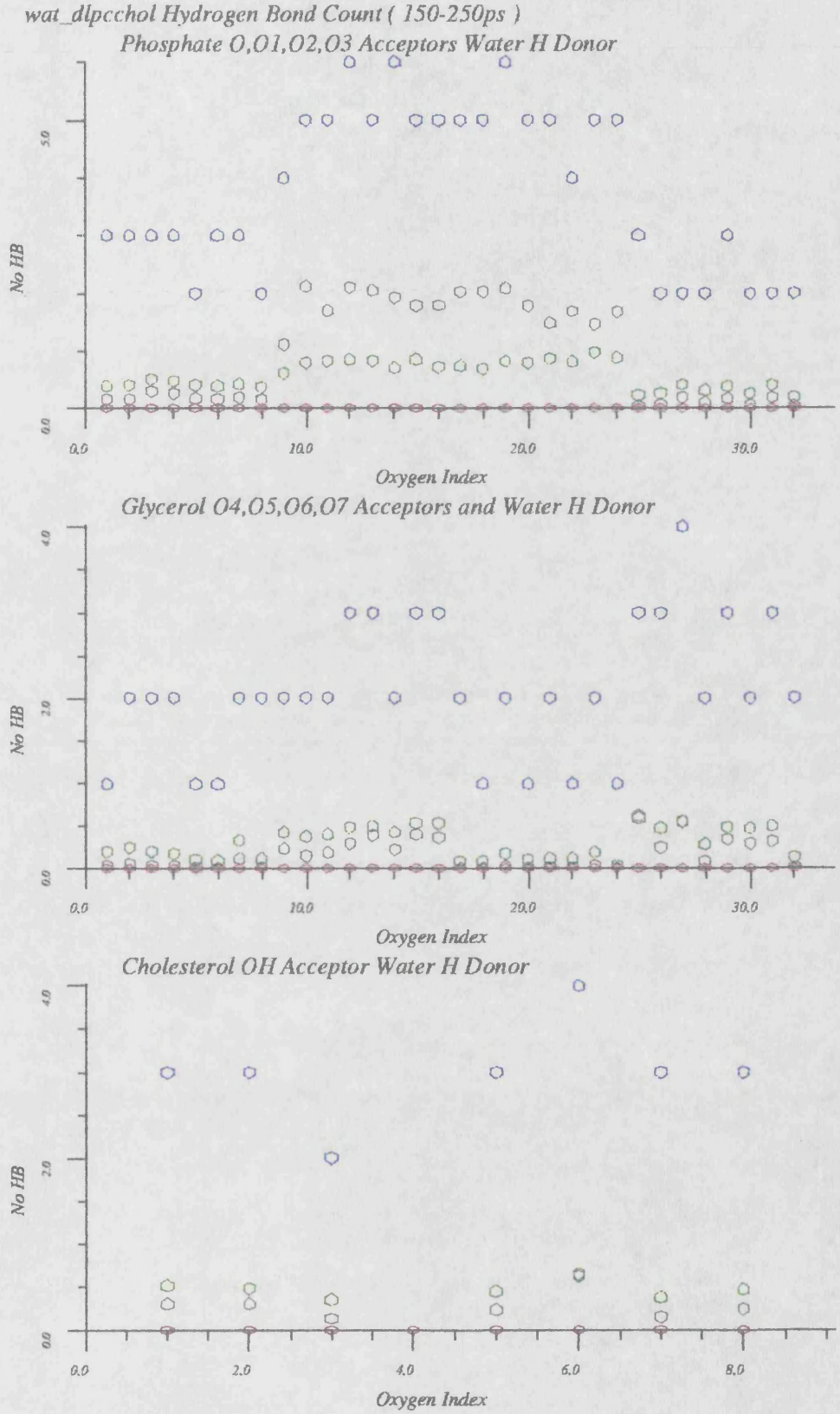
wat_dlpcchol Hydrogen Bond Count (150-250ps)
Phosphate O,O1,O2,O3 Acceptors Water H Donor
No HB
0.0
5.0
0.0
10.0
20.0
30.0
Oxygen Index
Glycerol O4,O5,O6,O7 Acceptors and Water H Donor
No HB
0.0
4.0
2.0
0.0
10.0
20.0
30.0
Oxygen Index
Cholesterol OH Acceptor Water H Donor
No HB
0.0
4.0
2.0
0.0
2.0
4.0
6.0
8.0
Oxygen Index

Figure 9.3.7b

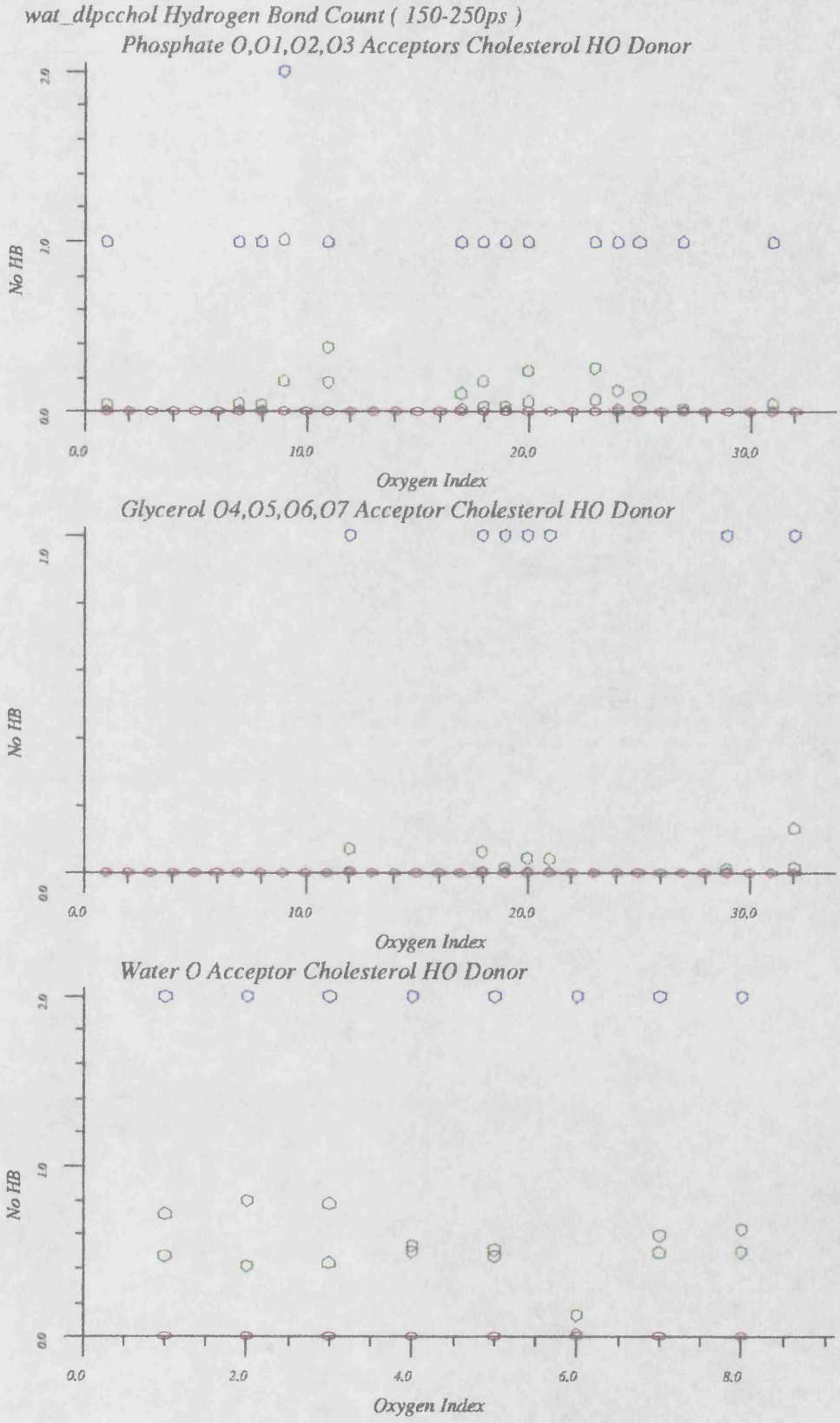
wat_dlpcchol Hydrogen Bond Count (150-250ps)
Phosphate O,O1,O2,O3 Acceptors Cholesterol HO Donor
No HB
0.0
1.0
2.0
0.0
10.0
20.0
30.0
Oxygen Index
Glycerol O4,O5,O6,O7 Acceptor Cholesterol HO Donor
No HB
0.0
1.0
0.0
10.0
20.0
30.0
Oxygen Index
Water O Acceptor Cholesterol HO Donor
No HB
0.0
1.0
2.0
0.0
2.0
4.0
6.0
8.0
Oxygen Index

motional polarisation of the hydrating waters.[2-4]

Examination of the calculated electrostatic potential in Figure 9.3.8 elucidates the boundary between bulk and hydrating waters to be at approximately 31Å from the centre of the unit cell in the bilayer normal direction. This interface is not well defined and suggests that there is a reduced polarisation of the water in proximity to the surface of the cholesterol doped bilayer. Given the increased surface area of the DLPC molecules separated by cholesterol molecules this is not unexpected. The boundary between the hydrating waters and dlpcchol bilayer is well defined, being at 19Å from the centre of the unit cell bilayer normal axis. The effect of the bilayer surface extends over 12Å from the bilayer water interface, giving rise to little evidence of bulk water. The net electrostatic potential ($\Delta\Phi$) is the difference in electrostatic potential between the bilayer (18Å) and centre of the liquid water (31Å) 0.22V. This agrees well with experimental results from similar bilayer systems[5-7] both in terms of the sign and magnitude of $\Delta\Phi$. This is smaller than the corresponding value for the *dlpc_wat* model.

Figure 9.3.8

wat_dlpcchol Electrostatic Potential 150-250ps

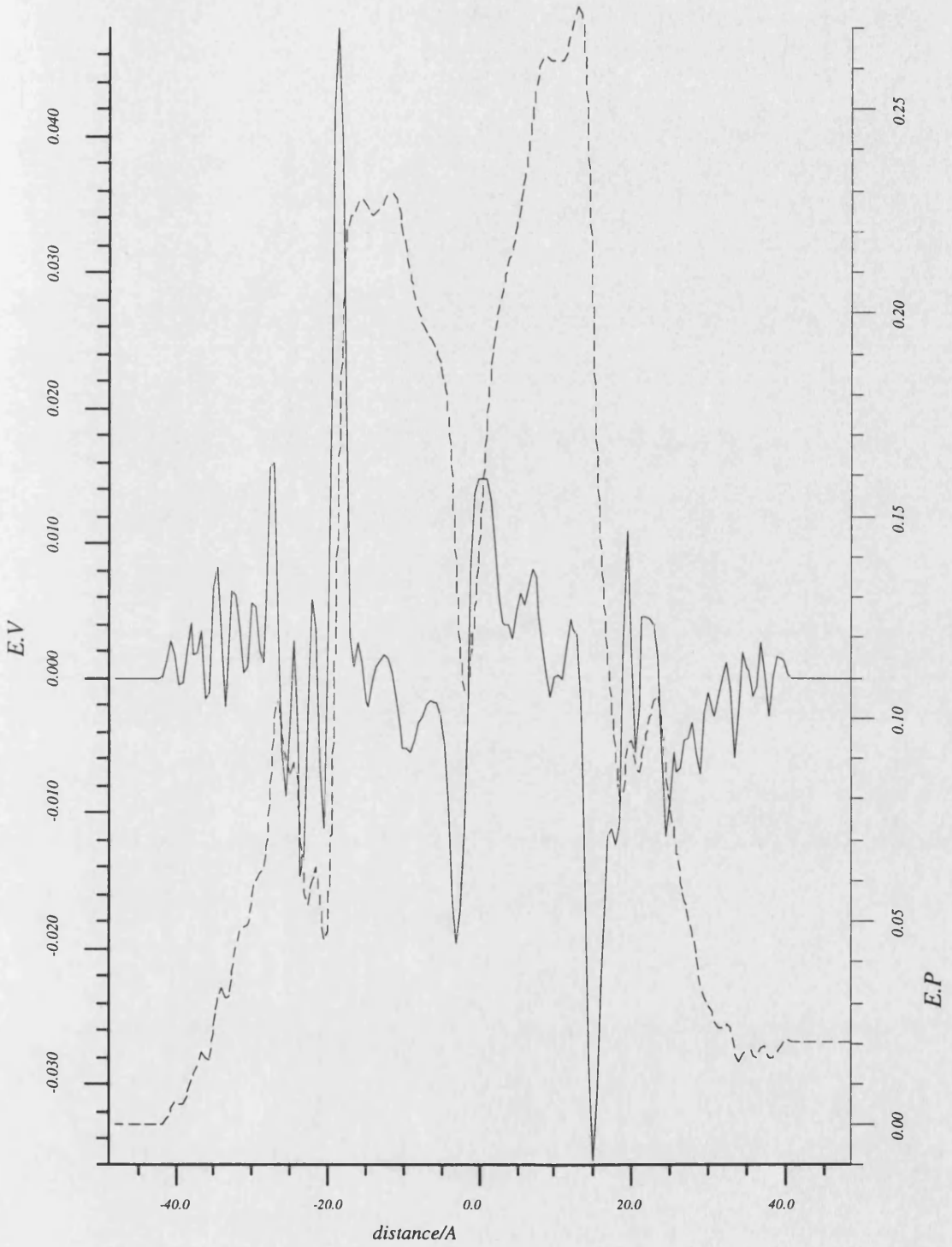

References

1. Scherer JR, *Biophysical J*, vol. 55, pp. 957-964, 1989.

2. Wilson MA, Pohorille A, and Pratt LR, *J Phys Chem*, vol. 91, no. 19, pp. 4873-4878, 1987.

3. Wilson MA, Pohorille A, and Pratt LR, *J Chem Phys*, vol. 88, no. 5, pp. 3281-3285, 1988.

4. Wilson MA and Pohorille A, *J of the American Chemical Society*, vol. 116, no. 4, pp. 1490-1501, 1994.

5. Smaby JM and Brockman HL, *Biophys J*, vol. 58, pp. 195-204, 1990.

6. Flewelling R and Hubbell W, *Biophysical J*, vol. 49, p. 477, 1986.

7. Latorre R and Hall HE, *Nature*, vol. 264, p. 361, 1976.

10. Discussion and Conclusions

The results from chapters 6-9 show the way forward towards improving the quality of bilayer simulations and equilibration. A number of problems have been highlighted and require addressing in order to improve the quality of the simulation results in terms of reproducing the experimental measurements. These include

1. The temperature differential between the hydrophilic and hydrophobic regions of the system. In particular the temperature difference between the water and lipid phases of the system.
2. The lack of fluidity of the acyl chain torsions of the lipid molecules.
3. The volume change of the system and the control of the area per head group under the pressure scaling algorithm.
4. The inhomogenity of the system. During the trajectory areas of high and low density are formed in the system altering the local dynamics of molecules in these locations.

It is the effect of these non-physical characteristics of the lipid bilayer and solvent system that have to be addressed in the methodology of the problem.

Solutions to these problems can be achieved by changing the methodology of the theoretical approach in the following areas:

1. Changing the method of calculating electrostatic interactions. The application of the Ewald sum method of calculating electrostatic interactions within a periodic system should improve the propagation of the long range electrostatic forces in the system.[1]
2. The size of the system must be increased in order to observe some of the longer wavelength interactions observed in real systems such as fluidisation of the hydrocarbon region.
3. The pressure scaling algorithm does not appear to work well for this size of system, sampling from the NVT / NVE ensembles is therefore more reliable.
4. A larger system should allow for the microdensity changes with out dominating the dynamics of the system as a whole.

10.1. Density and Torsional Flexibility

From examination of the torsional flexibility of the lauryl chains of the various lipid molecules, it is clear that the torsional flexibility and trans gauche transitions are not purely controlled by the torsion potential, although this is fundamental. Simulations run at the same

temperature and starting conformation of DLPC molecules give rise to results which may or may not exhibit fluidity (trans-gauche isomerism). Expanding the coordinates gives rise to an increase in fluidity and the presence of a gauche population. This indicates a density controlled mechanism for torsional transitions. This can be rationalised in terms of the extremes of density.

At high density, molecules in the system are packed to their limiting van der Waals radius and are consequently trapped in their local minima, torsional transitions being unfavourable on steric grounds. At extremely low density the molecules do not significantly interact with one another, acting more like kinetic gases. Their energy is distributed amongst the molecule's normal modes of motion. There is not sufficient energy in the torsions to escape the local minima and additional energy from collisions with neighbouring molecules is unavailable. At intermediate densities there will be a balance between the two effects. Hence the frequency of torsional transitions of a molecule and its flexibility are dependent upon its frequency of collision with neighbouring molecules leading to transfer of energy into modes of motion which lead to activation of the torsional transition.

Figure 10.1.1 and table 10.1.1 contain the equilibrium density of the bilayer models in this study. There are a number of models which are of considerably different densities. These include dmpc, dmpc_i and dlpc_wat which do not show a significant gauche population and exhibit reduced torsional flexibility. Figure 10.1.2 illustrates the average torsional flexibility from the lauryl chain torsion angles plotted against the average density of the bilayer systems. The bilayer models exhibit increased torsional flexibility between the densities 0.88-0.94g/ml outside of which the lauryl chain torsion angles exhibit a lower average standard deviation of approximately 5°. There is clearly a narrow band of density in which torsional flexibility is increased and significant gauche population is observed.

Figure 10.1.1

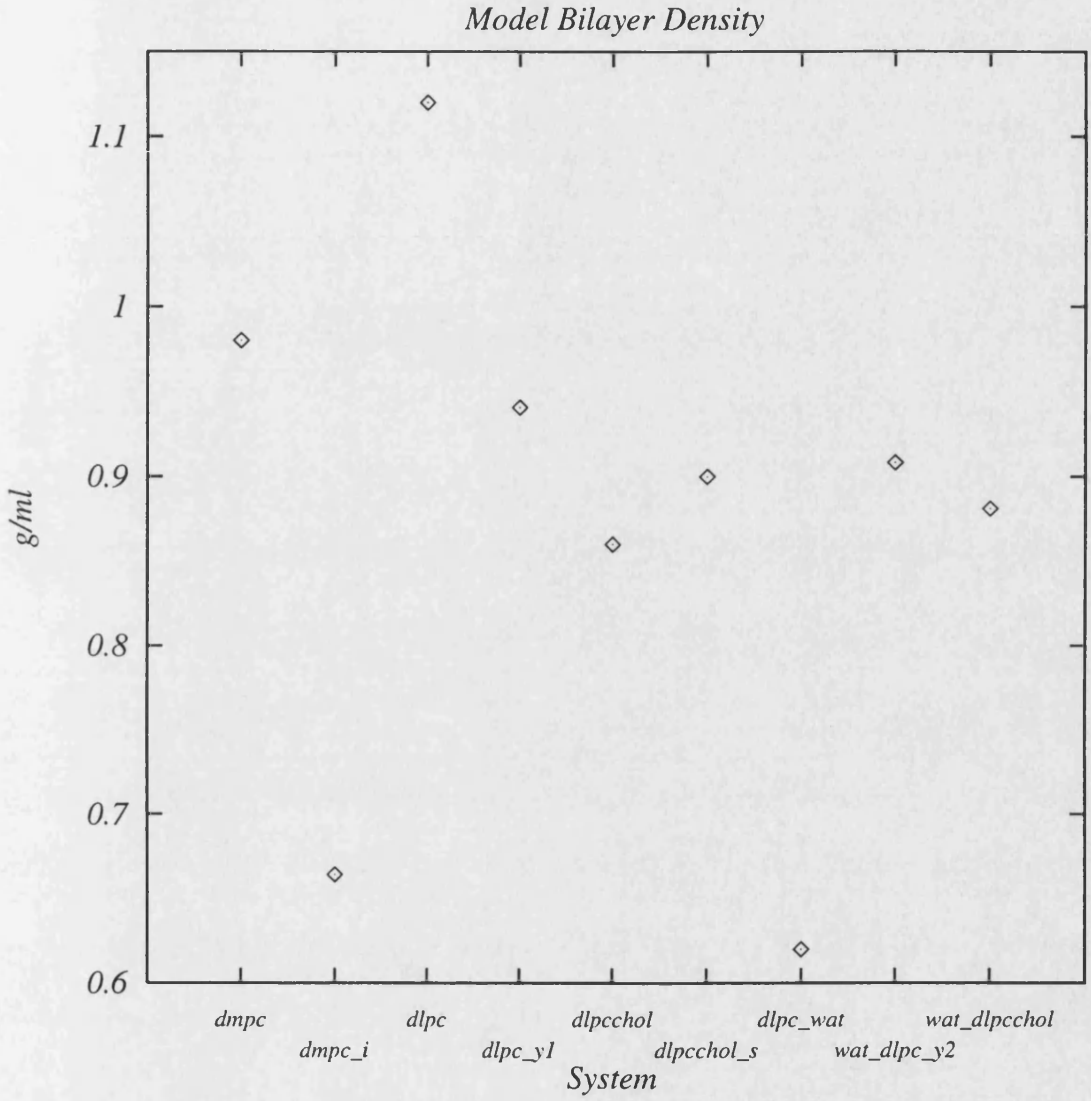
Model Bilayer Density
1.1
1
0.9
0.8
0.7
0.6
g/ml
dmpc
dmpc_i
dlpc
dlpc_y1
dlpcchol
dlpcchol_s
dlpc_wat
wat_dlpc_y2
wat_dlpcchol
System

Figure 10.1.2

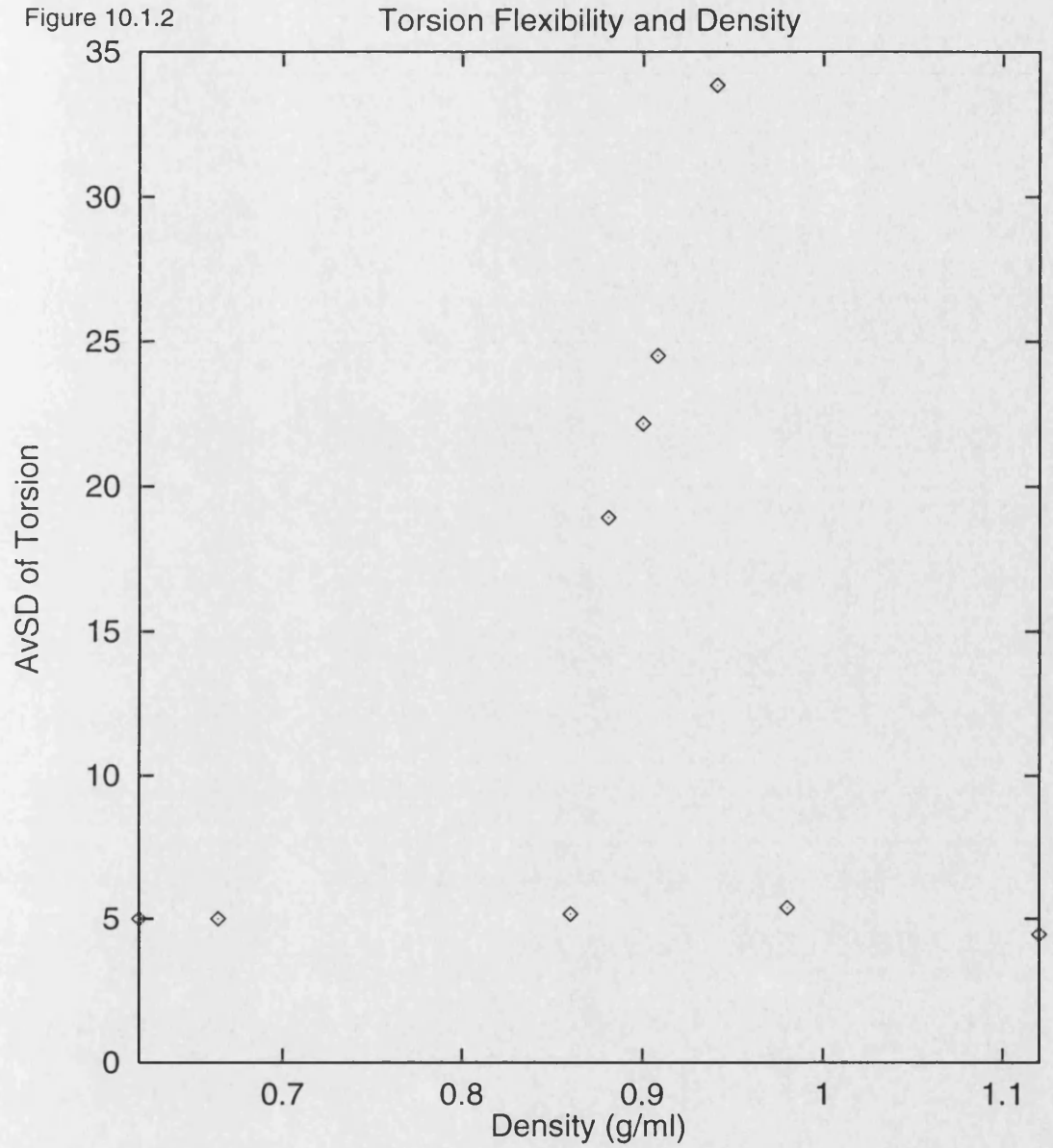
Torsion Flexibility and Density
AvSD of Torsion
Density (g/ml)
35
30
25
20
15
10
5
0
0.7
0.8
0.9
1
1.1

Table 10.1.1

Torsion SD and Density		
System	ρ(g/ml)	AvSD ϕ_c
dmpc	0.980	5.389
dmpc_i	0.664	5.0E
dlpc	1.120	4.456
dlpc_y1	0.941	33.85
dlpcchol	0.860	5.17
dlpcchol_s	0.900	22.17
dlpc_wat	0.620	5.0E
wat_dlpc_y2	0.908	24.51
wat_dlpcchol	0.881	18.92

ρ is the density calculated from the equilibrium cell volume and AvSD ϕ_c is the Average standard deviation of all lipid acyl chain torsions (not including cholesterol).

10.1.1. Decane simulations

In an attempt to probe further the relationship between density, torsional flexibility and gauche population a series of decane simulations were performed. These were simple 3x3 monolayers of decane molecules arranged in a hexagonal lattice. The density of the system was changed by varying the lattice spacing. Various density systems have been simulated which range across that of the bilayer simulation models. NVT ensemble trajectories were sampled for 100ps using a temperature constraint of 320K.

The final 50ps of the trajectory was used to sample the torsion angle trajectory from all 9 molecules in the unit cell. The central 7 torsion angles were sampled and the distribution of trans and gauche(±) torsions calculated. Tables 10.1.2(a-d) contain the extracted average distribution of torsion values for each molecule. These are the average distribution for all 7 torsion angles in each molecule. Tables 10.1.3(a-d) contain the average distribution for each torsion averaged over all molecules in the system.

In the high density (1.065g/ml) trajectory the decane molecule is on average in the all trans conformation, only 3 molecules at the edge of the unit cell exhibiting any torsional flexibility. This can be assigned to increased free volume at the edge of the unit cell. In the

0.772g/ml trajectory there is increased torsional flexibility although on average the molecules are in the all trans state. However at a density of less than 0.7 g/ml there is a marked increase in both the torsional flexibility and the population of gauche torsional states in the molecules. On average at a density of 0.421g/ml there are 4.15% g^+ and 2.99% g^- torsions in the decane molecules.

The distribution of torsion angle values at the higher densities are in the all trans conformation with one exception (ϕ_5 at 0.707g/ml). At the lower density alternate torsion angles exhibit gauche torsions (ϕ_2, ϕ_4, ϕ_6 and either ϕ_1 or ϕ_7). These tend to favour the g^- conformation with few exceptions. This may indicate some preferred arrangement of torsional populations within a linear molecule stacked in this liquid crystalline manner, but requires further study.

Table 10.1.2a

%Trans/Gauche Conformations per Molecule 1.065g/ml			
Mol	%t	$\%g^-$	$\%g^+$
1	71.43	6.69	1.22
2	79.43	0.02	10.82
3	85.86	0.00	8.71
4	99.71	0.00	0.00
5	99.86	0.00	0.00
6	98.86	0.00	0.00
7	99.86	0.00	0.00
8	99.71	0.00	0.00
9	99.86	0.00	0.00

Sampled over 50-100ps.

Table 10.1.2b

%Trans/Gauche Conformations per molecule 0.707g/ml			
Mol	%t	$\%g^-$	$\%g^+$
1	98.86	0.00	0.00
2	99.00	0.00	0.00
3	99.00	0.00	0.00
4	99.00	0.00	0.00
5	96.57	0.00	2.03
6	98.86	0.00	0.00
7	90.14	0.00	7.33
8	97.29	1.21	0.00
9	99.00	0.00	0.00

sampled over 50-100ps.

Table 10.1.2c

%Trans/Gauche Conformations per Molecule 0.503g/ml			
Mol	%t	$\%g^-$	$\%g^+$
1	86.43	11.24	0.00
2	91.86	0.00	5.47
3	97.29	1.45	0.00
4	98.43	0.00	0.00
5	96.00	0.00	2.16
6	90.14	1.54	4.96
7	91.14	1.80	4.35
8	81.71	5.44	9.05
9	90.71	0.00	6.92

Sampled over 50-100ps.

Table 10.1.2d

%Trans/Gauche Conformations per Molecule 0.421g/ml			
Mol	%t	$\%g^-$	$\%g^+$
1	87.57	9.29	0.67
2	85.14	4.73	7.09
3	98.14	0.00	0.00
4	95.00	1.34	1.51
5	88.86	8.35	0.00
6	92.43	1.35	3.34
7	89.14	5.19	2.59
8	77.86	7.13	11.72
9	98.43	0.00	0.00

Sampled over 50-100ps.

Table 10.1.3a

%Trans/Gauche Populations 1.065g/ml			
	%t	$\%g^-$	$\%g^+$
ϕ_1	99.00	0.00	0.00
ϕ_2	99.00	0.00	0.00
ϕ_3	99.00	0.00	0.00
ϕ_4	99.00	0.00	0.00
ϕ_5	100.00	0.00	0.00
ϕ_6	100.00	0.00	0.00
ϕ_7	100.00	0.00	0.00

Sampled over 50-100ps.

Table 10.1.3b

%Trans/Gauche Populations 0.707g/ml			
	%t	$\%g^-$	$\%g^+$
ϕ_1	98.00	0.00	0.00
ϕ_2	99.00	0.00	0.00
ϕ_3	99.00	0.00	0.00
ϕ_4	99.00	0.00	0.00
ϕ_5	83.00	0.00	14.19
ϕ_6	99.00	0.00	0.00
ϕ_7	99.00	0.00	0.00

Sampled over 50-100ps.

Table 10.1.3c

%Trans/Gauche populations 0.503g/ml			
ϕ_1	99.00	0.00	0.00
ϕ_2	77.00	0.00	19.75
ϕ_3	99.00	0.00	0.00
ϕ_4	98.00	0.00	0.00
ϕ_5	99.00	0.00	0.00
ϕ_6	93.00	0.00	3.24
ϕ_7	92.00	5.40	0.00

Sampled over 50-100ps.

Table 10.1.3d

%Trans/Gauche populations 0.421g/ml			
ϕ_1	68.00	22.91	4.68
ϕ_2	82.00	0.00	15.07
ϕ_3	98.00	0.00	0.00
ϕ_4	87.00	0.00	10.56
ϕ_5	98.00	0.00	0.00
ϕ_6	91.00	6.68	0.00
ϕ_7	99.00	0.00	0.00

Sampled over 50-100ps.

Figure 10.1.3

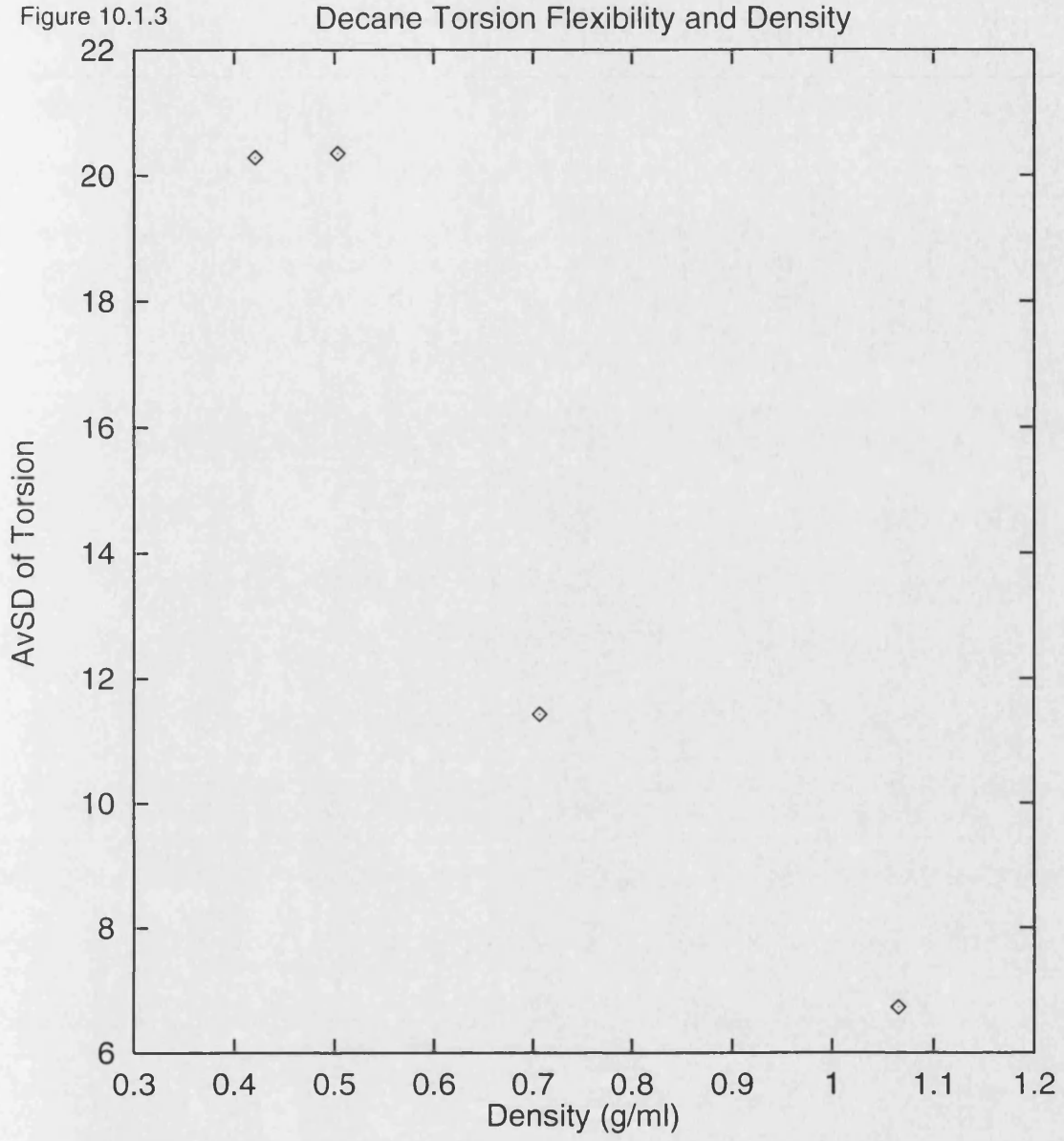

Figure 10.1.3 and table 10.1.4 contain the ensemble average standard deviation of all torsions in the decane system, over the sampled trajectory for each density of system. Clearly there is an increase in the torsional flexibility with decreasing density for this system. This appears to have reached a maximum at 0.421g/ml density, although this requires more data to increase the number of reference points.

This is sufficient however to demonstrate the link between density, torsion angle transitions and flexibility in long chain molecules arranged in a liquid crystalline configuration. Clearly the effect of the glycerol and PC groups tethering the chains to a relatively crystalline lattice will affect the torsion angle distribution for torsions in its locality and this requires more

study to define the precise nature of this interaction. This may be a primary mechanism for the order parameter plateau observed in experimental systems.

Table 10.1.4

Density and Average Torsion SD		
System	ρ(g/ml)	AvSD
1	1.065	6.721
2	0.707	11.424
3	0.503	20.35
4	0.421	20.288

Sampled over 50-100ps of NVT ensemble dynamics.

10.2. Cholesterol doping

The effect of cholesterol on the conformation and flexibility of the lipid membranes has been the subject of many studies. Experimentally it is observed to decrease fluidity in the L_α phase and increase fluidity in the L_β phase. In these systems the strict definitions of phase are not so clear. In the unexpanded model *dlpcchol* the DLPC molecules exhibit the characteristics of the L_β phase in a semirigid all trans conformation. The cholesterol gives rise to a decrease in the calculated order parameter profile, agreeing with the experimentally observed trend. The sterol ring system prevents efficient packing of the lauryl chains and decreases order in the gel state. However in the more fluid *dlpcchol_s* model the cholesterol increases order by virtue of the planarity of the sterol ring system, preventing fluidisation and mixing of the lauryl chains. This agrees well with a recent study in which cholesterol is observed to increase order and decrease fluidisation in a DMPC bilayer.[2]

This effect is maximised in the carbon segments in close proximity to the glycerol backbone, and where the planar sterol ring system is located. The calculated order parameters for the lower carbon segments out of range of the influence of the sterol ring system are in fact decreased in order providing further justification for this hypothesis.

The hydrogen bonding behaviour of the β-hydroxyl group of cholesterol in the *wat_dlpcchol* model compares well with that in a recent paper.[2] There is hydrogen bonding with the phosphate oxygens and on average 1.1 hydrogen bonds between the hydroxyl group and water. This compares with 1.5 hydrogen bonds in the study for cholesterols bound to

neighbouring lipid molecules.

10.3. Water Structure

In hydrated biological simulations the water model chosen is crucial. A number of water models are available[3-7] varying in complexity, from three site flexible waters to polarisible models. The water model used in this study is that of the CVFF force field and has been validated in several studies and reviewed along with other water models by Stouch[8] and coworkers. This study concludes that the CVFF water model reproduces the the structure and dynamics of water as well as the other equivalent water models.

In order to check the dynamic properties of the water model a molecular dynamics trajectory was sampled from a water box 30x30x30Å containing 302 waters. A 13Å cut off for nonbond interactions was used with no switching function, sampling from NVE ensemble for the first 50ps and 50-150ps from the NVT ensemble using a temperature constraint of 310K. 150ps of trajectory was sampled and the final 100ps used to calculated physical properties. This was repeated sampling from the NPT ensemble with temperature and pressure constraints of 310K and 1bar respectively. The radial distribution function for water oxygen atoms has been calculated for both systems (Figures 10.2.1(a,b)) These compare well with both experiment and previous theoretical studies[8] in terms of the position of both hydration shells and minima in the radial distribution.

Figure 10.2.1a & 10.2.1b

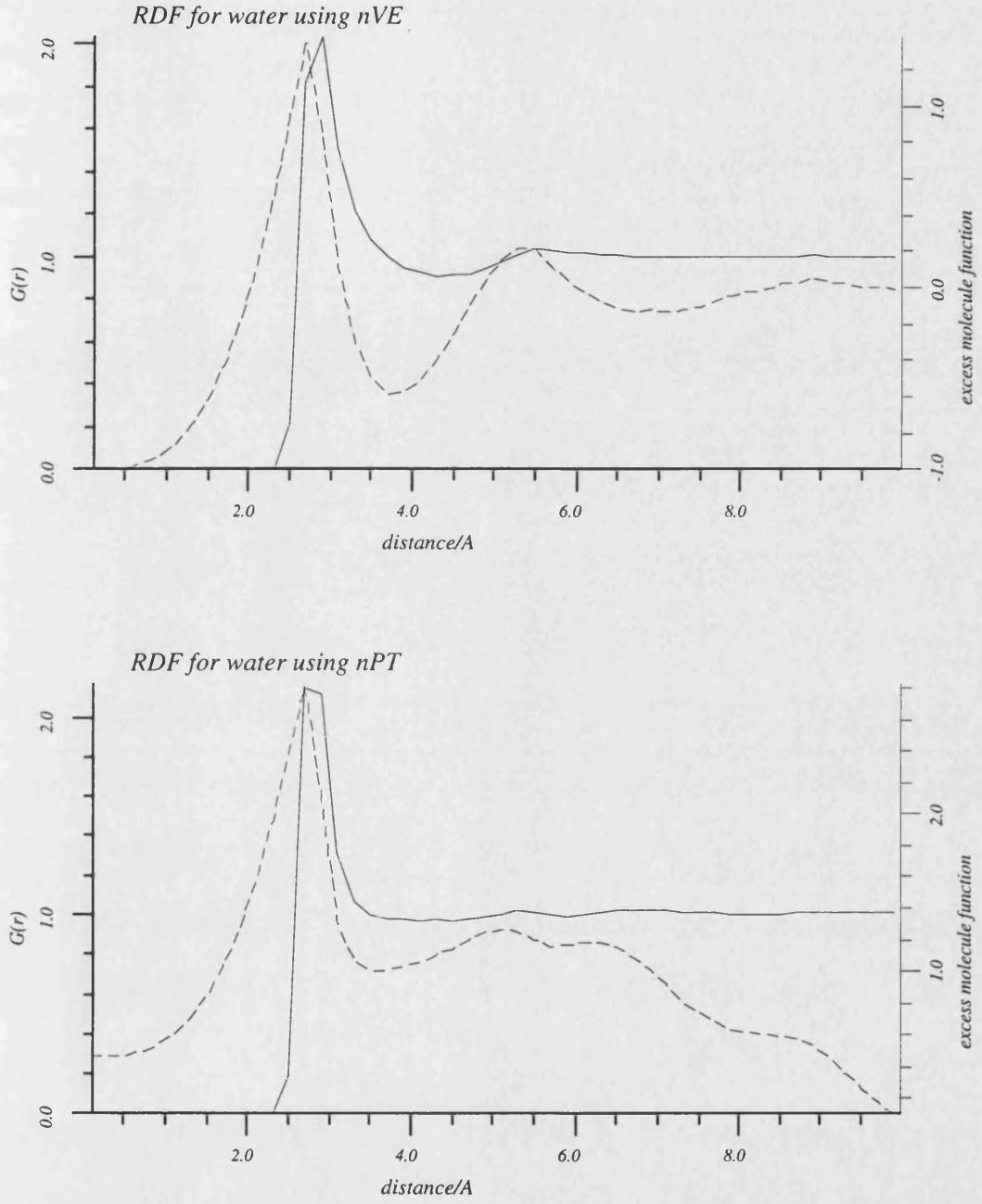

Sampled from 50-150ps. The dashed line is the integral of the normalised radial distribution function above 1.0 in molecules.

10.4. Hydrated Systems

From the results of the hydrated models, even given the imbalance of the thermal partitioning of the system, the water model reproduces the expected radial distribution function for

water oxygens, although the second hydration shell is not well pronounced. The hydrogen bonding elucidates a model in which there is significant hydrogen bonding to the nonesterified phosphate oxygens and little evidence of hydrogen bonding to the glycerol esterified oxygens and carbonyl oxygens of the fatty acid chains. This may be an artifact of the lack of equilibrium of the system. Clearly long simulations are required in order to allow the penetration of water into the hydrophilic head group region of the bilayer and allow the partitioning of the thermal energy to reach equilibrium through collisions of the water molecules and lipid head groups.

The measured electrostatic potentials agree well with experiment giving values in the order of 0.1-0.2V depending on the system. These values appear in better agreement with experiment than over recent simulations[9] although this maybe a function of the small size of the system. The reasons for the lack of agreement with experiment of other studies ave not been made clear.

10.5. Further Work

A number of features of both the simulation techniques and analysis require further examination and development.

1. Using the standard functions from within the FOCUS program it is possible to fourier transform the coordinates into the frequency domain and examine the characteristic frequencies of motion within the system. This allows for the comparison of characteristic stretching and bending frequencies of the DLPC molecule in a bilayer environment with those measured in experiment. These include

IR Frequencies	
Mode	μ/cm^{-1}
Anti-Sym CH_2 stretch	2918
Sym CH_2 stretch	2850
PO_2^- stretch	1090
Choline stretch	970
Water OH stretch	2800-3100
Water OH_2 bend	1640
CH stretch	2800-3100
CH_2 deformation	1400-1500
C-C stretch	1000-1200

2. A detailed examination of the time dependence of hydrogen bonding and its implications on the water's structure and dynamics is required. The orientational polarisation of water molecules by the bilayer surface as a function of the bilayer normal can then be examined.

3. Examination of the relationship between the segmental order parameter profile and the orientation of the DLPC molecules with respect to the bilayer normal is required. Clearly the insensitivity of the segmental order parameters to conformational disorder has been demonstrated.

4. An examination of the free volume available to various groups within the bilayer model would be of interest in examining the local dynamics of both the head groups and lauryl chains as a function of the bilayer normal.

5. An examination of the diffusion of water molecules within the aqueous layer above and below the bilayer will elucidate the effect of the motion of the DLPC head groups on the diffusional properties of the water molecules. This is of great interest especially due to its implications on ion transport properties of membranes.

6. The asymmetry of these bilayer simulations has been noted in several theoretical studies. The interactions within the two monolayers are not identical. There is much interest in the interactions and cooperativity amongst the acyl chains of these systems and in the interactions between the two monolayers. The interactions and cooperativity in the plane of the bilayer are more understood. There is a fine balance between having little interaction between the two monolayers leading in some circumstances to a vacuum being formed and introducing some degree of interdigitation which leads to a collapse of the hydrophobic region under the

dispersion forces between adjacent lauryl chains.

7. The imbalance of the thermal partitioning within the system which leads to the increased temperature of the aqueous phase in comparison with the lipid phase clearly requires further work. Some attempts have been undertaken to address this problem, the results of which are not presented here. These have included the implimentation of separate temperature baths for the lipid and aqueous phases in the system. Another approach applied used multiple boltzmann distributions at fixed intervals along the trajectory, reinitialising the distribution of atomic velocities within the system. It has been found that this improves the temperature differential reactivating all of the modes of motion of the molecule at each reinitialisation.

8. The course of the simulation depends fundermentally on the starting configuration and conformation of the lipid molecules. It is far from clear that the crystal structure represents a "reasonable" starting structure for an L_α phase bilayer. A more random starting structure based on the a pre-fluidised coordinate system may be of some benefit in achieving the L_α phase with less computational effort.

9. In mixed aqueous and lipid phase simulations careful pre-minimisation of both the aqueous and lipid phases independently and self-consistently is required in order to remove any strain from the system before sampling the molecular dynamics trajectory.

10. The pressure scaling within the system gives rise to a number of artifacts by virtue of its "sledgehammer" approach to pressure scaling. A more subtle method of pressure scaling will improve the stability of these systems.

10.6. Concluding Remarks

This study has attempted to simulate the liquid crystalline bilayer environment in order to allow for the structure and dynamics of membrane proteins to be calculated. Clearly there is much work to be done, before one could be satisfied that this model reproduces this phase correctly. A number of important issues and problems which must be addressed have been elucidated in this study and continuing effort is being made to address them in future studies. This study can therefore be used to pin point some of the possible pit falls of such simulations and allow others to improve on the results obtained here.

A number of tools have been developed to allow for the efficient and elegant analysis of such systems. These allow for the comparison of physical properties calculated from the obtained trajectories with both experimental and other theoretical studies.[10]

References

1. Allen MP and Tildesley DJ, in *Computer Simulation of Liquids*, Oxford Clarendon Press, 1987.

2. Robinson AJ, Richards WG, Thomas PJ, and Hann MM, *Biophysical J*, vol. 68, pp. 164-170, 1995.

3. Stillinger FH and Rahman A, *J Chem Phys*, vol. 60, no. 4, p. 1545, 1974.

4. Jorgensen WL, *J Am Chem Soc*, vol. 103, p. 335, 1981.

5. Jorgensen WL, *J Chem Phys*, vol. 77, pp. 4156-4163, 1982.

6. Jorgensen WL, Chandrasekhar J, and Madura JD, *J Chem Phys*, vol. 79, pp. 926-935, 1983.

7. Lie GC, Clementi E, and Yoshimine M, *J Chem Phys*, vol. 64, p. 2314, 1976.

8. Lau KF, Alper HE, Thatcher TS, and Stouch TR, *J Phys Chem*, vol. 98, pp. 8785-8792, 1994.

9. Schulten K and Zhou F, *J Phys Chem*, vol. 99, pp. 2194-2207, 1995.

10. Lemon A, Dauber-Osguthorpe P, and Osguthorpe DJ, *Computer Physics Communications (In Press 1995)*.

11. Appendix I

11.1. Potential Library

Coulombic parameters

h	0.10
c'	0.38
c	0.0
s	
c-	0.36
o-	-0.38
p	
cn	-0.16
h*	0.41

Bond Parameters

o	c	68.3	1.42	2.0
p	o	57.5	1.61	2.00
c	h	108.6	1.105	1.771
c	c	88.0	1.526	1.915
c	c'	76.0	1.52	1.93
c'	o'	145.0	1.23	2.06
n	c'	97.0	1.32	2.0
c	n	72.0	1.46	2.29
oh	ho	104.0	0.96	2.28
oh	c	96.0	1.42	2.00
o	ho	95.0	0.96	2.28
c'	h	108.6	1.105	1.771
c'	o	100.0	1.37	2.00
c'	o-	135.0	1.25	2.00
cp	h	116.0	1.08	1.77
cp	c	76.0	1.51	1.93
cp	oh	96.0	1.37	2.00
sh	hs	87.5	1.33	1.77

c	n3	68.0	1.47	2.29	
cp	n	70.0	1.34	2.00	
o*	h*	104.0	0.96	2.28	
p	oh	75.0	1.57	2.00	
p	o'	140.0	1.53	2.00	
p	o-	120.0	1.53	2.00	
p	h	56.0	1.50	2.00	
np	c	84.2	1.475	2.00	
c=	c'	80.7	1.50	2.00	
c=	c	80.7	1.50	2.00	
c=	c=	163.8	1.33	2.00	
c=	h	90.4	1.09	2.00	
cp	c'	80.7	1.50	2.00	
c'	oh	96.0	1.37	2.00	

Angle Parameters

h	c	h	39.5	106.4	0.0	0.0	0.0
h	c	c	44.4	110.0	0.0	12.6	38.4
c	c	c	46.6	110.5	28.5	60.2	60.2
c	c'	o'	68.0	120.0	25.0	2.0	30.0
h	c	c'	45.	109.5	2.0	2.0	38.4
c	c	c'	46.6	110.5	28.5	60.2	60.2
c'	n	c	111.0	118.0	25.3	31.5	30.0
n	c	c	50.0	109.5	25.	35.0	35.0
n	c	h	51.5	109.5	2.0	2.0	40.0
n	c	c'	50.0	109.5	25.	35.0	35.0
c	c'	n	53.5	114.1	45.9	2.0	31.5
o	c'	n	53.5	114.1	45.9	2.0	31.5
o'	c'	n	68.0	120.0	10.	2.	2.
c	o	ho	58.5	106.0	0.0	57.0	0.0
o	c	h	57.0	109.5	0.0	0.0	64.4
c	c	o	70.0	109.5	25.0	0.0	0.0
c'	c	o	70.0	109.5	25.0	0.0	0.0
c=	c	o	70.0	109.5	25.0	0.0	0.0

o'	c'	o	145.0	123.0	0.0		
o	c	o	115.01	113.0	66.61	60.51	60.51
c	c'	o	122.8	110.0			
c'	o	ho	50.0	112.0	0.0	00.0	00.0
h	c'	o	55.0	110.0			
h	c'	o'	55.0	120.0	25.0	2.0	30.0
o-	c'	o-	145.0	123.0	50.0		
c	c'	o-	68.0	120.0	50.0	0.0	30.0
h	c'	o-	55.0	120.0	50.0	0.0	30.0
c	n	c	37.0	120.0	50.0	50.0	50.0
h	c'	n	45.0	120.0			
cp	o	ho	50.0	109.0	0.0	0.0	0.0
h	c	n3	57.3	109.5			
c	n3	c	86.3	112.0			
c	c	n3	50.0	109.5			
n	c'	n	102.0	120.0			
cp	o	c	50.0	109.5			
n3	c	c'	50.0	109.5	25.	35.0	35.0
c	o	c	60.0	109.5	0.0	57.0	57.0
h*	o*	h*	50.0	104.5	-14.5	31.3	31.3
p	o	c	72.0	120.0			
p	o	p	72.0	120.0			
o	p	o	110.0	109.5	80.0		
o'	p	o	110.0	109.5	40.0		
o'	p	o'	110.0	109.5	40.0		
o-	p	o-	110.0	109.5	40.0		
o	p	o-	110.0	109.5	40.0		
h	p	o-	80.0	109.5	60.00		
np	c	o	80.0	109.5			
np	c	h	80.0	109.5			
np	c	c	80.0	109.5			
c	c	c=	46.6	110.5	28.5	60.2	60.2
c=	c'	n	53.5	114.1	45.9	2.0	31.5

c'	c=	c=		36.2	122.3	28.5	60.2	60.2
c	c=	c=		36.2	122.3	28.5	60.2	60.2
c	c=	h		37.5	120.0	0.0	38.4	0.0
c=	c	c=		46.6	110.5	28.5	60.2	60.2
h	c	c=		44.4	110.0	0.0	12.6	38.4
c=	c=	h		33.8	121.2	0.0	0.0	38.4
o'	c'	c=		50.0	120.0			
c	c=	c'		50.0	120.0			
c	c=	c		50.0	120.0			
cp	c'	n		53.5	114.1	45.9	2.0	31.5
cp	c'	o'		68.0	120.0	25.0	2.0	30.0
c'	o	c		50.0	109.5			

Torsion Parameters

*	c	c	*	1.4225	3.0	1.0	-10.5	
*	c	c'	*	0.0	0.0			
*	c	n	*	0.0	0.0			
*	c	o	*	0.39	3.0	1.0	0.0	
*	c	of	*	0.39	3.0	1.0	0.0	
*	c'	n2	*	6.0	2.0	-1.0	-	0.0
*	c'	o	*	4.5	2.0	-1.0		
*	n3	c	*	0.8	3.0	1.0	-10.5	
*	p	o	*	0.75	3.0	1.0		
*	c=	c=	*	16.3	2.0	-1.0		
*	c=	c	*	1.266	3.0	1.0		
*	c'	c=	*	1.8	2.0	-1.0		
c	c'	n	c	3.2	2.0	-1.0	-8.0	
o'	c'	n	c	3.8	2.0	-1.0	-8.0	
h	c'	n	c	3.2	2.0	-1.0	-8.0	
cp	c'	n	c	3.2	2.0	-1.0	-8.0	
o	c'	n	c	3.2	2.0	-1.0	-8.0	

Out of plane Parameters

c	c'	n	o'	*	10.0	2.0	-1.0	0.01
c	c'	n2	o'	*	10.0	2.0	-1.0	0.01

h	c'	n2	o'	*	10.0	2.0	-1.0	0.01
c	c'	o'	o'	*	11.6	2.0	-1.0	
h	c'	o'	o'	*	11.6	2.0	-1.0	
c'	n	c	c	*	0.05	2.0	-1.0	
h	c'	o'	n	*	0.05	2.0	-1.0	
n	c'	n2	n2	*	10.0	2.0	-1.0	0.01
c=	c'	n2	o'	*	10.0	2.0	-1.0	0.01
c	c=	c'	c=	*	11.1	2.0	-1.0	
h	c=	c	c=	*	11.1	2.0	-1.0	
cp	c'	n	o'	*	10.0	2.0	-1.0	0.01

c	(	c	c	)	c	-7.9
c	(	c	c'	)	o	0.0
c'	(	c	c	)	o	0.0
c	(	c	o	)	c'	0.0
c	(	c	o	)	o	0.0
c	(	c	o	)	c=	0.0
o	(	c	c	)	o	0.0
o	(	c	c	)	c=	0.0
o	(	c	c'	)	h	0.0
o	(	c	o	)	o	0.0
h	(	c	h	)	h	0.0
h	(	c	h	)	c	0.0
h	(	c	c	)	h	-7.9
h	(	c	c	)	c	-7.9
c	(	c	h	)	c	0.0
o	(	c	h	)	c=	0.0
h	(	c	h	)	c'	0.0
h	(	c	c'	)	h	-7.5
c	(	c	n	)	h	-7.9
c	(	c	h	)	n	-7.9
h	(	c	c	)	n	-7.9
c	(	c	c'	)	h	-7.9
c	(	c	h	)	c'	0.0

c'	(	c	c	)	h	-7.9
n	(	c	h	)	c'	-7.9
n	(	c	c'	)	h	-7.9
c'	(	c	n	)	h	-7.9
n	(	c	c	)	c'	-7.9
n	(	c	c'	)	c	-7.9
c	(	c	n	)	c'	-7.9
c	(	c'	o'	)	n	0.0
c	(	c'	n	)	o'	-7.5
n	(	c'	c	)	o'	0.0
h	(	c	n	)	h	-7.5
h	(	c	h	)	n	0.0
h	(	c	o	)	h	0.0
h	(	c	o	)	c=	0.0
h	(	c	h	)	o	0.0
h	(	c	c	)	o	0.0
h	(	c	o	)	c	0.0
c'	(	c	o	)	h	0.0
c	(	c	h	)	o	0.0
c'	(	c	h	)	o	0.0
c	(	c	c	)	o	0.0
c	(	c	o	)	c	0.0
c	(	c'	o'	)	o	0.0
c	(	c'	o	)	o'	0.0
o	(	c'	c	)	o'	0.0
o'	(	c'	h	)	o	0.0
h	(	c'	o'	)	o	0.0
h	(	c'	o	)	o'	0.0
h	(	c'	o-	)	o-	0.0
o-	(	c'	h	)	o-	0.0
c	(	c'	o-	)	o-	0.0
o-	(	c'	c	)	o-	0.0
c'	(	n	c	)	c	10.0

c	(	n	c'	)	c	10.0
h	(	c'	o'	)	n	0.0
o'	(	c'	n	)	h	0.0
o'	(	c'	h	)	n	0.0
cp	(	c	h	)	h	0.0
cp	(	c	c	)	h	-7.9
cp	(	c	h	)	c	0.0
s	(	c	h	)	h	0.0
sh	(	c	h	)	h	0.0
c	(	c	h	)	n3	0.0
c	(	c	n3	)	h	0.0
h	(	c	c	)	n3	0.0
h	(	c	h	)	n3	0.0
h	(	c	n3	)	h	0.0
c	(	n3	c	)	c	0.0
n	(	c'	n	)	n	0.0
c	(	c	n3	)	c'	-7.9
c	(	c	c'	)	n3	-7.9
c'	(	c	c	)	n3	-7.9
h	(	c	n3	)	c'	-7.9
h	(	c	c'	)	n3	-7.9
c'	(	c	h	)	n3	-7.9
c=	(	c	c	)	h	0.0
c	(	c	c=	)	h	0.0
c	(	c	c=	)	o	0.0
o	(	c	c=	)	h	0.0
c	(	c	h	)	c=	0.0
c	(	c=	c	)	c=	0.0
c	(	c	c=	)	c	0.0
c=	(	c	c	)	c	0.0
c=	(	c	h	)	c	0.0
c	(	c=	c=	)	c	0.0
o'	(	c'	n	)	c=	0.0

o'	(	c'	c=	)	n	0.0
n	(	c'	o'	)	c=	0.0
c	(	c=	c'	)	c=	0.0
c'	(	c=	c	)	c=	0.0
c	(	c=	c=	)	c'	0.0
h	(	c	c=	)	c=	0.0
h	(	c	c=	)	h	0.0
c=	(	c	h	)	c=	0.0
h	(	c	h	)	c=	0.0
np	(	c=	h	)	c=	0.0
h	(	c=	c	)	c=	0.0
h	(	c=	c=	)	c	0.0
c	(	c=	h	)	c=	0.0
o	(	p	o-	)	o-	0.0
o-	(	p	o-	)	o-	0.0
h	(	p	o-	)	o-	30.
o-	(	p	h	)	o-	30.
o'	(	p	o	)	o	0.0
o'	(	p	o	)	o'	0.0
o	(	p	o'	)	o	0.0
o'	(	p	o'	)	o	0.0
n	(	c	c	)	c	0.0
c	(	c	n	)	c	0.0
o'	(	c'	n	)	o	0.0
o'	(	c'	o	)	n	0.0
n	(	c'	o'	)	o	0.0

Non-Bond Parameters

h	-	7108.466	32.87076	12.
cg	-	1790340.724	528.4819	12.
o'	-	272894.7846	498.8788	12.
n	-	2266872.40	1230.557	12.
c'	-	2968753.359	1325.7081	12.
c	-	1981049.225	1125.998	12.

s	-	365906.4	250.8	12.
o*	-	629358.0	625.5	12.
h*	-	0.0025	0.0050	12.
p	-	6025894.0	2195.6	12.
c+	-	119025.0	240.25	12.

11.2. Atomic Charges and potential types

DMPC

Atom	pot	charge					
C	cn	-0.0800	1	H71	h	0.1000	31
HC1	h	0.1300	2	H72	h	0.1000	32
HC2	h	0.1300	3	O4	o	-0.3800	33
HC3	h	0.1300	4	C8	c'	0.3800	34
N	n3	-0.1600	5	O5	o'	-0.3800	35
C1	cn	-0.0800	6	C9	c2	-0.2000	36
H11	h	0.1300	7	H91	h	0.1000	37
H12	h	0.1300	8	H92	h	0.1000	38
H13	h	0.1300	9	C10	c2	-0.2000	39
C2	cn	-0.0800	10	H10	h	0.1000	40
H21	h	0.1300	11	H10	h	0.1000	41
H22	h	0.1300	12	C11	c2	-0.2000	42
H23	h	0.1300	13	H11	h	0.1000	43
C3	cn	-0.0300	14	H11	h	0.1000	44
H31	h	0.1300	15	C12	c2	-0.2000	45
H32	h	0.1300	16	H12	h	0.1000	46
C4	c2	-0.0400	17	H12	h	0.1000	47
H41	h	0.0600	18	C13	c2	-0.2000	48
H42	h	0.0600	19	H13	h	0.1000	49
O	o	-0.4800	20	H13	h	0.1000	50
P	p	1.3000	21	C14	c2	-0.2000	51
O1	o'	-0.7500	22	H14	h	0.1000	52
O2	o'	-0.7500	23	H14	h	0.1000	53
O3	o	-0.4800	24	C15	c2	-0.2000	54
C5	c2	-0.0400	25	H15	h	0.1000	55
H51	h	0.0600	26	H15	h	0.1000	56
H52	h	0.0600	27	C16	c2	-0.2000	57
C6	c1	0.1800	28	H16	h	0.1000	58
H61	h	0.2000	29	H16	h	0.1000	59
C7	c2	0.1800	30	C17	c2	-0.2000	60

H17	h	0.1000	61
H17	h	0.1000	62
C18	c2	-0.2000	63
H18	h	0.1000	64
H18	h	0.1000	65
C19	c2	-0.2000	66
H19	h	0.1000	67
H19	h	0.1000	68
C20	c2	-0.2000	69
H20	h	0.1000	70
H20	h	0.1000	71
C21	c3	-0.3000	72
H21	h	0.1000	73
H21	h	0.1000	74
H21	h	0.1000	75
O6	o	-0.3800	76
C22	c'	0.3800	77
O7	o'	-0.3800	78
C23	c2	-0.2000	79
H23	h	0.1000	80
H23	h	0.1000	81
C24	c2	-0.2000	82
H24	h	0.1000	83
H24	h	0.1000	84
C25	c2	-0.2000	85
H25	h	0.1000	86
H25	h	0.1000	87
C26	c2	-0.2000	88
H26	h	0.1000	89
H26	h	0.1000	90
C27	c2	-0.2000	91
H27	h	0.1000	92
H27	h	0.1000	93
C28	c2	-0.2000	94
H28	h	0.1000	95
H28	h	0.1000	96
C29	c2	-0.2000	97
H29	h	0.1000	98
H29	h	0.1000	99
C30	c2	-0.2000	100
H30	h	0.1000	101
H30	h	0.1000	102
C31	c2	-0.2000	103
H31	h	0.1000	104
H31	h	0.1000	105
C32	c2	-0.2000	106
H32	h	0.1000	107
H32	h	0.1000	108
C33	c2	-0.2000	109
H33	h	0.1000	110
H33	h	0.1000	111
C34	c2	-0.2000	112
H34	h	0.1000	113
H34	h	0.1000	114
C35	c3	-0.3000	115
H35	h	0.1000	116
H35	h	0.1000	117
H35	h	0.1000	118

DLPC

Atom	pot	charge					
C	cn	-0.0800	1	H72	h	0.1000	32
HC1	h	0.1300	2	O4	o	-0.3800	33
HC2	h	0.1300	3	C8	c'	0.3800	34
HC3	h	0.1300	4	O5	o'	-0.3800	35
N	n3	-0.1600	5	C9	c2	-0.2000	36
C1	cn	-0.0800	6	H91	h	0.1000	37
H11	h	0.1300	7	H92	h	0.1000	38
H12	h	0.1300	8	C10	c2	-0.2000	39
H13	h	0.1300	9	H101	h	0.1000	40
C2	cn	-0.0800	10	H102	h	0.1000	41
H21	h	0.1300	11	C11	c2	-0.2000	42
H22	h	0.1300	12	H111	h	0.1000	43
H23	h	0.1300	13	H112	h	0.1000	44
C3	cn	-0.0300	14	C12	c2	-0.2000	45
H31	h	0.1300	15	H121	h	0.1000	46
H32	h	0.1300	16	H122	h	0.1000	47
C4	c2	-0.0400	17	C13	c2	-0.2000	48
H41	h	0.0600	18	H131	h	0.1000	49
H42	h	0.0600	19	H132	h	0.1000	50
O	o	-0.4800	20	C14	c2	-0.2000	51
P	p	1.3000	21	H141	h	0.1000	52
O1	o'	-0.7500	22	H142	h	0.1000	53
O2	o'	-0.7500	23	C15	c2	-0.2000	54
O3	o	-0.4800	24	H151	h	0.1000	55
C5	c2	-0.0400	25	H152	h	0.1000	56
H51	h	0.0600	26	C16	c2	-0.2000	57
H52	h	0.0600	27	H161	h	0.1000	58
C6	c1	0.1800	28	H162	h	0.1000	59
H6	h	0.2000	29	C17	c2	-0.2000	60
C7	c2	0.1800	30	H171	h	0.1000	61
H71	h	0.1000	31	H172	h	0.1000	62

C18 c2	-0.2000	63
H181h	0.1000	64
H182h	0.1000	65
C19 c3	-0.3000	66
H191h	0.1000	67
H192h	0.1000	68
H193h	0.1000	69
O6 o	-0.3800	70
C20 c'	0.3800	71
O7 o'	-0.3800	72
C21 c2	-0.2000	73
H211h	0.1000	74
H212h	0.1000	75
C22 c2	-0.2000	76
H221h	0.1000	77
H222h	0.1000	78
C23 c2	-0.2000	79
H231h	0.1000	80
H232h	0.1000	81
C24 c2	-0.2000	82
H241h	0.1000	83
H242h	0.1000	84
C25 c2	-0.2000	85
H251h	0.1000	86
H252h	0.1000	87
C26 c2	-0.2000	88
H261h	0.1000	89
H262h	0.1000	90
C27 c2	-0.2000	91
H271h	0.1000	92
H272h	0.1000	93
C28 c2	-0.2000	94
H281h	0.1000	95
H282h	0.1000	96
C29 c2	-0.2000	97
H291h	0.1000	98
H292h	0.1000	99
C30 c2	-0.2000	100
H301h	0.1000	101
H302h	0.1000	102
C31 c3	-0.3000	103
H311h	0.1000	104
H312h	0.1000	105
H313h	0.1000	106

cholesterol

Atom	pot	charge		Atom	pot	charge	
OH	oh	-0.3800	1	C13	c1	-0.1000	32
HO	ho	0.3500	2	H13	h	0.1000	33
C2	c1	-0.0700	3	C14	c2	-0.2000	34
H2	h	0.1000	4	H141	h	0.1000	35
C1	c2	-0.2000	5	H142	h	0.1000	36
H11	h	0.1000	6	C15	c2	-0.2000	37
H12	h	0.1000	7	H151	h	0.1000	38
C	c2	-0.2000	8	H152	h	0.1000	39
HC1	h	0.1000	9	C16	c1	-0.1000	40
HC2	h	0.1000	10	H16	h	0.1000	41
C3	c2	-0.2000	11	C17	c3	-0.3000	42
H31	h	0.1000	12	H171	h	0.1000	43
H32	h	0.1000	13	H172	h	0.1000	44
C4	c=	0.0000	14	H173	h	0.1000	45
C5	c=	-0.1000	15	C18	c3	-0.3000	46
H5	h	0.1000	16	H181	h	0.1000	47
C6	c2	-0.2000	17	H182	h	0.1000	48
H61	h	0.1000	18	H183	h	0.1000	49
H62	h	0.1000	19	C19	c1	-0.1000	50
C7	c1	-0.1000	20	H19	h	0.1000	51
H7	h	0.1000	21	C20	c3	-0.3000	52
C8	c1	-0.1000	22	H201	h	0.1000	53
H8	h	0.1000	23	H202	h	0.1000	54
C9	c	0.0000	24	H203	h	0.1000	55
C10	c2	-0.2000	25	C21	c2	-0.2000	56
H101	h	0.1000	26	H211	h	0.1000	57
H102	h	0.1000	27	H212	h	0.1000	58
C11	c2	-0.2000	28	C22	c2	-0.2000	59
H111	h	0.1000	29	H221	h	0.1000	60
H112	h	0.1000	30	H222	h	0.1000	61
C12	c	0.0000	31	C23	c2	-0.2000	62

H231	h	0.1000	63
H232	h	0.1000	64
C24	c1	-0.1000	65
H24	h	0.1000	66
C25	c3	-0.3000	67
H251	h	0.1000	68
H252	h	0.1000	69
H253	h	0.1000	70
C26	c3	-0.3000	71
H261	h	0.1000	72
H262	h	0.1000	73
H263	h	0.1000	74

water

Atom	pot	charge	
O1	o*	-0.8200	1
H11	h*	0.4100	2
H12	h*	0.4100	3